Preparation, characterization and catalytic evaluation of zeolite catalysts for methyl tertiary butyl ether synthesis

Ali, Mohammed Ashraf

Award date:
1998

Awarding institution:
University of Bath

PREPARATION, CHARACTERIZATION AND CATALYTIC EVALUATION OF ZEOLITE CATALYSTS FOR METHYL TERTIARY BUTYL ETHER SYNTHESIS

Submitted by

Mohammed Ashraf Ali
(M.S. Chemistry)

for the Degree of Ph.D.
of the University of Bath
1998

COPYRIGHT

ProQuest LLC
789 East Eisenhower Parkway
P.O. Box 1346
Ann Arbor, MI 48106-1346

DEDICATION

This dissertation is dedicated

to my Wife

Shahnaz

and my Children

Wardah, Anadel and Haseeb

ACKNOWLEDGEMNT

I am very grateful to the Almighty, ALLAH, for providing me the opportunity and capability to effectuate this research work.

I wish to express my sincere thanks and appreciation to my supervisors, Professor W. J. Thomas and Dr. B. J. Brisdon for their technical support, guidance, advice and encouragement throughout this research work. I appreciate the suggestions and assistance of Dr. S. P. Perera during my visits to the University of Bath.

I am thankful to Dr. M. M. Abdillahi for motivating me to involve in catalyst research and development work and for his technical support and continuous contribution which resulted in the execution of this work. The support provided by the Catalysts Development Group at the Research Institute of the King Fahd University of Petroleum and Minerals is highly appreciated.

I am indebted to Dr. S. M. Zarook for his contribution in reviewing the manuscript and his help in finalizing this work.

I would like to thank my fellow postgraduates, Torsten, Bhardwaj and Ananya for their help and encouragement. I appreciate the help of Mrs. O'Reilly and Mr. Mac Forsyth during my stay at the University of Bath.

I am also obliged to my friends and colleagues at KFUPM for their help and suggestions during this work especially Ikram, Faiz, Javaid, Bari, Alam and Shakeel.

Most of all, I would like to acknowledge and esteem my parents, Mr. Ghulam Mohammed and Ms. Aisha who brought me up and educated me to the best of their efforts.

Finally, I would like to mention that, without the sacrifices, patience, prayers, encouragement and understanding of my wife and children it would not have been possible to complete this research work.

SUMMARY

MFI zeolites having silicon-to-aluminum molar ratios of 10 to 100 were synthesized successfully by a rapid crystallization method using silicon and aluminum compounds in the presence of a template in basic medium. The calcination of the synthesized zeolites was successfully achieved at 873 K and ion-exchange was accomplished efficiently using aqueous solution of hydrochloric acid. All synthesized zeolites were crystalline and of MFI type having chemical compositions agreed quite well with those of ZSM-5 zeolites. The crystals of the synthesized zeolites were spherical in shape. The synthesized zeolites were found stable up to 1323 K, and possess surface properties, and pore size comparable to ZSM-5 zeolites.

The activity of the synthesized zeolites, for the reaction of methanol and isobutene to produce MTBE, increased with decreasing Si/Al molar ratio of the zeolites and with increasing reaction temperature. The ZCIC-10 zeolite was found to have maximum MTBE yield among all synthesized zeolites. The substitution of boron and gallium did not enhance the activity of the zeolites. The hydrothermal modification using aluminum fluoride significantly enhanced the activities of zeolites for MTBE production.

The intrinsic kinetics determination for the reaction of methanol and isobutene to produce MTBE using ZCIC-10 zeolite showed that the surface reaction rate constant increased with increase in temperature whereas the thermodynamic equilibrium constants and adsorption equilibrium constants decreased with rise in temperature. The reaction was found to have activation energy of 140.8 kJ mol^{-1}. The reaction was found first order both in methanol and isobutene and 2.5 orders in MTBE. The reaction can be represented by a Langmuir-Hinshelwood model which is derived from the mechanism in which the methanol adsorbed on one site reacts with isobutene adsorbed on another site and produce MTBE which is then desorbed.

TABLE OF CONTENTS

Chapter	Title	Page
	SUMMARY	**i**
	NOMENCLATURE	xii
CHAPTER 1	**INTRODUCTION**	**1**
1.2.	ZEOLITE STRUCTURE AND ACIDITY	1
1.3.	OBJECTIVES OF THE STUDY	3
CHAPTER 2	**LITERATURE REVIEW**	**4**
2.1.	SYNTHESIS AND PRETREATMENT OF MFI ZEOLITES	4
2.1.1.	Synthesis of MFI Zeolites	4
2.1.2.	Pretreatment of Zeolites (Calcination and Ion-Exchange)	6
2.2.	ISOMORPHOUS SUBSTITUTION OF SILICON IN MFI ZEOLITES	8
2.3.	CHARACTERIZATION OF MFI ZEOLITES	9
2.3.1.	X-Ray Diffraction (XRD)	9
2.3.2.	Fourier Transform-Infrared Spectroscopy (FT-IR)	10
2.3.3.	Thermal Analysis (TG, DTA)	11
2.3.4.	Scanning Electron Microscopy (SEM)	11
2.3.5.	Elemental Analysis	12
2.3.6.	Surface Area and Pore Structure Determination	12
2.4.	CATALYSTS USED FOR MTBE SYNTHESIS	13
2.4.1.	Sulfuric Acid	13
2.4.2.	Clays	14
2.4.3.	Heteropoly Acids	14
2.4.4.	Acidic Resins	15
2.4.4.1.	Laboratory Synthesis of MTBE	15
2.4.4.2.	Commercial Production of MTBE	17
2.4.5.	Zeolites	18
2.5.	KINETICS OF MTBE SYNTHESIS	21
2.5.1.	Kinetics based on Rideal-Eley Mechanism	21
2.5.2.	Kinetics based on Langmuir-Hinshelwood Mechanism	22
CHAPTER 3	**EXPERIMENTAL**	**25**
3.1.	SYNTHESIS AND PRETREATMENT OF MFI ZEOLITES	25
3.1.1.	Synthesis of MFI Zeolites	25
3.1.1.1.	Experimental Set-up	25
3.1.1.2.	Synthetic Procedure	27
3.1.2.	Pretreatment of MFI Zeolites (Calcination and Ion-Exchange)	30
3.2.	ISOMORPHOUS SUBSTITUTION OF SILICON IN MFI ZEOLITES	30
3.2.1.	Chemicals and Equipment	31

3.2.2. Isomorphous Substitution by Boron and Gallium during Synthesis 31
3.2.3. Post-Synthesis Isomorphous Substitution by Boron and Gallium 32
3.2.3.1. Ammonium Fluoride and Boric Acid/Gallium Nitrate Hydrothermal Treatment 32
3.2.3.2. Solid State Method 32
3.2.3.3. Sodium Carbonate and Boric Acid Hydrothermal Treatment 33
3.2.4. Post-Synthesis Isomorphous Substitution by Aluminum 34
3.2.4.1. Aluminum Sulfate Hydrothermal Treatment 34
3.2.4.2. Ammonium Fluoride and Aluminum Sulfate Hydrothermal Treatment 34
3.2.4.3. Aluminum Fluoride or Aluminum Chloride Hydrothermal Treatment 34
3.3. CHARACTERIZATION OF MFI ZEOLITES 35
3.3.1. X-Ray Diffraction 35
3.3.2. Fourier Transform-Infrared Spectroscopy 35
3.3.3. Thermal Analysis 35
3.3.4. Scanning Electron Microscopy 36
3.3.5. Elemental Analysis 36
3.3.5.1. Sample Preparation for the Determination of Silicon and Aluminum 36
3.3.5.2. Alternate Methods of Determination of Silicon and Aluminum Contents 37
3.3.5.3. Determination of Sodium by Flame Photometry 37
3.3.5.4. Determination of Fluoride Contents by Potentiometric Titration 37
3.3.6. Surface Area and Pore Structure Determination 38
3.4. CATALYTIC EVALUATION OF MFI ZEOLITES 38
3.4.1. Synthesized Aluminosilicate MFI Zeolites 38
3.4.1.1. Experimental Set-up 38
3.4.1.2. Reaction Procedure 40
3.4.2. Isomorphously Substituted MFI Zeolites 41
3.4.2.1. Experimental Set-up 41
3.4.2.2. Reaction Procedure 41
3.4.3. Reaction Product Analysis 42
3.5. DETERMINATION OF INTRINSIC KINETICS 43
3.5.1. Reaction System Set-up 43
3.5.2. Reaction Procedure 45
3.5.3. Methodology for Determining Intrinsic Kinetics 47

3.5.3.1. Optimization of Reaction Variables 47
3.5.3.2. Determination of Order of Reaction for Isobutene 48
3.5.3.3. Determination of Order of Reaction for Methanol 48
3.5.3.4. Effect of Temperature on the Rate of Reaction 49
3.5.3.5. Product (MTBE) Inhibition Experiment 49
CHAPTER 4 RESULTS AND DISCUSSION 51
4.1. SYNTHESIS AND PRETREATMENT OF MFI ZEOLITES 51
4.1.1. Synthesis of MFI Zeolites 51
4.1.2. Zeolite Pretreatment (Calcination and Ion-Exchange) 51
4.2. ISOMORPHOUS SUBSTITUTION OF SILICON IN MFI ZEOLITES 52
4.3. CHARACTERIZATION OF MFI ZEOLITES 52
4.3.1. X-Ray Diffraction 52
4.3.2. Fourier Transform Infrared Spectroscopy 56
4.3.3. Thermal Analysis 59
4.3.4. Scanning Electron Microscopy 66
4.3.5. Elemental Analysis 66
4.3.6. Surface Area and Pore Structure Determination 72
4.4. CATALYTIC EVALUATION OF MFI ZEOLITES 73
4.4.1. Synthesized Aluminosilicate MFI Zeolites 73
4.4.2. Isomorphously Substituted MFI Zeolites 75
4.5. DETERMINATION OF INTRINSIC KINETICS 79
4.5.1. Optimization of Reaction Variables 79
4.5.1.1. Effect of Stirring Speed on the Rate of Reaction 79
4.5.1.2. Effect of Catalyst Amount on the Rate of Reaction 79
4.5.1.3. Effect of MTBE addition on Product Formation 79
4.5.2. Determination of Order of Reaction using Initial Rate Method. 85
4.5.2.1 Determination of Order of Reaction for Isobutene 86
4.5.2.2. Determination of Order of Reaction for Methanol 86
4.5.3. Effect of Temperature on the Rate of Reaction 87
4.5.4. Kinetic Modelling of the Reaction 93
CHAPTER 5 CONCLUSIONS AND RECOMMENDATIONS 104
5.1. CONCLUSIONS 104
5.2. RECOMMENDATIONS 106
CHAPTER 6 REFERENCES 107
APPENDICES 119
APPENDIX A X-RAY DIFFRACTION PATTERNS 120
APPENDIX B FT-IR SPECTRA 124
APPENDIX C THERMOGRAMS 129
APPENDIX D SCANNING ELECTRON MICROGRAPHS 132
APPENDIX E METHOD OF REACTION PRODUCT ANALYSIS 136

APPENDIX F DERIVATION OF THE MODEL EQUATIONS 138
APPENDIX G PROPERTIES OF MTBE, METHANOL AND ISOBUTENE .. 142
APPENDIX H KINETIC REACTION STUDY DATA 146
H1. Effect of stirring speed on the rate of reaction 146
H2. Effect of amount of catalyst on the rate of reaction 148
H3. Effect of MTBE in the reaction mixture on the rate of reaction .. 150
H4. Effect of reaction temperature on the rate of reaction 152
APPENDIX I PARAMETER ESTIMATION RESULTS 156
I1. Rideal-Eley mechanism in which methanol (reactant A) is adsorbed and reacts with isobutene (reactant B) in solution to produce MTBE and surface reaction is the rate controlling step of the reaction (ks is the surface reaction rate constant). 156
I2. Rideal-Eley mechanism in which isobutene (reactant B) is adsorbed and reacts with methanol (reactant A) in solution to produce MTBE and surface reaction is the rate controlling step of the reaction (ks is the surface reaction rate constant). 157
I3. Langmuir-Hinshelwood mechanism in which both methanol (reactant A) and isobutene (reactant B) are adsorbed on separate sites and react to produce MTBE and surface reaction is the rate controlling step of the reaction (ks is the surface reaction rate constant) 158
I4. Langmuir-Hinshelwood mechanism in which adsorption of methanol (reactant A) is the rate controlling step of the reaction (K_a is the adsorption rate constant) 159
I5. Langmuir-Hinshelwood mechanism in which desorption of MTBE (reactant C) is the rate controlling step of the reaction (K_d is the desorption rate constant) 160

LIST OF FIGURES

Figure	Title	Page
Figure 2.1.	Mechanism of ZSM-5 structure synthesis. (a) double 5-membered rings, (b) dimeric unit of 5-membered ring, (c) chain layer or pentasil layer, (d) basic unit or seed for ZSM-5 structure, (e) sheet projection of ZSM-5 structure showing the chain building units, (f) hollow tube representation of ZSM-5 structure, and (g) 10-membered rings showing straight and sinusoidal channels.	7
Figure 2.2.	Molecular mechanism for the MTBE synthesis. (a) methanol adsorption on one site, (b) isobutene adsorption on two sites, (c) MTBE adsorption on two sites, and (d) surface reaction through a concerted mechanism.	24
Figure 3.1.	Schematic of the autoclave used for rapid crystallization of MFI zeolites.	26
Figure 3.2.	Scheme used for the synthesis of MFI zeolites.	28
Figure 3.3.	Schematic of the packed-bed reaction system used for catalytic evaluation of MFI zeolite catalysts.	39
Figure 3.4.	Schematic of the batch reaction system used in the kinetic study.	44
Figure 3.5.	Schematic of the isobutene measuring and feed tube.	46
Figure 4.1.	X-ray powder diffraction pattern of (a) ZCIC-10 zeolite compared with (b) standard MFI zeolite.	53
Figure 4.2.	FT-IR spectra of zeolite having Si/Al molar ratio of 10 in its different forms. (a) as-synthesized(ZAS-10) (b) calcined(ZC-10) (c) ion-exchanged with aqueous ammonium nitrate solution(ZCI-10) and (d) calcined after ion-exchanging(ZCIC-10).	57
Figure 4.3.	FT-IR spectra of (a) MZ-25 zeolite and (b) aluminum fluoride-modified MZ-25 zeolite.	60
Figure 4.4.	Thermogram of ZAS-10 zeolite.	61
Figure 4.5.	Water and TPAOH contents as a function of Si/Al molar ratio of the as-synthesized zeolites.	63
Figure 4.6.	Thermograms of (a) B-MFI zeolite and (b) Ga-MFI zeolite.	64
Figure 4.7.	Thermograms of (a) MZ-25 zeolite and (b) aluminum fluoride modified MZ-25 zeolite.	65
Figure 4.8.	Scanning electron micrograph of ZCIC-10 zeolite. (a) at lower magnification and (b) at higher magnification.	67
Figure 4.9.	Surface area as a function of Si/Al molar ratio of the synthesized	

zeolites..... 73

Figure 4.10. MTBE produced as a function of reaction temperature..... 75

Figure 4.11. MTBE produced as a function of Si/Al molar ratio of the zeolites..... 75

Figure 4.12. Plot of MTBE concentration as a function of reaction time at different stirring speed..... 81

Figure 4.13. Plot of Initial rate as a function of stirring speed..... 81

Figure 4.14. Plot of rate of reaction as a function of amount of catalyst. The amount of isobutene was 119 grams (2.13 moles)..... 82

Figure 4.15. Plot of rate of reaction as a function of amount of catalyst. The amount of isobutene was 200 grams (3.58 moles)..... 82

Figure 4.16. Plot of MTBE concentration as a function of reaction time at 343 K reaction temperature..... 83

Figure 4.17. Plot of MTBE concentration as a function of reaction time at 353 K reaction temperature..... 83

Figure 4.18. Plot of MTBE concentration as a function of reaction time at 363 K reaction temperature..... 84

Figure 4.19. Plot of MTBE concentration as a function of reaction time at 373 K reaction temperature..... 84

Figure 4.20. Plot of initial rate as a function of initial isobutene concentration at 343-373 K..... 88

Figure 4.21. Plot of initial rate as a function of initial methanol concentration at 343-373 K..... 89

Figure 4.22. Plot of concentration of methanol, isobutene and MTBE in the reaction mixture as a function of reaction time at 343 K..... 89

Figure 4.23. Plot of concentration of methanol, isobutene and MTBE in the reaction mixture as a function of reaction time at 353 K..... 90

Figure 4.24. Plot of concentration of methanol, isobutene and MTBE in the reaction mixture as a function of reaction time at 363 K..... 90

Figure 4.25. Plot of concentration of methanol, isobutene and MTBE in the reaction mixture as a function of reaction time at 373 K..... 91

Figure 4.26. Plot of isobutene conversion as a function of reaction time in the temperature range 343 to 373 K..... 91

Figure 4.27. Plot of initial rate of reaction as a function of temperature in the range 343 to 373 K..... 92

Figure 4.28. Plot of thermodynamic equilibrium constant as a function of reaction temperature..... 92

Figure 4.29. Arrhenius plot for k_S 101

Figure 4.30. van't Hoff plot for K_A 101

Figure 4.31. van't Hoff plot for K_B 102

Figure 4.32. van't Hoff plot for K_C 102

Figure 4.33. Plot of rate of reaction as a function of temperature on a log-log scale. 103

Figure A1. X-ray powder diffraction pattern of ZCIC-15 zeolite. 120

Figure A2. X-ray powder diffraction pattern of ZCIC-20 zeolite. 120

Figure A3. X-ray powder diffraction pattern of ZCIC-25 zeolite. 121

Figure A4. X-ray powder diffraction pattern of ZCIC-50 zeolite. 121

Figure A5. X-ray powder diffraction pattern of ZCIC-75 zeolite. 122

Figure A6. X-ray powder diffraction pattern of ZCIC-100 zeolite. 122

Figure A7. X-ray powder diffraction pattern of B-MFI zeolite. 123

Figure A8. X-ray powder diffraction pattern of Ga-MFI zeolite. 123

Figure B1. FT-IR spectrum of ZCIC-15 zeolite 124

Figure B2. FT-IR spectrum of ZCIC-20 zeolite 124

Figure B3. FT-IR spectrum of ZCIC-25 zeolite 125

Figure B4. FT-IR spectrum of ZCIC-50 zeolite 125

Figure B5. FT-IR spectrum of ZCIC-75 zeolite 126

Figure B6. FT-IR spectrum of ZCIC-100 zeolite 126

Figure B7. FT-IR spectrum of ZAS-10 zeolite calcined at 500 °C for 5 hours. 127

Figure B8. FT-IR spectrum of ZAS-10 zeolite calcined at 600 °C for 3 hours. 127

Figure B9. FT-IR spectrum of B-MFI zeolite. 128

Figure B10. FT-IR spectrum of Ga-MFI zeolite. 128

Figure C1. Thermogram of ZCIC-15 zeolite. 129

Figure C2. Thermogram of ZCIC-20 zeolite. 129

Figure C3. Thermogram of ZCIC-25 zeolite. 130

Figure C4. Thermogram of ZCIC-50 zeolite. 130

Figure C5. Thermogram of ZCIC-75 zeolite. 131

Figure C6. Thermogram of ZCIC-100 zeolite. 131

Figure D1. Scanning electron micrograph of ZCIC-15 zeolite. 132

Figure D2. Scanning electron micrograph of ZCIC-20 zeolite. 132

Figure D3. Scanning electron micrograph of ZCIC-25 zeolite. 133

Figure D4. Scanning electron micrograph of ZCIC-50 zeolite. 133

Figure D5. Scanning electron micrograph of ZCIC-75 zeolite. 134

Figure D6. Scanning electron micrograph of ZCIC-100 zeolite..... 134

Figure D7. Scanning electron micrograph of B-MFI zeolite..... 135

Figure D8. Scanning electron micrograph of Ga-MFI zeolite..... 135

Figure G1. Vapor pressure of MTBE as a function of temperature..... 144

Figure G2. Vapor pressure of methanol as a function of temperature..... 145

Figure G3. Vapor pressure of isobutene as a function of temperature. 145

LIST OF TABLES

Table	Title	Page
Table 2.1.	Kinetic models used for Rideal-Eley and Langmuir-Hinshelwood mechanisms	23
Table 3.1.	Detailed synthesis and post-synthesis parameters of MFI zeolite.	29
Table 3.2.	Hydrothermal treatment conditions of MZ-25 zeolite with aqueous solutions containing ammonium fluoride and boric acid or gallium nitrate.	33
Table 3.3.	Hydrothermal treatment of MZ-25 with ammonium fluoride at 383 K for 18 hours, followed by reaction with sodium tetraborate	33
Table 3.4.	Gas chromatographic specifications and operating conditions.	42
Table 3.5.	Reaction conditions used for optimization of reaction variables for determining intrinsic kinetics of the reaction.	48
Table 3.6.	Reaction conditions used to determine the order of reaction for isobutene and methanol.	50
Table 4.1.	X-ray diffraction data of synthesized zeolites compared with data from a standard MFI zeolite.	54
Table 4.1.	X-ray diffraction data of synthesized zeolites compared with data from a standard MFI zeolite(continued).	55
Table 4.2.	FT-IR data obtained for as-synthesized zeolites in the range 1500 and 400 cm^{-1}.	58
Table 4.3.	FT-IR absorbance data of absorption bands A and B obtained for as-synthesized zeolites.	58
Table 4.4.	Percent weight loss results obtained for as-synthesized zeolites using thermal analysis.	63
Table 4.5.	Si/Al molar ratio of the gel prepared for the synthesis of zeolites. The weight of sodium metasilicate pentahydrate in the gel was 100 grams (0.471 moles of silicon).	66
Table 4.6.	Elemental analysis and unit cell composition of as-synthesized zeolites	68
Table 4.7.	Elemental analysis and unit cell composition of calcined and ion-exchanged zeolites	69
Table 4.8.	Elemental composition and molar ratios of isomorphously boron substituted zeolites.	70

Table 4.9. Elemental composition and molar ratios of isomorphously gallium substituted zeolites. 71

Table 4.10. Elemental composition and molar ratios of aluminum fluoride treated MFI zeolites with parent zeolites 72

Table 4.11. Surface area and pore structure characterization results of calcined ion-exchanged calcined (ZCIC) zeolites. 73

Table 4.12. Catalytic evaluation results obtained for zeolites in a packed-bed reaction system. The reaction conditions were; catalyst weight = 3.5 g, isobutene flow = 11.6 x 10^{-2} mol h^{-1} (6.51 g h^{-1}), methanol flow = 23.4 x 10^{-2} mol h^{-1} (7.49 g h^{-1}), total flow = 35.0 x 10^{-2} mol h^{-1} (14.0 g h^{-1}), WHSV = 4.0 and methanol -to-isobutene molar ratio = 2.0. 74

Table 4.13. Catalytic evaluation results of the synthesized and isomorphously substituted zeolites at 353 K reaction temperature. 78

Table 4.14. The initial rate and isobutene concentration data at 343-373 K. The concentration of methanol was 28.3 x 10^{-2} mol g^{-1} for all reaction runs. 86

Table 4.15 The initial rate and methanol concentration data at 343-373 K. The isobutene in the reaction mixture were 15 moles and the amount of catalyst was 1.5 grams. 87

Table 4.16. Results of parameter estimation for five model equations using the order of reactions a=1, b=1 and c=2.5. $\sqrt{\Sigma r^2}$ represents the square root of the sum of the squares of the residuals. 97

Table 4.17. A comparison of estimated parameters obtained in this study with those determined by other investigators. 98

Table 4.18. A comparison of activation energy obtained for MTBE synthesis in this study with those determined by other investigators. 99

Table G1. Physical, chemical and thermal properties of MTBE. 142

Table G2. Physical, chemical and thermal properties of methanol. 143

Table G3. Physical, chemical and thermal properties of isobutene. 144

NOMENCLATURE

$-r_A$	Rate of disappearance of methanol or rate of reaction
a	Order of reaction of methanol
Å	Angstrom
Al	Aluminum
$[Al(OH)_4]^-$	Aluminum hydroxide anion
$Al_2(SO_4)_3 \cdot 16H_2O$	Aluminum sulfate hexadecahydrate
Al_2O_3	Aluminum oxide
ASTM	American Society for Testing and Materials
b	Order of reaction of isobutene
BET	Brunauer, Emmett, and Teller
c	Order of reaction of MTBE
C_2H_4	Ethylene
C_3H_6	Propylene
C_4H_8	Butene
C_A	Concentration of methanol, mol g^{-1} of catalyst
C_B	Concentration of isobutene, mol g^{-1} of catalyst
C_C	Concentration of MTBE, mol g^{-1} of catalyst
$(CH_3)_2C=CH_2$	Isobutene
$(CH_3)_2CH\text{-}CH_3$	Isobutane
$(CH_3)_3C\text{-}O\text{-}CH_3$	MTBE
$(CH_3)_3C\text{-}OH$	Tertiary butyl alcohol (TBA)
$CH_3\text{-}O\text{-}CH_3$	Dimethyl ether (DME)
$CH_3\text{-}OH$	Methanol
CH_4	Methane
CO	Carbon monoxide
CO_2	Carbon dioxide
$[(CH_3)_2C=CH_2]_2$	Diisobutene
cP	Centipoise
cSt	Centistoke
DTA	Differential thermal analysis
DTG	Differential thermogravimetry
DVB	Divinyl benzene
E	Activation Energy
EPA	Environmental protection agency
ETBE	Ethyl tertiary butyl ether
FID	Flame ionization detector
FT-IR	Fourier transform infrared spectroscopy
GC	Gas chromatography
H_2	Hydrogen

H_2O	Water
H_2SO_4	Sulfuric acid
H_3PO_4	Phosphoric acid
He	Helium
HPA	Heteropoly acid
HPLC	High performance liquid chromatography
HSZ	High-silica zeolite
IB	Isobutene (B)
ICP	Inductively coupled plasma
JCPDS	Joint Committee of Powder Diffraction Data Service
K	Kelvin
K_A	Adsorption equilibrium constant for methanol
K_{Ao}	Preexponential factor for K_A
K_B	Adsorption equilibrium constant for isobutene
K_{Bo}	Preexponential factor for K_B
K_C	Adsorption equilibrium constant for MTBE
K_{Co}	Preexponential factor for K_C
K_e	Thermodynamic equilibrium constant
k_s	Surface reaction rate constant
K_{so}	Preexponential factor
MAS NMR	Magic angle spinning nuclear magnetic resonance
MeOH	Methanol (A)
MFI	A structure type code for zeolites having similar topology
MON	Motor octane number
MS	Mass spectrometry
MTBE	Methyl tertiary butyl ether (C)
MZ-25	A commercial MFI zeolite having a Si/Al molar ratio of 25
$Na_2SiO_3 \cdot 5H_2O$	Sodium metasilicate pentahydrate
NaCl	Sodium chloride
NaOH	Sodium hydroxide
Nb_2O_5	Niobium oxide
NH_3	Ammonia
NH_4NO_3	Ammonium nitrate
o.d.	Outer diameter
O_2	Oxygen
ppm	Parts per million
R	Gas constant, 8.314 J mol^{-1} K^{-1}
RON	Research octane number
SAXS	Small angle X-ray scattering
SBA	Secondary butyl alcohol
SEM	Scanning electron microscopy

Si	Silicon
Si/Al	Silicon-to-aluminum molar ratio
SiF_4	Silicon tetrafluoride
$[SO_3H]^+$	Sulfonic acid group
T	Temperature (Kelvin)
TAEE	Tertiary amyl ethyl ether
TAME	Tertiary amyl methyl ether
TBA	Tertiary butyl alcohol
TCD	Thermal conductivity detector
TFA	Trifluoromethane sulfonic acid
TG	Thermogravimetry
$[TPA]^+$	Tetrapropyl ammonium cation
TPA•Br	Tetrapropyl ammonium bromide
TPA•OH	Tetrapropyl ammonium hydroxide
TPD	Temperature-programmed desorption
WHSV	Weight hourly space velocity
XPS	X-ray photon spectroscopy
XRD	X-ray diffraction
ZAS	As-synthesized form of zeolite
ZC	Calcined form of zeolite
ZCI	Calcined ion-exchanged form of zeolite
ZCIC	Calcined ion-exchanged calcined form of zeolite
ZCIC-10	Synthesized MFI synthesized zeolite having Si/Al molar ratio of 10
ZCIC-15	Synthesized MFI synthesized zeolite having Si/Al molar ratio of 15
ZCIC-20	Synthesized MFI synthesized zeolite having Si/Al molar ratio of 20
ZCIC-25	Synthesized MFI synthesized zeolite having Si/Al molar ratio of 25
ZCIC-50	Synthesized MFI synthesized zeolite having Si/Al molar ratio of 50
ZCIC-75	Synthesized MFI synthesized zeolite having Si/Al molar ratio of 75
ZCIC-100	Synthesized MFI synthesized zeolite having Si/Al molar ratio of 100
ZSM-5	MFI type zeolite
$[AlO_4]^{5-}$	Aluminate
$[SiO_4]^{4-}$	Silicate
ΔH_A	Heat of adsorption of methanol, J mol^{-1}
ΔH_B	Heat of adsorption of isobutene, J mol^{-1}
ΔH_C	Heat of adsorption of MTBE, J mol^{-1}

CHAPTER 1 INTRODUCTION

Alkyl lead compounds have been used in gasoline for decades as octane booster additives. The United States has now imposed a complete ban on the use of alkyl lead compounds in gasoline, and European and Asian countries are following the US lead in this regard. The use of alkyl lead compounds is being discouraged worldwide because the exhaust emissions from vehicles operating on leaded gasoline contain lead particulates which cause serious health hazards [New Scientist, 1982]. Consequently, other additives are needed to replace alkyl lead compounds. A number of oxygenates are currently being blended with gasoline to produce lead free high octane gasoline. These include alcohols, namely methanol, ethanol, tertiary butyl alcohol (TBA), and ethers such as methyl tertiary butyl ether (MTBE), ethyl tertiary butyl ether (ETBE), tertiary amyl methyl ether (TAME), tertiary amyl ethyl ether (TAEE) and diisopropyl ether (DIPE). Among these, MTBE has been found to be one of the best choices because of economics, performance and compatibility and it is being blended with gasoline up to 15 volume percent [Csikos, et al., 1980]. MTBE has shown very good performance especially in the boiling range where gasoline typically shows its lowest antiknock characteristics [Gupta and Prakesh, 1980]. The addition of MTBE not only increases the octane number but also reduces the concentration of carbon monoxide and hydrocarbons in the exhaust of vehicles. Contrary to leaded gasoline, vehicles operating on MTBE-gasoline blends can be installed with catalytic converters to further reduce the concentration of toxic constituents in exhaust emissions.

The commercial production of MTBE is carried out in the liquid phase below 373 K by the reaction of methanol and isobutene over sulfonated ion-exchange resins such as Amberlyst 15. In this reaction, diisobutene and TBA are the by-products formed by dimerization of isobutene, and reaction of water with isobutene, respectively. The amount of diisobutene formed increases with rise in temperature. TBA formation becomes significant with the presence of moisture. Even though the performance of Amberlyst 15 is good, it has several drawbacks such as thermal instability, acid leaching from the resin surface and high sensitivity to the methanol-to-isobutene ratio.

The application of zeolite catalysts for MTBE production has the potential of overcoming the temperature limitations of the existing commercial resin catalyst. Zeolite catalysts have improved stability and activity. They are also more selective towards MTBE formation because of their restricted pore size, and thus they are more environmentally favorable.

1.2. ZEOLITE STRUCTURE AND ACIDITY

Zeolites are highly crystalline aluminosilicates consisting of three-dimensional frameworks of SiO_4 and AlO_4 tetrahedra, each of which contains a silicon or an aluminum atom in the center. The oxygen atoms are shared between adjoining tetrahedra, which can be present

in various ratios and linked in a variety of ways. Zeolites may be represented chemically in terms of a mixed oxide formulation by the following empirical formula:

$$M_{2/n}O{\bullet}xAl_2O_3{\bullet}ySiO_2{\bullet}zH_2O$$

where M represents the exchangeable cation, generally from group I or II elements, n indicates the valence of the cation, x is equal or greater than 2 because Al^{3+} ions do not occupy adjacent tetrahedral sites, y is 2 to 10, and z represents the number of water molecules located in the channels and cavities. Zeolites may also be represented in terms of a crystallographic unit cell, the smallest repeat unit of the structure, by the following structural formula:

$$M_{x/n}[(AlO_2)_x(SiO_2)_y]{\bullet}zH_2O$$

The bracketed term is the crystallographic unit cell. The metal cation of valance n is present to produce electrical neutrality, since for each aluminum tetrahedron in the lattice there is a net charge of -1. The values of x and y represent the total number of AlO_4 and SiO_4 tetrahedra per unit cell. Zeolites possess a number of catalytically favorable properties such as well-defined crystalline structure, uniform pores, high surface area, good thermal stability, a wide range of acidity, and shape selectivity. The channels and cavities in zeolites have various diameters depending on the framework structure formed by the SiO_4 and the AlO_4 tetrahedra. The pores or channel openings in zeolite range from 3 to 8 Å [Szostak, 1989]. However, the catalytically important classes of zeolites, have pore diameters defined by 8, 10 and 12-membered rings of oxygen atoms. Shape selectivity is the result of intimate interactions of dimension, geometry and tortuosity of zeolite channels with the size, shape and configuration of the molecules taking part in a reaction. Depending on the physical and chemical properties of reactants, intermediate or products, one can distinguish among three types of shape selectivity: reactant selectivity, product selectivity and transition state molecular shape selectivity. ZSM-5 zeolite in its sodium form has the following general formula.

$$Na_n{\bullet}Al_nSi_{96-n}{\bullet}O_{192}{\bullet}16H_2O \quad \text{with } n<27$$

ZSM-5 contains a zigzag channel system intersecting a straight 10-membered ring of oxygen atoms to produce the three-dimensional pore system having pore size 5.4 x 5.6 and 5.1 x 5.5 Å.

The most important commercial application of acid catalysis by zeolites is the transformation of hydrocarbons in petroleum refining and petrochemical processes by catalytic cracking, isomerization, oligomerization and etherification. The acidity of a zeolite is due to the presence of protons which are required to maintain electrical neutrality in the structure. The strength of the acidic sites is related to the zeolite structure type, T-O-T bond angles and lengths where T represent an atom in the tetrahedra TO_4 unit, and

crystal resonance energy. Large T-O-T bond angles, as found in ZSM-5 zeolites, enhance the electronegativity of oxygen atoms which results in a relatively high positive charge on hydrogen and thus stronger protic acidity. The number of acid sites is dependent upon the presence of aluminum or other trivalent cations in the framework. The number of these trivalent cations can be varied and adjusted to specific needs, either by synthesis or by post-synthesis modification. The Si/Al molar ratio is, therefore, one of the most frequently used parameters to classify acidity of zeolites.

1.3. OBJECTIVES OF THE STUDY

The main objective of this study is the synthesis, modification, characterization and catalytic evaluation of MFI zeolites for MTBE synthesis, and the determination of intrinsic kinetics for this reaction. MFI is the structure type code allocated (by the Structure Commission of the International Zeolite Association) to a number of zeolites having similar topology, such as ZSM-5 and silicalite. The main tasks of this study were:

1. Synthesis of MFI type zeolites using silicon and aluminum source compounds.

2. Isomorphous substitution of MFI zeolites both at synthesis level and post synthesis modification.

3. Characterization of MFI synthesized and isomorphously substituted zeolites for their crystallinity, structure type, thermal characteristics, morphology, elemental composition, surface area and pore size determination.

4. Catalytic evaluation of the synthesized and isomorphously substituted zeolites for the reaction of methanol and isobutene to produce MTBE.

5. Determination of intrinsic kinetics of the reaction of methanol and isobutene to produce MTBE in the absence of intraparticle diffusion and interparticle mass transfer.

CHAPTER 2 LITERATURE REVIEW

2.1. SYNTHESIS AND PRETREATMENT OF MFI ZEOLITES

2.1.1. Synthesis of MFI Zeolites

Systematic studies in zeolite synthesis began in Barrer's laboratory in 1938, where the replication of natural zeolites was achieved as well as the hydrothermal synthesis of new forms of zeolites [Barrer, 1982]. Hydrothermal synthesis of zeolites follows the laws of thermodynamics and hence proceeds in a direction corresponding to a decrease in free energy of the system [Jiru, 1982]. The precursor hydrogel prepared from silica and alumina sources is always supersaturated with respect to its chemical constituents under hydrothermal conditions. The supersaturated gel undergoes nucleation and converts into a metastable zeolite phase that further transforms to a more stable crystalline phase.

The main variables in the synthesis of zeolite types are pH, temperature, reaction time, source of silica, silica-to-alumina ratio of the gel and type of template if present. The crystallization of a particular type of zeolite depends strongly upon the pH of the gel. A pH of 10 is considered best for MFI type zeolite synthesis. Kulkarni et al., [1989] showed that a pH of 6.7 was the highest acidity limit for the crystallization of MFI type zeolites but their formation required at least thirty days. A minimum period of three days has been reported for the isothermal synthesis of MFI structures in the pH range of 9 to 11 [Szostak, 1989].

The crystallization of a particular zeolite structure from a matrix system and the rate of crystallization depends strongly upon the silica-to-alumina ratio of the starting gel mixture [Araya and Lowe, 1985]. The rate of crystallization generally decreases with an increase in the aluminum content of the gel. This is because the apparent activation energy of nucleation and crystal growth are higher in the presence of aluminum in the gel [Erdem and Sand, 1979]. Argauer and Landolt [1972] patented the preparation of crystalline ZSM-5 formed at a silica-to-alumina ratio of 15 to infinity.

The mineralizing property of water is the basis of hydrothermal chemistry, and in zeolite synthesis it is an essential guest species that stabilizes the host lattice. In hydrothermal systems, water promotes mixing, transport of materials, and hence facilitates nucleation as well as crystal growth. Water stabilizes zeolite crystals by filling the cavities [Barrer and Cole, 1970]. Suzuki et al., [1987] found that the average diameter of the MFI zeolite crystallites increases as the water content of the reaction mixture is increased.

The temperature at which a zeolite can be synthesized depends upon the pore volume. For example, zeolites having small pore volume are synthesized at higher temperatures while large pore zeolites are crystallized at lower temperatures. A maximum temperature of 623 K has been suggested for hydrothermal synthesis [Mostowicz and Sand, 1982]. This illustrates that there is a direct relationship between pore volume and synthesis

temperature. The higher the synthesis temperature, the smaller the water content and the lower the intracrystalline porosity of the zeolite. MFI type zeolites are synthesized in the temperature range 398 to 473 K. If the temperature of the reaction mixture is near the upper limit, the crystallization time is minimized.

Alkalinity is another important parameter in zeolite synthesis as it controls the rate of crystallization. An increasing $[OH]^-$ concentration generally decreases nucleation time and accelerates crystal growth [Barrer, 1981]. High alkalinity causes a high degree of supersaturation with silicate and aluminate, and the formation of a large number of nuclei. The aluminum hydroxide anion $[Al(OH)_4]^-$ has been observed to be the predominant aluminum species at higher pH values [Derouane et al., 1982]. The hydroxide concentration can also induce a change in the crystalline phase and composition of the zeolite produced. Inorganic or organic cations not only influence the structure of the crystalline zeolite but they also influence the morphology and crystal size of the material. The presence of cations in the reaction mixture also minimizes the crystallization time and produces a more stable zeolite phase. It has been suggested that hydrated sodium ions function as a template in the synthesis of ZSM-5 [Nastro et al., 1985].

The function of the organic additive such as tetrapropyl ammonium bromide can be visualized as an entity around which the components assemble and the zeolite structure grows with certain pore structures or subunits being stabilized. The organic cation organizes oxide tetrahedra into a particular geometric topology around itself and thus provides the initial pattern for a particular structural type at the nucleation stage [Derouane et al., 1981]. The tetrapropyl ammonium cation $[TPA]^+$ has been used to promote ZSM-5 structure formation. Crystallographic examination of the $[TPA]^+$ in the MFI structure has indicated a channel-directing role for this cation, as the trapped amine is oriented in the channel intersections with the propyl groups acting as tentacles extended into the straight and sinusoidal channels of the zeolite structure [Price et al., 1982]. ZSM-5 has also been synthesized without a template [Grose and Flanigen, 1981; Schwieger et al., 1989] but it required more time for crystallization. It has been suggested that organic additives act as surfactants and help in higher mobility of the fragments forming the crystal lattice as well as reversibility of polymerization-depolymerization processes. This assures more homogeneous distribution of the aluminum and silicon atoms in the zeolite structure compared to the zeolites obtained without organic additives [Golubovskaya et al., 1985].

The source of silica has an effect on the rate of crystallization. Crystallization of MFI using either Ludox (colloidal silica) or silicate produced rapid nucleation of the desired structure after five hours [Mostowicz and Sand, 1982]. The use of precipitated silica resulted in a longer period of induction before crystals were observed. Barrer et al., [1959] have proposed that nucleation is a result of polymerization of various aluminate, silicate and possibly more complex ions in the liquid phase, the ions being continuously supplied by the dissolution of the solid hydrogel material. Flanigen and Breck [1960] showed that

crystallization occurs from the solid-gel phase. The induction period was postulated to be a time during which the nuclei formed in the solid phase growing to a definite size. Derouane et al., [1981, 1982] suggested that both the liquid phase ion transformation mechanism, and the solid hydrogel phase transformation mechanism, are important in studying the synthesis of MFI zeolite.

Santen et al., [1986] have proposed a synthesis mechanism in which, ZSM-5 zeolite forms through a ring opening and polymerization of double 5-ring silicate anions, which they observed to present in silicate solutions. These double 5-ring structure combines to produce a dimeric unit that further grows into a chain layer called pentasil layer. Two of these layers combines to produce the basic unit or seed for the ZSM-5 structure. This mechanism is given in Figure 2.1.

2.1.2. Pretreatment of Zeolites (Calcination and Ion-Exchange)

Calcination of zeolites is needed to remove both organic template and moisture after the synthesis, and to deammoniate the zeolite after ion-exchange with an ammonium salt. Templates are present within the pores of the zeolite. Due to its porous nature, the zeolite also adsorbs moisture when exposed to the atmosphere. In calcination, the zeolite sample is heated in a furnace, in the presence of air, at a controlled temperature. The process of calcination clears the zeolite pores so that exchange of ions can take place easily and completely. The calcination of ZSM-5 zeolite is usually carried out at 823 to 873 K but it can also be accomplished at lower temperature under vacuum [Jacobs and Ballmoos, 1982]. Higher temperatures may result in dehydroxylation (loss of structural water from the lattice), which is accompanied by a small decrease in crystallinity and some dealumination [Nayak and Choudhary, 1982].

Ion-exchange within the zeolites involves substitution of one type of cation present in the structure with another such as protons. The number of exchanges and amount of exchange solution required depends upon the quantities of sodium present in the zeolite and the concentration of the ion-exchange solution. Proton exchange can be carried out directly using an aqueous dilute acid solution such as hydrochloric acid. Alternatively an aqueous solution of an ammonium salt such as ammonium nitrate will result in the introduction of $[NH_4]^+$ ions. Concentrated acid solutions may cause dealumination which results in entire destruction of the zeolite framework. It has been observed that one molar aqueous ammonium nitrate solution provides optimum ion-exchanging conditions for the cations without damaging the zeolite framework [Inui et al., 1984].

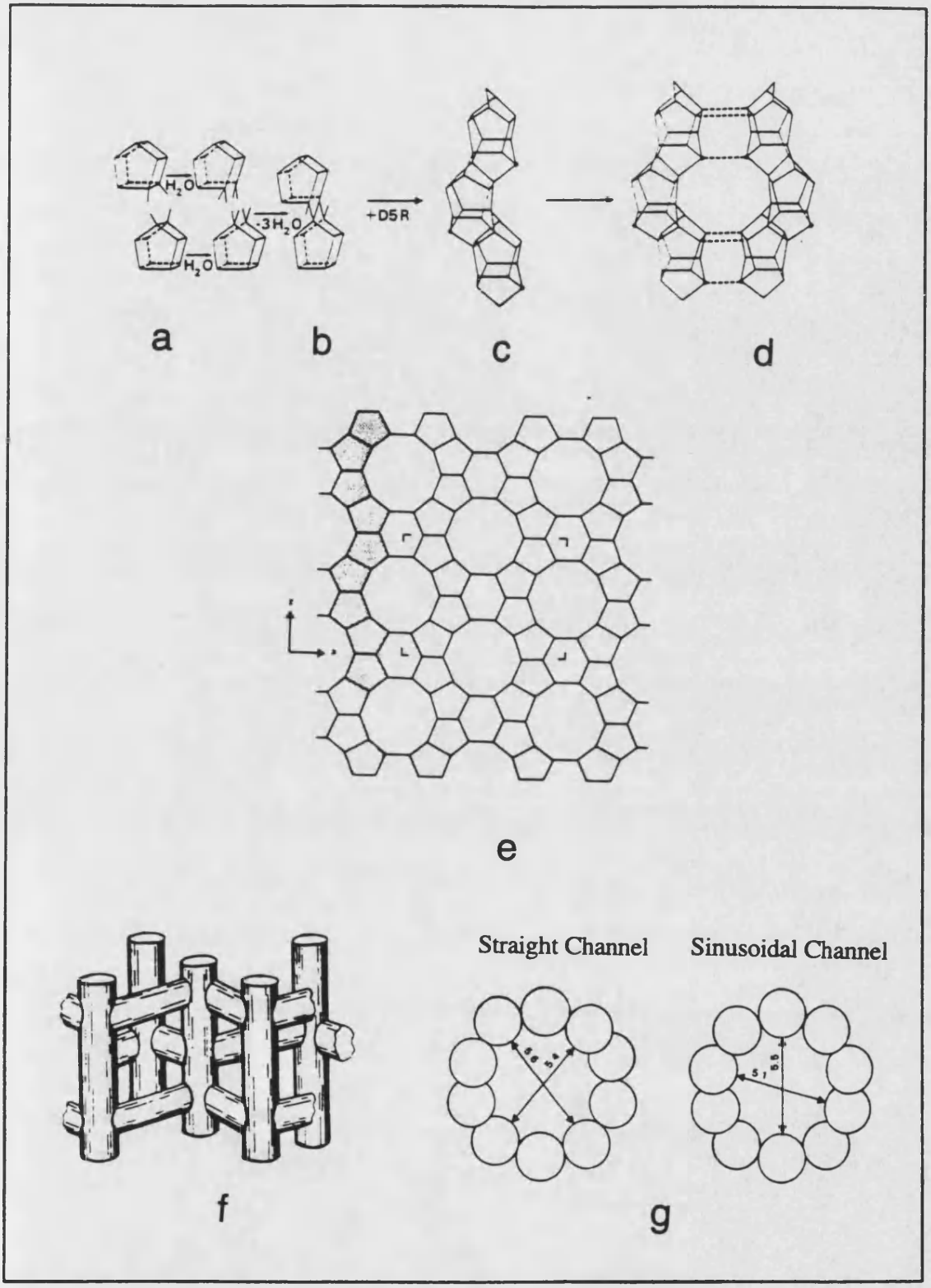

Figure 2.1. Mechanism of ZSM-5 structure synthesis. (a) double 5-membered rings, (b) dimeric unit of 5-membered ring, (c) chain layer or pentasil layer, (d) basic unit or seed for ZSM-5 structure, (e) sheet projection of ZSM-5 structure showing the chain building units, (f) hollow tube representation of ZSM-5 structure, and (g) 10-membered rings showing straight and sinusoidal channels.

After ion-exchanging with ammonium salt solution, deammoniation of the zeolite is carried out at 823 K to decompose the ammonium ion. This process releases ammonia gas and leaves protons within the zeolite structure which provide active sites for reaction.

2.2. ISOMORPHOUS SUBSTITUTION OF SILICON IN MFI ZEOLITES

Isomorphous substitution in zeolites can be achieved through two routes. 1. Incorporation of desired metal at the synthesis stage through crystallization under hydrothermal conditions, and 2. modification of existing zeolites for framework composition through post synthesis modification.

A number of researchers have reported isomorphous substitution of silicon by boron in MFI type zeolites under hydrothermal conditions [Trong et al., 1995; Axon and Klinowski, 1994; Xu et al., 1993; Datka and Kawalek, 1993; Simon et al., 1992; Cornaro and Wojceichowski, 1989; Sayed et al., 1989; Kofke et al., 1989; Datka and Piwowarska, 1989; Ratnasamy et al., 1989; Jansen et al., 1988; Bodart et al., 1986; Coudurier and Védrine, 1986; Chu and Chang, 1985; Ione et al., 1985, Howden, 1985; Chang et al., 1985; Derouane et al., 1985; Gablica et al., 1984]. Han and coworkers [1994] have reported isomorphous substitution of silicon by boron in commercial ZSM-5 zeolite. In this method, the ZSM-5 zeolite was heated at 358 K for 18 hours with a dilute aqueous solution of ammonium tetrafluoroborate (NH_4BF_4) buffered to pH 7.3 with ammonium acetate. The substituted zeolite was characterized using solid state MAS NMR technique. The reaction was believed to proceed via a metathesis pathway wherein the desired metal ion inserts into the T-atom vacancy created by the formation of soluble aluminum or silicon fluorides. A T-atom vacancy is created on removal of an atom such as Si or Al bonded tetrahedrally by oxygen atoms in a zeolite framework.

Mao et al., [1995] described a method for the removal of silicon from ZSM-5 by heating the zeolite with an aqueous solution of sodium carbonate and sodium hydroxide at 353 K. As a result, silicon was removed, the degree of crystallinity was decreased from 100 percent (parent zeolite) to 88 percent. The pore size distribution showed the presence of a certain amount of narrow pores. The healing process was promoted by a temperature programmed heating that resulted in homogeneous pore size distribution. The modified zeolite in the hydrogen form can be stabilized by inserting aluminum or another metal in the T-atom vacancies created by the leached silicon.

Isomorphous substitution of gallium into MFI type zeolites at the synthesis stage has been reported in a number of studies [Arean et al., 1996; Kosslick et al., 1995; Liu and Klinowski, 1992; Handreck et al., 1989; Meriaudeau et. al., 1989; Kucherov et al., 1989; Simmons et al., 1987; Inui et al., 1987]. Gallium has been substituted in pure silicalite using an impregnation technique in which the zeolite was mixed with an aqueous solution of gallium nitrate, the solution evaporated and the residue calcined at 773 K for 6 hours in

a flow of oxygen. MAS NMR indicated the presence of tetrahedral gallium in the zeolite framework [Lalik et al., 1992]. Others have tried substitution through impregnation [Dooley et al., 1995] or solid state exchange [Kucherov and Slinkin, 1994] but their attempts failed to introduce the desired metal into the framework.

Isomorphous substitution of silicon by aluminum into high silica ZSM-5 and B-ZSM-5 has been carried out in the presence of alumina beads under hydrothermal conditions at 423-443 K. This treatment resulted in the transportation of aluminum atoms from the beads into tetrahedral positions in the zeolite framework. The substituted zeolite was found to have increased acidity after this treatment [Clarence et al., 1985]. Aluminum fluoride has been reported to induce an increase in hydrophobicity of the zeolites, perhaps due to the removal of aluminum from the framework. These fluoride modified zeolites were observed to have a high degree of crystallinity and increased activity. This is attributed to the presence of active non-framework aluminum fluoride containing species such as $AlF_x(OH)_y$ [Fishel, 1968].

2.3. CHARACTERIZATION OF MFI ZEOLITES

Characterization of MFI zeolite samples in terms of their chemical composition, surface properties, thermal behavior, morphology and crystallinity provides a framework for understanding their performance in the reaction process. Several techniques have been used to characterize the zeolite catalysts at different levels of synthesis, post synthesis pretreatment, isomorphous substitution, and when spent after catalytic reaction studies. The characterization helps in the understanding of the relationship between the properties of a zeolite and its performance. Typical characterization techniques include X-ray diffraction, Fourier transform-infrared spectroscopy, thermal analysis, scanning electron microscopy, elemental analysis, surface area measurement, and pore size determination.

2.3.1. X-Ray Diffraction (XRD)

X-ray diffraction is a technique in which the sample in the powder form is subjected to irradiation by X-rays. The X-rays are scattered from the sample and an X-ray diffraction pattern is obtained. The information obtained from the XRD pattern of a zeolite sample includes the degree of crystallinity of the sample, the presence of a single phase or a mixture of phases, type of structure formed and an indication of new structure formation. XRD is also used to study the modification of zeolites as a result of chemical and/or thermal treatment. Identification by XRD is based on the Bragg equation giving the lattice d-spacing that acts as a fingerprint of any crystalline phase.

$$\lambda = 2\,\delta\,\mathrm{Sin}\,\theta$$

where λ = wavelength of the X-rays, δ = interplanar spacing between a family of equidistant parallel atomic planes having indices hkl, and θ = angle between both the

incident and diffracted beams and the atomic planes. The d-spacing values and the relative intensities of the diffraction peaks are recorded and compared with the strongest peak (equal to 100). The synthesized zeolite can be identified by comparing these values with known data provided by the Joint Committee of Powder Diffraction Data Service (JCPDS). X-ray diffraction provides a method of determining the purity of a synthesized zeolite sample. Purity can be estimated by comparing the peak intensities of a sample with those of a standard pure zeolite of the same composition and crystal size [Derouane et al., 1981]. The intensities of the diffraction peaks are determined mainly by the amount of the crystalline material present in the sample. XRD is also a powerful tool in examining structural defects in zeolite structures and has been used routinely to characterize boron and gallium substituted MFI zeolites [Trong et al., 1995; Simon et. al., 1992; Liu and Klinowski, 1992; Coudurier and Védrine, 1986].

2.3.2. Fourier Transform-Infrared Spectroscopy (FT-IR)

Infrared spectroscopy provides structural information in terms of chemical bonds present in zeolites. The FT-IR technique has also been applied in the determination of crystallinity of MFI zeolites. Bands in the infrared spectrum of a ZSM-5 zeolite can be classified into two groups of vibrations: (a) the internal vibrations of the framework TO_4, which are insensitive to structural variation, and (b) vibrations related to the external linkage of the TO_4 units in the structure. The internal SiO_4 tetrahedra have asymmetric stretching absorption bands around 1220 cm^{-1}, symmetric stretching modes around 668 and T-O bending modes around 450 cm^{-1}. The external linkages show absorption bands at around 542 cm^{-1} for double five-membered rings, symmetric stretching of SiO_4 tetrahedra at about 790 and asymmetric stretching at 1080 cm^{-1} [Flanigen et al., 1971]. A weak signal at around 1650 cm^{-1} has been assigned to water contained within the zeolite. Shifts in band positions in the symmetric and asymmetric stretching vibrations were observed with variations in silica-to-alumina ratios of zeolites. Wu and Kaeding [1984] assigned the absorption band at 1035 cm^{-1} to Si-O bond stretching and the band around 600 cm^{-1} to Al-O bond stretching. Attributing these bands to external vibrational modes of chainlets of tetrahedra allows one to explain their presence in all zeolites, particularly in MFI structures. Transition metal (TMe) substitution in high-silica zeolites results in an observed asymmetric vibration appearing at lower wavenumber than the Si-O-Si-(Al) vibration, because of the heavier mass of the Si-O-TMe oscillations. The relative intensities of absorption bands near 550 cm^{-1} (band A) and 450 cm^{-1} (band B) apparent in most zeolite structures have been used as a measure of crystallinity [Jacobs et al., 1981].

Infrared spectroscopy has also been used to characterize boron and gallium substituted MFI zeolites [Arean et al., 1996; Trong et al., 1995; Datka and Kawalek, 1993; Liu and Klinowski, 1992]. Szostak and Thomas [1986] concluded that the asymmetric and symmetric absorption bands which appear between 600 and 1200 cm^{-1} in zeolites can be attributed to Si-O-T vibrations. Changing the mass or charge of the T atom affects the

position of these bands. In the case of gallosilicates, the asymmetric stretching vibration was reported to shift to lower wavenumber by 20 cm^{-1} due to the presence of Si-O-Ga linkages. This was due to the increase in the mass of the T atom. In the case of boron containing ZSM-5 zeolites, the stretching vibration band is shifted towards higher wavenumber because of the reduced mass of the T atom [Kosslick et al., 1991].

2.3.3. Thermal Analysis (TG, DTA)

Catalytic reactions are normally carried out at elevated temperatures. The zeolite catalyst should therefore be thermally stable over the range of operating temperatures. Thermal analysis is carried out to study thermally induced changes which take place in the zeolite properties. Thermal analysis describes a group of techniques in which a physical property of a substance is measured as a function of temperature while the substance is subjected to an elevated temperature under controlled heating and other conditions. Characteristic parameters of a physical or chemical nature that alter under thermal treatment are measured as a function of temperature in order to provide information on the thermal behavior of the material. Thermogravimetry (TG) is a technique in which the change in mass of a substance is measured as a function of temperature. Applications best suited for TG include determination of thermal stability of materials, moisture and volatiles determinations, accelerated aging tests, and investigation of redox reactions. The technique of differential thermal analysis (DTA) determines the amount of heat evolved or absorbed and the temperature at which these changes take place within the material. The temperature difference between the substance and a reference material is measured as a function of temperature under controlled conditions. By careful analysis and interpretation of DTA and TG results, the type of reactions that occur in or on the substance during heating may be identified. Reactions that may be identified through thermal analysis include decomposition, adsorption, desorption and dehydration. Phase transformations may also be identified including fusion, melting, vaporization, sublimation, and crystalline transition. Thermogravimetry has been employed to characterize gallium substituted MFI zeolites [Liu and Klinowski, 1992].

2.3.4. Scanning Electron Microscopy (SEM)

Scanning electron microscopy (SEM) is the most versatile technique to study the morphology and particle size distribution of zeolites. In SEM, the zeolite sample in powder form is subjected to an electron beam. Signals such as secondary electrons, back scattered electrons, X-rays, and transmitted electrons are generated from the sample and provide information about the area of the sample on which the SEM picture is obtained. Size of a zeolite particle can be determined in the range of about 1 nanometer to 30 micrometers. Different forms of ZSM-5 zeolite obtained, with varying silica source and concentration in the gel, have been studied using SEM [Jansen and Wilson, 1991]. SEM has been used to determine the effect of synthesis process conditions on the crystal morphology [Sanders,

1985]. . The effect of substitution of boron and gallium in ZSM-5 have also been studied using SEM [Axon and Klinowski, 1989].

2.3.5. Elemental Analysis

Elemental analysis of a zeolite sample is required to determine its bulk composition. It is very important that the identity and quantity of all trace elements present in the zeolite and its precursors are known. They can become very significant in determining the overall zeolite composition and properties. Chemical analysis is usually performed using atomic absorption spectroscopy or inductively coupled plasma spectroscopy. Sometimes wet chemistry methods are needed for determining specific components. The elements most frequently determined in zeolite analysis are sodium, potassium, aluminum and silicon. During post synthesis modification such as ion-exchange, the determination of sodium is very important to verify the efficiency of the ion-exchanging process.

2.3.6. Surface Area and Pore Structure Determination

Catalytic reactions take place on the surface of the catalysts, and the activity of solid catalysts depends initially on their total surface area and their surface composition. The principal method of measuring the total surface area and porosity of a catalyst is by adsorption of nitrogen gas onto its surface. For determining the surface area, the amount of nitrogen adsorbed at equilibrium at its normal boiling point is measured over a range of nitrogen pressures below 1 atmosphere. The most common method of determining surface area of a solid is the one developed by Brunauer, Emmett, and Teller (BET method), in which the Langmuir adsorption isotherm is extended to multilayer adsorption [Brunauer et al., 1938]. In the Langmuir approach, the rate of evaporation is taken to be equal to the rate of condensation, and the heat of adsorption is considered independent of coverage for the first layer. For layers beyond the first layer, the rate of adsorption is considered to be proportional to the fraction of the lower layer still vacant, and the rate of desorption is proportional to the amount present in that layer. The heat of adsorption for all other layers, except the first, is taken to be equal to the heat of liquefaction of the adsorbed gas. Nitrogen is normally used for surface area measurement since it is cheap and readily available in high purity. Other gases such as krypton and argon can also be used but are expensive relative to nitrogen [Emmett and Cines, 1947].

The T-plot is an accurate tool for displaying the micropore volume of a given microporous zeolite sample [Broekhoff and Linsen, 1970]. The relative pressure (P/P_o) is proportionally related to the thickness(t) of the adsorbed nitrogen assuming the substrate is nonporous. According to IUPAC (International Union of Pure and Applied Chemistry) recommendations, pores smaller than about 2 nanometer in diameter are called micropores, those larger than 50 nanometer are macropores and the pores between 2 and 50 nanometer are termed as mesopores [Sing et al., 1985]. T-plot surface area and BET area should be

identical in the absence of micropores. The area of the nonzeolite part of a catalyst is called the matrix area of that catalyst. In a structure containing both micro and mesopores, extrapolation of a linear T-plot to t=0 yields the micropore area [Johnson, 1978]. This is the basis of the ASTM (American Society for Testing and Materials) method D-4365 used for determining the zeolite area of a catalyst which is the difference between total area and the matrix area [ASTM D-4365]. It has been proved to be a valuable method of characterizing complex mixed materials or the nonzeolite part of a catalyst such as FCC catalyst containing zeolite.

2.4. CATALYSTS USED FOR MTBE SYNTHESIS

A wide variety of acid catalysts has been used for the synthesis of MTBE from methanol and isobutene.

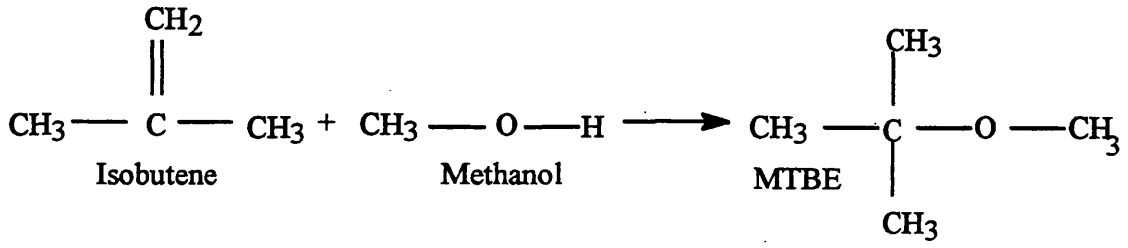

For example, heteropolytungstic or molybdic acids doped with phosphorus, silicon or boron [Izumi, 1979; Todo et al., 1979], various acidified ion-exchange resins [Ancillotti et al., 1977; Ancillotti et al., 1978; Torck et al., 1980; Stouthamer and Kwantes, 1980], acid alumina [Ancillotti et al., 1978] and sulfuric acid [Evans and Edlund, 1936]. Clays have also been used to catalyze synthesis of ethers from 1-alkenes, and the interlayer water naturally present in clays [Adams et al., 1979]. Several investigators have reported catalytic applications of zeolites for MTBE synthesis from methanol and isobutene or TBA. These zeolites include Y types, MFI types, silicalites, mordenites and their acidified and metal-substituted forms. The available literature on the synthesis of MTBE is discussed below according to the type of catalyst.

2.4.1. Sulfuric Acid

MTBE has been synthesized from methanol and TBA or isobutene in the presence of mineral acids such as sulfuric acid [Norris and Rigby, 1932]. However, the reaction was not selective for MTBE due to by-product formation mainly as a result of dehydration reactions. Using sulfuric acid, the reaction was found to be reversible and reached equilibrium [Evans and Edlund, 1936]. Among the C_4 isomers, isobutene reacted selectively with methanol in the presence of sulfuric acid and excess methanol. The excess methanol prevented the radical polymerization of unsaturated components while the homogeneous phase ensured uniform distribution of catalyst [Csikos et al., 1980; Mafki, 1980]. The drawbacks of using sulfuric acid are dehydration reactions leading to by-

products formation, difficulty in the separation of the catalyst from the reaction products and corrosion of different parts of the reaction system.

2.4.2. Clays

Clays have been used to catalyze the reaction of isobutene with methanol to produce MTBE. Using smectite exchanged with different interlamellar trivalent cations such as Fe^{3+}, Cr^{3+} or Al^{3+} at a reaction temperature of 333 K, yields of MTBE greater than 50% were obtained. A yield of 8% was achieved in the presence of monovalent or divalent cations such as Na^{+}, Cu^{2+}, Pb^{2+}, Ni^{2+}, Co^{2+} and Ca^{2+}. The catalysts were found to be very active in the presence of 1,4-dioxan as a solvent as compared to n-pentane, diethylene glycol, diethyl ether, tetrahydrofuran or tetrahydropyran. Copper-exchanged bentonite has also been used to synthesize MTBE from methanol and isobutene, and the rate of reaction was observed higher than the sulfuric acid catalyzed reaction of isobutene and methanol [Bylina et al., 1980]. Montmorillonite clay exchanged with Ti^{3+} showed an activity similar to Amberlyst 15 resin, but higher than Al^{3+} exchanged montmorillonite for the synthesis of MTBE from methanol and either isobutene or TBA. In the presence of 1,4-dioxan as solvent, the activation energy of the reaction was 44 kJ mol^{-1} for Al^{3+}-montmorillonite as compared to 25 kJ mol^{-1} for Amberlyst 15. In the absence of a solvent, the rates of reaction were considerably slower for both the clay- and resin-catalyzed reactions. The performance of the Al^{3+}-montmorillonite catalyst was increased by reducing its water content under vacuum [Adams et al., 1986]. Using trifluoromethane sulfonic acid-montmorillonite at 393 K, a molar MTBE selectivity of 77% was achieved with 68% TBA conversion. The montmorillonite clay modified with trifluoroethane sulfonic acid showed no change in catalytic activity [Knifton, 1992]. The disadvantages of using clay in the reaction of methanol and isobutene are high pore size which allow formation of by-products and thus have reduced MTBE selectivity.

2.4.3. Heteropoly Acids

Zirconium and titanium phosphates have been used as catalysts for the synthesis of MTBE from methanol and isobutene at temperatures (e.g. 443 K) required to activate their Brönsted acidic sites. Their phenylsulfonic acid derivatives show higher activity toward MTBE formation at relatively lower temperatures [Cheng et al., 1991]. Amorphous niobium phosphate and phosphoric acid treated-niobium oxide (H_3PO_4-Nb_2O_5) have been found to catalyze the reaction of TBA and methanol to form MTBE [Okazaki and Wada, 1993]. Gamma alumina and gamma alumina-doped with 1.0 wt% phosphoric acid have also been used for the reaction of methanol and TBA to produce MTBE. It was found that phosphoric acid-doped alumina calcined at 573 K was almost 100% selective for MTBE under all conditions [Aboul-Gheit et al., 1994]. Cesium salts of 12-tungstophosphoric acid ($H_3PW_{12}O_{40}$) and 12-tungstosilicic acid ($H_4SiW_{12}O_{40}$) showed moderate activities and selectivities for MTBE synthesis from methanol and TBA at 323 K. Kinetic studies showed

that three reactions take place simultaneously, namely, dehydration of TBA to form isobutene, reaction of isobutene with methanol to produce MTBE and TBA reaction with methanol to form MTBE [Matouq and Goto, 1993].

- Dehydration of TBA

$(CH_3)_3C\text{-}OH$ ----------> $(CH_3)_2C{=}CH_2 + H_2O$

- Reaction of isobutene with methanol

$(CH_3)_2C{=}CH_2 + CH_3\text{-}OH$ ----------> $(CH_3)_3C\text{-}O\text{-}CH_3$

- Reaction of TBA with methanol

$(CH_3)_3C\text{-}OH + CH_3\text{-}OH$ ----------> $(CH_3)_3C\text{-}O\text{-}CH_3 + H_2O$

It was observed that TBA dehydration is significant in the case of Amberlyst 15 resin as compared to HPA. From the viewpoint of selectivity, HPA proved to be a better catalyst than Amberlyst 15 [Matouq et al., 1994]. The heteropoly acids are oxygen-rich compounds and possess a kind of structure called keggin ion systems composed of a central atom of phosphorous or silicon connected to oxygen atoms which are surrounded by a network of molybdenum or tungsten atoms bounded by oxygen atoms. The terminal molybdenum or tungsten atoms have exchangeable protons which provide the acidity to these systems.

2.4.4. Acidic Resins

A variety of acidic resin catalysts are being used commercially. Amberlyst 15 produced by Rohm and Haas is a strongly acidic cation-exchange resin containing sulfonic acid (SO_3H^+) groups. This resin is prepared by the sulfonation of a copolymer made of polystyrene and divinyl benzene [Brockwell et al., 1991; Izqulerdo et al., 1992]. This resin has a surface area of 43 $m^2\ g^{-1}$ and a mean pore diameter of 240 Å. This resin has an acid capacity of 4.8 miliequivalent SO_3H^+ per gram of the catalyst [Rohm and Haas, 1992]. Recently, Amberlyst 35 has been introduced by Rohm and Haas which is claimed to have better activity and selectivity than Amberlyst 15 resin. This resin has a surface area of 44 $m^2\ g^{-1}$, particle size 0.4 to 1.25 mm, porosity 0.35 $cm^3\ g^{-1}$, an average pore diameter of 300 Å and acid capacity of 5.4 miliequivalent per gram of the catalyst [Rohm and Haas, 1996].

2.4.4.1. Laboratory Synthesis of MTBE

The use of Amberlyst 15 as a catalyst for the reaction of tertiary olefins and alcohols to produce ethers was first reported by Ancillotti and his coworkers [Ancillotti et al., 1977]. From the initial reaction rates, the reactivity of primary alcohols with isobutene was observed to follow the order n-butanol > n-propanol > ethanol > methanol. The results also showed a zero order dependence of rate on methanol concentration and a first order dependence on isobutene concentration. A strong dependence of rate of reaction on acid group concentration was also observed. It was found that the initial rates of the reaction between methanol with isobutene could be explained by different reaction mechanisms,

depending on the ratio of the reactants. At stoichiometric or higher methanol-to-isobutene ratios, the initial rates were zero order with respect to methanol and first order with respect to isobutene. In this case, the experimental data agreed with an ionic mechanism in which the protonation of the isobutene by the solvated methanol was the rate determining step as given below:

- Solvation of methanol

$CH_3\text{-}OH + A\text{-}15(H^+)$ ----------> $CH_3\text{-}OH(H^+)$

- Protonation of isobutene

$(CH_3)_2C{=}CH + CH_3\text{-}OH(H^+)$ ----------> $CH_3\text{-}OH + (CH_3)_2C{=}CH_2(H^+)$

- Reaction of protonated isobutene and methanol

$(CH_3)_2C{=}CH_2(H^+) + CH_3\text{-}OH$ ----------> $(CH_3)_3C\text{-}O\text{-}CH_3 + H^+$

On decreasing the methanol-to-isobutene ratios, the rate increased to a maximum. A further reduction in the ratio led to zero order in the isobutene and first order in methanol. In addition, at higher isobutene concentrations, dimerization of isobutene was observed [Ancillotti et al., 1978]. The rates for the reaction of methanol with three olefins at 353 K were determined as follows: isobutene, 1×10^{-2}; butadiene, 2×10^{-6} and cis-2-butene, 2×10^{-7} per acid equivalent per second. The results showed that the reaction rate for butadiene is greater than with n-butene but less than that of isobutene. This order of rates was reflected in the relative stability of the carbenium ion according to the two-step reaction mechanism where olefin protonation was regarded as the first and rate controlling step. The reactivity difference between isobutene and butadiene was large enough to allow isobutene to react selectively, but only in a narrow range of operating conditions [Ancillotti et al., 1987].

Amberlyst 35 compared with Amberlyst 15 for MTBE synthesis from isobutene and methanol showed a 2 to 5 % increase in maximum conversion. Both catalysts were similar in selectivity. The concentration-based equilibrium constants for Amberlyst 35 were 870-2500 compared to 300-850 for Amberlyst 15 at temperature ranging from 313 to 343 K [Ladisch et al., 1993]. The average equilibrium constant determined for MTBE synthesis using a macroporous sulfonic acid resin K-2631 manufactured by Bayer were found between 117 to 26 in the temperature range 313 to 353 K [Izquierdo et al., 1994]. Pannerman and Beenackers [1995] found that the catalytic activity of various strong acidic ion-exchange resin for the synthesis of MTBE from methanol and isobutene decreased when part of the protons were exchanged by sodium ions. The intrinsic rate constant was found to be higher than the apparent rate constant due to diffusional limitations. At higher temperature, the intrinsic rate constant of the resins with larger particle sizes were found significantly lower than for smaller particle size resins probably because of the long diffusional pathways of the reactants to the acid sites located inside the highly crosslinked microparticles.

2.4.4.2. Commercial Production of MTBE

MTBE is commercially produced by the reaction of methanol and isobutene over a resin catalyst such as Amberlyst 15 [Brockwell et al., 1991; Izqulerdo et al., 1992]. The catalyst life in commercial operation is about two years. The MTBE synthesis reaction is exothermic yielding 37.7 kJ mol^{-1} of energy. The isobutene is obtained from cracking reactions and from the isomerization of n-butene or dehydrogenation of isobutane. The methanol is produced from syngas obtained from the steam reforming of natural gas. Followings are the reactions for methanol and isobutene production.

- Steam reforming of methane

$2CH_4 + O_2$ ----------> $2CO + 4H_2$

- Methanol synthesis from syngas

$CO + 2H_2$ ----------> $CH_3\text{-}OH$

- Isomerization of n-butane to isobutane

$CH_3\text{-}CH_2\text{-}CH_2\text{-}CH_3$ ----------> $(CH_3)_2CH\text{-}CH_3$

- Dehydrogenation of isobutane to isobutene

$(CH_3)_2CH\text{-}CH_3$ ----------> $(CH_3)_2C{=}CH_2 + H_2$

- Isomerization of n-butene to isobutene

$CH_3\text{-}CH_2\text{-}CH{=}CH_2$ ----------> $(CH_3)_2C{=}CH_2$

The Amberlyst 15 resin is unstable above 373 K [Rohm and Haas, 1992]. At higher temperatures, large quantities of sulfonic and sulfuric acids are released from the strongly acidic cation-exchange resin and the deterioration of the catalyst resin is accelerated. Even at a low temperature, a small quantity of acid is released into the reaction mixture, and when the mixture is fed into the succeeding separation step of the process (achieved by distillation), some decomposition or reversal of the reaction leading to the main product occurs, and thus reduced yields are obtained. In addition, parts of the equipment are corroded by the presence of strong acids [Takezono and Fujiwara, 1980]. Current commercial operations are carried out in the liquid phase below 373 K and at about 15 bar. Under these conditions, all C_4 hydrocarbons are inert except isobutene. In this reaction, diisobutene and TBA are the by-products formed by dimerization of isobutene and reaction of water with isobutene respectively. The amount of diisobutene formed increases with rise in temperature [Chu and Kohl, 1987]. TBA formation is insignificant as long as the feedstocks are thoroughly dried. Followings are the reactions leading to by-products formation.

- Diisobutene formation

$(CH_3)_2C{=}CH_2 + (CH_3)_2C{=}CH_2$ ----------> $[(CH_3)_2C{=}CH_2]_2$

- TBA formation

$(CH_3)_2C{=}CH_2 + H_2O$ ----------> $(CH_3)_3C\text{-}OH$

- Dimethyl ether formation

$CH_3\text{-}OH + CH_3\text{-}OH$ ----------> $CH_3\text{-}O\text{-}CH_3 + H_2O$

According to LeChatlier's principle, the reaction equilibrium for MTBE formation is more favorable at lower temperatures, but reaction rate is considerably decreased. Thus current operation temperatures appear to be limited by three factors: (1) resin catalyst instability at temperature above 363 K, (2) poor selectivity due to dimerization above 363 K, and (3) equilibrium conversion limitation.

A number of commercial processes based on resin catalysts are in operation. These includes Hüls/UOP process, Snamprogetti/Ecofuel/John Brown process, ARCO process, BP Etherol process and Mobil Olefins to Gasoline/MTBE (MOG/MTBE) process.

2.4.5. Zeolites

The utilization of zeolite catalysts for MTBE production has the potential advantage of overcoming the temperature limitations of the existing commercial resin catalysts. Zeolites are more thermally stable and have been found to be more selective towards MTBE formation, and thus environmentally more favorable. Some of the zeolites have found to have improved activity towards MTBE formation [Chu and Kohl, 1987]. A number of studies have been reported in the literature for the catalytic application of synthesized and commercial zeolites for the production of MTBE from methanol and isobutene [Kazi et al., 1995; Kogelbaur et al., 1995; Mao et al., 1990; Briscoe et al., 1989].

The liquid phase synthesis of MTBE using zeolite H-Nu-2 has been reported at 363 K and a methanol-to-isobutene molar ratio of 2.4 [Briscoe et al., 1989]. The study showed high activity and selectivity (up to 99%) which was believed to be due to the unique pore system of the catalyst allowing the reactants to have free access to acid sites. Knifton [1989] described a patented method in which TBA was reacted with methanol using Y-zeolites, super acid aluminas, Ni-zeolites and silicates. Up to 38 weight percent MTBE was obtained. Knifton and Sanderson have patented a similar reaction using Y zeolites modified with fluorophosphoric acid [1993] and hydrogen fluoride [1994]. Using fluorophosphoric-modified Y zeolite at 413 K, TBA conversion was 49 wt% and the MTBE molar selectivity was 59%. For a hydrogen fluoride-modified Y zeolite, a molar selectivity of 64% and a conversion of 56 wt% was achieved.

Kogelbauer et al., [1994] studied partially alkali exchanged HY zeolites containing lithium, sodium or rubidium cations, which possessed similar proton concentrations but different acid strengths in the order lithium > sodium > rubidium. All zeolites showed initial activities for MTBE formation below 373 K. However, steady-state activities were found to be strongly influenced by the different deactivation behavior of the zeolites. Rubidium-exchanged zeolites showed a loss of activity, perhaps due to pore blocking by bulky cations. In another study, Kogelbauer and coworkers [1995] studied the adsorption

behavior of HY and H-ZSM-5 zeolites and their impact on activity and selectivity for MTBE synthesis. The experiments carried out showed that 2.5 molecules of methanol were adsorbed per acid site on HY and H-ZSM-5 zeolites whereas isobutene was found to produce a 1:1 adsorption complex. The excess methanol was found to be weakly bonded, probably via hydrogen bonds. Conversely, equal amounts of methanol and isobutene were adsorbed on Amberlyst 15. The higher amount of methanol adsorbed on the zeolites resulted in higher selectivity for MTBE compared to resin catalysts. This increased methanol adsorption was thought to play a key role in suppressing the formation of by-products due to isobutene dimerization and oligomerization, by decreasing the isobutene adsorption on the active sites and thereby preserving these sites for reaction.

Kazi and coworkers [1995] observed that MTBE cannot be formed on lithium and palladium metal sites from the reaction of isobutene and methanol precursors. MTBE yields were higher for H-ZSM-5 compared to HY zeolite, and this was attributed to a higher deactivation resistance of H-ZSM-5. Similar results were also observed by Nikolopoulos and coworkers [1992, 1994a] in a vapor phase synthesis of MTBE using a packed bed reactor over zeolite HY, silica-alumina and Amberlyst 15 resin. Their catalytic study showed that the zeolites were superior to resins in terms of acidity and MTBE selectivity. It was found that the very strong acidity of the resin favors many secondary reactions leading to extensive by-product formation. The results of this study suggested that acid strength has a major influence on the catalytic behavior of zeolites for MTBE synthesis. Kinetic data indicated that increased acid strength is favorable for MTBE formation but it also facilitates deactivation of the catalyst. Low acid density tends to reduce overall MTBE formation. The selectivity to MTBE was decreased with increase in temperature due to thermodynamic equilibrium limitations and enhanced by-product formation. Among all the catalysts investigated, H-ZSM-5 was found to be the best zeolite for the synthesis of MTBE at high temperature because of its superior selectivity towards MTBE and low selectivity towards isobutene dimerization, and its slow rate of deactivation.

The vapor phase reaction carried out using Amberlyst 15 resin, ZSM-5, zeolite Y, and trifluoromethane sulfonic acid (TFA) modified H-ZSM-5 and H-Y zeolites [Mao et al., 1990] showed a higher yield of MTBE for both zeolites compared to Amberlyst resin at 358 K. Zeolite Y was found to be less active than the ZSM-5 zeolite because of its weaker acid strength, although its acid density was much higher. TFA loaded zeolite Y exhibited a similar MTBE yield with lower by-products formation. Chang et al. [1992] reported the vapor phase reaction of methanol and isobutene over isomorphous substituted titanium silicalites at 343 to 383 K. The results showed that titanium silicalite had a higher MTBE selectivity than H-ZSM-5 zeolite. The results also indicated that the acid sites responsible for MTBE formation were mainly of weak to medium acid strength. The strength of the acid sites and the adsorption strength of titanium silicalite were found to be weaker than those of the H-ZSM-5 catalyst.

The catalytic activity of H-ZSM-5 zeolite evaluated for liquid phase MTBE synthesis in a packed bed microreactor at temperatures from 343 to 388 K [Pien and Hatcher, 1990] showed 10 to 89 percent isobutene conversion and 100% MTBE selectivity. Dimerization was believed to be hindered by the unique pore system of the zeolite. Reaction temperature and the isobutene to catalyst ratios were the significant process variables. Pressure had no significant effect on conversion of the reactants. At 348 K, Amberlyst 15 was approximately 11 times more active than H-ZSM-5 zeolite. However, at 373 K, the two catalysts had about the same activity. This illustrated the instability of resin catalyst at higher temperatures. Selectivity with the zeolite catalyst was better than the resin catalyst. Yavaraski and Hatcher [1989] suggested that the absence of isobutene dimers in the product was not due to the shape selectivity of H-ZSM-5 catalyst, but perhaps due to the very high coverage of active sites by methanol which prevented two isobutene molecules from reacting together. The results showed that methanol adsorption was about three times that of isobutene. In the presence of excess methanol, the rate of reaction was found to be zero order in methanol and first order with respect to isobutene.

Chu and Kohl [1987] showed that the medium pore zeolites such as ZSM-5 and ZSM-11 gave the highest isobutene conversion and MTBE selectivity. The zeolite beta and mordenite showed poorest selectivity. On the other hand, the small pore zeolites e.g. ferrierite were found inactive for this reaction, since isobutene cannot enter the zeolite cage structure. The authors explained the relative reactivity and selectivity of zeolites in terms of the differences in diffusion rates of the reactants within the zeolite channels. For the medium pore zeolites, ZSM-5 (pore size 5.4 x 5.6 and 5.1 x 5.5 Å) and ZSM-11 (pore size 5.1 x 5.6 Å), methanol (molecular size 3.7 x 4.2 Å) diffuses more rapidly than isobutene (molecular size 3.9 x 5.4 Å), and therefore an isobutene molecule migrating within the zeolite pore system encounters a high excess of adsorbed methanol and reacts to form MTBE selectively. The lower selectivity observed for mordenite and zeolite beta were due to the lack of shape selectivity in the diffusion of methanol and isobutene as compared to large pore zeolite Y. The high selectivity observed for rare earth exchanged zeolites Y was due to the preferential adsorption of methanol by the more polar zeolite with a lower SiO_2/Al_2O_3 ratio. Both large pore zeolite Y and Amberlyst 15 resin catalysts exhibited higher selectivity for MTBE with rise in temperature, whereas this effect was not observed for ZSM-5 and ZSM-11 catalysts. ZSM-5 illustrated superior selectivity for MTBE over the broad range of methanol-to-isobutene ratios as compared to Amberlyst 15. This study demonstrated the low temperature application of zeolite catalysts. It was concluded that zeolites ZSM-5 and ZSM-11 offer a number of distinct advantages over the Amberlyst 15 catalyst. These advantages are high thermal stability, no acid effluent, high selectivity to MTBE, lower sensitivity to methanol-to-isobutene ratio, excellent selectivity (even at methanol to isobutene molar ratios approaching unity), high MTBE output (despite unfavorable thermodynamic equilibrium) and ease of regeneration of the catalyst [Chu and Kohl, 1987]

From this literature review, it is clear that MFI type zeolites are a viable alternative to resin based catalysts for producing MTBE.

2.5. KINETICS OF MTBE SYNTHESIS

The literature on the kinetics of MTBE synthesis revealed that there are two mechanism types proposed by which the reaction of methanol and isobutene can be interpreted. The Rideal-Eley mechanism in which the rate determining step is the reaction between the methanol or isobutene adsorbed on the catalyst surface and the isobutene or methanol in solution. In Langmuir-Hinshelwood mechanism, the rate-determining step is the reaction between methanol adsorbed on one site and isobutene adsorbed on one or more active sites. The Langmuir-Hinshelwood approach was popularized by Hougen-Watson and it is therefore sometime called the Langmuir-Hinshelwood-Hougen-Watson (LHHW) mechanism. The details of some of the kinetic studies are described here. The kinetic model equations are given in Table 2.1.

2.5.1. Kinetics based on Rideal-Eley Mechanism

The batch reaction of isobutene and methanol to produce MTBE using Amberlyst 15 resin showed that methanol is preferentially adsorbed on the ion-exchange resin catalyst. The catalyst was found to be more active at lower methanol-to-isobutene ratios. The reaction rate constant increased with rise in temperature, and the reaction had an activation energy of 87.9 kJ mol^{-1}. The reaction data obtained under the conditions investigated fitted a Rideal-Eley mechanism whose rate determining step is the reaction between the methanol adsorbed on the surface and the isobutene in solution. The thermodynamic equilibrium constant and the adsorption equilibrium constants for methanol and MTBE decreased with rise in temperature. The reaction was found to be first order in methanol, half order in isobutene and 1.5 order in MTBE [Al-Jarallah et al., 1988]. A similar reaction mechanism was reported by Caetano et al., [1994] using Amberlyst 18 resin in a batch reactor in the liquid phase over a temperature range 323 to 338 K. The forward reaction was first order in isobutene and the activation energy determined was 130.2 kJ mol^{-1}. Parra et al., [1994] also reported a similar mechanism using a Bayer resin catalyst K2631 in a liquid phase reaction in a continuous differential reactor operated at 318-363 K. The activation energy was found to be 81.1 kJ mol^{-1}.

2.5.2. Kinetics based on Langmuir-Hinshelwood Mechanism

Gicquel and Torck [1983] conducted the vapor phase synthesis of MTBE in the temperature range 323-368 K and concluded that resin catalysts are sensitive to the concentration of methanol. Furthermore, at a given temperature, the variation in the apparent equilibrium constant was due mainly to the variation of the methanol activity coefficient as a function of its mole fraction. The vapor phase synthesis of MTBE from methanol and isobutene studied using Amberlyst 15 in the temperature range of 313 to 325

K under a high degree of agitation showed an increase in the reaction rate with rise in catalyst concentration and reaction temperature. There was no significant difference in the conversion using 0.238 mm and 0.405 mm particle size catalyst. The reaction data were analyzed using homogeneous and heterogeneous kinetic models based on Langmuir-Hinshelwood rate equations and yielded apparent activation energies of 79.0 and 76.7 kJ mol^{-1} respectively [Subramanium and Bhatia, 1987]. A similar study conducted by Ali and Bhatia [1990] in the temperature range 328 to 348 K demonstrated that a Langmuir-Hinshelwood-Hougen-Watson (LHHW) model fitted the kinetic data well. Zhang and Dutta [1995] also proposed that the reaction mechanism of MTBE synthesis was based on a LHHW mechanism in which the rate determining step is the surface reaction between adsorbed methanol and adsorbed isobutene.

The vapor phase reaction of methanol and isobutene over Amberlyst 15 catalyst was studied by Tejero et al. [1988, 1989] in a continuous differential reactor in the temperature range of 314.0 to 334.5 K. It was found that an equilibrium mixture of methanol and isobutene did not change the temperature of the catalyst bed. The equilibrium constants obtained in this study were found to agree with those predicted from literature data. Fifteen different mechanisms were tested. The data fitted statistically with an LHHW kinetic model which derives from a mechanism in which the rate-determining step is the reaction between the methanol adsorbed on one active site and the isobutene adsorbed onto two sites. The molecular mechanism proposed by Tejero et al., [1987] is given in Figure 2.2. This kinetic model was also found satisfactory by Chang et al., [1992] for the vapor phase reaction of methanol and isobutene in the temperature range 343 to 373 K using titanium silicalite.

Table 2.1. Kinetic models used for Rideal-Eley and Langmuir-Hinshelwood mechanisms.

Reference	Kinetic Equation
1. Al-Jarallah, et al., 1988	$-r_A = k_S K_A^a \dfrac{C_A^a C_B^b - C_C^c / K_e}{\left(1 + K_A C_A + K_C C_C\right)^a}$
2. Caetano et al., 1994	$-r_A = k_f \dfrac{C_A C_B - C_C / K_e}{C_B + D C_C}$
3. Parra et al., 1994	$-r_A = \dfrac{C_A C_B - C_C / K_e}{\left(K_A C_A + K_C C_C\right)^2}$
4. Gicquel and Torck, 1983	$-r_A = \dfrac{k_f C_A C_B - k_r R C_C}{C_A + R C_C}$
5. Subramanium and Bhatia, 1987	$-r_A = \dfrac{k_f C_A C_B - k_r R C_C}{C_A + R C_C}$
6. Ali and Bhatia, 1990	$-r_A = \dfrac{k_f C_A C_B - k_r R C_C}{C_A + R C_C}$
7. Zhang and Dutta, 1995	$-r_A = \dfrac{k_r K_B}{K_A}\left(\dfrac{a_B}{a_A}\dfrac{1}{K_e}\dfrac{a_C}{{a_A}^2}\right)$
8. Tejero et al., 1989; Chang et al., 1992	$-r_A = k_S K_A K_B \left(p_A p_B - \dfrac{p_C}{K_e}\right)\left[\dfrac{\left[\left(1 + K_A p_A\right)^2 + 8\left(K_B p_B + K_C p_C\right)\right]^{1/2} - \left(1 + K_A p_A\right)}{4\left(K_B p_B + K_C p_C\right)}\right]^3$

where subscript A, B and C represent methanol, isobutene and MTBE respectively; superscript a, b and c are the order of reaction of methanol, isobutene and MTBE respectively; K_A, K_B and K_C are the adsorption equilibrium constants of methanol, isobutene and MTBE respectively; C_A, C_B and C_C are the molar concentration of methanol, isobutene and MTBE respectively; k_S is the surface reaction rate constant; K_e is the thermodynamic equilibrium constant; k_f is the forward reaction rate constant; k_r is the reverse reaction rate constant; D is the ratio of the adsorption and desorption equilibrium constants of MTBE and methanol respectively; R is the ratio of MTBE and methanol adsorption coefficients; and p_A, p_B and p_C are the partial pressures; and a_A, a_B and a_C are the activity of methanol, isobutene and MTBE respectively.

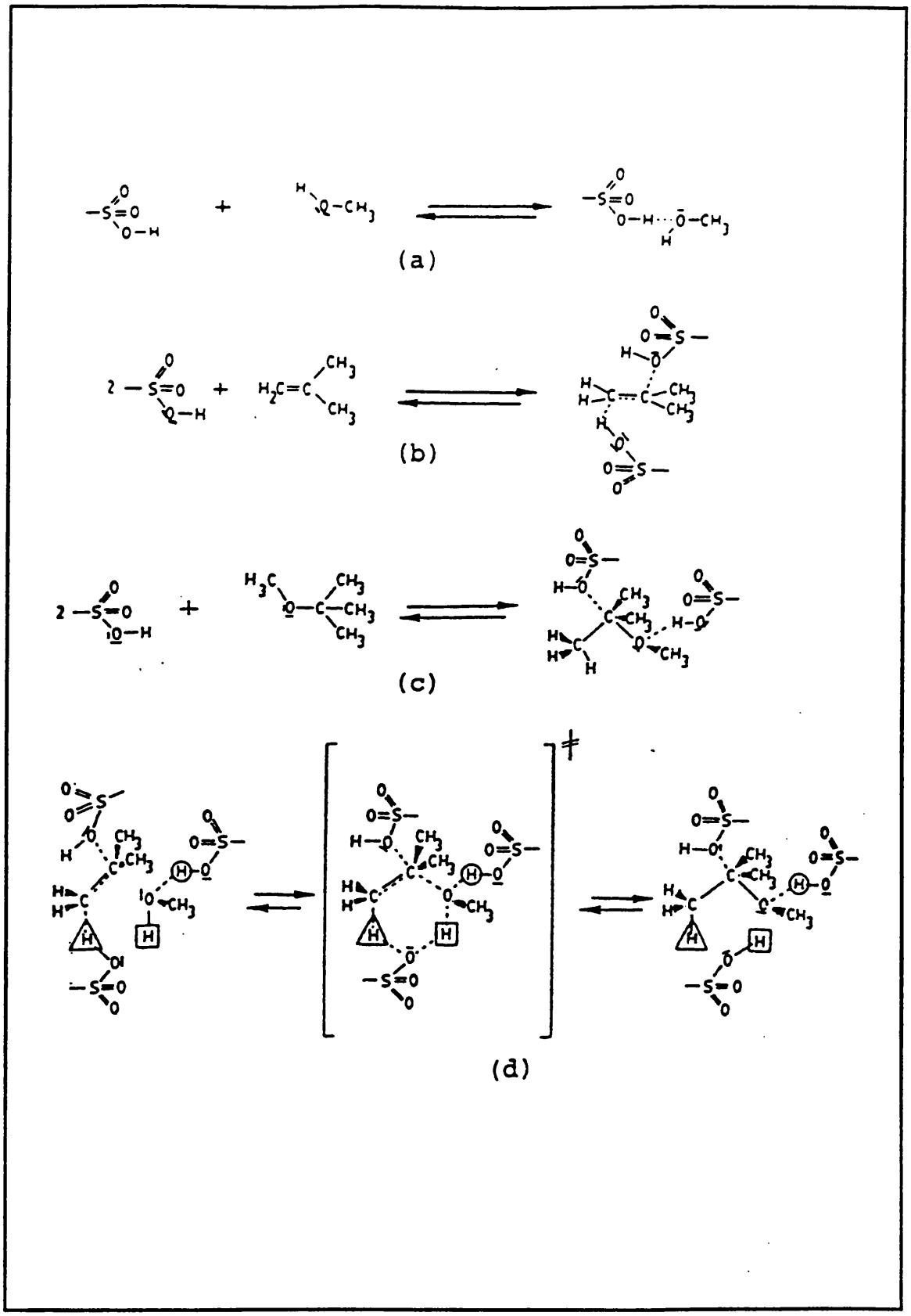

Figure 2.2. Molecular mechanism for the MTBE synthesis. (a) methanol adsorption on one site, (b) isobutene adsorption on two sites, (c) MTBE adsorption on two sites, and (d) surface reaction through a concerted mechanism.

CHAPTER 3 EXPERIMENTAL

3.1. SYNTHESIS AND PRETREATMENT OF MFI ZEOLITES

3.1.1. Synthesis of MFI Zeolites

3.1.1.1. Experimental Set-up

A standard high pressure reactor (manufactured by Parr Instrument Company, Moline, Illinois, USA) was employed in the rapid crystallization of zeolites and it is shown diagramatically in Figure 3.1. The zeolite synthesis reactor consisted of a reactor vessel or bomb, reactor head or bombhead assembly, heater, and temperature and stirrer speed controllers. It was fitted with both pressure and temperature indicators.

The reactor vessel was a one liter stainless steel 316 cylindrical pressure vessel into which the gel was charged and the synthesis carried out. The bomb was closed with the bombhead assembly using split ring closures. The bombhead assembly was equipped with all required fittings such as an inlet valve, a sampling valve, an internal cooling coil, a gas release valve, a rupture disk, a pressure gauge, a stirrer driving system and a thermowell for holding the thermocouple. A safety rupture disk of 0.25 inch (6.25 mm) size made of Inconel material and having a burst rating of 3008 psig, was provided for safety. The pressure gauge with a stainless steel Bourdon tube, having a range of 0-600 psi, was provided to monitor the pressure in the reactor. The magnetic stirrer drive was provided for driving an internal stirrer while maintaining a tight seal around the stirrer shaft. A universal coupling was provided on the upper end of the shaft to compensate for any slight misalignment in the stirring system. Vigorous mixing of the reactants as well as uniform distribution of the catalyst or suspended solid was achieved by impellers that were located on the stirring rod near the bottom of the vessel. A thermowell extended to a point near the bottom of the reactor. A thermocouple was inserted into the thermowell and connected to the temperature controller. Another thermocouple was inserted from the back, reaching the heating coil to control the temperature of the reactor. The bomb and bombhead assembly were closed by split ring closure. The split ring system allowed easy access to the reactor vessel. The head was clamped to the cylinder by a hardened steel ring that had been split into two sections. These sections slid into place from the side without interfering with any fittings attached to the head. The closing force was developed by simply tightening a set of eight cap screws into the ring section with a hand wrench. The heater was made of a 1500 Watt Sheathed calrod element built into a rugged stainless steel and aluminum housing and mounted on a 16 inch square base plate. The stirrer drive motor was mounted on a pivoting support bracket attached to the top of the heater and connected to the reactor with a moveable v-belt. A removable guard covered the entire system.

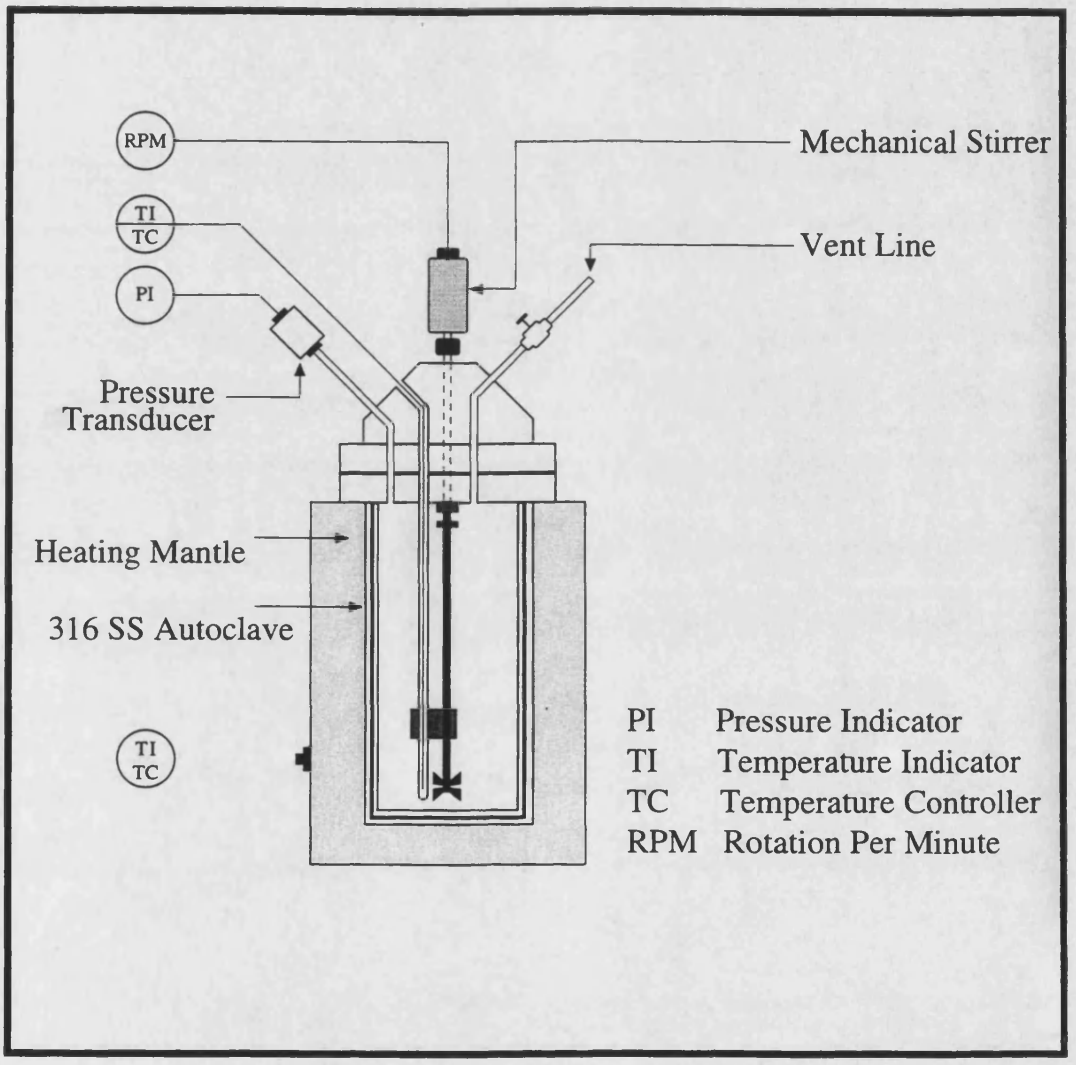

Figure 3.1. Schematic of the autoclave used for rapid crystallization of MFI zeolites.

The reactor vessel simply slid into the heater and sat on the top plate. The heater provided uniform heat distribution around the sides and the bottom of the vessel. The controller maintained the temperature of the autoclave and the speed of the stirrer. A dial setting established the set point at any temperature within the range 273 to 673 K. The temperature was controlled with a thermocouple which has both low and high heating rate options. The speed of the stirrer was controlled by an adjustable speed motor. The controller was completely housed in an enclosure containing all necessary switches, relays and indicator light.

3.1.1.2. Synthetic Procedure

The following high purity reagents were used for the synthesis of zeolites: sodium metasilicate pentahydrate ($Na_2SiO_3 \cdot 5H_2O$), sodium hydroxide (NaOH), sodium chloride (NaCl), aluminum sulfate hexadecahydrate ($Al_2(SO_4)_3 \cdot 16H_2O$), concentrated sulfuric acid (H_2SO_4) and tetrapropylammonium bromide (TPA•Br). These chemicals were obtained from Fluka. Zeolites with silicon-to-aluminum molar ratios ranging from 10 to 100 were prepared by altering the aluminum content of the synthesis precursors. Three solutions were prepared separately. Solution A was prepared by dissolving the aluminum sulfate hexadecahydrate in distilled water containing tetrapropylammonium bromide and sodium chloride. Solution B was obtained by dissolving the sodium metasilicate pentahydrate in distilled water at 343 K. Solution C consisted of the tetrapropylammonium bromide template and sodium cations. Solutions A and B were mixed together and then solution C was added with vigorous stirring. Gelation took place and the gel obtained was stirred for 5 minutes and then the pH was adjusted to 10.0 by careful dropwise addition of concentrated sulfuric acid. The semi-homogeneous gel was stirred vigorously for 80 minutes to make the gel homogeneous and the pH was checked and maintained. The gel was allowed to age overnight under stirring. The pH was finally checked and maintained at 10.0 ± 0.1 until the gel was charged into the zeolite synthesis reactor vessel, which was heated in a temperature programmed mode. Rapid crystallization was achieved by heating the gel with constant stirring at a rate of 2 °C min^{-1} up to 433 K and subsequently at 10 °C min^{-1} up to 483 K. The heating was regulated at this point overnight. The contents of the reactor vessel were then allowed to cool to ambient temperature. The contents were mixed with an equal volume of distilled water and stirred for an hour to wash out impurities and extraneous ions from the zeolite particles. The contents were then filtered through ashless filter paper No. 4 and washed several times until the washing was neutral. The crystals finally obtained were dried overnight at 393 K. The scheme used for the synthesis of MFI zeolites is summarized in Figure 3.2 showing different steps of the synthesis and the conditions used. The details of the synthesis procedure at different stages are given in Table 3.1. The zeolite obtained after drying was designated as as-synthesized (ZAS).

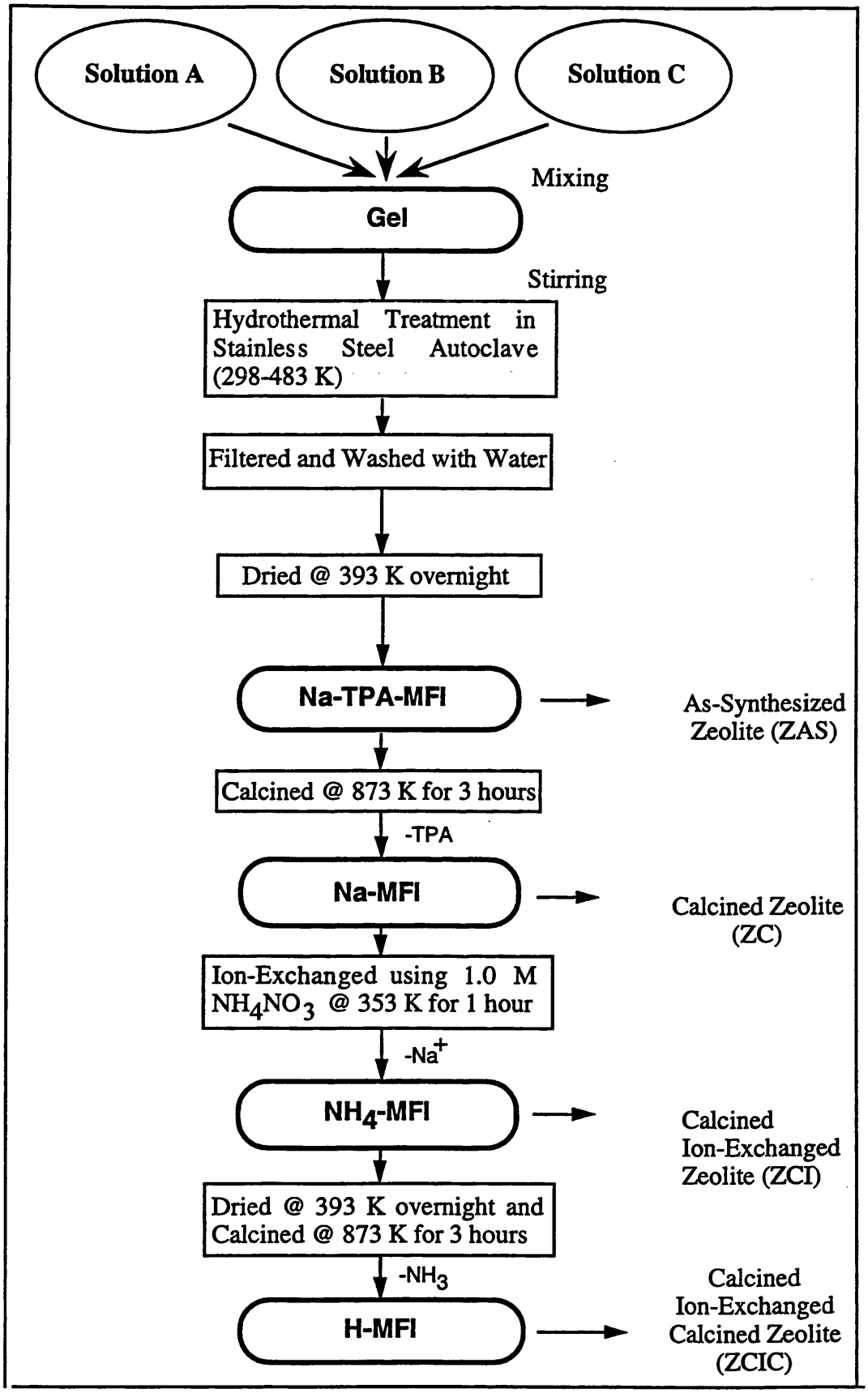

Figure 3.2. Scheme used for the synthesis of MFI zeolites.

Table 3.1. Detailed synthesis and post-synthesis parameters of MFI zeolite.

Synthesis Parameters	
Parameter	**Quantity/Value**
1. Preparation of Precursors	
Solution A	
a. $Al_2(SO_4)_3 \cdot 16H_2O$	0.2 - 15.0 g
b. Distilled Water	60.0 g
c. TPA•Br (Template)	6.0 g
d. NaCl	5.0 g
Solution B	
a. Distilled Water	100.0 g
b. $Na_2SiO_3 \cdot 5H_2O$	100.0 g
Solution C	
a. NaCl	47.5 g
b. Distilled Water	200 g
c. TPA•Br	2.16 g
d. NaOH	2.39 g
2. Gel Formation	
a. Order of addition of solutions	(A+B)+C
b. Stirring time	5 min
c. pH after mixing and stirring	13.0 to 13.5
d. pH after addition of H_2SO_4	10.0
e. Time of mechanical stirring	80 min
f. pH after addition of H_2SO_4	10.0
g. Aging	stirring overnight
3. Hydrothermal Reaction	
a. Reactor material	Stainless Steel 316 one liter Parr reactor
b. Temperature programming	298-433 K (2 °C min^{-1}) then 433-483 K(10 °C min^{-1})
c. Pressure	300 psi (2.1 MPa)
d. Stirring speed	1000 rpm during heating and cooling

Post-Synthesis Parameters	
Parameter	**Purpose/Method**
4. Filtration and Washing	to filter and wash all impurities @ 298 K temperature
5. Drying	to remove moisture @ 393 K temperature overnight
6. Weighing	to determine yield of as-synthesized zeolite
7. Calcination	to remove template @ 873 K temperature for 3 hours
8. Ion-Exchanging	to replace the sodium ions with hydrogen ions.
9. Filtration and Washing	to filter and wash all impurities @ 298 K temperature
10. Drying	to remove moisture @ 393 K temperature overnight
11. Calcination	to remove moisture @ 873 K temperature for 3 hours
12. Weighing	to determine the yield of acid form of zeolite

3.1.2. Pretreatment of MFI Zeolites (Calcination and Ion-Exchange)

Calcination of zeolites was performed in order to remove the template material after the synthesis, and to decompose ammonia after ion-exchange with ammonium nitrate. The zeolites were calcined at 873 K temperature for three hours in 100 cm^3 min^{-1} of air flow. The temperature of the furnace was programmed at 10 °C min^{-1}. After the calcination, the zeolite samples were ion-exchanged to replace sodium ions for hydrogen ions present on the active sites in the zeolites framework. An aqueous solution of 0.1 molar hydrochloric acid was used for ion-exchange in the experiments. The catalyst-to-acid solution ratio was 1g to 150 cm^3 and the stirring time was one hour. In case of zeolites having a high aluminum content, the ion-exchange procedure was repeated two to three times to completely exchange hydrogen ions for the sodium ions, without damaging the zeolite structure. Alternatively, a 1.0 molar aqueous solution of ammonium nitrate was used at 353 K for carrying out ion-exchange, the catalyst-to-solution ratio being the same as for the acid solution. After ion-exchange, the zeolite was again calcined to activate the catalytic sites.

3.2. ISOMORPHOUS SUBSTITUTION OF SILICON IN MFI ZEOLITES

The main objective of this part of the program was to produce a modified MFI zeolite having enhanced activity towards MTBE formation by isomorphous substitution of silicon (T-atom) by an appropriate heteroatom. Substitution was attempted at both the synthesis and post-synthesis modification stages. Gallium and boron were selected for evaluation in this study. Attempts were also made to substitute more aluminum in the zeolite to enhance its activity. The main tasks involved were

1. To perform isomorphous substitution of silicon by boron and gallium in MFI zeolites using two procedures, (i) during zeolite synthesis and (ii) by post-synthesis modification.

2. To perform isomorphous substitution of silicon by aluminum in MFI zeolites using post-synthesis modification.

3. To characterize the substituted zeolites to establish a relationship between their structure and properties.

4. To evaluate the effect of isomorphous substitution by boron, gallium and aluminum on the catalytic activity of MFI zeolites for MTBE synthesis.

3.2.1. Chemicals and Equipment

The chemicals used were sodium carbonate (Fluka, 99.5 %), boric acid (BDH, 99.8%), sodium tetraborate decahydrate (Riedel-De Haen AG, 99%), aluminum fine powder (BDH, 98%), ammonium fluoride (Fisher, 98% pure), gallium nitrate nanohydrate (Riedel-De Haen AG, 99%), hydrofluoric acid (BDH, 34%), hydrochloric acid (BDH, 35%), sulfuric acid (Fluka, 97%), aluminum sulfate hexadecahydrate (Fluka, 98%) and ammonium nitrate (Fisons, 99%). Teflon screw capped thick-walled bottles of 500 cm^3 volume were used for hydrothermal treatment. Each bottle was checked for leaks using pure water up to 400 K temperature.

3.2.2. Isomorphous Substitution by Boron and Gallium during Synthesis

A sample of MFI zeolite containing boron (B-MFI) was prepared from a gel having a Si/B molar ratio of 10. In this preparation, boric acid was used as the source of boron. Similarly, a gallium containing MFI zeolite (Ga-MFI) was prepared from a gel having a Si/Ga molar ratio of 10. Gallium nitrate nanohydrate was used as the source of gallium. The crystallization method and conditions were the same as mentioned earlier in Section 3.1.1 for synthesizing aluminum containing MFI zeolites. The synthesis procedure is described below:

Three solutions were prepared separately. Solution A was prepared by dissolving 2.92 g of boric acid in 60.0 g of distilled water having 6.0 g of tetrapropylammonium bromide and 5.0 g of sodium chloride. Solution B was obtained by dissolving 100.0 g of sodium metasilicate pentahydrate in 45.0 g of distilled water at 343 K. Solution C consisted of 2.16 g of tetrapropylammonium bromide, 2.4 g of sodium hydroxide and 47.5 g of sodium chloride in 200.0 g of distilled water. Solutions A and B were mixed together and then solution was added with vigorous stirring. Gelation took place and the gel obtained was stirred for 5 minutes. Then the pH was adjusted to 10.0 by dropwise addition of concentrated sulfuric acid. The semi-homogeneous gel was then stirred vigorously to ensure homogeneity and the pH finally adjusted to 10.0 ± 0.1 and the gel was charged into the zeolite synthesis reactor vessel. The reactor vessel was sealed and heated in a temperature programmed mode. Rapid crystallization was performed by heating the gel with constant stirring at a rate of 2 °C min^{-1} to 433 K. The heating rate was then increased to 10 °C min^{-1} up to 483 K. This temperature was maintained overnight. The contents of the reactor vessel were then allowed to cool to ambient temperature, mixed with equal volume of distilled water and stirred for an hour to wash out the impurities and extraneous ionic species from the zeolite particles. The product were then filtered through ashless filter paper No. 4 and washed several times until the washings were neutral. The resulting crystals were finally dried overnight at 393 K. The same procedure was repeated using 9.82 g of gallium nitrate nanohydrate instead of boric acid in solution A in order to synthesize Ga-MFI zeolite.

3.2.3. Post-Synthesis Isomorphous Substitution by Boron and Gallium

A number of methods were attempted for the isomorphous substitution of silicon in MFI zeolites by boron or gallium. These procedures were carried out on ZCIC-10 and MZ-25 zeolites. MZ-25 is a commercial MFI zeolite having a Si/Al molar ratio of 25, which was obtained from Mobil R & D corporation. ZCIC-10 refers to the synthesized MFI zeolite having a Si/Al molar ratio of 10.

3.2.3.1. Ammonium Fluoride and Boric Acid/Gallium Nitrate Hydrothermal Treatment

In this method, MZ-25 zeolite was treated at different temperatures with aqueous solutions having a predetermined concentration of ammonium fluoride and either boric acid or gallium nitrate. The hydrothermal treatment conditions are summarized in Table 3.2. Four batches, each of 2 grams of zeolite in a 500 cm^3 Teflon screw capped bottle were treated with 200 cm^3 of an aqueous solution which was 1.0 to 2.0 molar in ammonium fluoride and 0.25 to 0.50 molar in boric acid. The bottles were sealed and then heated in an oven at 363-383 K for 18 hours. The contents were allowed to cool, filtered and washed with distilled water several times. The resultant solids were dried at 393 K overnight and then calcined at 873 K for 3 hours and were designated as S-01 to S-04. Similarly, four batches, each of 2 grams of zeolite were treated with aqueous solutions having a concentration of 1.0 to 2.0 molar ammonium fluoride and 0.25 to 0.50 molar gallium nitrate. The treatment was performed at 363-383 K for 18 hours. After the hydrothermal treatment, the mixture was allowed to cool, filtered and washed several times with distilled water. The resultant solid was dried at 393 K overnight and then calcined at 823 K to decompose ammonium ions. These samples were designated as S-05 to S-08.

3.2.3.2. Solid State Method

Six batches of 2 grams of MZ-25 zeolite were first treated with 200 cm^3 of ammonium fluoride solution at 383 K for 18 hours in 500 cm^3 Teflon screw capped bottles. After cooling, the contents of the bottles were filtered, washed and dried in an oven at 393 K. Three of the treated zeolites were calcined at 873 K for 3 hours to decompose ammonium ions. The resultant solids from all six batches were then mixed separately with different amounts of finely divided solid sodium tetraborate in six crucibles and heated in a temperature programmed oven. All six samples were initially heated from 298 to 473 K at a rate of 3 _C min^{-1} and maintained at this temperature for 1 hour. The temperature was then raised to 573 K and maintained for 1 hour. Then, the temperature was raised to 673 K and maintained for 1 hour. Finally, the temperature was increased to 773 K and maintained for 2 hours to achieve maximum substitution. The heating rate was 3 _C min^{-1} at all temperatures. The mixture was then cooled to room temperature, mixed with 200 cm^3 of distilled water and heated at 383 K for 1 hours. This treatment was carried out to remove

unreacted sodium tetraborate. The resultant solids were then filtered, washed and dried at 393 K. The hydrothermal treatment and solid state exchange conditions are given in Table 3.3. These samples were designated as S-09 to S-14.

Table 3.2. Hydrothermal treatment conditions of MZ-25 zeolite with aqueous solutions containing ammonium fluoride and boric acid or gallium nitrate.

Sample Designation	Molarity of Boric Acid	Molarity of Ammonium Fluoride	Reaction Time, hour	Reaction Temperature, K
S-01	0.25	1.0	18	363
S-02	0.50	2.0	18	363
S-03	0.25	1.0	18	383
S-04	0.50	2.0	18	383

Sample Designation	Molarity of Gallium Nitrate	Molarity of Ammonium Fluoride	Reaction Time, hour	Reaction Temperature, K
S-05	0.25	1.0	18	363
S-06	0.50	2.0	18	363
S-07	0.25	1.0	18	383
S-08	0.50	2.0	18	383

Table 3.3. Hydrothermal treatment of MZ-25 with ammonium fluoride at 383 K for 18 hours, followed by reaction with sodium tetraborate.

Sample Designation	Molarity of Ammonium Fluoride	Calcination at 823 K for 3 hours after hydrothermal treatment	Weight of sodium tetraborate used for solid state exchange
S-09	2.0	No	6.0
S-10	1.0	No	3.0
S-11	0.5	No	1.5
S-12	2.0	Yes	6.0
S-13	1.0	Yes	3.0
S-14	0.5	Yes	1.5

3.2.3.3. Sodium Carbonate and Boric Acid Hydrothermal Treatment

In this method, 5.0 grams of ZCIC-10 zeolite was stirred with 150 cm^3 of 1.0 molar aqueous solution of sodium carbonate in a Teflon beaker and heated to 353 K for 4 hours. The mixture was then cooled, the suspended solid allowed to settle, and then the upper liquid was removed. This procedure was repeated three times and the total process was

completed in 12 hours. The resultant solid was filtered, washed several times, mixed with 150 cm^3 of distilled water and heated at 353 K for 3 hours under gentle stirring. The mixture was then cooled, the solid allowed to settle and the upper liquid removed. This process was repeated three times to remove excess sodium ions from the zeolite. The product obtained after the selective removal of silicon was filtered and washed, and then mixed with a solution of boric acid and heated at 353 K for 12 hours. The resultant solid was filtered at room temperature, washed and dried at 373 K [Mao et al., 1993]. This sample was designated as S-15.

3.2.4. Post-Synthesis Isomorphous Substitution by Aluminum

3.2.4.1. Aluminum Sulfate Hydrothermal Treatment

Two grams of aluminum sulfate hexadecahydrate was dissolved in 200 cm^3 of water and mixed with 2.0 g of ZCIC-10 in a 500 cm^3 stainless steel autoclave and heated at 423 K for 18 hours. The mixture was allowed to cool, the solid was filtered, washed several times with distilled water and calcined at 873 K. This sample was designated as S-16.

3.2.4.2. Ammonium Fluoride and Aluminum Sulfate Hydrothermal Treatment

Ammonium fluoride and aluminum sulfate hexadecahydrate were dissolved in 200 cm^3 of water to produce a solution which was 2.0 molar in ammonium fluoride and 0.5 molar in aluminum sulfate hexadecahydrate. Three grams of ZCIC-10 zeolite was added to this solution and the mixture heated for 18 hours at 353 K in 500 cm^3 Teflon screw capped bottle. The treated solid was filtered, washed and dried at 373 K, then calcined at 873 K for three hours to decompose ammonium ions. This sample was designated as S-17.

3.2.4.3. Aluminum Fluoride or Aluminum Chloride Hydrothermal Treatment

Isomorphous substitution was carried out using aluminum chloride and aluminum fluoride which were prepared in the laboratory. Aluminum chloride was prepared by combining 10.0 g hydrochloric acid (30%) with 0.64 g aluminum powder at ambient temperature. In this reaction, hydrogen gas was evolved and aluminum chloride was produced. The solution was evaporated and the product was dried at 373 K overnight. Aluminum fluoride was prepared by reacting 10.0 g hydrofluoric acid (40%) with 1.07 g aluminum powder using an analogous procedure [Bailer et al., 1973; Brauer, 1963]. Aluminum chloride, 0.33 g, was added in 50 cm^3 water and mixed with 1.5 g of ZCIC-10. The mixture was heated at 373 K in a Teflon screw capped 500 cm^3 bottle for 18 hours. The resultant solid was filtered, washed with distilled water and dried at 373 K. This sample was designated as S-18. Similarly, 1.5 g of zeolite was treated with 0.33, 0.66 and 1.0 g of aluminum fluoride in three separate preparations. All other conditions were the same as used for the aluminum chloride treatment. These samples were designated as S-19, S-20 and S-21 respectively.

MZ-25 zeolite, 1.5 g was also treated with 1.0 g of aluminum fluoride in 50 cm^3 of distilled water at 373 K for 18 hours in a separate preparation. The product was designated as S-22.

3.3. CHARACTERIZATION OF MFI ZEOLITES

A variety of characterization techniques were used to characterize the various MFI zeolites prepared in this program for their chemical composition, crystallinity, thermal behavior, and morphology. These techniques are described in the following section.

3.3.1. X-Ray Diffraction

Powdered zeolite samples were analyzed using a JEOL JDX-3530 X-ray diffractometer. The operating conditions of the XRD analysis were as follows: A Cu fine focus X-ray tube at a generator potential of 40 kV and a generator current of 30 mA; divergence and scatter slit at 1 degree: receiving slit at 0.2 mm; a nickel filter was used; scanning was continuous and the scanning speed and interval of data collection was 0.01 degree 2θ/sec and the angles scanned were from 4 to 50 degree 2θ.

3.3.2. Fourier Transform-Infrared Spectroscopy

FT-IR spectra were recorded in the range 4000-400 cm^{-1} as thin wafers of KBr in which the zeolite was dispersed. For this purpose, 2 mg of dried zeolite was mixed with 200 mg of dried KBr and made into a homogeneous mixture by mechanical agitation. Twenty milligram of this mixture was pressed at a pressure of 15,000 psi (103 MPa) so forming a very thin transparent wafer. The FT-IR spectra of this wafer was recorded using Perkin Elmer Model 1600 Infrared Spectrophotometer.

3.3.3. Thermal Analysis

Thermal analyses were carried out using a Simultaneous Thermal Analyzer Model STA 429, manufactured by Netzsch, West. Germany, which performed thermogravimetry and differential thermal analysis simultaneously. The equipment consisted of two sections, one for measuring and the other for controlling. A microprocessor based data acquisition system was used to couple the recording and control to a computer system. The furnace temperature was programmed and controlled by the control system. 100 mg of the zeolite sample was grounded to 125-mesh size and placed in one alumina crucible. The same weight of pre-calcined ultrex grade aluminum oxide was placed in an identical alumina crucible as a reference sample. The temperature of the sample was measured by thermocouples made of platinum containing 10 percent rhodium. The sample holder was placed in the middle of the vertical furnace and the temperature was raised at a uniform rate of 10 °C min^{-1} from ambient to 1423 K in an air flow at a rate of 100 cm^3 min^{-1}. In the thermograms, the weight loss, the differential temperature, and the temperature of the

sample were plotted simultaneously. The endothermic peaks are shown downwards and the exothermic peaks are shown upward with respect to the base line.

3.3.4. Scanning Electron Microscopy

The zeolite samples were characterized by SEM technique using a JEOL scanning microscope model JSM-T330. The samples in powdered form were dried at 453 K overnight and mounted on aluminum disks. In this process, a thin layer of sample powder was spread and deposited on an aluminum disk having carbon pads. These samples were then evacuated at 1.3 Pascal vacuum for 2 hours using an Edwards freeze dryer, and then immediately coated with gold. Coating was performed for 6 minutes at 610 Pascal in an Edwards sputter coater. The gold coated disks were then mounted in the sample holder of the instrument and the data collected in the range 5,000-20,000 magnification power.

3.3.5. Elemental Analysis

The determination of aluminum, silicon, boron and gallium contents in zeolite samples was carried out using standard inductively coupled plasma (ICP) methods. Blanks were also run during the analyses to ensure accuracy in the results obtained. Alternatively, silicon and aluminum contents of aluminosilicate zeolites were checked using spectrophotometry and complexometric titrimetric methods. Sodium contents were determined using flame photometry.

3.3.5.1. Sample Preparation for the Determination of Silicon and Aluminum

One gram pellets of sodium hydroxide (analytical reagent grade) were weighed in a 10 cm^3 platinum crucible and heated to melting until homogenized. The melt was cooled to room temperature, treated with 100 mg of zeolite sample and heated slowly until a clear fused melt was obtained. Platinum tipped tongs were used to hold the crucible in order to avoid any contamination from the tong material. The melt was transferred to a muffle furnace at 673 K and heated for 15 minutes to complete dissolution. The crucible was cooled to room temperature and the contents were transferred to a 100 cm^3 polyethylene beaker containing about 70 cm^3 of de-ionized water. The mixture was stirred well using a Teflon coated stirring bar and a magnetic stirrer, and then the solution was transferred quantitatively to a 100 cm^3 plastic volumetric flask and made up to the mark with water. This solution was used to determine silicon and aluminum contents.

3.3.5.2. Alternate Methods of Determination of Silicon and Aluminum Contents

Silicon was determined by the molybdosilicic acid spectrophotometric method. An aliquot from the fused zeolite sample was acidified with aqueous molybdic acid at pH 1-2 to produce yellow molybdosilicic acid complex, $H_4SiMo_{12}O_{40}$ which obeys Beer's law in the range of 10-100 mg $liter^{-1}$ silicon and is used as the basis for the spectrophotometric

determination of silicon. All measurements were made at 400 nm in a one cm path length cell, using a Shimadzu UV/Visible Spectrophotometer Model 260. A calibration curve was prepared using four standards solutions (10, 20, 30 and 40 mg liter^{-1} silicon).

Aluminum was determined by complexometric titration. The pH of an aliquot from the fused zeolite solution was adjusted to 3.5 using dilute hydrochloric acid. A measured amount of 0.01 molar aqueous solution of disodium salt of ethylenediamine tetraacetic acid (EDTA) was added to it and the contents of the beaker were gently heated to boiling for 3 to 5 minutes. At this temperature, the EDTA complexed all the aluminum quantitatively. The beaker was cooled to room temperature. The excess EDTA was back titrated with standard 0.01 molar zinc solution at pH 5.5. A buffer was used to maintain this pH. Xylenol orange indicator was used to detect the end point. The amount of EDTA which complexed the aluminum was directly proportional to the aluminum content. As a check, the EDTA bound to aluminum was freed by adding sodium fluoride. The released EDTA was then titrated with standard zinc solution. Since the zeolite samples do not contain metal impurities which could also complex with EDTA, the EDTA estimations were found to be very similar in both cases.

3.3.5.3. Determination of Sodium by Flame Photometry

For the determination of sodium, 100 mg of zeolite sample was weighed into a platinum dish. A small amount of de-ionized water was added to form a paste. Three cm^3 of hydrofluoric acid was added slowly and the platinum dish was placed on a hot plate at low heat. Volatile silicon tetrafluoride (SiF_4) evaporated from the platinum dish yielding a solid residue. Ten cm^3 of diluted HCl was added to dissolve this residue and the mixture was heated for 10 minutes. The solution was quantitatively transferred to a 100 cm^3 volumetric polyethylene flask and made up to the mark with de-ionized water. The sodium content of the solution was determined on a Dr. Lange flame photometer which had been calibrated with standard sodium chloride solutions.

3.3.5.4. Determination of Fluoride Contents by Potentiometric Titration

For determining the fluoride contents of zeolites, an equimolar mixture of solid lithium tetraborate ($Li_2B_4O_7$) and anhydrous Na_2CO_3 was prepared. A known amount of zeolite sample was mixed with the mixture in the ratio of 1:3 and the mixture fused at 1273 K for 30 minutes in a platinum crucible. The fused sample was dissolved in deionized water at room temperature. The solution thus obtained was analyzed by potentiometric titration using a fluoride selective electrode. A number of standard solutions of sodium fluoride were analyzed to calibrate the instrument.

3.3.6. Surface Area and Pore Structure Determination

Surface area and pore structure measurements were carried out using a fully automated ASAP 2000 equipment (Micromeritics, U.S.A.). The operation of the ASAP 2000 was monitored and controlled by a microcomputer. The zeolite samples were heated overnight in an oven at 473 K in order to remove moisture. A weighed quantity of dry zeolite sample was placed in a clean tared tube and connected to the degas port of the ASAP unit. After degassing overnight at 573 K and attaining a vacuum of 3 μm Hg, the sample was allowed to cool, reweighed and connected to the analysis port as quickly as possible in order to avoid any readsorption of moisture. At the analysis port, nitrogen was fed into the tube and adsorption of the gas took place. From this point onward, the adsorption and desorption steps were controlled by the computer and data were recorded continuously until the analysis was complete.

3.4. CATALYTIC EVALUATION OF MFI ZEOLITES

3.4.1. Synthesized Aluminosilicate MFI Zeolites

3.4.1.1. Experimental Set-up

The packed-bed reaction system used for screening of MFI zeolite catalysts for MTBE synthesis is shown in Figure 3.3. The apparatus consisted of four parts: feed section, preheating section, reactor section and product section. Experiments were carried out at atmospheric pressure in a fixed bed tubular stainless steel reactor. The feed section was designed to supply the feed to the reaction system under controlled pressure and flow rate. It consisted of a methanol storage tank, methanol feed pump, air, nitrogen and isobutene gas cylinders, and a Brook's mass flow meter. The feed tank was equipped with pressure indicators, filling port and a side Teflon tube to show the liquid level inside the tank. Methanol liquid was fed to the unit by a Milton Roy Minipump (Model 396-57). Isobutene gas from the cylinder was supplied at a regulated flow rate using Brooks mass flow meter (Model 5850C) which mixed with methanol before the preheating zone. The different feeds were delivered to the reaction system through lines constructed of 10 mm o.d. stainless steel tubing. The preheater was made of 10 mm o.d. stainless steel coiled tube insulated with a high heat-resistant heating tape to preheat the feed and to maintain stable temperature during the operation. The preheater temperature was measured using a thermocouple and controlled using an Omega temperature controller.

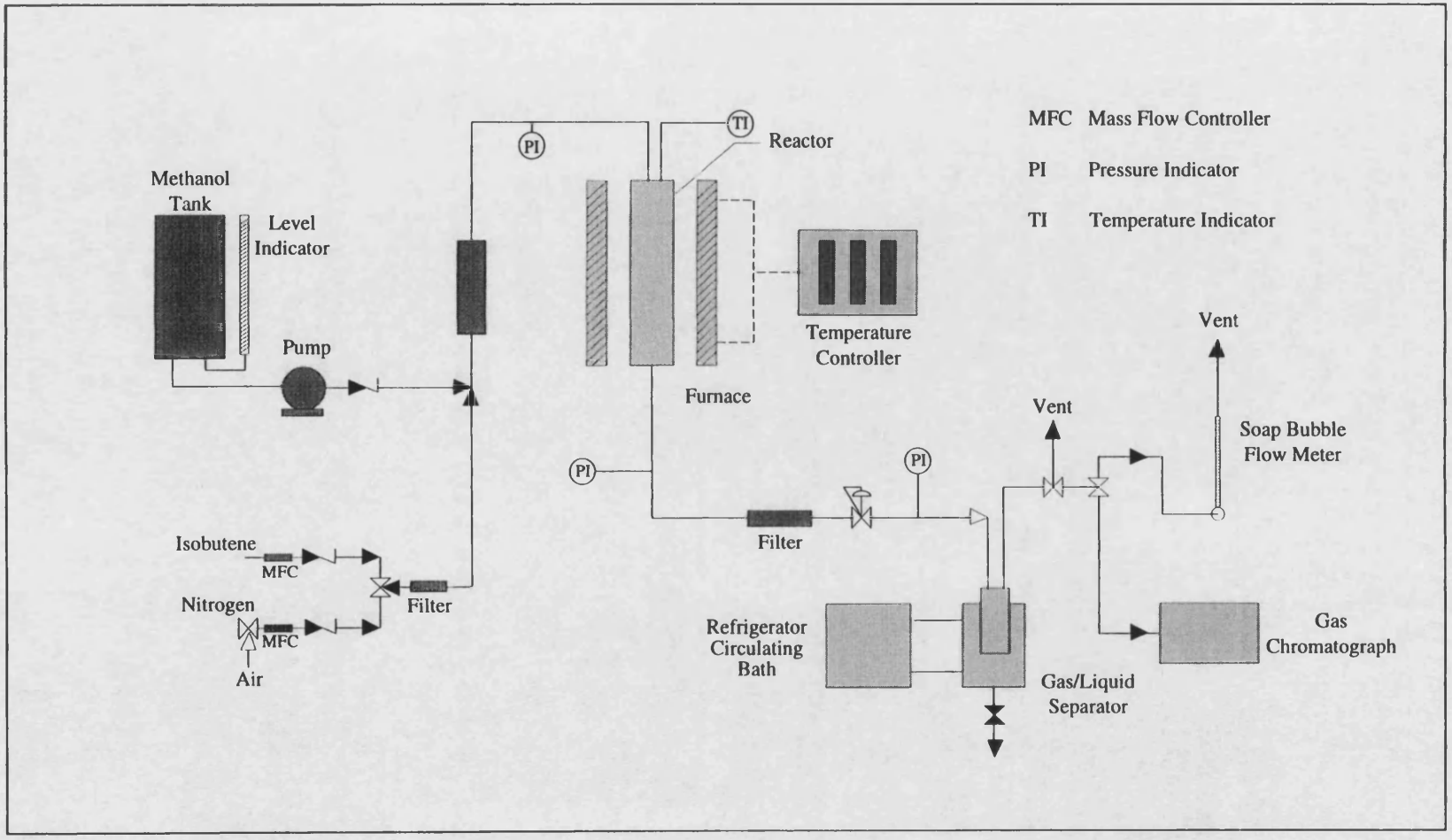

Figure 3.3. Schematic of the packed-bed reaction system used for catalytic evaluation of MFI zeolite catalysts.

The reactor used was a 380 mm long tubular stainless steel having 9.0 mm i.d. and 1.0 mm thickness. The reactor was housed in three zone furnace and the temperatures of the reactor were measured at the inlet, center and outlet of the reactor. The reactor was fitted with a mesh screen at the inlet, to distribute the feed mixture uniformly across the reactor radius. The heating rate and the temperature were maintained by a temperature controller. The product collection section was designed to collect and separate the reaction products into liquid and gaseous fractions. It consisted of a two stage cooling system supplied by Brinkman Instrument Co. USA. A mixture of ethylene glycol and water was used as the circulating medium. Condensed products were collected at sampling times through down-flow drain valve located at the bottom of the product collector which was maintained at 263 K.

3.4.1.2. Reaction Procedure

The ion-exchanged calcined zeolite powder was converted into 1 to 2 mm size pellets needed for catalytic reaction. For this purpose, the zeolite powder was placed in a special die and a pressure of 15,000 psi (103 MPa) was applied to produce a disk of about 2 mm thickness. This zeolite disk was broken on a sieve to produce 1 to 2 mm size pellets. Prior to packing the zeolite catalyst into the reactor, the bulk density of the pellets was determined by weighing a known volume of the catalyst in a 10 cm^3 graduate cylinder. For all catalytic runs, 7 grams of zeolite catalysts was packed in the reactor. The catalyst was placed in the center of the reactor between layers of glass wool. The bottom of the reactor contained some glass beads between the catalyst bed and the silica wool. The reactor was then mounted in position on the three-zone electric furnace enclosing the reactor. The reaction system was then pressure tested to ensure that the unit was leak-free.

The zeolite catalyst was calcined in-situ at 773 K for three hours in an air stream having a flow of 100 cm^3 min^{-1}. The purpose of the in-situ calcination was to purge water and other volatile impurities within the zeolite pores. The calcination involved stepwise heating of the sample from ambient to 773 K. The temperature was raised at a rate of 10 °C min^{-1} from ambient to 423 K and was maintained for 20 minutes. The temperature was then raised to 573 K and then 673 K at the same rate and maintained for 20 minutes at each stage. Finally, the temperature was raised to 773 K, and maintained for 3 hours. Following the in-situ calcination, the reactor was allowed to cool. When the temperature reached 473 K, the air flow was replaced by a nitrogen flow to purge the residual calcination products from the catalyst bed. The nitrogen flow was maintained overnight at 100 cm^3 min^{-1}. The reactor was allowed to cool to the reaction temperature. After the reactor reached the desired reaction temperature, the preheater heating and product collector cooling were started and allowed to reach their equilibrium temperature. The temperature of the preheater was same as that of the reactor while the product collector was set at 263 K. The methanol pump was started and the different sections of the reaction system were then

closely monitored until methanol reached the catalyst bed and then collected at the product collection section. At this moment, the flow rate of methanol was measured. Then, the isobutene flow was started and the methanol-isobutene mixture was preheated to the required reaction temperature and fed into the reactor. The reaction temperature was monitored by a thermocouple located at the center of the catalyst bed. The reaction was carried out at atmospheric pressure (gas phase) and the reaction products were collected after the system reached the steady state. A methanol to isobutene ratio of 2:1 was used to avoid the formation of diisobutene which is formed by the dimerization of isobutene. For each run, the catalyst charged to the reactor was 7.0 grams. The methanol and isobutene flow rates were 23.4 x 10^{-2} mol h^{-1} (7.49 g h^{-1}) and 11.6 x 10^{-2} mol h^{-1} (6.51 g h^{-1}) respectively. The weight hour space velocity was kept at 2.0. Physical, chemical and thermal properties of MTBE, methanol and isobutene are given in Appendix G. All catalysts were evaluated at 343, 353, 363 and 373 K temperatures. The products of the reaction were collected on an hourly basis. Liquid products were collected in preweighed chilled glass vials to avoid loss of isobutene and were then weighed. A number of parameters were recorded at each sampling event. These included sampling time, total run duration, total weight of the product obtained and reactor temperature.

3.4.2. Isomorphously Substituted MFI Zeolites

3.4.2.1. Experimental Set-up

The catalytic reactions were carried out in a batch reactor (manufactured by Parr Instrument Company, Moline, Illinois, USA). The reactor vessel was a 500 cm^3 stainless steel 316 cylindrical pressure vessel into which the reactants and catalyst were charged. The heater was made of a 590 Watt Sheathed calrod element built into a aluminum housing. The construction of this reactor system was similar to the one used for synthesis of MFI zeolites and has been described in Section 3.1.1.1 (Figure 3.1).

3.4.2.2. Reaction Procedure

The reactor was charged with 32 grams of methanol (1.0 mole) together with 1 gram of catalyst and was then closed. A known volume of isobutene, 47 cm^3 (0.5 mole), was taken into the isobutene measuring and feed tube. The schematic of this tube is given in Figure 3.5. Isobutene was charged into the reactor through the inlet valve of the reactor head assembly. This yielded a methanol-to-isobutene molar ratio of 2:1. The reactor was then pressurized at room temperature with nitrogen to 200 psi. The reaction was carried out at 353 K under constant stirring. The reaction time was 3 hours after the temperature of the reactor had reached 353 K. This temperature was reached in 20 minutes. At the end of the run, the reactor was allowed to cool and the contents were centrifuged to separate the fine particles of zeolite catalyst from the reaction product. The products were analyzed quickly to avoid loss of volatile components.

3.4.3. Reaction Product Analysis

The reaction products were analyzed using an HP 5890 gas chromatograph equipped with a flame ionization detector. The components of the reaction product were separated on a HP Ultra-1 capillary column having poly(dimethylsiloxane) as stationary phase. Helium was used as a carrier gas. The detector and injector were maintained at 523 and 573 K temperatures respectively. The injection volume was 0.2 µl. During the analysis, the column was maintained at 303 K isothermally. The components of the reaction products were analyzed using internal standard method. The reaction product was mixed with a known amount of diisopropyl ether as an internal standard and was injected into the gas chromatograph. The gas chromatographic specification and operating conditions are given in Table 3.4.

Table 3.4. Gas chromatographic specifications and operating conditions.

Instrument:	HP 5890 series II Gas Chromatograph interfaced with IBM compatible computer installed with Chemstation HP 3365.	
Detector:	Flame Ionization Detector (FID).	
Column:	Capillary Column, Ultra 1, 50 m x 0.32 mm x 0.52 µm film thickness.	
Gases:	Air	99.9%, 40 psi (276 kPa) , 400 cm^3 min^{-1}
	Hydrogen	99.9%, 30 psi (207 kPa) , 30 cm^3 min^{-1}
	Helium (Carrier)	99.9%, 60 psi (414 kPa), 1.4 cm^3 min^{-1}
	(purified using 5A molecular sieve column and oxygen scrubber)	
Operating Conditions:		
	Split ratio	100:1
	Injection volume	0.2 µl
	Injection port temperature	523 K
	Detector temperature	573 K
	Equilibrium time	3 min
	Oven temperature	303 K Isothermal
	Run time	10 min

3.5. DETERMINATION OF INTRINSIC KINETICS

3.5.1. Reaction System Set-up

A standard high pressure Parr reactor was used for the kinetic study of the reaction of methanol and isobutene. A schematic of the batch reaction system is shown in Figure 3.4. The main components of the reaction system are the reactor, preheater, thermostat oil bath circulation system, isobutene measuring and feed tube, isobutene cylinder and nitrogen gas cylinder.

The reactor (manufactured by Parr Instrument Company, Moline, Illinois, USA) consisted of two liter reaction vessel or bomb, reactor head or bombhead assembly, heater, controller for temperature and stirrer speed, and pressure and temperature indicators. The reactor, controller and the heater were similar to those used in the synthesis of zeolites. Additionally, the reactor head assembly was provided with a sampling valve, inlet valve, an internal cooing coil, a gas releasing valve and a dip tube for product sampling. The sampling valve was used for withdrawing samples from the pressurized reactor. It was connected at the top to a sampling tube and high pressure nitrogen gas supply and at the bottom to a dip tube extended to the bottom of the reactor having a 0.5 micron Hastelloy filter at the tip. The Hastelloy filter allowed only the pressurized liquid through it while preventing any catalyst particles from entering the sampling tube. This ensured that the sample withdrawn was representative of the reaction mixture and free from catalyst particles. The internal cooling coil was provided to circulate the cooling medium to maintain the temperature.

The preheater was also a Parr reactor consisting of bomb, bombhead assembly having a thermowell, inlet and outlet valves, heater, temperature controller, and pressure and temperature indicators. The inlet valve was used for charging the isobutene into the preheater while the outlet valve was used for transferring the isobutene to the reactor. The outlet valve was connected to a dip tube extended to the bottom of the reactor. This ensured that the isobutene was completely transferred to the reactor. A safety rupture disk of 0.25 inch size made of Inconel material was provided having a burst rating of 3008 psig. The pressure gauge with a stainless steel Bourdon tube, having a range of 0 to 600 psi was provided to monitor the pressure in the preheater. The preheater head was fitted with a thermowell extending to the bottom of the reactor. A thermocouple was inserted into the thermowell and connected to the temperature controller to maintain the temperature of the preheater. The bomb, heater and the temperature controller were similar to those with the reactor. The oil bath was used for maintaining the temperature of the reactor and to remove heat generated during the exothermic reactions. The oil was circulated through stainless steel tubing covered with insulated material in order to avoid heat loss during circulation.

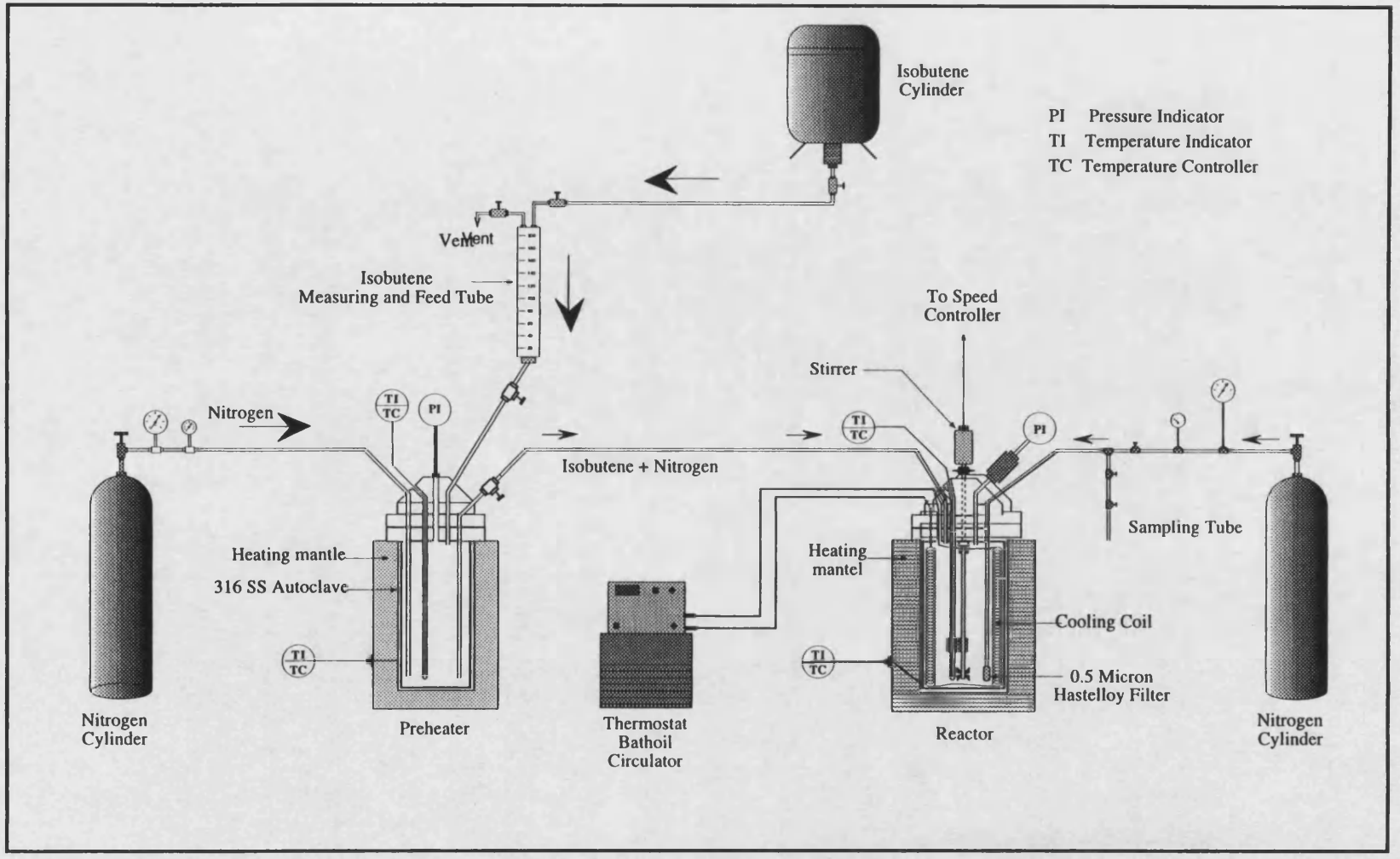

Figure 3.4. Schematic of the batch reaction system used in the kinetic study.

This tubing was connected to the internal cooling coil located at the bombhead of the reactor. The oil bath was provided with a temperature setting device and a valve for variable flow of the oil.

The isobutene measuring and feed tube was made of thick QVF glass tube of 1.0 inch internal diameter and 18.0 inch in length. It was fitted at the top with a flange holding two valves, a vent valve and a valve connected to the inverted isobutene cylinder for allowing the isobutene in the tube. A second flange with a valve was attached at the bottom end for feeding isobutene to the preheater. This tube was calibrated to provide an accurate measure of the volume of isobutene fed into the preheater. The schematic of the isobutene measuring and feed tube is given in Figure 3.5.

3.5.2. Reaction Procedure

The reactions were carried out in a batch reactor in the liquid phase. Prior to a reaction run, the preheating and reaction system including the connecting lines and valves were pressurized at the operating pressure using nitrogen gas. Leaks were detected using a soap solution and by observing the change in pressure of the reactor and preheater for a period of 24 hours. A measured volume of methanol (reagent grade, 99.9% pure from Fluka) was charged into the reactor together with a weighed amount of the catalyst. The reactor was then inserted into the heater assembly and closed by means of the reactor head using split ring closures. The reactor was connected to the preheater and all other connections were completed using stainless steel tubing. Thermocouples were inserted into the reactor and preheater and connections were made to controllers and temperature indicators. Nitrogen gas was passed through the empty isobutene tube to purge the air and to test for any possible leaks in the isobutene measuring and fed tubing system. Then, liquid isobutene (99.9% pure from Fluka) was allowed to flow from the inverted isobutene cylinder to the fed tube. At this point, the valve 1 was opened fully and valve 2 (vent valve) was slightly opened to allow isobutene in the tube. During filling of the tube, valve 3 was closed. After the required amount of isobutene was filled in the tube, valves 1 and 2 were closed completely. To fed the isobutene from the tube to the preheater, the inlet valve of the preheater was opened and the outlet valve was closed.

The valve 2 of the tube was connected to the nitrogen gas cylinder and valve 3 was opened. A slight positive nitrogen pressure was applied to force the isobutene into the preheater. When all the isobutene liquid was fed to the preheater, valve 3 and then the inlet valve of the preheater was closed. Then, the heating of the reactor and preheater was started and the controllers were set at the desired reaction temperatures. The circulating oil bath was also started and set at the desired reaction temperature. The temperature of the preheater and reactor were monitored by the digital temperature indicators. The stirrer was switched on and maintained at the desired rpm during the experimental run.

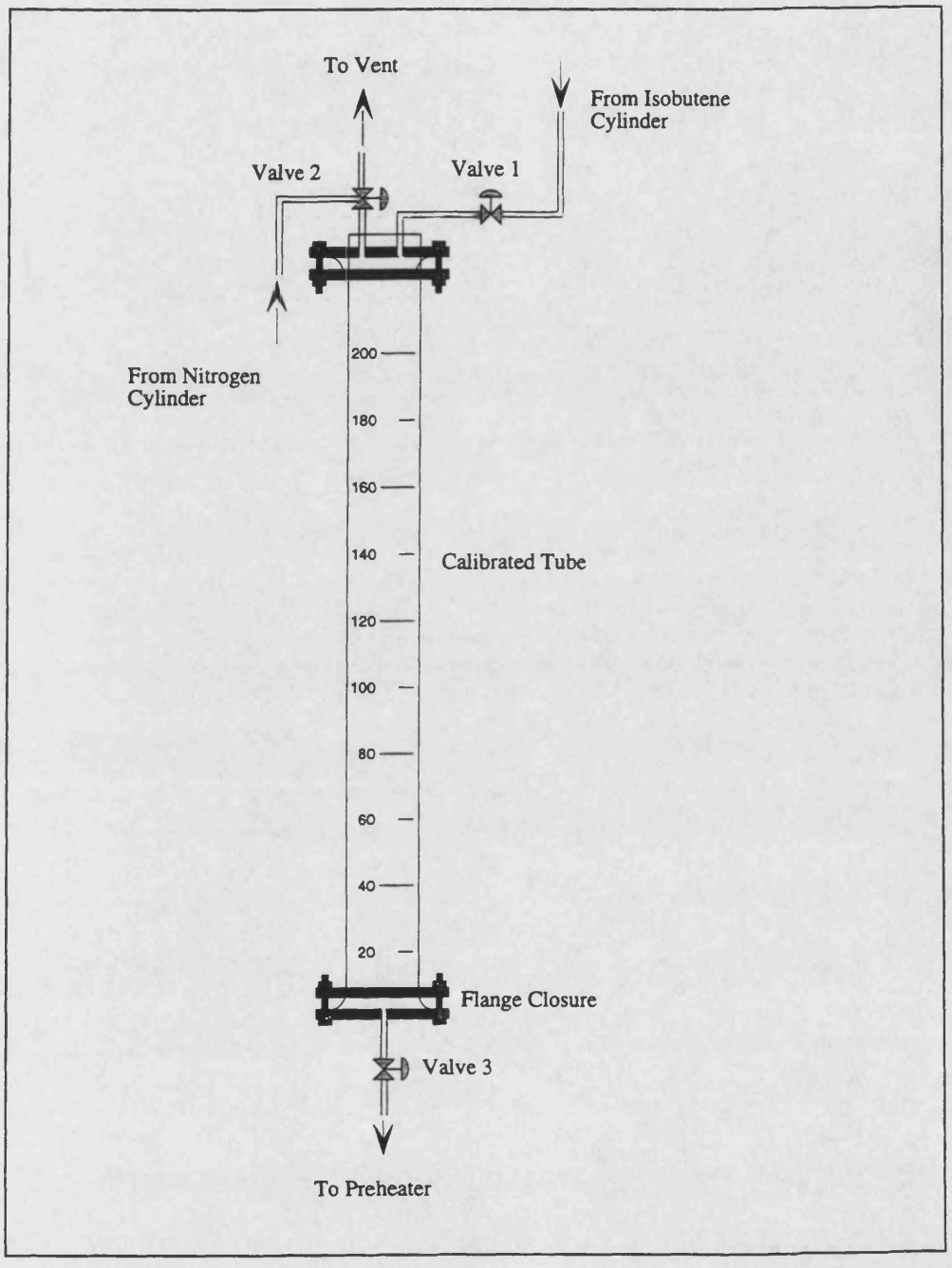

Figure 3.5. Schematic of the isobutene measuring and feed tube.

When the desired temperatures of the reactor and preheater were achieved, the preheater was connected to a nitrogen cylinder and it was pressurized to a pressure corresponding to the reaction temperature at which the isobutene would be in the liquid phase. When the desired pressure was achieved, the outlet valve of the preheater and inlet valve of the reactor were opened and the liquid isobutene was fed from the preheater into the reactor and the reactor was pressurized to the required pressure. The time of addition of isobutene to the reactor was taken as the starting point of the reaction. Samples were collected in a stainless steel sampling tube having valves at both ends. Prior to taking any sample by opening the sampling valve, nitrogen gas pressure was applied through the dip tube to force back into the reactor any reaction product present in the dip tube. This was necessary to collect a representative sample of the reaction mixture at that particular time. The sampling tube was weighed and connected to the sampling valve. The sampling valve and the sampling tube valves were opened, and the tube was filled with pressurized sample. After taking the sample, the sampling valve and the sampling tube valve were closed, and the tube was disconnected and reweighed to determine the amount of sample collected. The sample was poured slowly in a preweighed glass vial. The reaction products were analyzed by gas chromatography using diisopropyl ether as internal standard. The procedure for reaction product analysis has been described earlier in Chapter 3.4.3. The concentrations of methanol, isobutene and MTBE were calculated using the method mentioned in Appendix E. Duplicate analyses were performed to ensure that the results obtained were accurate.

3.5.3. Methodology for Determining Intrinsic Kinetics

The intrinsic kinetics of the reaction between isobutene and methanol to produce MTBE was determined in the absence of interparticle mass transfer and intraparticle diffusion effects. The mass transfer effects were eliminated by employing very small particle size of the catalyst and high speed of agitation of the reaction mixture. A methodology was adopted to optimize the reaction conditions used in obtaining the data for the determination of intrinsic kinetics of the reaction. The catalyst used in this study was ZCIC-10 having a Si/Al molar ratio of 10. This zeolite possess the maximum aluminum content which was achieved during the zeolite synthesis. This catalyst gave a maximum MTBE yield during screening experiments of the synthesized zeolite catalysts. The reaction data produced during the kinetic experiments is given in Appendix H.

3.5.3.1. Optimization of Reaction Variables

Prior to establishing a temperature and rate of reaction relationship, the reaction was carried out at 353 K to determine the right amount of catalyst and to select the appropriate stirrer speed to produce data for modeling. The effect of the amount of catalyst on the rate of reaction was determined at 353 K temperature at four different amounts, 2.5, 7.5, 12.0 and 15.0 grams. The methanol-to-isobutene molar ratio was 2 and the total amount of the

reactants was 255 grams (136 grams methanol and 119 grams isobutene). The stirring speed was 1000 rpm.

The effect of stirring speed on the rate of reaction was determined at 353 K temperature at three different stirring speeds which were 600, 800 and 1000 rpm. The methanol-to-isobutene molar ratio was 2 and the amount of the catalyst used for each reaction run was 15 grams. The total amount of the reactants was 255 grams (136 grams methanol and 119 grams isobutene). All reactions for producing kinetics data were performed in the liquid phase at 250 to 300 psi. The reaction conditions are given in Table 3.5.

Table 3.5. Reaction conditions used for optimization of reaction variables for determining intrinsic kinetics of the reaction.

Run No.	Operating Temperature, K	MeOH/IB Molar Ratio	Catalyst Weight, gram	Stirrer Speed, rpm
Effect of amount of catalyst on the rate of reaction				
1	353	2.0	2.5	1000
2	353	2.0	7.5	1000
3	353	2.0	12.0	1000
4	353	2.0	15.0	1000
Effect of stirrer speed on the rate of reaction				
5	353	2.0	15.0	600
6	353	2.0	15.0	800
7	353	2.0	15.0	1000

3.5.3.2. Determination of Order of Reaction for Isobutene

To determine the order of reaction with respect to isobutene, the concentration of methanol in the reaction mixture was increased. Reactions were carried out at 343, 353, 363 and 373 K temperatures and at three different isobutene concentrations of 10.6×10^{-3}, 7.0×10^{-3} and 3.5×10^{-3} mol g^{-1} of catalyst while the methanol concentration was kept constant, 28.3×10^{-2} mol g^{-1} of catalyst. The amount of catalyst was 15 grams. This corresponds to a methanol-to-isobutene molar ratio of 26.7, 40.4 and 80.9 respectively. The reaction conditions are given in Table 3.6.

3.5.3.3. Determination of Order of Reaction for Methanol

To determine the order of reaction with respect to methanol, the concentration of isobutene in the reaction mixture was increased while the methanol concentration was decreased in order to produce a reaction mixture having an isobutene concentration at least 10 times that of methanol (Table 3.6). The amount of catalyst was 1.5 grams. Reactions were carried out at 343, 353, 363 and 373 K temperatures and at three different methanol concentrations of

1.0, 0.83 and 0.67 mol g^{-1} of catalyst while the isobutene concentration was 10 mol g^{-1} of catalyst. This corresponds to a isobutene-to-methanol molar ratio of 10, 12.1 and 14.9 respectively.

3.5.3.4. Effect of Temperature on the Rate of Reaction

The effect of reaction temperature on the rate of reaction was determined at 343, 353, 363 and 373 K temperatures. The methanol-to-isobutene molar ratio was 2.0 and the amount of catalyst was 15 grams. The total amount of the reactants was 255 grams (136 grams methanol and 119 grams isobutene). The stirrer speed was 1000 rpm. The reaction was conducted up to the point where the composition of the reaction product become constant.

3.5.3.5. Product (MTBE) Inhibition Experiment

Catalytic reaction runs were conducted to determine the effect of presence of the product (MTBE) in the reaction mixture on the rate of reaction at four temperatures, 343, 353, 363 and 373 K. The amount of MTBE added was 2.53 grams while the methanol was 136 grams and the isobutene was 119 grams. On the mole basis, the MTBE was 2.9×10^{-2} moles while the methanol and isobutene were 4.25 and 2.13 moles respectively. The amount of catalyst was 15.0 grams. The reactions were performed in the liquid phase at 250 to 300 psi.

Table 3.6. Reaction conditions used to determine the order of reaction for isobutene and methanol.

Run No.	Reaction Temperature, K	Methanol moles	Isobutene moles	Catalyst Weight, gram	Stirrer Speed, rpm
Determination of order of reaction for isobutene					
1	343	4.25	0.16	15.0	1000
2	343	4.25	0.11	15.0	1000
3	343	4.25	0.05	15.0	1000
4	353	4.25	0.16	15.0	1000
5	353	4.25	0.11	15.0	1000
6	353	4.25	0.05	15.0	1000
7	363	4.25	0.16	15.0	1000
8	363	4.25	0.11	15.0	1000
9	363	4.25	0.05	15.0	1000
10	373	4.25	0.16	15.0	1000
11	373	4.25	0.11	15.0	1000
12	373	4.25	0.05	15.0	1000
Determination of order of reaction for methanol					
13	343	1.50	15.0	1.5	1000
14	343	1.25	15.0	1.5	1000
15	343	1.00	15.0	1.5	1000
16	353	1.50	15.0	1.5	1000
17	353	1.25	15.0	1.5	1000
18	353	1.00	15.0	1.5	1000
19	363	1.50	15.0	1.5	1000
20	363	1.25	15.0	1.5	1000
21	363	1.00	15.0	1.5	1000
22	373	1.50	15.0	1.5	1000
23	373	1.25	15.0	1.5	1000
24	373	1.00	15.0	1.5	1000

CHAPTER 4 RESULTS AND DISCUSSION

4.1. SYNTHESIS AND PRETREATMENT OF MFI ZEOLITES

4.1.1. Synthesis of MFI Zeolites

Zeolites having Si/Al molar ratio in the range 10-100 were synthesized using reagent grade high purity chemicals. The yields of these zeolites were around 30 grams per batch of synthesis.

4.1.2. Zeolite Pretreatment (Calcination and Ion-Exchange)

The occluded organic template species, located in the pores of the as-synthesized zeolite, were removed by calcination at 873 K temperature maintained for 3 hours. These conditions were found to be optimum for the removal of template as verified by thermal analysis which showed that above 873 K, there was a very little loss of the weight from the zeolite. FT-IR spectroscopy also showed that calcination under these conditions completely removed the template molecules. Ion-exchange reactions on the calcined zeolites were performed using a 0.1 molar aqueous solution of hydrochloric acid at 298 K. Alternatively, an aqueous 1.0 molar ammonium nitrate solution was used at 353 K. Sodium ions were efficiently removed by employing the acid solution without affecting the zeolite structure. The crystallinity was monitored by FT-IR spectra and X-ray diffraction patterns of the zeolite before and after the ion-exchange process. The sodium contents of the calcined and ion-exchanged zeolites showed that the ion-exchange treatment was very efficient. In the case of zeolites having a low Si/Al ratio (less than 25), one time ion-exchange reaction was not enough and was repeated two to three times to effect complete exchange. The process of ion-exchange and calcination is shown below:

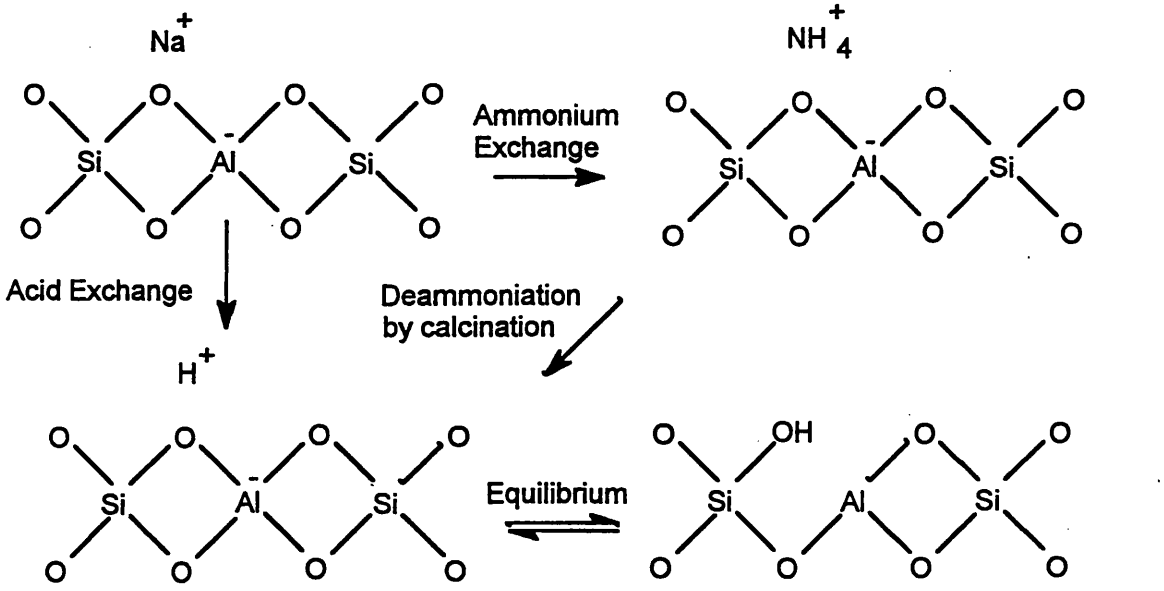

4.2. ISOMORPHOUS SUBSTITUTION OF SILICON IN MFI ZEOLITES

A number of methods were explored for the isomorphous substitution of silicon by boron, gallium and aluminum in order to achieve enhanced activity of the zeolite for MTBE formation. The efficiency of these methods was determined by evaluating the catalytic activity of the substituted zeolites in a batch reactor.

4.3. CHARACTERIZATION OF MFI ZEOLITES

4.3.1. X-Ray Diffraction

The X-ray diffraction pattern of the ZCIC-10 zeolites is given in Figure 4.1 together with the X-ray diffraction pattern of a standard MFI zeolite [Ballmoos and Higgins, 1990]. The XRD data for synthesized zeolites were compared with the XRD data of standard MFI type zeolites (Table 4.1). The good matching of both the pattern and data clearly showed that the synthesized zeolites are of the MFI types. The X-ray diffraction patterns of synthesized zeolites ZCIC-15 to ZCIC-100 are given in Figures A1-A6 (Appendix A). In case of ZCIC-10 to ZCIC-20 zeolites, the intensities of the peaks with 2θ values of 8.0 and 8.8 are lower than those of the zeolites ZCIC-25 to ZCIC-100. This was because the particles were larger and more regular in the case of ZCIC-25 to ZCIC-100 zeolites and thus they tended to pack in the XRD sample holder in a preferred orientation. This produced the observed drastic change in diffraction pattern peak intensity and as a result, the 2θ peak near 8.8 increases significantly in intensity while the peak near 8.0 emerged as the most intense peak in the XRD pattern [Nastro and Sand, 1983]. The large particle size of ZCIC-25 to ZCIC-100 zeolites are evident from their scanning electron micrographs given in Figures D3-D6 (Appendix D). The XRD pattern of synthesized B-MFI and Ga-MFI zeolites are shown in Figures A7-A8 (Appendix A). A comparison of these patterns with the standard MFI zeolite shows that these zeolites are also of the MFI type. The XRD patterns of zeolites ZCIC-10 to ZCIC-20 contains broad peaks and low area counts due to the fact that their crystallinity was below 100% and contain some amorphous material as shown by their scanning electron micrographs.

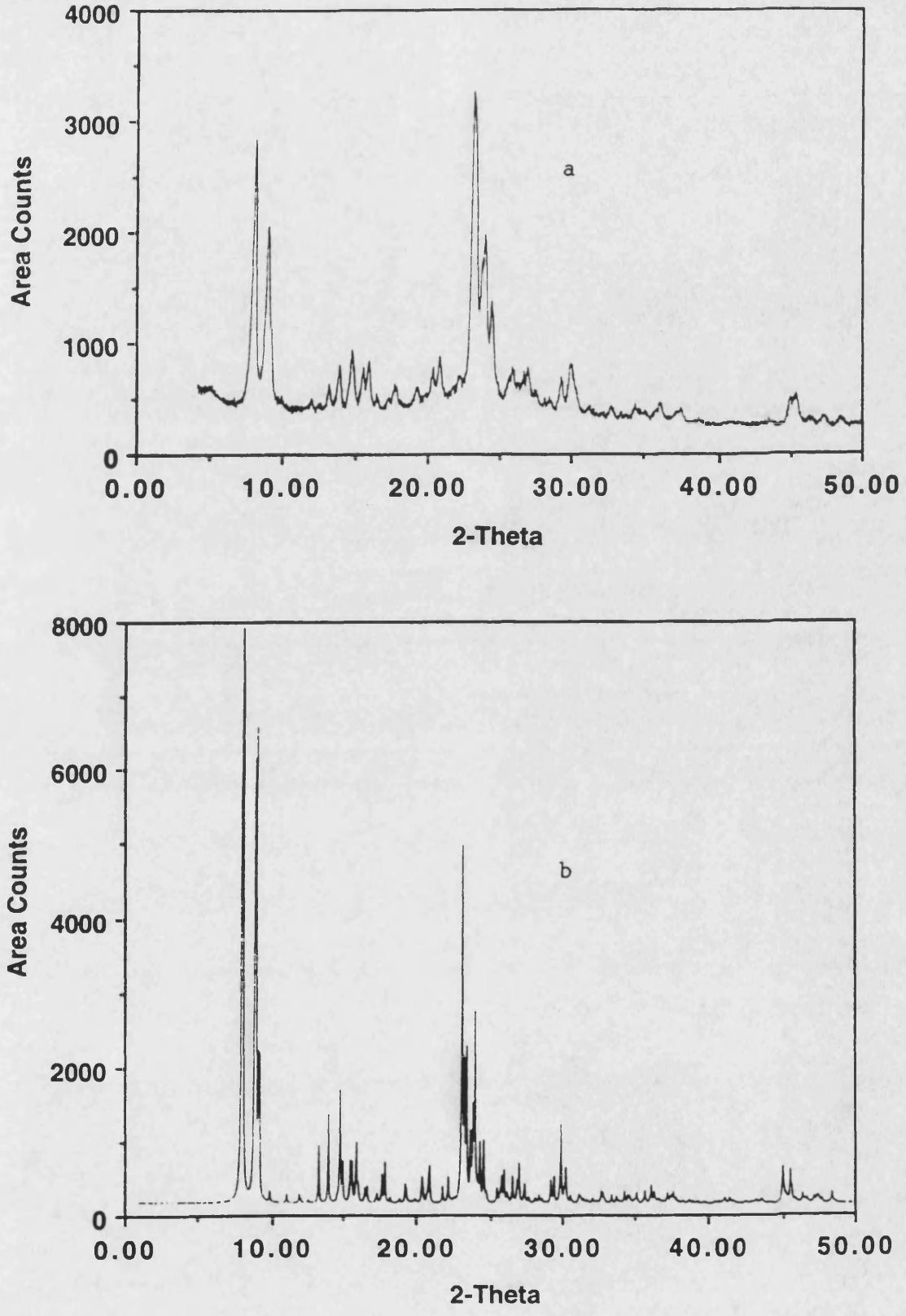

Figure 4.1. X-ray powder diffraction pattern of (a) ZCIC-10 zeolite compared with (b) standard MFI zeolite.

Table 4.1. X-ray diffraction data of synthesized zeolites compared with data from a standard MFI zeolite.

	Standard Calcined MFI		Sample No 1 ZCIC-10		Sample No. 2 ZCIC-15		Sample No. 3 ZCIC-20	
No.	Angle [2θ]	d-value α1[Å]	Angle [2θ]	d-value α1[Å]	Angle [2θ]	d-value α1[Å]	Angle [2θ]	d-value α1[Å]
1	8.01	11.03	8.00	11.04	7.98	11.07	7.96	11.11
2	8.80	10.05	8.82	10.02	8.79	10.05	8.84	10.00
3	9.07	9.75	9.10	9.71	9.12	9.69	9.10	9.71
4	11.88	7.45	11.89	7.44	11.91	7.43	11.91	7.43
5	13.25	6.68	13.23	6.69	13.22	6.69	13.25	7.08
6	13.96	6.34	13.95	6.34	13.88	6.38	13.96	6.34
7	14.79	5.99	14.74	6.01	14.79	5.99	14.79	5.99
8	15.50	5.72	15.47	5.73	15.50	5.71	15.55	5.69
9	15.92	5.57	15.96	5.55	15.94	5.56	15.93	5.56
10	16.50	5.37	16.51	5.36	16.49	5.37	16.50	5.37
11	17.24	5.14	17.28	5.13	17.25	5.14	17.25	5.14
12	17.64	5.03	17.68	5.01	17.68	5.01	17.67	5.02
13	17.85	4.97	17.77	4.99	17.69	5.01	17.83	4.97
14	18.20	4.87	18.39	4.82	-	-	-	-
15	19.24	4.61	19.20	4.62	19.25	4.61	19.25	4.61
16	20.37	4.36	20.31	4.37	20.31	4.37	20.37	4.36
17	20.86	4.26	20.84	4.26	20.87	4.25	20.87	4.25
18	22.20	4.01	22.20	4.00	22.15	4.01	22.13	4.01
19	23.27	3.82	23.32	3.81	23.29	3.82	23.28	3.82
20	23.69	3.76	23.70	3.75	23.69	3.75	23.71	3.75
21	23.94	3.72	23.88	3.72	23.87	3.73	23.98	3.71
22	24.35	3.66	24.38	3.65	24.36	3.56	24.41	3.64
23	25.54	3.49	25.56	3.48	25.52	3.49	25.55	3.48
24	25.85	3.45	25.84	3.45	25.84	3.45	25.90	3.44
25	26.59	3.35	26.87	3.32	-	-	26.58	3.35
26	27.37	3.26	27.37	3.26	27.46	3.25	27.41	3.25
27	28.43	3.14	28.42	3.14	28.40	3.14	28.46	3.13
28	29.22	3.06	29.23	3.05	29.18	3.06	29.24	3.05
29	29.95	2.98	29.95	2.98	29.87	2.99	29.83	2.99
30	30.30	2.95	30.34	2.94	30.37	2.94	30.35	2.94
31	32.74	2.74	32.71	2.74	32.75	2.73	32.72	2.74
32	33.46	2.68	33.49	2.67	33.38	2.68	33.45	2.68
33	34.34	2.61	34.30	2.61	34.21	2.62	34.35	2.61
34	37.50	2.40	37.48	2.40	37.50	2.40	37.51	2.40
35	45.09	2.01	45.06	2.01	45.00	2.01	45.03	2.01
36	45.64	1.99	45.50	1.99	45.45	1.99	45.52	1.99
37	46.50	1.95	46.43	1.95	46.44	1.95	46.48	1.95
38	47.48	1.92	47.36	1.92	47.47	1.91	47.42	1.92
39	48.55	1.88	48.49	1.88	48.47	1.88	48.54	1.87

Table 4.1. X-ray diffraction data of synthesized zeolites compared with data from a standard MFI zeolite(continued).

	Sample No 4 ZCIC-25		Sample No. 5 ZCIC-50		Sample No. 6 ZCIC-75		Sample No. 7 ZCIC-100	
No.	Angle [2θ]	d-value α1[Å]	Angle [2θ]	d-value α1[Å]	Angle [2θ]	d-value α1[Å]	Angle [2θ]	d-value α1[Å]
1	7.97	11.08	7.96	11.11	7.98	11.07	7.96	11.11
2	8.84	10.00	8.87	9.97	8.83	10.01	8.81	10.03
3	9.11	9.71	9.11	9.70	9.15	9.66	9.13	9.68
4	11.91	7.43	11.91	7.43	11.91	7.42	11.88	7.44
5	13.25	6.68	13.20	6.71	13.27	6.67	13.26	6.67
6	13.95	6.35	13.93	6.35	13.95	6.34	13.95	6.34
7	14.78	5.99	14.75	6.00	14.79	5.99	14.79	5.99
8	15.53	5.70	15.52	5.71	15.54	5.70	15.51	5.71
9	15.95	5.55	15.96	5.55	15.97	5.54	15.89	5.57
10	16.51	5.37	16.52	5.36	16.54	5.36	16.50	5.37
11	17.25	5.14	17.26	5.14	17.29	5.13	17.24	5.14
12	17.67	5.02	17.63	5.03	17.65	5.02	17.62	5.03
13	17.83	4.97	17.80	4.98	17.86	4.96	17.83	4.97
14	18.17	4.88	18.17	4.88	18.22	4.87	18.20	4.87
15	19.20	4.62	19.26	4.61	19.28	4.60	19.23	4.61
16	20.37	4.36	20.33	4.37	20.37	4.36	20.37	4.36
17	20.87	4.25	20.80	4.27	20.87	4.25	20.86	4.25
18	22.19	4.00	22.22	4.00	22.20	4.00	22.17	4.01
19	23.31	3.81	23.29	3.82	23.31	3.81	23.32	3.81
20	23.66	3.76	23.69	3.75	23.71	3.75	23.69	3.75
21	23.90	3.72	23.94	3.72	23.97	3.71	23.93	3.72
22	24.37	3.65	24.39	3.65	24.44	3.64	24.33	3.66
23	25.52	3.49	25.54	3.49	25.59	3.48	25.52	3.49
24	25.87	3.44	25.86	3.44	25.92	3.43	25.80	3.45
25	26.57	3.35	26.59	3.35	26.59	3.35	26.55	3.36
26	27.44	3.25	27.41	3.25	27.42	3.25	27.44	3.25
27	28.40	3.14	28.38	3.14	28.46	3.13	28.37	3.14
28	29.24	3.05	29.29	3.05	29.29	3.05	29.23	3.05
29	29.89	2.99	29.83	2.99	29.92	2.98	29.90	2.99
30	30.36	2.94	30.35	2.94	30.36	2.94	-	-
31	32.77	2.73	32.72	2.74	32.80	2.73	32.73	2.74
32	33.45	2.68	33.37	2.68	33.45	2.68	33.42	2.68
33	34.35	2.61	34.34	2.61	34.42	2.60	34.31	2.61
34	37.46	2.40	37.52	2.40	37.56	2.39	37.60	2.39
35	45.03	2.01	45.04	2.01	45.08	2.01	45.02	2.01
36	45.47	1.99	45.44	1.99	45.58	1.99	45.56	1.99
37	46.49	1.95	46.45	1.95	46.53	1.95	46.47	1.95
38	47.41	1.92	47.46	1.91	47.51	1.91	47.47	1.91
39	48.56	1.87	48.54	1.87	48.61	1.87	48.46	1.88

4.3.2. Fourier Transform Infrared Spectroscopy

The FT-IR spectra of the synthesized zeolites were recorded in the range 4000 to 400 cm^{-1}. Figure 4.2 shows the infrared spectra of ZCIC-10 zeolite in its different forms which are as-synthesized, calcined, ion-exchanged and calcined after ion-exchanging. These spectra show the appearance and disappearance of different absorption bands during the pretreatment procedure. The spectrum of as-synthesized zeolite shows weak C-H stretching absorption bands in the region 2980-2880 cm^{-1} due to presence of the template. These infrared spectra showed two broad peaks at 3670 and 3460 cm^{-1} assigned to O-H stretching modes due to the presence of moisture. When the zeolite was calcined, the template present in the pores was decomposed and removed resulting in the disappearance of absorption bands in the region 2980-2880 cm^{-1} in its infrared spectrum. Other absorption bands were not affected. Following ion-exchange with aqueous solution of ammonium nitrate, the sodium ions attached to the oxygen atom of the zeolite framework were replaced by ammonium ions. This was evidenced by the infrared spectrum of ion-exchanged zeolite having a new band at 3170 cm^{-1} due to N-H stretching vibration and another at 1400 cm^{-1} due to a N-H bending mode. Following ion-exchange with dilute hydrochloric acid solution, the infrared spectrum did not change significantly other than the appearance of more intense O-H stretching bands. When the ammoniated zeolite was calcined to produce hydrogen form of the zeolite, the bands at 3170 and 1400 cm^{-1} disappeared while the intensity of O-H stretching bands were increased. The FT-IR spectra of the synthesized zeolites having Si/Al molar ratio of 15 to 100 are given in Figures B1-B6 (Appendix B).

Table 4.2 contains infrared absorption data in the range of 1500 to 400 cm^{-1}. The infrared absorption bands around 791 and 450 cm^{-1} as well as around 1080 and 1219 cm^{-1} are characteristic of SiO_4 tetrahedron units [Trong et al., 1995]. The data shows that the asymmetric stretching vibration frequencies at 1219 and 1080 cm^{-1} increase with an increase in their Si/Al molar ratio. The absorptions at 1219 and 542 cm^{-1} provide information on the differences between these zeolites with other zeolite types. The external asymmetric stretching vibration near 1219 cm^{-1} is due to the presence of structures containing four chains of 5-membered rings arranged around a two-fold screw axis (Figure 2.1) as in the case of ZSM-5 structure [Jansen et al., 1984]. The absorption band around 542 cm^{-1} indicates the presence of five membered rings present in ZSM-5 zeolites. The absorption band around 1080 cm^{-1} is attributed to the internal asymmetric stretching vibration of Si-O-T linkage and is observed to be shifted towards higher wavenumber with increasing Si/Al molar ratio of the zeolites.

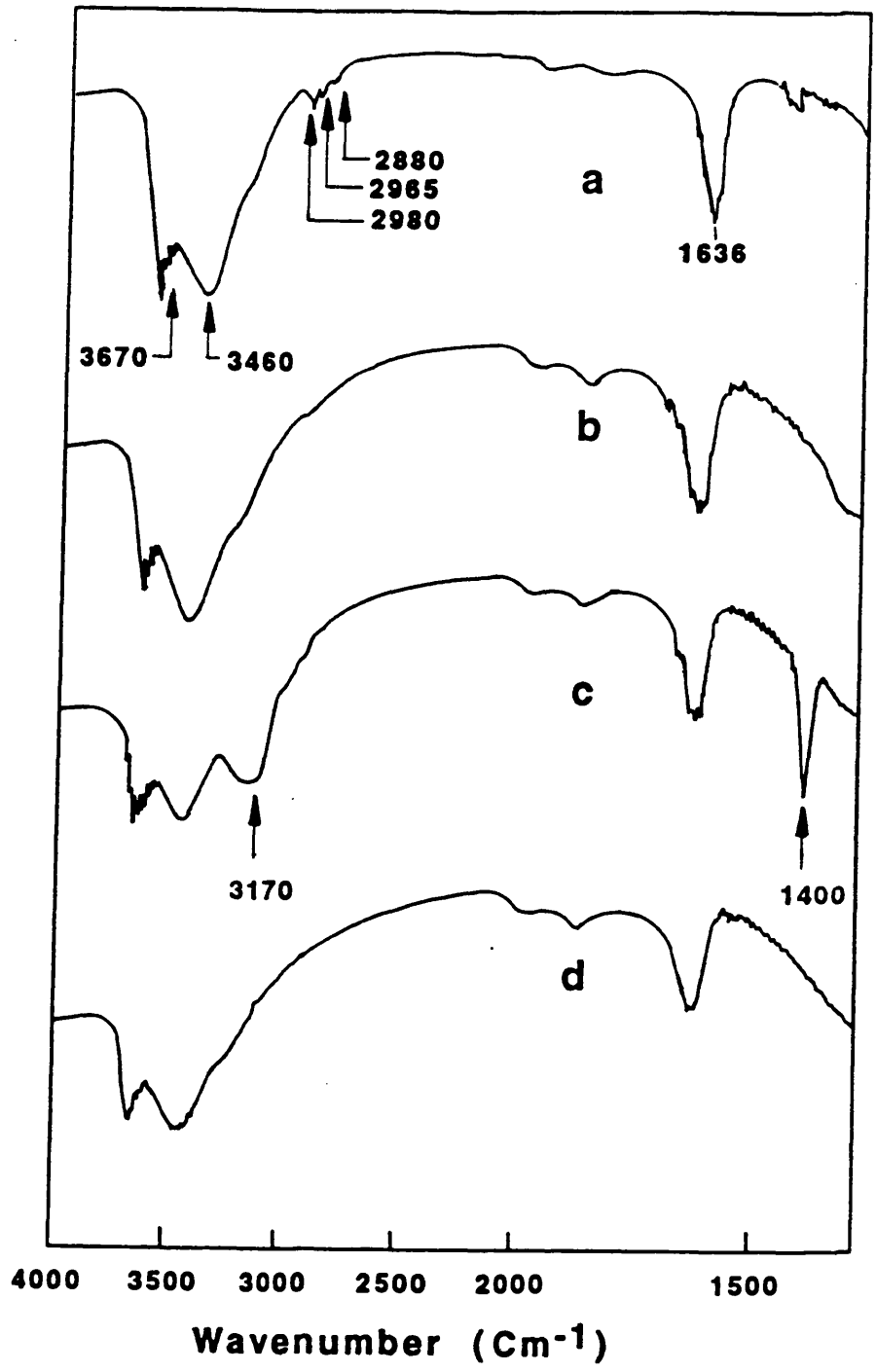

Figure 4.2. FT-IR spectra of zeolite having Si/Al molar ratio of 10, in its different forms. (a) as-synthesized(ZAS-10) (b) calcined(ZC-10) (c) ion-exchanged with aqueous ammonium nitrate solution(ZCI-10) and (d) calcined after ion-exchanging(ZCIC-10).

Table 4.2. FT-IR data obtained for as-synthesized zeolites in the range 1500 and 400 cm^{-1}.

Zeolite	Asymmetric Stretching External	Asymmetric Stretching Internal	Double Ring External	Symmetric Stretching External	Symmetric Stretching Internal	T-O Bending
ZAS-10	1219	1080	542	791	668	450
ZAS-15	1220	1090	542	791	668	450
ZAS-20	1220	1078	542	792	668	450
ZAS-25	1223	1086	542	792	668	450
ZAS-50	1223	1086	542	793	668	450
ZAS-75	1223	1098	546	795	668	450
ZAS-100	1223	1098	544	796	668	450

This shift in Si-O-T asymmetric stretching was due to the slightly lower mass of aluminum as compared to silicon [Szostak and Thomas, 1986]. In the case of significant mass difference between the Si and the T atom such as gallium, then another absorption band appears. The absorption near 790 cm^{-1} is due to the symmetric stretching of the external linkages. In the region near 542 cm^{-1}, absorption is attributed to a structure sensitive vibration caused by the double 5-membered rings of the external linkages. The absorption band near 450 cm^{-1} is due to the T-O bending vibrations of the SiO_4 and AlO_4 internal tetrahedra. The presence of absorption bands around 542 and 450 cm^{-1} has been taken as being characteristic of the ZSM-5 crystalline structure. The ratio of the absorption of these latter peaks provides an estimation of the percent crystallinity of a zeolite sample. A linear decrease in this ratio has been observed with increasing amount of amorphous material. Table 4.3 provides absorbance data of vibration bands at 542 and 450 cm^{-1}. The ratio of the absorbance of these absorption bands was calculated and found to be between 0.73 and 0.81. These values compared to a literature value of 0.8 (suggested for pure ZSM-5 zeolites) indicated that the synthesized zeolites are fairly crystalline [Jacobs et al., 1981; Coudurier et al., 1982; Jansen et al., 1984].

Table 4.3. FT-IR absorbance data of absorption bands A and B obtained for as-synthesized zeolites.

Zeolite Type	Absorbance of Band A @ 542 cm^{-1}	Absorbance of Band B @ 450 cm^{-1}	Ratio of Absorbance A/B
ZAS-10	0.93	1.17	0.79
ZAS-15	0.99	1.27	0.78
ZAS-20	1.24	1.59	0.78
ZAS-25	1.18	1.61	0.73
ZAS-50	0.93	1.14	0.81
ZAS-75	0.97	1.25	0.81
ZAS-100	0.97	1.15	0.81

FT-IR spectroscopy was also used for evaluating the efficiency of template decomposition during the calcination. Absorption bands were found initially in the region 2980-2880 cm^{-1} due to the C-H stretching mode of propyl groups of the template. Some zeolite samples were calcined at 773 and others at 873 K temperatures separately. In the case of zeolites calcined at 773 K for 5 hours, weak absorption bands were still found in the region 2980-2880 cm^{-1} showing the presence of traces of template. In the case of zeolites calcined at 873 K for 3 hours, the absorption bands in the region 2980-2880 cm^{-1} disappeared indicating the complete decomposition and removal of the organic template present in the pores of the zeolite. This is shown in Figures B7-B8 (Appendix B). Completely removal of the template from the pores of the zeolite was necessary before ion-exchange.

The FT-IR spectra of the synthesized B-MFI and Ga-MFI zeolites contained two characteristics absorption bands at 542 and 450 cm^{-1} showing that the synthesized zeolites containing boron and gallium are of the MFI type. This is shown in Figures B9-B10 (Appendix B). The FT-IR spectra of ammonium fluoride and boric acid treated MZ-25 zeolite samples (S-01 to S-04) as well as ammonium fluoride and gallium nitrate treated MZ-25 zeolite samples (S-05 to S-08) showed appearance of absorption bands due to ammoniation of the zeolite. An absorption band appeared at 3170 cm^{-1} due to N-H stretching and another at 1400 cm^{-1} assigned to an N-H bending vibration. The infrared spectra of these samples were similar to ammoniated form of ZCIC-10 zeolite (Figure 4.2c) and confirms that the above mentioned treatment of MZ-25 zeolite resulted in ammoniation besides boron and gallium substitution. Figure 4.3 shows the FT-IR spectra of MZ-25 and its aluminum fluoride modified form. These spectra reveals that after the hydrothermal treatment with aluminum fluoride, the absorption band for hydroxyl groups become sharp and reduced in intensity indicating loss of hydroxyl groups due to substitution of fluoride for hydroxyl group.

4.3.3. Thermal Analysis

Thermal analysis was carried out to determine the thermal stability of the synthesized zeolites and also loss due to the removal of water and template present in these zeolites. Thermogram of the ZAS-10 zeolite is given in Figure 4.4. The exotherm seen in the thermogram is due to the decomposition of template present in the zeolite pores in the presence of air. The thermograms of as-synthesized zeolites ZAS-15 to ZAS-100 are given in Figures C1-C6 (Appendix C). Some of the thermograms showed more than one peak representing template decomposition events occurring at different temperatures during the thermal treatment.

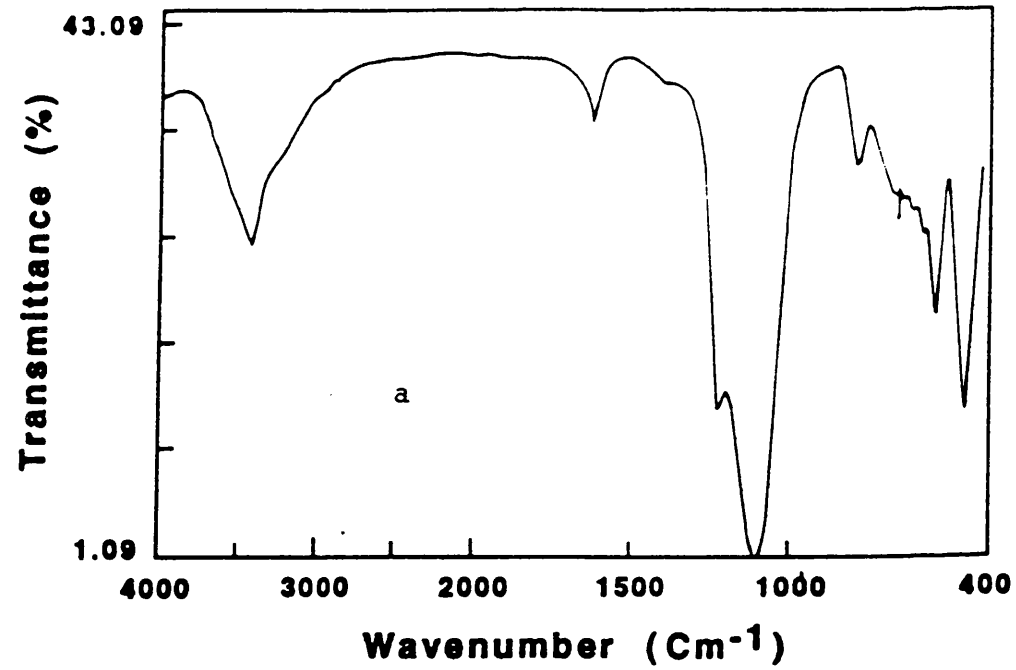

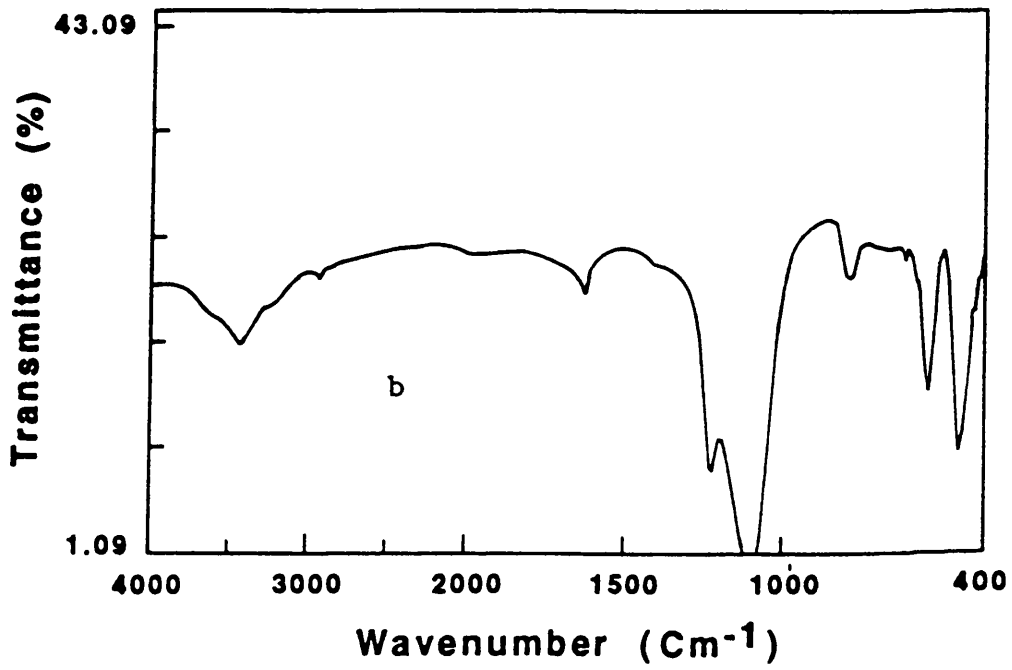

Figure 4.3. FT-IR spectra of (a) MZ-25 zeolite and (b) aluminum fluoride-modified MZ-25 zeolite.

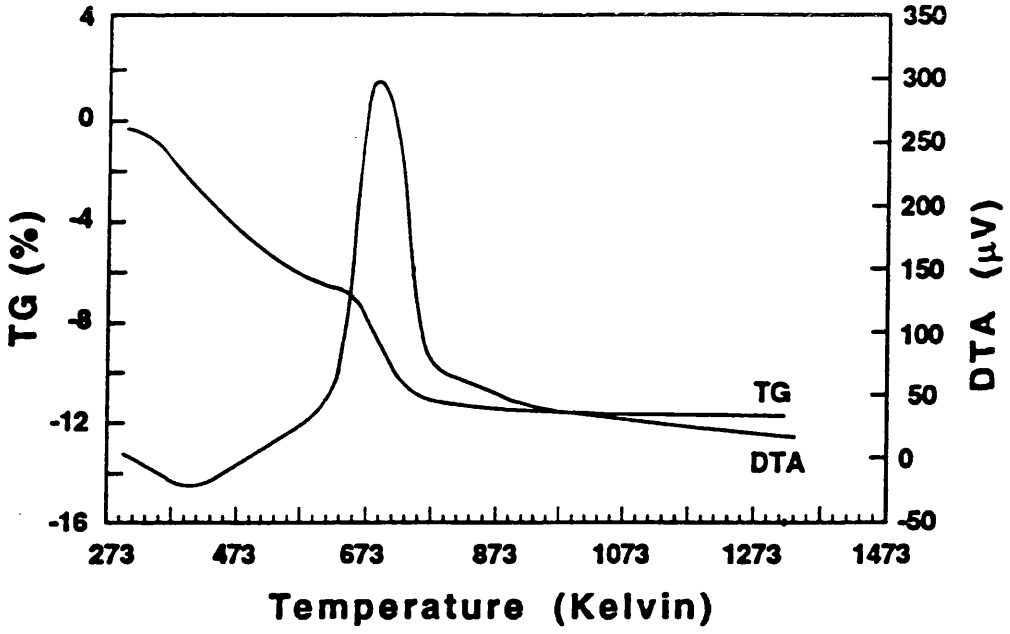

Figure 4.4. Thermogram of ZAS-10 zeolite.

Table 4.4 summarizes the thermal loss data for as-synthesized zeolites. The percent weight losses in the temperature range 293-873 K include total loss due to water present in the zeolite as well as the template decomposition. The weight loss in the temperature range 293-573 K was due to the loss of water present in the zeolite, and it shows a decreasing trend with increasing Si/Al ratio of the zeolites. This is because the acidity of the zeolite decreases with increasing Si/Al ratio thus increasing its hydrophobic nature and therefore less water is present in the zeolite. The weight loss due to the removal of template in the temperature range 573-873 K has a reverse trend of increasing with increasing Si/Al ratio of the zeolites. The water and template contents of the as-synthesized zeolites plotted vs Si/Al molar ratio in Figure 4.5 show that the water content decreases sharply with increase in Si/Al molar ratio from 10 to 25, and then the decrease is relatively little. It seems that the water content of zeolites having Si/Al molar ratio of 100 and above do not change appreciably. The following relationships were observed between Si/Al molar ratios in the range 10 to 100 and the water and template contents of as-synthesized zeolites.

Water content (wt%) $= 13.0 \times \text{Si/Al molar ratio}^{(-0.36)}$ $(R = 0.99)$

Template content (wt%) $= 2.9 \times \text{Si/Al molar ratio}^{(0.28)}$ $(R = 0.98)$

Thermograms of the synthesized B-MFI and Ga-MFI zeolites are given in Figure 4.6 which show that a phase change phenomenon occurred at 1193 and 1263 K. This can be attributed to the lower thermal stability of B-OH and Ga-OH functional groups in these zeolites towards dehydroxylation compared to the Al-OH groups in aluminosilicate zeolites which are stable up to 1350 K [Szostak, 1989]. This led to rapid dehydroxylation of the framework, which finally changed from an MFI phase into another phase [Suzuki et al., 1985]. In aluminosilicate zeolites, no phase change was observed up to 1373 K and thus they were more thermally stable. In summary, the thermal stability of the as-synthesized zeolites follows the following trend:

$$\text{B(Si)-MFI} < \text{Ga(Si)-MFI} < \text{Al(Si)-MFI}$$

Figure 4.7 also shows thermograms of MZ-25 and its aluminum fluoride modified form. As can be seen, MZ-25 is stable thermally up to 1373 K. The aluminum fluoride-modified form shows a phase change around 1073 K and is thus less stable than the ammoniated form. This can be explained as follows. During the hydrothermal treatment of zeolite with aluminum fluoride, some of the hydroxyl groups are replaced by fluoride groups and thus result in decreased hydroxyl groups of the treated zeolite. The loss of hydroxyl groups was indicated by a decrease in the intensity of hydroxyl group absorption bands at 3670 and 3460 cm^{-1} in the FT-IR spectra. Dehydroxylation at elevated temperature involves the elimination of water from two active sites to form different types of sites [Bolton and Lanewala, 1970]. The process of dehydroxylation is followed by dealumination of the

zeolite framework [Nayak and Choudhary, 1982] and this results in the collapse of the zeolite framework at a lower temperature compared to untreated MZ-25.

Table 4.4. Percent weight loss results obtained for as-synthesized zeolites using thermal analysis.

Zeolite Type	293-873 K Total loss	293-573 K Loss of Water	573-873 K Loss of Template
ZAS-10	11.6	6.2	5.4
ZAS-15	10.9	4.7	6.2
ZAS-20	11.2	4.5	6.7
ZAS-25	11.1	3.7	7.4
ZAS-50	11.4	3.2	8.2
ZAS-75	12.6	2.9	9.7
ZAS-100	13.2	2.5	10.7

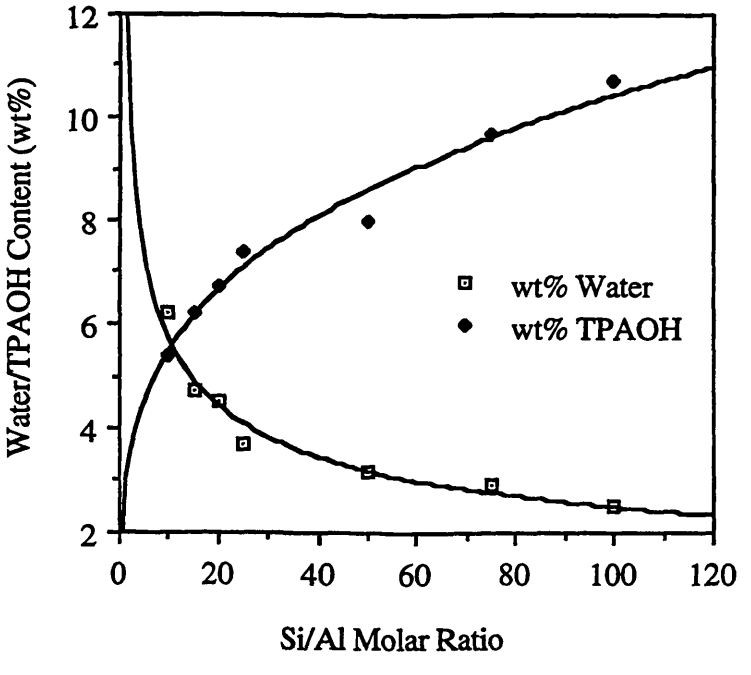

Figure 4.5. Water and TPAOH contents as a function of Si/Al molar ratio of the as-synthesized zeolites.

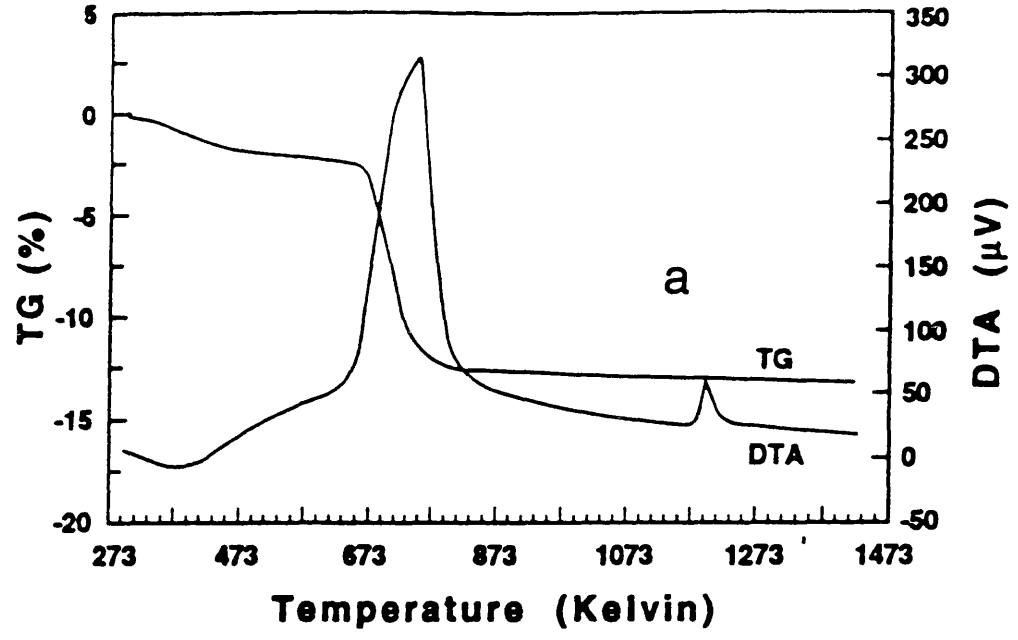

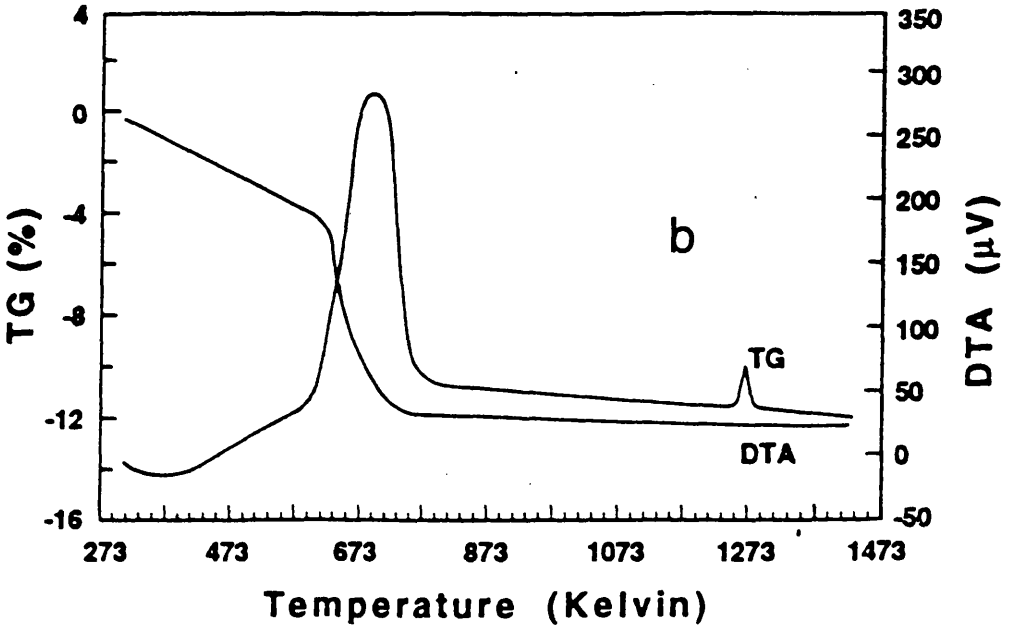

Figure 4.6. Thermograms of (a) B-MFI zeolite and (b) Ga-MFI zeolite.

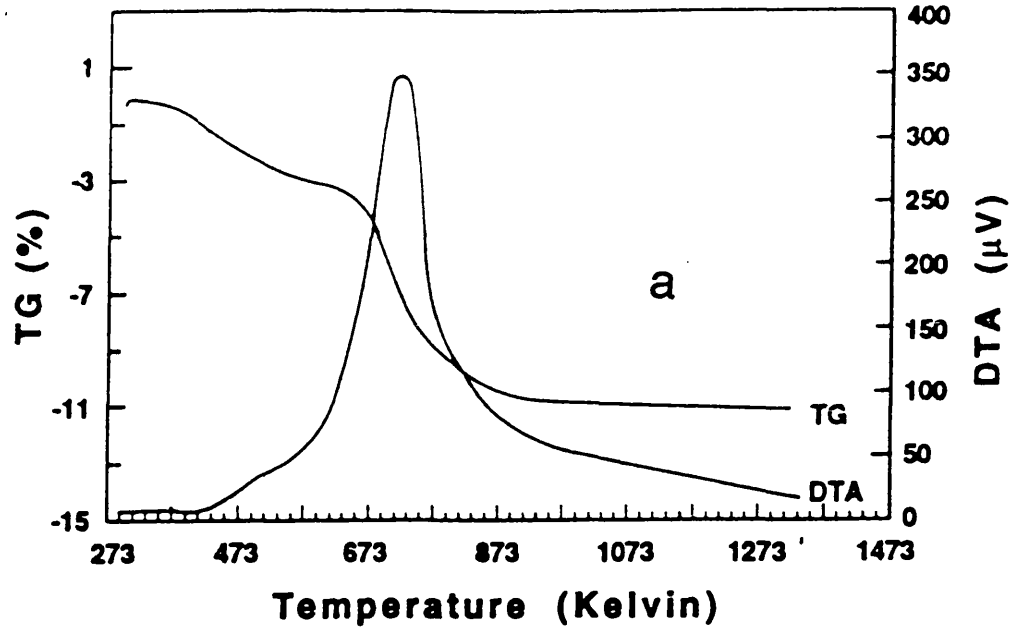

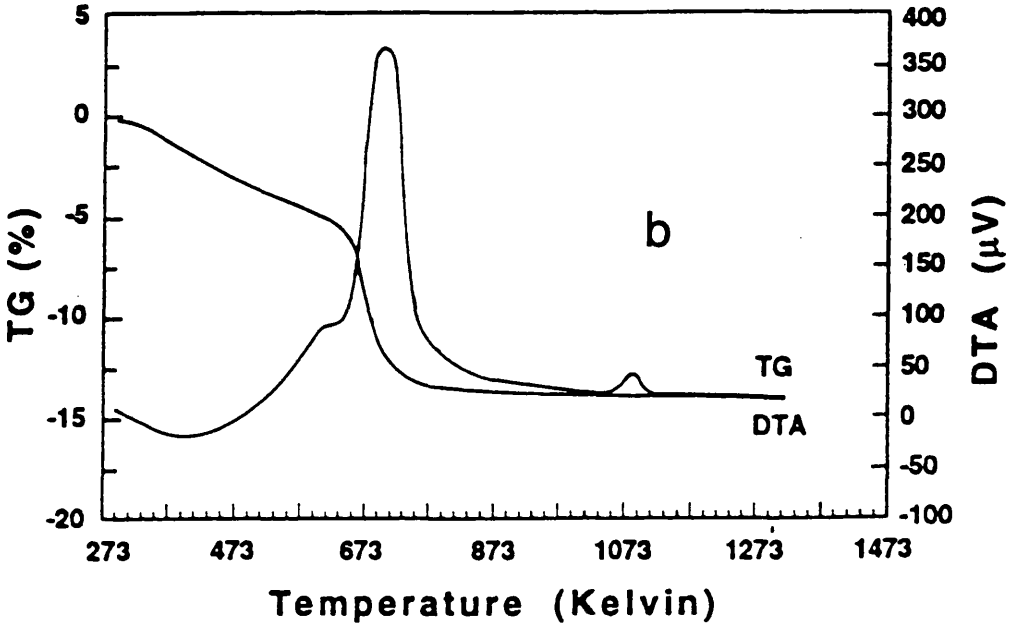

Figure 4.7. Thermograms of (a) MZ-25 zeolite and (b) aluminum fluoride modified MZ-25 zeolite.

4.3.4. Scanning Electron Microscopy

The scanning electron micrograph of ZCIC-10 zeolite is shown in Figure 4.8 both at low and high magnification. The SEM at lower magnification shows the agglomeration of crystals and presence of some amorphous material. The SEM of other synthesized zeolites are given in Figures D1-D6 (Appendix D). The SEM of B-MFI and Ga-MFI synthesized zeolites are given in Figures D7-D8 (Appendix D). The micrographs show that the synthesized aluminosilicate zeolites are crystalline, having spherical shape crystals [Jacobs and Martens, 1987], and are free from amorphous material. The crystals of B-MFI and Ga-MFI appear to be of square shape.

4.3.5. Elemental Analysis

Table 4.5 shows the Si/Al molar ratio of the gel prepared for the syntheses. The Si/Al molar ratio was calculated using the composition and amount of sodium metasilicate pentahydrate and aluminum sulfate hexadecahydrate used for the gel preparation.

Table 4.5. Si/Al molar ratio of the gel prepared for the synthesis of zeolites. The weight of sodium metasilicate pentahydrate in the gel was 100 grams (0.471 moles of silicon).

Gel Type	Grams of $Al_2(SO_4)_3.16H_2O$	Moles of aluminum	Si/Al molar ratio
Gel-10	14.858	0.047	10
Gel-15	9.906	0.031	15
Gel-20	7.431	0.024	20
Gel-25	5.945	0.019	25
Gel-50	2.974	0.009	50
Gel-75	1.989	0.006	75
Gel-100	1.486	0.005	100

Table 4.6 shows elemental analysis results for the as-synthesized zeolites in terms of silicon, aluminum and sodium contents together with water and TPAOH contents obtained from thermal analysis. A comparison of the Si/Al ratio of the gel given in Table 4.5 with that of the as-synthesized zeolites (Table 4.6) shows that the Si/Al ratio of as-synthesized zeolites is slightly lower than that of the gel which means that almost all of the aluminum present in the gel was incorporated into the zeolite framework. Table 4.6 also shows the unit cell composition of the as-synthesized zeolites which was calculated from the elemental analysis data.

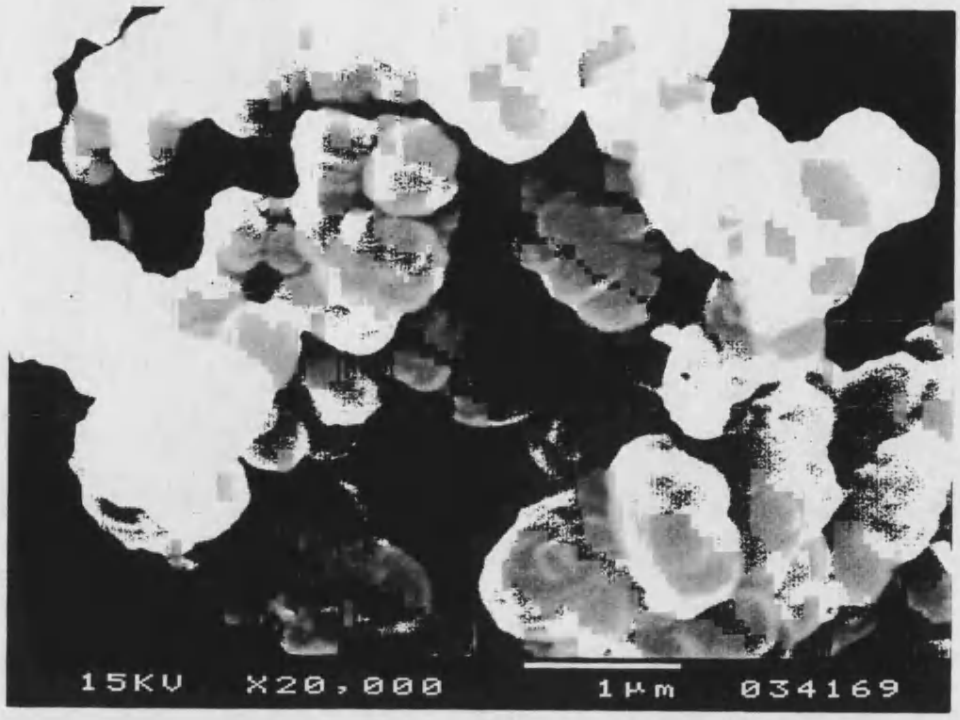

b

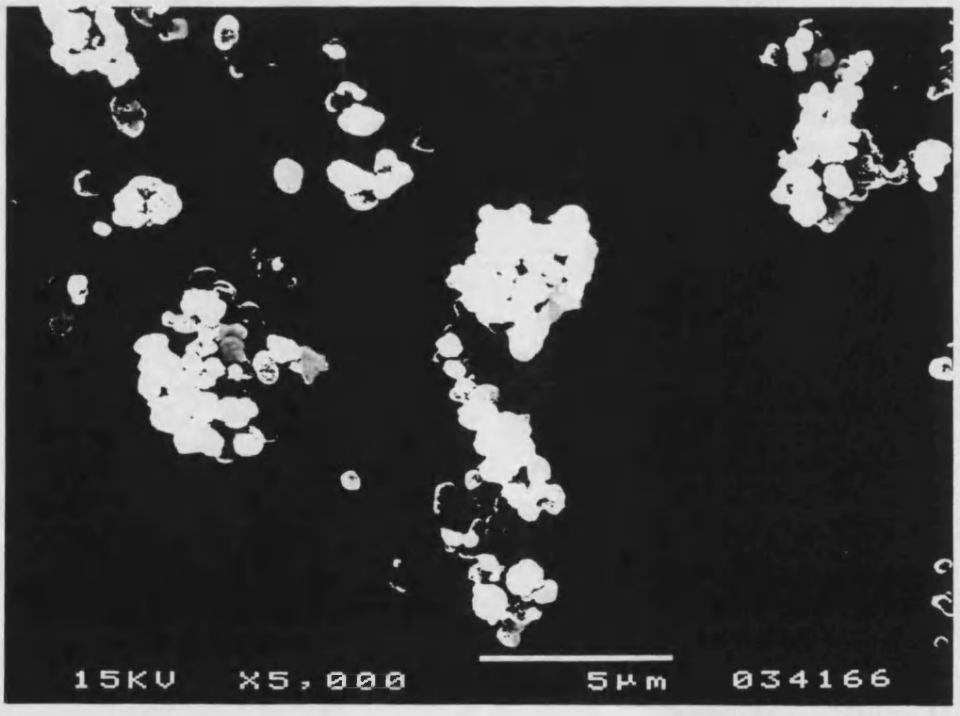

a

Figure 4.8. Scanning electron micrograph of ZCIC-10 zeolite.
(a) at lower magnification and (b) at higher magnification.

This illustrates very clearly that as the Si/Al molar ratio increase, the aluminum, sodium and water contents decrease while the silicon and TPAOH contents increase as shown in the unit cell composition of the zeolites. The zeolites with high Si/Al molar ratio possess low concentrations of sodium ions because of their low aluminum content.

Table 4.6. Elemental analysis and unit cell composition of as-synthesized zeolites.

Zeolite Type	Silicon wt%	Aluminum wt%	Sodium wt%	Water wt%	TPAOH wt%
ZAS-10	38.7	3.81	3.11	6.2	5.0
ZAS-15	39.2	2.62	2.05	4.7	6.2
ZAS-20	41.8	2.07	1.62	4.5	6.7
ZAS-25	41.9	1.67	1.30	3.7	7.4
ZAS-50	42.3	0.82	0.63	3.2	8.2
ZAS-75	42.5	0.55	0.41	2.9	9.7
ZAS-100	42.6	0.41	0.30	2.5	10.7

Zeolite Type	Silicon mole	Aluminum mole	Sodium mole	Water mole	TPAOH mole	Si/Al molar ratio
ZAS-10	1.38	0.14	0.14	0.34	0.03	9.7
ZAS-15	1.40	0.10	0.09	0.26	0.03	14.4
ZAS-20	1.48	0.08	0.07	0.25	0.03	19.8
ZAS-25	1.49	0.06	0.06	0.21	0.04	24.0
ZAS-50	1.51	0.03	0.04	0.18	0.04	49.5
ZAS-75	1.52	0.02	0.04	0.16	0.05	73.4
ZAS-100	1.52	0.02	0.03	0.14	0.05	99.0

Zeolite Type	Unit Cell Composition
ZAS-10	$Na_{8.81}[Al_{8.90}{\bullet}Si_{87.1}{\bullet}O_{192}]{\bullet}H_2O_{20.5}{\bullet}TPAOH_{1.6}$
ZAS-15	$Na_{6.19}[Al_{6.24}{\bullet}Si_{89.8}{\bullet}O_{192}]{\bullet}H_2O_{18.9}{\bullet}TPAOH_{2.0}$
ZAS-20	$Na_{4.61}[Al_{4.69}{\bullet}Si_{91.3}{\bullet}O_{192}]{\bullet}H_2O_{17.8}{\bullet}TPAOH_{2.1}$
ZAS-25	$Na_{3.79}[Al_{3.84}{\bullet}Si_{92.2}{\bullet}O_{192}]{\bullet}H_2O_{14.5}{\bullet}TPAOH_{2.3}$
ZAS-50	$Na_{1.85}[Al_{1.90}{\bullet}Si_{94.1}{\bullet}O_{192}]{\bullet}H_2O_{13.1}{\bullet}TPAOH_{2.6}$
ZAS-75	$Na_{1.20}[Al_{1.29}{\bullet}Si_{94.7}{\bullet}O_{192}]{\bullet}H_2O_{12.5}{\bullet}TPAOH_{3.1}$
ZAS-100	$Na_{0.88}[Al_{0.96}{\bullet}Si_{95.0}{\bullet}O_{192}]{\bullet}H_2O_{11.2}{\bullet}TPAOH_{3.5}$

Table 4.7 contains the elemental analysis results of calcined zeolites (ZC) together with their Si/Al molar ratios and unit cell composition. The weight percent silicon increases while weight percent aluminum decreases with increase in Si/Al ratio of the zeolites. The quantities of silicon and aluminum were greater in calcined zeolites compared to as-synthesized zeolites. This is because the TPAOH removal increases the weight percent of these elements.

Table 4.7. Elemental analysis and unit cell composition of calcined and ion-exchanged zeolites.

Zeolite Type	Silicon wt%	Aluminum wt%	Silicon mole	Aluminum mole	Si/Al molar ratio
ZC-10	40.9	4.01	1.46	0.15	9.7
ZC-15	41.6	2.79	1.48	0.10	14.4
ZC-20	44.8	2.21	1.60	0.08	19.8
ZC-25	45.2	1.80	1.61	0.07	24.0
ZC-50	46.4	0.90	1.65	0.03	49.5
ZC-75	46.6	0.61	1.66	0.02	73.4
ZC-100	47.4	0.46	1.69	0.02	99.0

Zeolite Type	Unit Cell Composition
ZC-10	$Na_{8.81}[Al_{8.90}{\cdot}Si_{87.1}{\cdot}O_{192}]{\cdot}H_2O_{20.5}$
ZC-15	$Na_{6.19}[Al_{6.24}{\cdot}Si_{89.8}{\cdot}O_{192}]{\cdot}H_2O_{18.9}$
ZC-20	$Na_{4.61}[Al_{4.69}{\cdot}Si_{91.3}{\cdot}O_{192}]{\cdot}H_2O_{17.8}$
ZC-25	$Na_{3.79}[Al_{3.84}{\cdot}Si_{92.2}{\cdot}O_{192}]{\cdot}H_2O_{14.5}$
ZC-50	$Na_{1.85}[Al_{1.90}{\cdot}Si_{94.1}{\cdot}O_{192}]{\cdot}H_2O_{13.1}$
ZC-75	$Na_{1.20}[Al_{1.29}{\cdot}Si_{94.7}{\cdot}O_{192}]{\cdot}H_2O_{12.5}$
ZC-100	$Na_{0.88}[Al_{0.96}{\cdot}Si_{95.0}{\cdot}O_{192}]{\cdot}H_2O_{11.2}$

Zeolite Type	Unit Cell Composition
ZCIC-10	$H_{8.88}{\cdot}Na_{0.02}[Al_{8.90}{\cdot}Si_{87.1}{\cdot}O_{192}]{\cdot}H_2O_{20.5}$
ZCIC-15	$H_{6.21}{\cdot}Na_{0.02}[Al_{6.23}{\cdot}Si_{89.8}{\cdot}O_{192}]{\cdot}H_2O_{18.9}$
ZCIC-20	$H_{4.67}{\cdot}Na_{0.02}[Al_{4.69}{\cdot}Si_{91.3}{\cdot}O_{192}]{\cdot}H_2O_{17.8}$
ZCIC-25	$H_{3.83}{\cdot}Na_{0.01}[Al_{3.84}{\cdot}Si_{92.2}{\cdot}O_{192}]{\cdot}H_2O_{14.5}$
ZCIC-50	$H_{1.89}{\cdot}Na_{0.01}[Al_{1.90}{\cdot}Si_{94.1}{\cdot}O_{192}]{\cdot}H_2O_{13.1}$
ZCIC-75	$H_{1.27}{\cdot}Na_{0.02}[Al_{1.29}{\cdot}Si_{94.7}{\cdot}O_{192}]{\cdot}H_2O_{12.5}$
ZCIC-100	$H_{0.94}{\cdot}Na_{0.02}[Al_{0.96}{\cdot}Si_{95.0}{\cdot}O_{192}]{\cdot}H_2O_{11.2}$

Table 4.7 also shows the unit cell composition of the calcined ion-exchanged zeolites (ZCIC). The difference between these and calcined zeolites is the replacement of sodium ions with hydrogen ions to produce the acid forms of the zeolites. The sodium contents of these zeolites were found to be in the range 5.0×10^{-3} to 7.0×10^{-3} weight percent, which shows that almost all the sodium ions were replaced by hydrogen ions.

The elemental analysis data obtained for isomorphously synthesized and substituted zeolites are given in Table 4.8. These show that boron has been incorporated in the zeolite. MZ-25 is the parent zeolite that was used in the substitution experiments, and it has a Si/Al molar ratio of 25. B-MFI is a synthesized zeolite that contains boron in the structure with a Si/B molar ratio of 10. The data show that during the hydrothermal treatment of the zeolite samples (S-01 to S-04), some of the aluminum was also lost together with silicon. In the zeolites samples obtained by solid state method (S-09 to S-14), boron was not found during elemental analysis. Silicon and aluminum contents were found to decrease thus increasing the Si/Al molar ratio of these samples (S-09 to S-14). This resulted in increasing the Si/Al molar ratio in the modified zeolite.

Table 4.8. Elemental composition and molar ratios of isomorphously boron substituted zeolites.

Sample Designation	Silicon wt%	Aluminum wt%	Boron wt%	Si/Al molar ratio	Si/(Al+B) molar ratio
B-MFI	40.9	0.04	1.56	981	10.1
MZ-25	42.7	1.61	0.00	25.5	25.5
S-01	41.9	1.24	0.02	32.5	31.1
S-02	40.5	1.21	0.02	32.2	30.7
S-03	40.9	1.22	0.03	32.3	30.4
S-04	40.6	1.19	0.03	32.8	30.9
S-09	42.5	1.25	0.00	32.7	32.7
S-10	42.2	1.23	0.00	33.0	33.0
S-11	42.6	1.25	0.00	32.8	32.8
S-12	42.5	1.24	0.00	33.0	33.0
S-13	42.6	1.27	0.00	32.3	32.3
S-14	42.5	1.24	0.00	32.9	32.9
S-15	40.8	1.14	0.00	33.0	34.4
S-16	42.4	1.60	0.00	25.5	25.5
S-17	41.8	1.05	0.00	32.9	38.3

The modification of MZ-25 using sodium carbonate and boric acid (S-15) did not led to boron substitution. Instead, more aluminum was lost from the zeolite structure. The hydrothermal treatment of MZ-25 with aluminum sulfate at 423 K (S-16) provided no

change in the composition of the zeolite but the material turned brownish. The treatment of MZ-25 with ammonium fluoride and aluminum sulfate decreased the aluminum content (S-17). This is because the aluminum present in the zeolite framework reacts with other species in the reaction mixture and produce water soluble compounds which were removed during washing of the sample.

The elemental analysis data obtained for Ga-MFI and isomorphously gallium substituted zeolites are given in Table 4.9 which shows that gallium has been incorporated in the zeolite. The silicon-to-gallium molar ratio of the gel prepared for synthesizing Ga-MFI zeolite was 10, but Ga-MFI synthesized zeolite was found to have a silicon-to-gallium molar ratio of 15.6 which shows that all the gallium present in the gel was not incorporated in the zeolite synthesis. This was probably due to the larger size of gallium compared to boron and aluminum atoms and the difficulty of incorporating it into the zeolite framework. The data also show that during the hydrothermal treatment of the MZ-25 zeolite, some of the aluminum was also lost together with silicon (S05-S08). This resulted in an increase in the Si/Al molar ratio of the modified zeolite. The amount of gallium incorporated in the zeolite was considerably less than that of the boron incorporated due to the larger size of gallium.

Table 4.9. Elemental composition and molar ratios of isomorphously gallium substituted zeolites.

Sample Designation	Silicon wt%	Aluminum wt%	Gallium wt%	Si/Al molar ratio	Si/(Al+Ga) molar ratio
Ga-MFI	25.2	0.03	3.94	621	15.6
S-05	40.9	1.14	0.02	34.5	34.3
S-06	41.1	1.18	0.02	33.5	33.3
S-07	39.1	1.14	0.01	33.0	32.8
S-08	41.1	1.21	0.02	32.6	32.4

The elemental composition of the parent zeolite and the aluminum fluoride-modified zeolites is shown in Table 4.10 together with the Si/Al, Si/F and Al/F molar ratios. The results show that the aluminum fluoride treatment of ZCIC-10 zeolite resulted in an increase in both aluminum and fluoride content and a decrease in silicon content. The aluminum and fluoride contents were found to increase with the increase in the amount of aluminum fluoride used for the treatment. MZ-25 zeolite also showed an increase in aluminum and fluoride content and a decrease in silicon content. Aluminum and fluorine contents were higher in ZCIC-10 as compared to MZ-25. The silicon contents were significantly less in ZCIC-10 zeolite as compared to MZ-25. As a result of increase in aluminum content, the Si/Al molar ratio of aluminum fluoride-modified MZ-25 and ZCIC-10 were decreased significantly. The Al/F molar ratio was found higher for ZCIC-10 compared to MZ-25 as expected due to the higher aluminum content of ZCIC-10 zeolite.

Table 4.10. Elemental composition and molar ratios of aluminum fluoride treated MFI zeolites with parent zeolites

Sample Designation	Silicon wt%	Aluminum wt%	Fluorine wt%	Si/Al molar ratio	Si/F molar ratio	Al/F molar ratio
ZCIC-10	40.9	4.01	<0.02	9.7	-	-
S-19	36.7	6.23	1.39	5.7	17.8	3.2
S-20	34.0	7.23	1.70	4.5	12.6	3.0
S-21	33.7	7.73	1.94	4.2	11.8	2.8
MZ-25	42.7	1.61	<0.02	25.5	-	-
S-22	42.0	3.74	0.47	10.6	59.2	5.6

4.3.6. Surface Area and Pore Structure Determination

Table 4.11 summarizes the results of surface area and pore size determinations for the synthesized zeolites in their ZCIC form, together with their Si/Al molar ratios. The surface area results are plotted in Figure 4.9 and show that the BET and Langmuir surface area increases with increasing Si/Al molar ratio of the zeolites. The T-Plot micropore area was found to decrease with increasing Si/Al ratio of the zeolites. This is because the template loss was greater for zeolites with higher Si/Al ratio than those with lower Si/Al ratios. The single point surface area and BET surface area values are similar, whereas a higher Langmuir surface area was observed. The BET surface area of MZ-25, a commercial MFI zeolite, was found to be 383 $m^2 g^{-1}$. The median pore diameter determined for synthesized zeolites matches very closely that of the standard MFI zeolite and confirms the MFI type structure. The measured BET surface area values indicate that Ga-MFI and B-MFI zeolites have surface area of 300 $m^2 g^{-1}$ and 333 $m^2 g^{-1}$ respectively.

Table 4.11. Surface area and pore structure characterization results of calcined ion-exchanged calcined (ZCIC) zeolites.

Surface Property	Si/Al Molar Ratio						
	10	15	20	25	50	75	100
BET Surface Area(m^2 g^{-1})	321	369	394	420	454	453	442
Langmuir Surface Area(m^2 g^{-1})	424	489	526	558	630	621	612
Single Point Surface Area(m^2 g^{-1})	328	375	400	425	458	455	439
T-Plot Micropore area(m^2 g^{-1})	237	259	282	283	283	224	157
Horvath Kawazoe median pore diameter (Å)	5.1	5.0	5.4	4.9	5.3	6.7	6.0

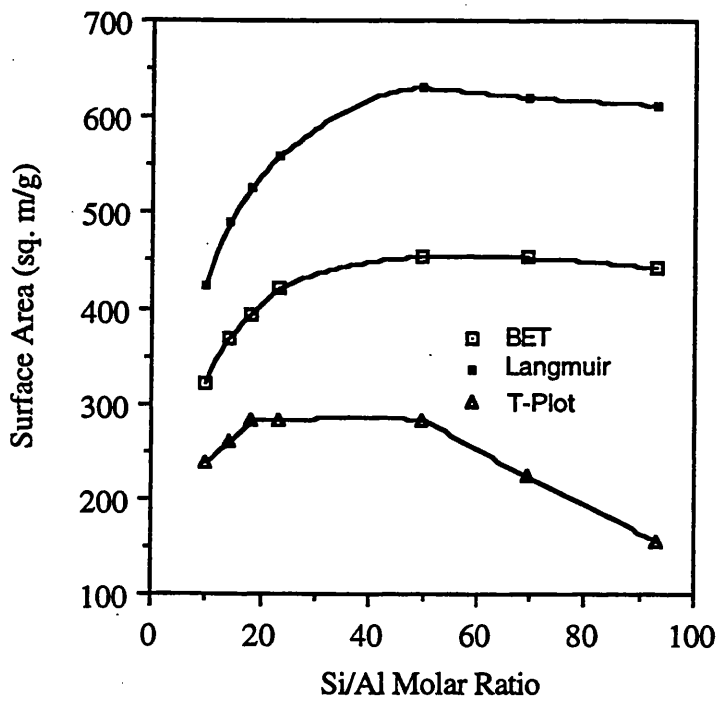

Figure 4.9. Surface area as a function of Si/Al molar ratio of the synthesized zeolites.

4.4. CATALYTIC EVALUATION OF MFI ZEOLITES

4.4.1. Synthesized Aluminosilicate MFI Zeolites

The synthesized zeolites having a Si/Al molar ratio of 10-100 in the calcined and ion-exchanged forms were tested in a packed-bed reactor and the catalytic results obtained are given in Table 4.12. These data are also plotted in Figures 4.10 and 4.11. The results show that MTBE production increases with increase in reaction temperature. The MTBE produced was also found to increase with decrease in Si/Al molar ratio or increase in aluminum content of the zeolites. During this screening of the synthesized zeolites, ZCIC-10 was found the best for catalytic activity giving the maximum MTBE yield, and thus it

was chosen for kinetic study as well as for isomorphous substitution studies aimed at enhancing its activity.

Table 4.12. Catalytic evaluation results obtained for zeolites in a packed-bed reaction system. The reaction conditions were; catalyst weight = 3.5 g, isobutene flow = 11.6 x 10^{-2} mol h^{-1} (6.51 g h^{-1}), methanol flow = 23.4 x 10^{-2} mol h^{-1} (7.49 g h^{-1}), total flow = 35.0 x 10^{-2} mol h^{-1} (14.0 g h^{-1}), WHSV = 4.0 and methanol -to-isobutene molar ratio = 2.0.

Catalyst Type	Temperature K	MTBE Produced mol g^{-1} h^{-1}	MTBE Produced mole h^{-1}	Unreacted Methanol mol h^{-1}	Unreacted Isobutene mol h^{-1}	Percent Isobutene Conversion
ZCIC-10	343	5.0E-03	17.50E-03	21.69E-02	98.60E-03	15.1
ZCIC-15	343	4.8E-03	16.63E-03	21.78E-02	99.48E-03	14.3
ZCIC-20	343	4.3E-03	14.88E-03	21.95E-02	10.12E-02	12.8
ZCIC-25	343	3.5E-03	12.25E-03	22.22E-02	10.39E-02	10.6
ZCIC-50	343	3.0E-03	10.50E-03	22.39E-02	10.56E-02	09.0
ZCIC-75	343	1.8E-03	61.25E-04	22.83E-02	11.00E-02	05.3
ZCIC-100	343	1.0E-03	35.00E-04	23.09E-02	11.26E-02	03.0
ZCIC-10	353	7.5E-03	26.25E-03	20.82E-02	89.85E-03	22.6
ZCIC-15	353	7.1E-03	24.68E-03	20.97E-02	91.43E-03	21.3
ZCIC-20	353	6.8E-03	23.63E-03	21.08E-02	92.48E-03	20.3
ZCIC-25	353	6.3E-03	22.05E-03	21.24E-02	94.05E-03	19.0
ZCIC-50	353	4.5E-03	15.75E-03	21.87E-02	10.04E-02	13.6
ZCIC-75	353	2.7E-03	94.50E-04	22.50E-02	10.67E-02	08.1
ZCIC-100	353	1.8E-03	63.00E-04	22.81E-02	10.98E-02	05.4
ZCIC-10	363	1.4E-02	50.40E-03	18.40E-02	65.70E-03	43.4
ZCIC-15	363	1.4E-02	47.60E-03	18.68E-02	68.50E-03	41.0
ZCIC-20	363	1.3E-02	44.80E-03	18.96E-02	71.30E-03	38.6
ZCIC-25	363	1.2E-02	40.60E-03	19.38E-02	75.50E-03	35.0
ZCIC-50	363	8.2E-03	28.70E-03	20.57E-02	87.40E-03	24.7
ZCIC-75	363	4.8E-03	16.80E-03	21.76E-02	99.30E-03	14.5
ZCIC-100	363	2.8E-03	98.00E-04	22.46E-02	10.63E-02	08.4
ZCIC-10	373	2.3E-02	80.08E-03	15.43E-02	36.02E-03	69.0
ZCIC-15	373	2.2E-02	77.00E-03	15.74E-02	39.10E-03	66.3
ZCIC-20	373	2.1E-02	74.69E-03	15.97E-02	41.41E-03	64.3
ZCIC-25	373	2.0E-02	70.84E-03	16.36E-02	45.26E-03	61.0
ZCIC-50	373	1.4E-02	50.05E-03	18.44E-02	66.05E-03	43.1
ZCIC-75	373	9.7E-03	33.88E-03	20.05E-02	82.22E-03	29.2
ZCIC-100	373	5.5E-03	19.25E-03	21.52E-02	96.85E-03	16.6

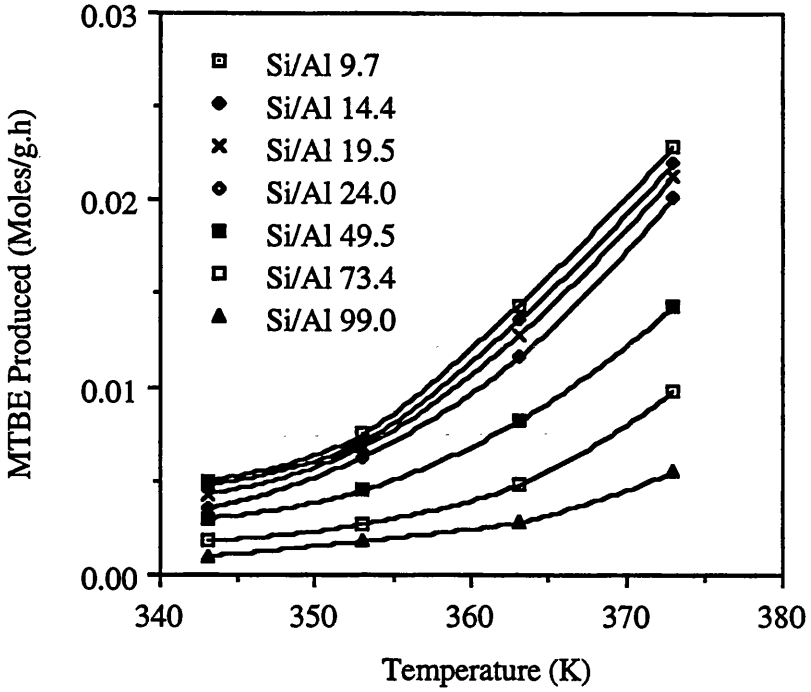

Figure 4.10. MTBE produced as a function of reaction temperature.

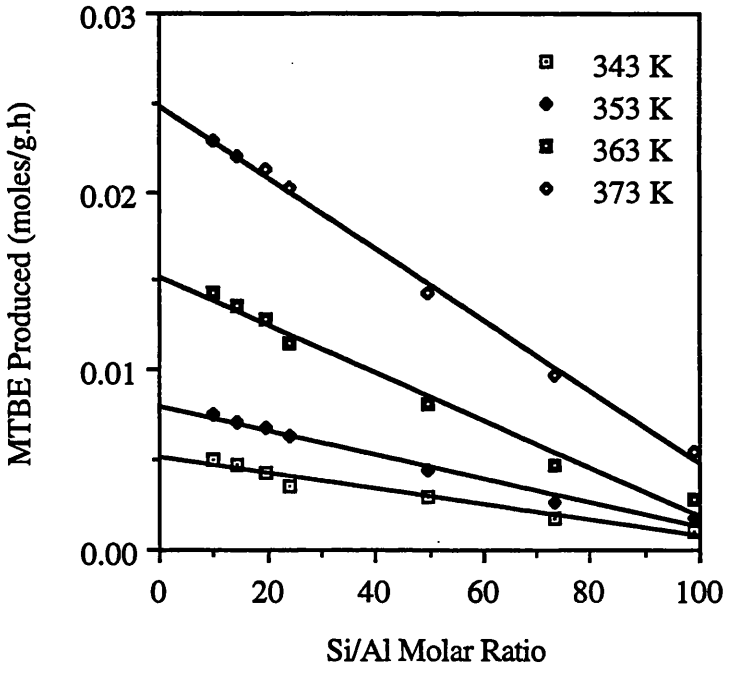

Figure 4.11. MTBE produced as a function of Si/Al molar ratio of the zeolites.

4.4.2. Isomorphously Substituted MFI Zeolites

The catalytic evaluation results of the isomorphously substituted MFI zeolites for the reaction of methanol and isobutene to produce MTBE are shown in Table 4.13. It was observed that the activity of the substituted zeolites (S01-S14) was lower than the parent MZ-25 zeolite. The decrease in catalytic activity of the substituted zeolites was due to the loss of aluminum from the framework during the thermal treatment, although the

substitution of gallium and boron was achieved to some extent. This results in the decrease of the acidity and activity of the substituted zeolites. This was observed from the elemental analysis results of the parent and substituted zeolites (Table 4.8). The loss of aluminum was due to the presence of fluoride ion in the system which has high affinity for aluminum. It has been reported that fluorination of ZSM-5 and other types of zeolite is accompanied with the loss of substantial amount of aluminum. The degree of dealumination is found to be directly proportional to the fluorine content of the substituted zeolites [Becker and Kowalek, 1989; Lok et al., 1982]. If only silicon loss had occurred with no loss in aluminum on substitution of boron or gallium, the substituted zeolites would be expected to exhibit increased activity. The Brönsted acidity of the zeolites are expected to follow the following trend:

$$Si(OH)Si < B(OH)Si < Ga(OH)Si < Al(OH)Si$$

This is due to the increasing strength of the T-O bond, which increases the positive charge on the proton of the O-H bond. The treatment of MZ-25 first with sodium carbonate and then with boric acid (S-15) did not increase the activity of the zeolite. This was due to the removal of aluminum from the zeolite framework although some amount of boron was substituted. A similar trend has been found in the literature for substitution of boron and gallium in ZSM-5 zeolite. Derouane et al., 1985 have found that post-synthesized incorporation of boron was accompanied with a decrease in the aluminum contents of ZSM-5 zeolites. Similarly, Sayed et al., [1989] studied the effect of boron incorporation in ZSM-5 zeolites and found that boron substitution resulted in the decrease in activity for acid type reactions due to the removal of aluminum from the framework. Coudurier and Vedrine [1986] have shown that impregnation of aluminum containing pentasil zeolites with boric acid and their further calcination at 773 K results in partial substitution of lattice aluminum by boron and therefore the aluminum contents were decreased. Gallium substitution has also been reported in pure silicalite using impregnation technique [Lalik et al., 1992]. MAS NMR technique indicated the presence of gallium in the zeolite framework but aluminum content data of the substituted zeolites was not reported. The treatment of MZ-25 with aluminum sulfate decreased the activity of the catalyst perhaps due to the deactivation of the active sites by the presence of sulfur species in the reaction mixture (S-16 to S-17).

Another technique used to enhance the activity of the zeolites involves the chlorination or fluorination of a zeolite. The catalytic reactions carried out show that treatment of ZCIC-10 with aluminum chloride slightly increased the activity of the zeolite (S-18). The treatment of the ZCIC-10 with aluminum fluoride significantly improved the activity of the catalyst. Increasing the aluminum fluoride concentration of the treating solution from 0.33 to 0.66 g per 50 cm^3, further increased the activity of the zeolites (S-19 to S-20). Increasing still further the concentration of aluminum fluoride to 1.0 gram per 50 cm^3 of the solution did

not significantly increase the yield of MTBE (S-21). The treatment of MZ-25 with aluminum fluoride (S-22) also increased the activity of the catalyst, but not as much as was observed for ZCIC-10 zeolite (S-21). Salts of fluoride have been found to increase the activity of the zeolites [Becker and Kowalak, 1989]. It has been suggested that during fluorination, some of the surface hydroxyl groups are replaced by fluorine and the acidity of the remaining OH groups is enhanced by the inductive effect of the fluorine. The inductive effect of fluorine linked to aluminum weakens the O-H bond in the bridging O-H group thereby enhancing their acidity [Gosh and Kydd, 1985]. Further fluorination of the zeolite results in dealumination which then exists as non-framework aluminum fluoride containing hydroxide, such as $AlF_X(OH)_Y$ [Fishel, 1968]. The activity of the zeolite was increased due to the presence of these active aluminum fluoride containing hydroxide species. Pure aluminum fluoride was also tested as a catalyst in the batch reactor but it showed no activity for the formation of MTBE from methanol and isobutene. The hydrothermal treatment of MFI zeolite with aluminum fluoride was found to be a suitable method for enhancing the activity of the zeolites for the reaction of methanol and isobutene to produce MTBE. The mechanisms of fluorination followed by dehydroxylation and dealumination is illustrated by the following reactions:

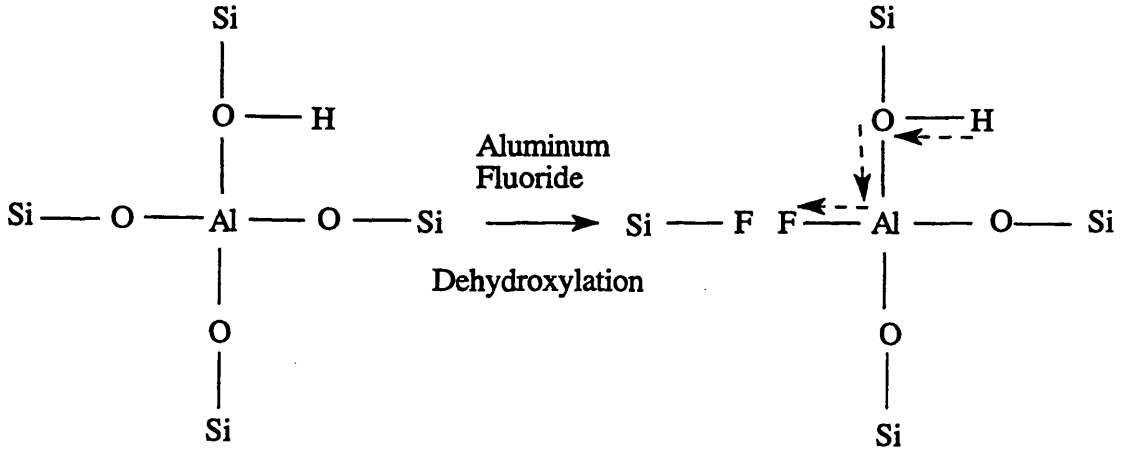

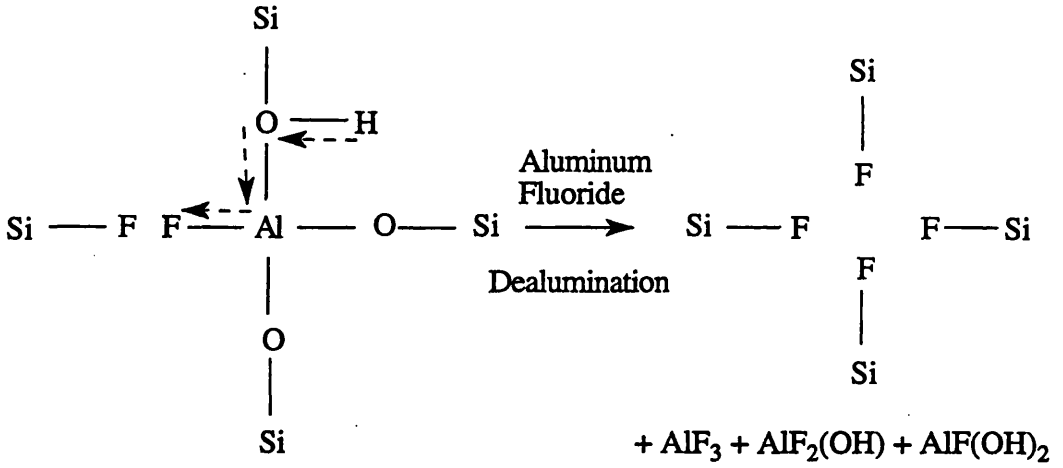

Table 4.13. Catalytic evaluation results of the synthesized and isomorphously substituted zeolites at 353 K reaction temperature.

Zeolite Sample Designation	MTBE Produced, mol g^{-1} h^{-1}
Isomorphously Synthesized Zeolites	
B-MFI	6.5E-03
Ga-MFI	3.1E-03
Parent Zeolites	
ZCIC-10	7.4E-03
MZ-25	7.0E-03
Isomorphously Substituted Zeolites	
S-01	6.8E-03
S-02	6.9E-03
S-03	6.7E-03
S-04	6.5E-03
S-05	5.5E-03
S-06	5.8E-03
S-07	5.1E-03
S-08	5.6E-03
S-09	6.7E-03
S-10	6.7E-03
S-11	6.6E-03
S-12	6.5E-03
S-13	6.6E-03
S-14	6.4E-03
S-15	5.2E-03
S-16	1.8E-03
S-17	2.5E-03
S-18	9.8E-03
S-19	22.3E-03
S-20	32.2E-03
S-21	32.4E-03
S-22	11.7E-03

4.5. DETERMINATION OF INTRINSIC KINETICS

4.5.1. Optimization of Reaction Variables

4.5.1.1. Effect of Stirring Speed on the Rate of Reaction

The concentrations of MTBE obtained were plotted against time at three different agitation speeds, 600, 800 and 1000 rpm, and polynomials were obtained which provided a best fit for the data (Figure 4.12). These polynomials were differentiated with respect to time and the initial rates of the reaction were obtained. The initial rates were plotted against the stirring speed as shown in Figure 4.13. This shows that the initial rates increased with increasing stirring speed from 600 to 1000 rpm. The increase in the rate of reaction from 800 to 1000 rpm was relatively small. If the reaction had been carried out above 1000 rpm, very little or no increase in the initial rates would be expected. On this basis, the stirrer speed of 1000 rpm was selected to obtain reaction data uninhibited by fluid to solid mass transfer effects. This stirrer speed was used for the zeolite having particle size less than 0.05 mm. Subraminium and Bhatia [1987] conducted the liquid phase synthesis of MTBE from methanol and isobutene in a batch reactor utilizing 15.0 grams of catalyst and a stirrer speed of 650 rpm in order to produce kinetic data free from mass transfer effects. Al-Jarallah et al., [1988] employed 12.4 grams of catalyst which produced the highest initial rate in the liquid phase synthesis of MTBE from methanol and isobutene in a batch reactor. They used this amount of catalyst and a stirrer speed of 600 rpm to exclude mass transfer effects and to obtained data for kinetic modeling of the reaction. In this work, a stirrer speed of 1000 rpm was employed to exclude any mass transfer effect. This stirring rate was much higher than those used by the other investigators. The catalyst used in our study had a particle size less than 0.05 mm compared to 0.20 to 0.40 mm particle size range used by other investigators [Al-Jarallah et al., 1988; Subraminium and Bhatia, 1987].

4.5.1.2. Effect of Catalyst Amount on the Rate of Reaction

It has been shown that for small particle sized catalysts (less than 0.05 mm) and at relatively high stirring speed (1000 rpm), the reaction is neither influenced by intraparticle diffusion nor interparticle mass transfer. The inference drawn from the above set of experiments is that the reaction is occurring in the chemical control regime. In turn, this means that the rate of reaction should be directly proportional to the catalyst surface area and therefore directly proportional to the mass of the catalyst loaded in the reactor. Figures 4.14 and 4.15, in which the rate of reactions are plotted as a function of amount of catalysts loaded, demonstrate that indeed this is the case for two different initial concentrations of the reactants.

4.5.1.3. Effect of MTBE addition on the Product Formation

The MTBE concentration obtained with and without MTBE addition to the reaction mixture was plotted against reaction time at each temperature. The results showed that in the presence of MTBE, the MTBE concentration decreased in the temperatures range 343 to 373 K (Figures 4.16-4.19). This was because MTBE is the product of the reaction and it is desorbed from the catalyst site after it is formed. When MTBE was present in the reaction mixture before the reaction, some of the active sites were already occupied by MTBE and were not available for the reaction. This resulted in the decrease of active sites and thus a decrease in the rate of the reaction and reduced MTBE concentration in the reaction product.

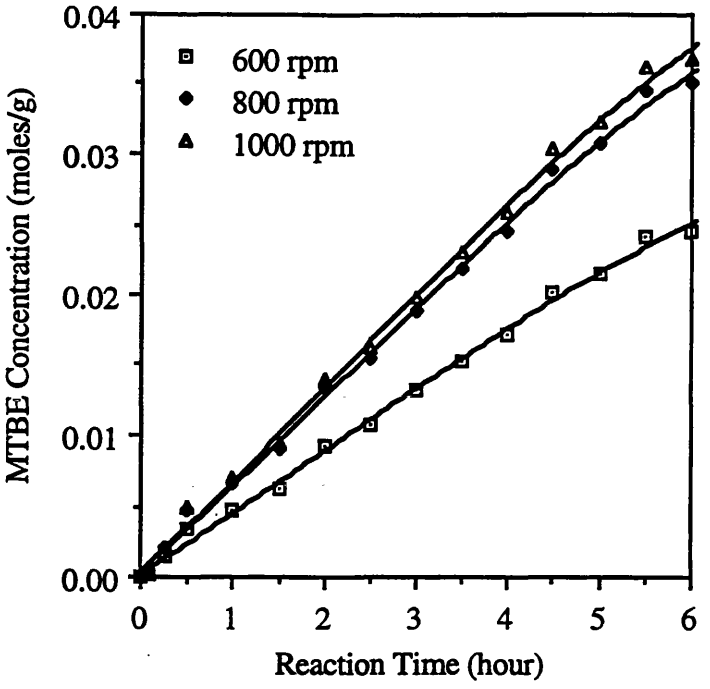

Figure 4.12. Plot of MTBE concentration as a function of reaction time at different stirring speed.

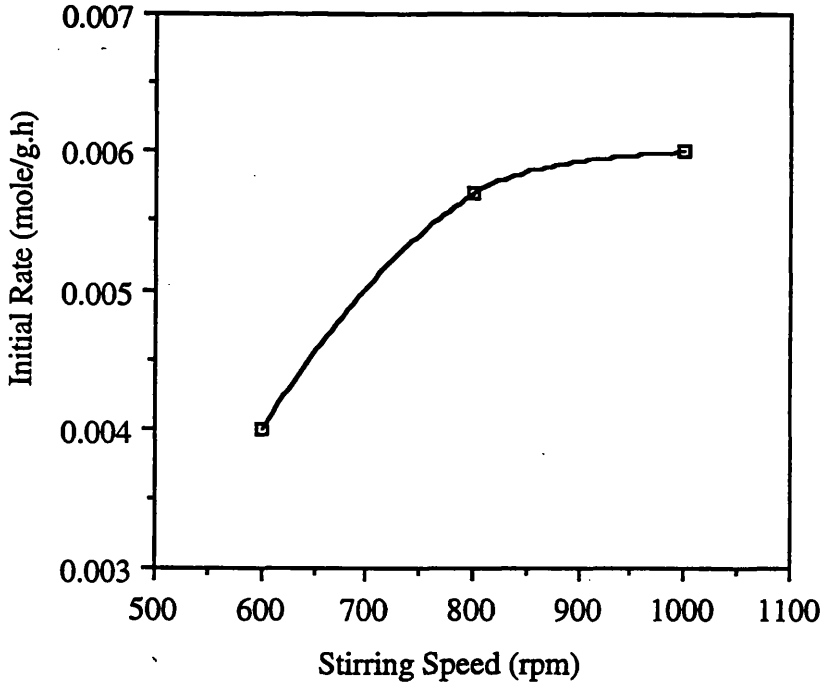

Figure 4.13. Plot of Initial rate as a function of stirring speed.

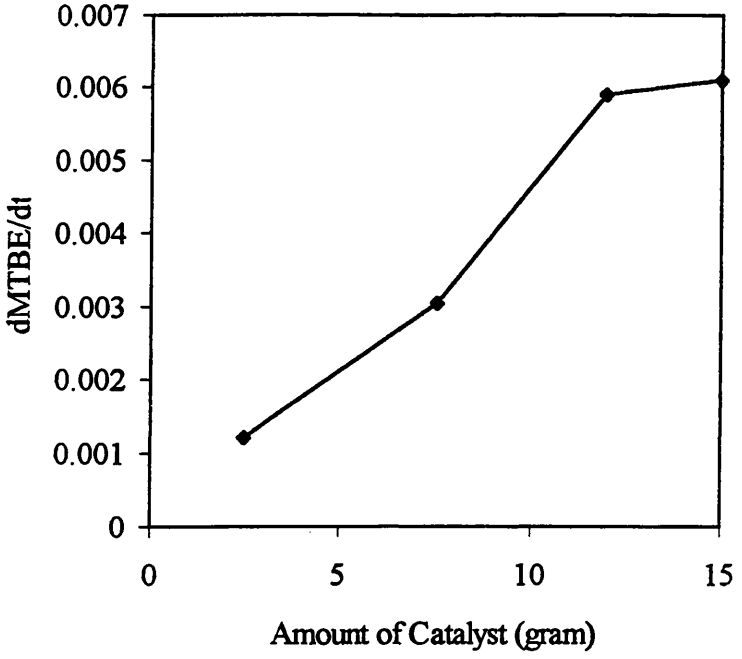

Figure 4.14. Plot of rate of reaction as a function of amount of catalyst. The initial amount of isobutene was 119 grams (2.13 moles).

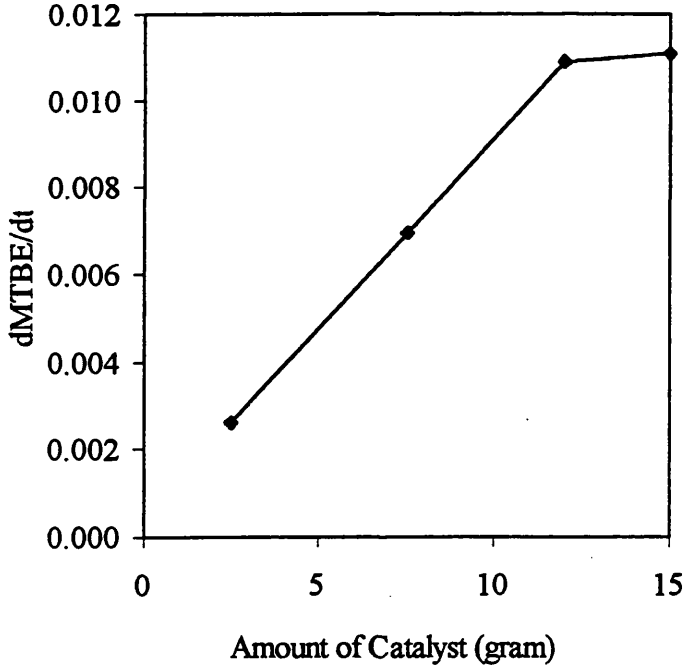

Figure 4.15. Plot of rate of reaction as a function of amount of catalyst. The initial amount of isobutene was 200 grams (3.58 moles).

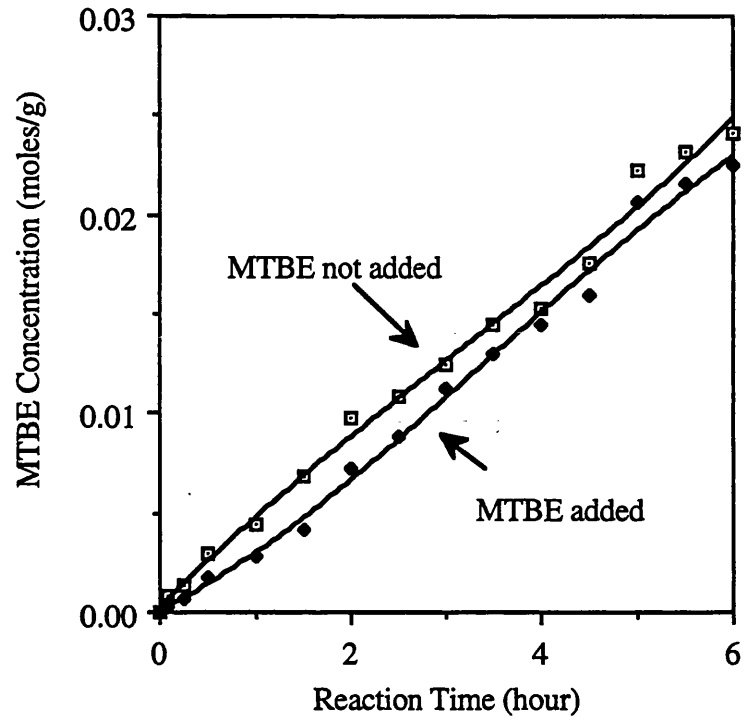

Figure 4.16. Plot of MTBE concentration as a function of reaction time at 343 K reaction temperature.

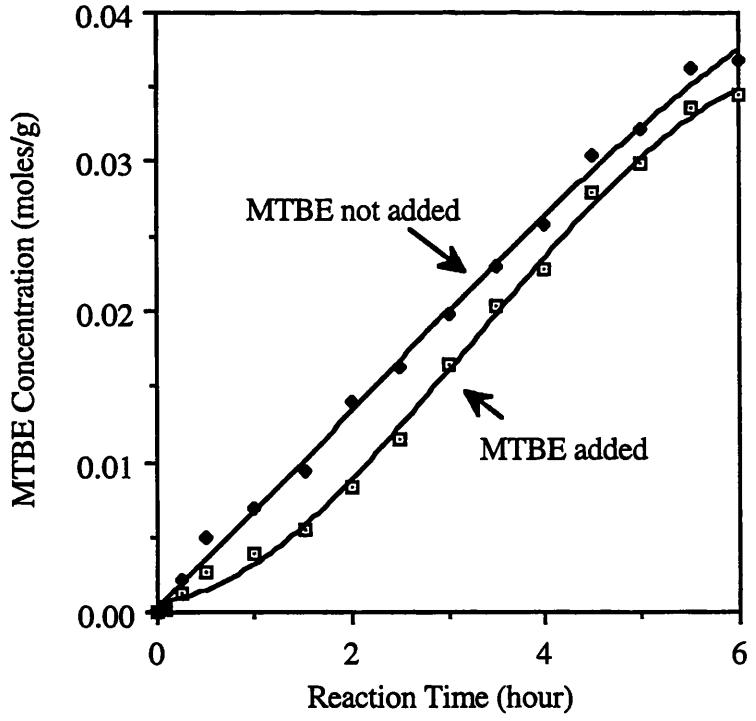

Figure 4.17. Plot of MTBE concentration as a function of reaction time at 353 K reaction temperature.

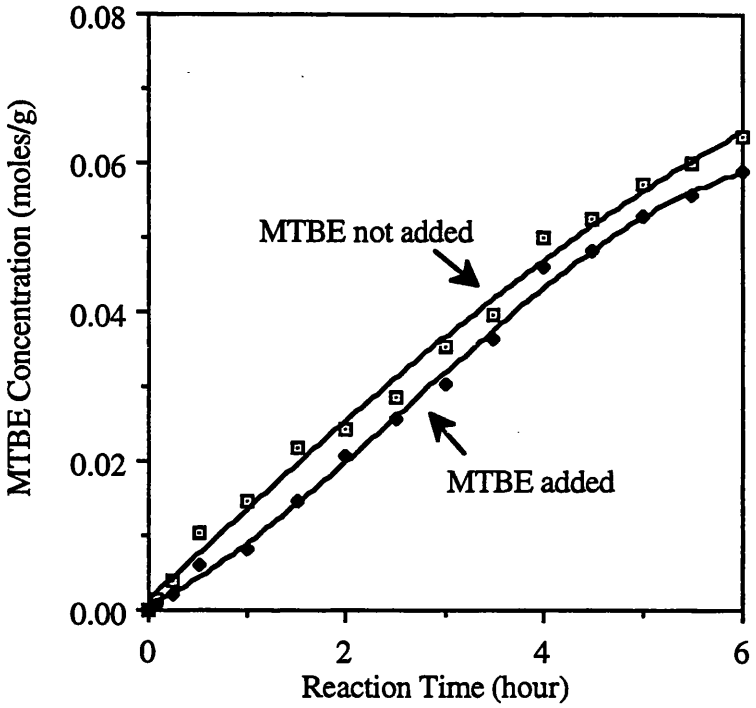

Figure 4.18. Plot of MTBE concentration as a function of reaction time at 363 K reaction temperature.

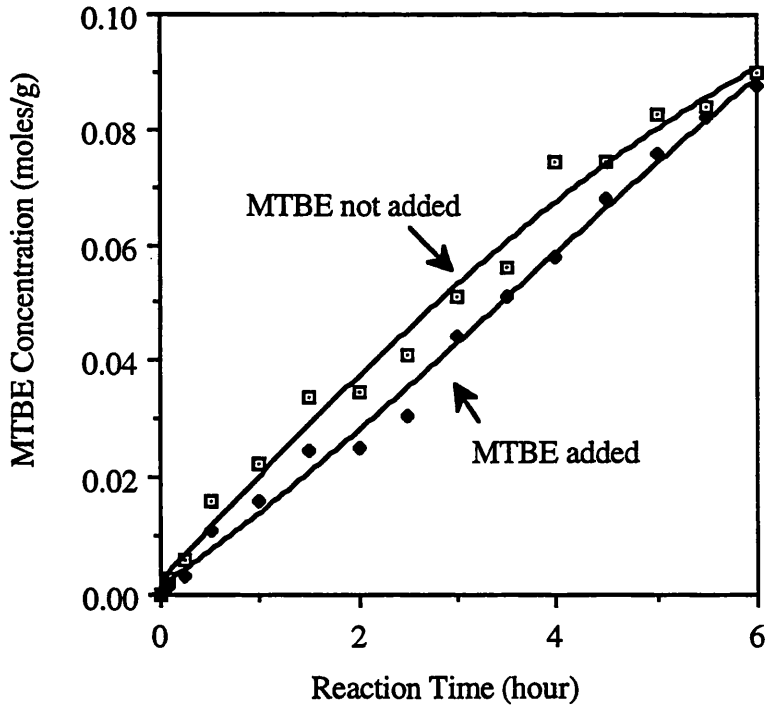

Figure 4.19. Plot of MTBE concentration as a function of reaction time at 373 K reaction temperature.

4.5.2. Determination of Order of Reaction using Initial Rate Method

The orders of reaction in the model equations are unknown and these had first to be determined before proceeding to curve fitting the experimental data. To determine the order of reaction with respect to individual components, one of the two reactants was used in excess in the reaction such that the concentration of that reactant remains virtually constant. The reaction of methanol (A) and isobutene (B) to produce MTBE (C) can be represented as follows:

$$aA + bB = cC$$

where a, b and c denote the order of reaction with respect to methanol, isobutene and MTBE respectively. The rate expression can be written as

$$Rate = \frac{dC_c}{dt} = k_+ C_A^a C_B^b - k_- C_C^c \qquad \text{(i)}$$

where k_+ and the k_- are forward and reverse reaction rate constants respectively and C_A, C_B and C_C are the concentrations (mol g^{-1}) of methanol, isobutene and MTBE respectively. At time zero, the rate is called initial rate and is given by the following equation:

$$\text{Initial Rate} = \left[\frac{dC_c}{dt}\right]_{t=0} = k_+ C_A^a C_B^b \qquad \text{(ii)}$$

In the logarithmic term, the equation can be written as follows:

$$\text{Log [Initial Rate]} = Log\left[\frac{dC_c}{dt}\right]_{t=0} = Logk_+ + aLogC_A + bLogC_B \qquad \text{(iii)}$$

If the reactant A is taken in excess such that $C_A >> C_B$ then the change in the concentration of A will be negligible as compared to reactant B. In such a case, the concentration of A remains constant and the above equation can be rewritten as

$$\text{Log [Initial Rate]} = Log\left[\frac{dC_c}{dt}\right]_{t=0} = Logk'' + bLogC_B \qquad \text{(iv)}$$

In this equation, a plot of log [Initial Rate] vs. log C_B will yield a slope b which is the order of reaction with respect to reactant B.

Similarly, if we use an excess amount of reactant B such that $C_B >> C_A$, then the above equation will take the form:

$$\text{Log [Initial Rate]} = Log\left[\frac{dC_e}{dt}\right]_{t=0} = Logk''' + aLogC_A \qquad \text{(v)}$$

In this case, a plot of log [Initial Rate] vs. log C_A will yield a slope that is the order of reaction with respect to reactant A.

4.5.2.1 Determination of Order of Reaction for Isobutene

The concentration of the MTBE obtained at different temperatures and isobutene concentrations was plotted against time to obtain polynomials that were differentiated with respect to time and initial rates were calculated (Table 4.14). A plot of log of initial rate against log of initial concentration of isobutene was obtained whose slope was the order of the reaction with respect to isobutene (Figure 4.20). The slopes obtained were 0.94, 0.98, 0.97 and 0.91 at 343, 353, 363 and 373 K reaction temperatures respectively showing that the reaction is first order with respect to isobutene in the temperature range 343 to 373 K.

Table 4.14. The initial rate and isobutene concentration data at 343-373 K. The concentration of methanol was 28.3 x 10^{-2} mol g^{-1} for all reaction runs.

Methanol-to-Isobutene ratio	Initial conc. of isobutene (mol g^{-1})	Initial Rates (mol g^{-1} h^{-1})			
		343 K	353 K	363 K	373 K
26.7	10.6E-03	2.5E-03	5.2E-03	10.5E-03	15.0E-03
40.4	7.0E-03	1.8E-03	3.9E-03	7.9E-03	11.2E-03
80.9	3.5E-03	0.9E-03	1.8E-03	3.7E-03	5.6E-03

4.5.2.2. Determination of Order of Reaction for Methanol

In determining the order of reaction for methanol, the amount of methanol was reduced while that of isobutene was increased to have a concentration of isobutene at least 10 times compared to methanol. Due to the presence of a large amount of isobutene and catalyst, an undesired side reaction of isobutene dimerization was observed, which affected the selectivity of MTBE formation. For this reason, the amount of the catalyst was reduced to 1.5 grams so that isobutene dimerization was minimized. The appreciable increase in the concentration of products other than MTBE would lead to inaccuracy in the determination of the order of reaction for methanol. The concentration of the MTBE was plotted as a function of time to obtain a third degree polynomial that was differentiated with respect to time, and the initial rates were calculated for all three isobutene-to-methanol molar ratios (Table 4.15). A plot of log initial rate vs. log of initial concentration of methanol was obtained (Figure 4.21) whose slope was the order of reaction with respect to methanol. The order of reaction obtained with respect to methanol were 0.94, 0.96, 0.90 and 0.95 at

343, 353, 363 and 373 K temperatures respectively showing that the reaction is first order with respect to methanol in the temperature range 343 to 373 K.

Table 4.15. The initial rate and methanol concentration data at 343-373 K. The isobutene concentration in the in the reaction mixture was 10 mol g^{-1} and the amount of catalyst was 1.5 grams.

Isobutene-to Methanol ratio	Initial conc. of methanol (mol g^{-1})	Initial Rates (mol g^{-1} h^{-1}) 343 K	353 K	363 K	373 K
10	1.0	2.5E-03	5.3E-03	11.5E-03	15.0E-03
12.1	0.83	2.0E-03	4.5E-03	9.8E-03	12.3E-03
14.9	0.67	1.7E-03	3.6E-03	8.0E-03	10.2E-03

4.5.3. Effect of Temperature on the Rate of Reaction

The reaction data were obtained to the point at which the reaction reached equilibrium. The MTBE, isobutene and methanol concentration obtained at 343, 353, 363 and 373 K temperatures were plotted versus time as shown in Figures 4.22 to 4.25 which illustrates that MTBE concentration increase while the isobutene and methanol concentration were decreased in the reaction mixture with the passage of time. The percent isobutene conversion was found to increase with increasing reaction time for all temperatures but the equilibrium concentration of MTBE was found to decrease at higher temperature (Figure 4.26). The initial rates of reaction were observed to increase at higher temperature (Figure 4.27). The data for all three components, methanol, isobutene and MTBE were fitted by polynomials. A polynomial was obtained for each component at all four temperatures. These polynomials were used to obtain values of concentrations of the three components (C_A, C_B and C_C) at different times (t). The polynomial obtained for MTBE (mol g^{-1} h^{-1}) at 343 to 373 K are given below:

At 343 K,

$$MTBE = 4.94 \times 10^{-4} + 4.10 \times 10^{-3}\, t - 1.63 \times 10^{-5}\, t^2 - 2.19 \times 10^{-7}\, t^3 \quad \text{(vi)}$$

At 353 K,

$$MTBE = 4.05 \times 10^{-4} + 6.80 \times 10^{-3}\, t - 7.93 \times 10^{-5}\, t^2 - 3.68 \times 10^{-7}\, t^3 \quad \text{(vii)}$$

At 363 K,

$$MTBE = 1.50 \times 10^{-3} + 1.24 \times 10^{-2}\, t - 3.51 \times 10^{-4}\, t^2 + 3.04 \times 10^{-6}\, t^3 \quad \text{(viii)}$$

At 373 K,

$$MTBE = 2.20 \times 10^{-3} + 1.93 \times 10^{-2}\, t - 7.90 \times 10^{-4}\, t^2 + 8.04 \times 10^{-6}\, t^3 \quad \text{(ix)}$$

These polynomials were differentiated with respect to time in order to calculate the rate of reaction (dMTBE/dt). The values of the thermodynamic equilibrium constant (K_e) of the reaction at different temperatures were determined by the following equation.

$$\ln K_e = 7300/T - 4.75 \ln T + 1.17 \times 10^{-2}\ T - 4.8 \times 10^{-6}\ T^2 + 2.5 \times 10^{-9}\ T^3 + 4.8 \quad (x)$$

This equation has been used by a number of researchers (Tejero et al., 1988, Tejero et al., 1989; Chang et al., 1992). A plot of thermodynamic equilibrium constant as a function of reaction temperature is shown in Figure 4.28. This shows that K_e decreases with increase in reaction temperature.

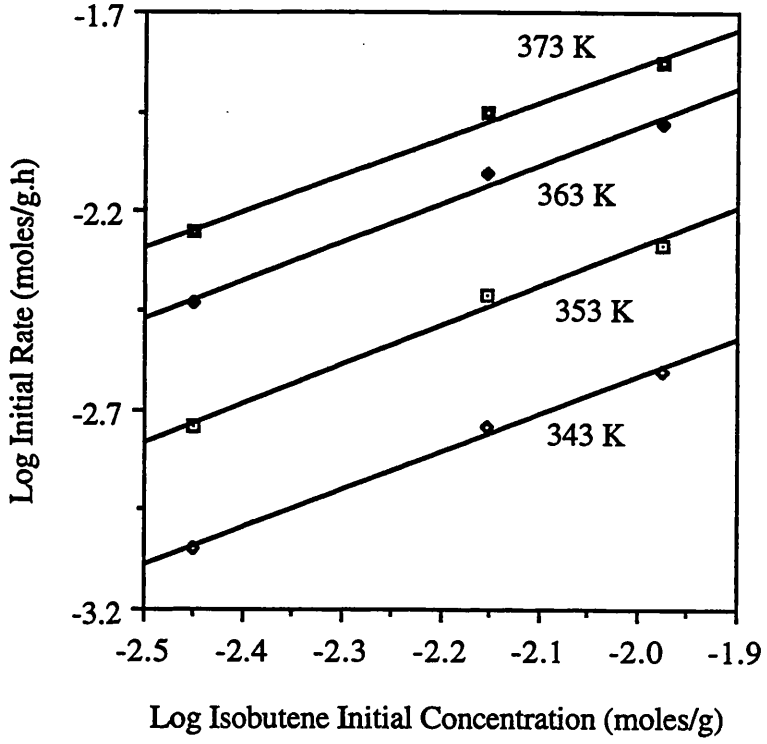

Figure 4.20. Plot of initial rate as a function of initial isobutene concentration at 343-373 K.

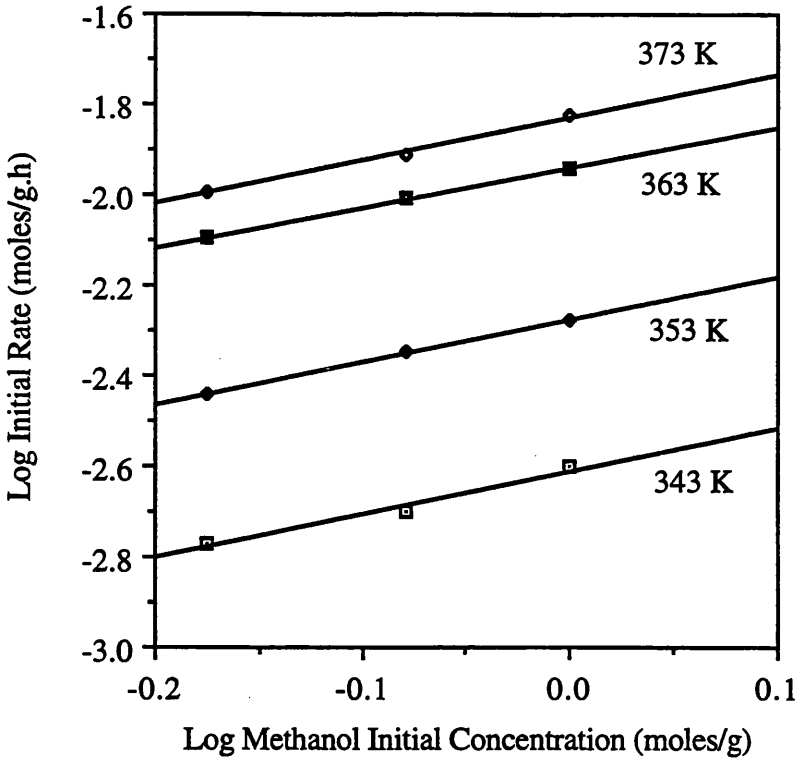

Figure 4.21. Plot of initial rate as a function of initial methanol concentration at 343-373 K.

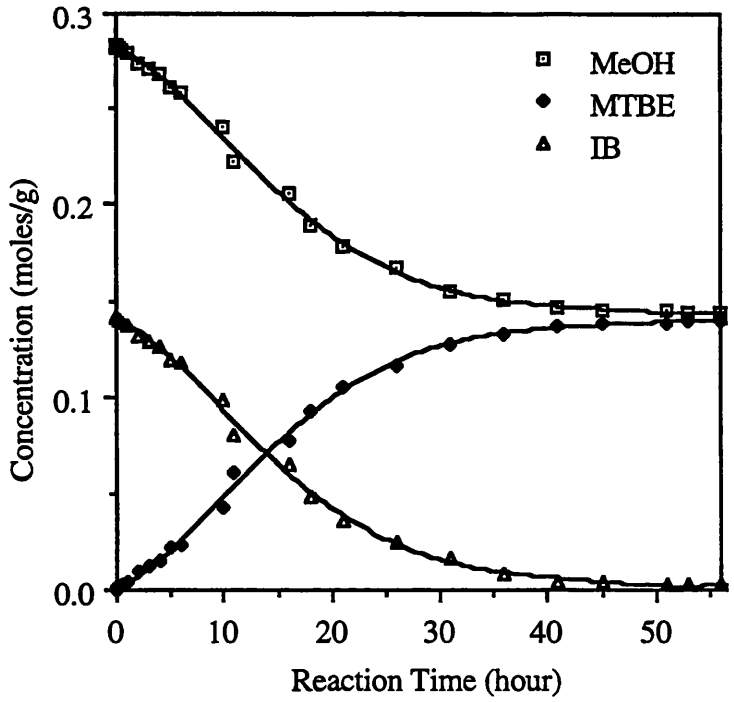

Figure 4.22. Plot of concentration of methanol, isobutene and MTBE in the reaction mixture as a function of reaction time at 343 K.

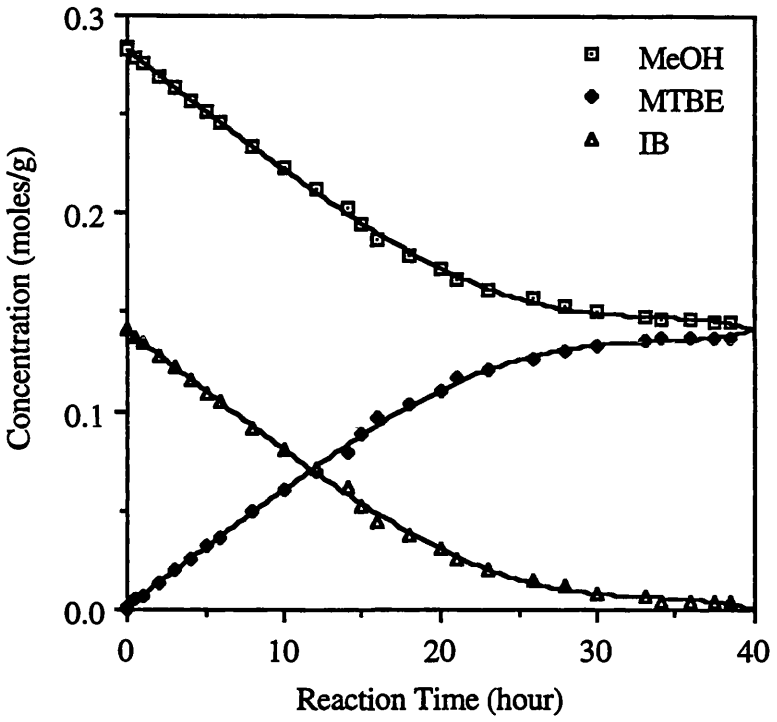

Figure 4.23. Plot of concentration of methanol, isobutene and MTBE in the reaction mixture as a function of reaction time at 353 K.

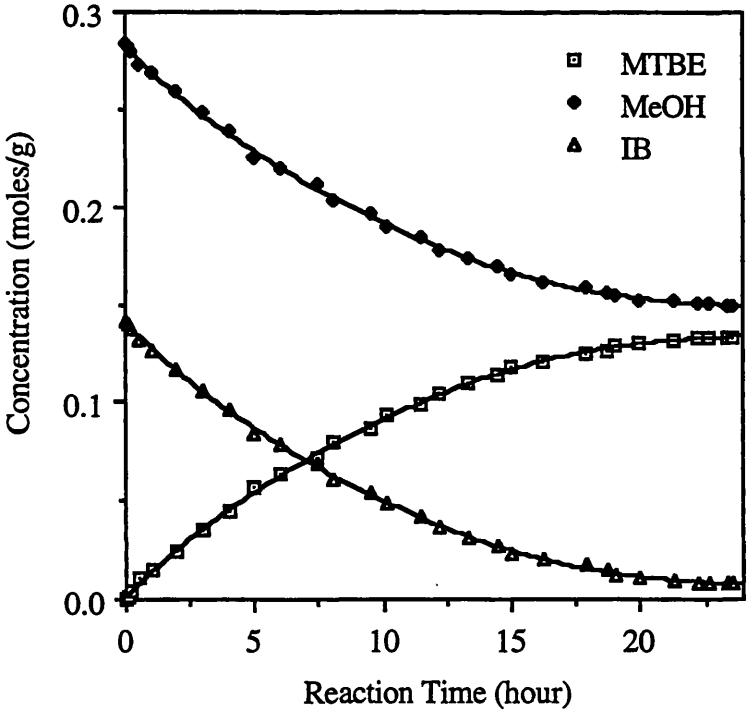

Figure 4.24. Plot of concentration of methanol, isobutene and MTBE in the reaction mixture as a function of reaction time at 363 K.

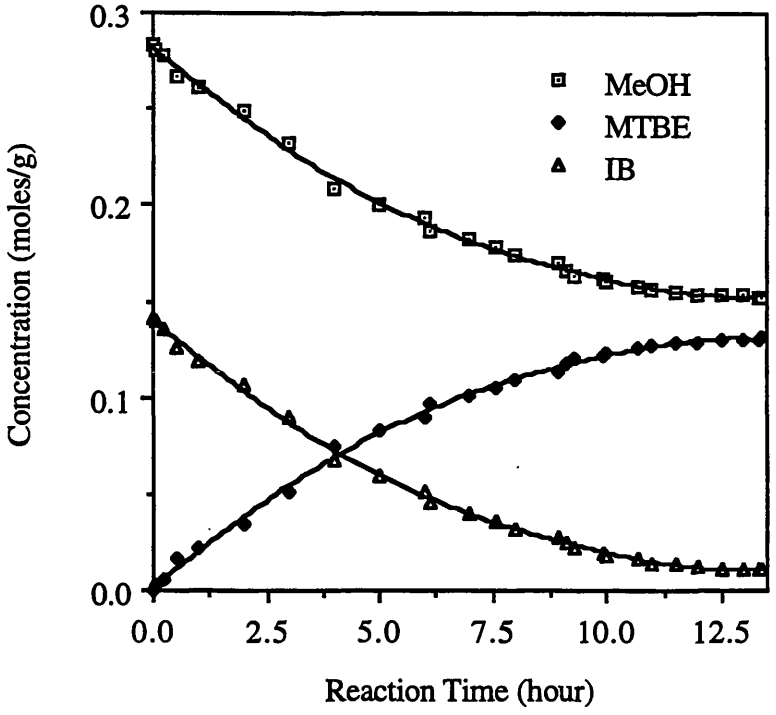

Figure 4.25. Plot of concentration of methanol, isobutene and MTBE in the reaction mixture as a function of reaction time at 373 K.

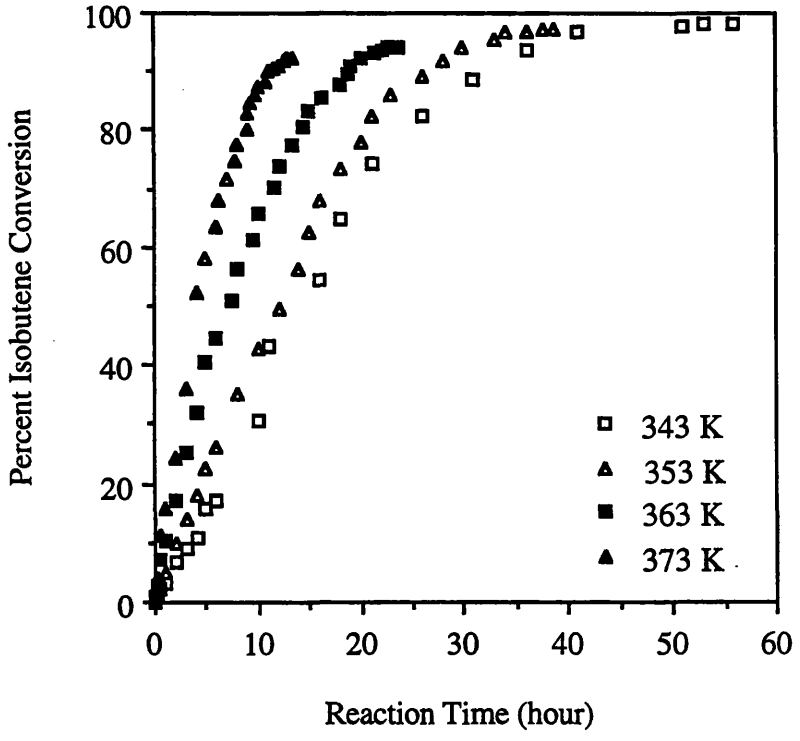

Figure 4.26. Plot of isobutene conversion as a function of reaction time in the temperature range 343 to 373 K.

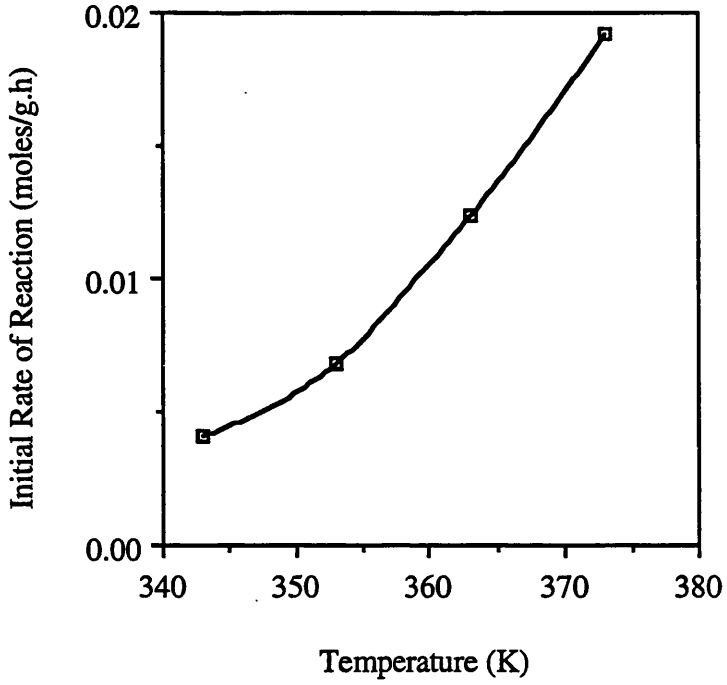

Figure 4.27. Plot of initial rate of reaction as a function of temperature in the range 343 to 373 K.

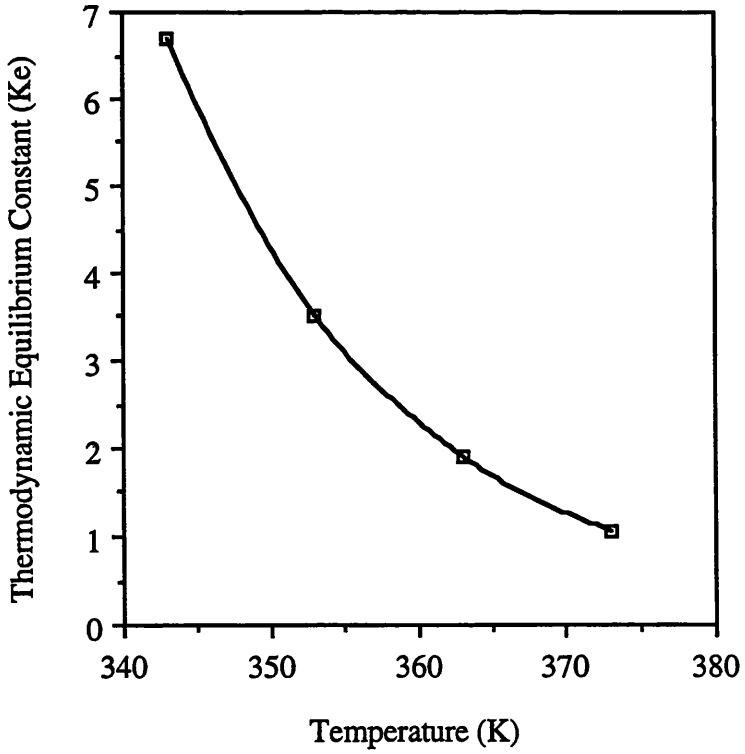

Figure 4.28. Plot of thermodynamic equilibrium constant as a function of reaction temperature.

4.5.4. Kinetic Modelling of the Reaction

The reaction of isobutene and methanol can be represented by the following equation:

$$A + B = C$$

where A, B and C stand for methanol, isobutene and MTBE respectively. The overall process by which this reaction proceeds, can be broken down into the sequence of individual steps described as follows:

1. Mass transfer of the reactants (methanol and isobutene) from the bulk of the fluid to the external surface of the zeolite catalyst particles.

2. Diffusion of the reactants (methanol and isobutene) from the zeolite pore mouth through the catalyst pores to the immediate vicinity of the internal catalytic surface.

3. Adsorption of the reactants (methanol or isobutene or both) onto the catalyst surface.

4. Reaction of the reactants (methanol and isobutene) on the catalyst surface.

5. Desorption of the product (MTBE) from the surface.

6. Diffusion of the product (MTBE) from the surface to the zeolite pore mouth through the catalyst pores at the external surface of zeolite particles.

7. Mass transfer of the product (MTBE) from the external surface of the zeolite catalyst particles to the bulk of the fluid.

These steps show the complexity of the reaction involved in a heterogeneous chemical reaction. Even if the mass transfer and diffusion steps are eliminated, the adsorption, surface reaction and desorption steps are so complex that it is very difficult to select a straightforward model which could accurately describe the reaction process. In this situation, a number of rate equations were derived which were tested against the experimental observations. In deriving rate equations for this reaction, the following assumptions were taken into consideration.

1. The mass transfer and diffusion (steps 1, 2, 6 and 7) of the reactants to and from the catalyst surface are very fast compared to the reaction steps 3, 4 and 5 and thus do not affect the overall rate of the reaction.

2. The surface reaction (step 4) is the rate limiting or rate controlling step in this reaction, since more than 75% of all heterogeneous reactions, that are not diffusion limited, are surface reaction limited. The surface reaction is assumed to occur through three possible mechanisms that are described as follows:

1. Reaction between adsorbed molecule A and nonadsorbed molecule B.
2. Reaction between adsorbed molecule B and nonadsorbed molecule A.
3. Reaction between adsorbed molecules A and B on adjacent active sites.

The first two mechanisms are referred to as Rideal-Eley mechanism and the third one is the Langmuir-Hinshelwood mechanism. The rate equations representing the above mentioned three mechanisms are given below. The derivations of these equations are given in Appendix F.

$$-r_A = k_S K_A^a \frac{C_A^a C_B^b - C_C^c / K_e}{\left(1 + K_A C_A + K_C C_C\right)^a} \tag{1}$$

$$-r_A = k_S K_B^b \frac{C_A^a C_B^b - C_C^c / K_e}{\left(1 + K_B C_B + K_C C_C\right)^b} \tag{2}$$

$$-r_A = k_S K_A^a K_B^b \frac{C_A^a C_B^b - C_C^c / K_e}{\left(1 + K_A C_A + K_B C_B + K_C C_C\right)^{a+b}} \tag{3}$$

Sigma Plot software package installed on an IBM PC was used for estimation of parameters unknown in the models. The SigmaPlot curve fitter uses the Marquardt-Levenberg algorithm to find the coefficients (parameters) of the independent variables that give the best fit between the equation and the data. This algorithm seeks the values of the parameters that minimize the norm of the residuals (square root of the sum of the squares of the residuals). Residuals are the differences between the observed values and predicted values of the dependent variable. This process is iterative. SigmaPlot begins with a guess at the parameters, checks to see how well the equation fits, then continues to make better guesses. When the absolute value of the differences between the norm of the residuals, from one iteration to the next, is less than the value of the tolerance (default value 0.0001), the iteration stops. This condition is called convergence.

Non-linear least square regression analysis was performed on the three models proposed in the literature. During estimation of parameters, values ranging from 0.5 to 3.0 were used for the order of reaction with respect to MTBE in the model equation.

The parameters estimated were surface reaction rate constant (k_S) and adsorption equilibrium constants (K_A, K_B and K_C) for all four temperatures. These estimated constants must meet the following criteria.

1. The estimated surface reaction rate constant and adsorption equilibrium constants should be positive.

2. The estimated surface reaction rate constant should have an increasing trend with rise in temperature while the adsorption equilibrium constants should decrease with increase in temperature.

The log of estimated parameters were plotted against reciprocal of absolute temperature to give an Arrhenius plot (ln k_S vs. 1/T) and three van't Hoff plots (ln K_A, ln K_B & ln K_C vs. 1/T). These plots must meet the following criteria.

1. Plot of the log of surface reaction rate constant (k_S) vs. reciprocal of absolute temperature (Arrhenius plot) should be linear with a negative slop (-E/R). i.e. for an exothermic reaction, the rate of reaction decreases with increase in temperature.

2. Plot of the log of each adsorption equilibrium constants (K_A, K_B and K_C) vs. reciprocal of absolute temperature (van't Hoff plots) should be linear with positive slopes ($\Delta H/R$).

3. The goodness of the fit was indicated by the lowest value of the square root of the sum of the squares of the residuals ($\sqrt{\Sigma r^2}$).

Satisfying the above mentioned criteria, the best fit was obtained by using a=1, b=1 and c=2.5. This combination of a, b and c estimated the parameters at the lowest value of the square root of the sum of the squares of the residuals. The results of parameters estimation using the proposed model equations are given in Table 4.16. As can be seen, the experimental data fitted the model equation 3 better than model 1 and 2. The value of the surface reaction rate constant (k_S) showed an increasing trend with rise in temperature whereas the values of adsorption equilibrium constants (K_A, K_B and K_C) decreased with increased in temperature. The values of the square root of the sum of squares of the residuals ($\sqrt{\Sigma r^2}$) were found lowest for model equation 3 as compared to model equations 1 and 2.

To further rule out any possibility that the rate determining step in this reaction is adsorption of methanol or desorption of MTBE, two more model equations were tested for the data. These model equations are based on adsorption of methanol controlling and desorption of MTBE controlling mechanisms and are given as follows:

Adsorption of methanol (A) controlling (K_a is the adsorption rate constant)

$$-r_A = K_a \frac{C_A^a - C_c^c / K_e C_B^b}{\left(1 + K_B^b C_B^b + K_A^a C_C^c / K_e C_B^b + K_C^c C_C^c\right)} \qquad (3a)$$

Desorption of MTBE (C) controlling (K_d is the desorption rate constant)

$$-r_A = K_d K_C^c \frac{C_A^a C_B^b - C_c^c / K_e}{\left(1 + K_A^a C_A^a + K_B^b C_B^b + K_C^c K_e C_A^a C_B^b\right)} \qquad (3b)$$

As compared to model equation 3, model equations 3a and 3b did not give satisfactory results. Based on the results of curve fitting, the model which fitted the experimental data very well was the surface reaction controlling mechanism (model equation 3) in which both methanol and isobutene were adsorbed on active sites and reacted together to form MTBE which was then desorbed. A comparison of estimated parameters with the literature (Table 4.17) indicated that the surface reaction rate constant values estimated in our study are lower than the literature values in the same temperature range due to the relative decreased rate of reaction.

Table 4.16. Results of parameter estimation for five model equations using the order of reactions a=1, b=1 and c=2.5. $\sqrt{\Sigma r^2}$ represents the square root of the sum of the squares of the residuals.

Model Equation 1						
T, K	K_e	k_s	K_A	K_B	K_C	$\sqrt{\Sigma r^2}$
343	6.71	3.54E-02	2.64E+04	-	4.23E-04	7.20E-03
353	3.51	5.83E-02	1.24E+04	-	2.33E-05	1.04E-02
363	1.91	1.00E-01	2.07E+04	-	1.11E-04	1.72E-02
373	1.07	3.32E-01	3.24E+00	-	2.22E-08	4.65E-02
Model Equation 2						
T, K	K_e	k_s	K_A	K_B	K_C	$\sqrt{\Sigma r^2}$
343	6.71	1.68E-02	-	9.41E+01	2.44E-01	4.29E-03
353	3.51	3.14E-02	-	3.42E+01	9.20E-02	9.56E-03
363	1.91	6.78E-02	-	1.62E+01	1.42E-01	1.67E-02
373	1.07	2.64E-01	-	3.00E+00	7.14E-09	4.61E-02
Model Equation 3						
T, K	K_e	k_s	K_A	K_B	K_C	$\sqrt{\Sigma r^2}$
343	6.71	1.78E-02	6.59E+01	8.80E+01	4.05E-01	3.70E-03
353	3.51	4.35E-02	4.15E+01	2.49E+01	1.35E-01	8.90E-03
363	1.91	1.76E-01	1.22E+01	3.70E+00	4.35E-02	1.63E-03
373	1.07	9.36E-01	1.30E+00	1.12E+00	1.34E-02	4.60E-03
Model Equation 3a						
T, K	K_e	K_a	K_A	K_B	K_C	$\sqrt{\Sigma r^2}$
343	6.71	1.24E-02	2.19E+02	2.59E-08	5.39E-08	2.56E-03
353	3.51	1.04E-02	1.40E+02	3.29E-08	8.42E-02	4.60E-03
363	1.91	1.05E-02	1.03E+02	3.30E-08	9.16E-10	7.17E-03
373	1.07	9.28E-03	5.35E+01	1.65E-12	8.48E-03	1.54E-02
Model Equation 3b						
T, K	K_e	K_d	K_A	K_B	K_C	$\sqrt{\Sigma r^2}$
343	6.71	1.94E+02	2.00E-06	4.44E+03	6.56E-01	3.18E-03
353	3.51	1.74E+02	3.26E-06	2.50E+03	6.63E-01	7.39E-03
363	1.91	2.18E+02	1.67E-05	6.25E+03	1.11E+00	1.40E-02
373	1.07	2.80E+02	1.50E-04	1.39E+04	1.73E+00	3.95E-02

Table 4.17. A comparison of estimated parameters obtained in this study with those determined by other investigators.

Al-Jarallah et al., 1988					
T, K	K_e	k_s	K_A	K_B	K_C
343	38.0	0.512	359.8	-	202.1
353	15.8	1.065	159.8	-	73.3
363	13.0	2.537	47.6	-	18.5
373	6.9	6.080	25.5	-	7.64
Tejero et al., 1989					
T, K	K_e	k_s	K_A	K_B	K_C
343	6.71	3.5	53.0	3.8	12.7
353	3.51	8.7	34.4	2.6	12.0
363	1.91	16.7	29.8	1.41	9.1
373	1.07	27.0	17.4	1.33	8.5
This Study					
T, K	K_e	k_s	K_A	K_B	K_C
343	6.71	1.78E-02	6.59E+01	8.80E+01	4.05E-01
353	3.51	4.35E-02	4.15E+01	2.49E+01	1.35E-01
363	1.91	1.76E-01	1.22E+01	3.70E+00	4.35E-02
373	1.07	9.36E-01	1.30E+00	1.12E+00	1.34E-02

The dependence of the surface reaction rate constant, k_s on the temperature was determined from the Arrhenius equation given below:

$$k_s = K_{so} \exp(-E/RT) \tag{4}$$

Where K_{so} and E are preexponential factor and activation energy respectively. The values of K_{so} (3.92×10^{19}) and E (140,806 J mol^{-1}) were found from the least squares fit of the equation 4 as shown in Figure 4.29. Thus

$$k_s = 3.92x10^{19} \exp(-140{,}806/RT) \tag{5}$$

The activation energy has been described as the minimum energy which must be possessed by the reaction molecules before the reaction occur. A comparison of activation energy is given in Table 4.18. The activation energy determined for MFI zeolite catalyst was found to be 140.8 ± 0.1 kJ mol^{-1} and it is higher than reported in the literature for the same reaction using Amberlyst 15 catalyst, which is in the range 71.2 to 92.4 kJ mol^{-1}. The higher value of activation energy obtained for the MFI zeolite catalyst was due to lower acidic strength of acidic sites present in zeolite. This higher value of activation energy is

also reflected in the higher values of heat of adsorption of the reactants and product. One of the studies [Caetano et al., 1994] using Amberlyst 18 resin reported an activation energy of 130.2 kJ mol^{-1} which is quite comparable to the value obtained in our work.

Table 4.18. A comparison of activation energy obtained for MTBE synthesis in this study with those determined by other investigators.

No.	E (kJ mol^{-1})	Catalyst	Reaction System	Reference
1.	82.0	Amberlyst 15	Heterogeneous(Batch)	Gicquel & Torck, 1983
2.	74.1	Amberlyst 15	Heterogeneous(PB)	Gicquel & Torck, 1983
3.	71.2	Amberlyst 15	Heterogeneous(IR)	Ancillotti et al, 1978
4.	79.0	Amberlyst 15	Homogeneous	Subraminium & Bhatia, 1987
5.	76.7	Amberlyst 15	Heterogeneous	Subraminium & Bhatia, 1987
6.	68.9	Amberlyst 15	Heterogeneous	Ali & Bhatia, 1989
7.	87.9	Amberlyst 15	Heterogeneous(Batch)	Al-Jarallah et al., 1988
8.	61.9	Amberlyst 15	Heterogeneous	Tejero et al., 1988
9.	85.4	Amberlyst 15	Heterogeneous(PB)	Zhang & Dutta, 1995
10.	92.4	Amberlyst 15	Heterogeneous(CSTR)	Rehfinger & Hoffmann, 1990a
11.	130.2	Amberlyst 18	Heterogeneous(Batch)	Caetano et. al., 1994
12.	140.8	ZCIC-10	Heterogeneous(Batch)	This Study

PB=Packed-bed, IR=Initial rates

The dependence of the adsorption equilibrium constants (K_A, K_B and K_C) on the temperature was determined from the van't Hoff equations given below:

$$K_A = K_{Ao} \exp(-\Delta H_A / RT) \tag{6}$$

$$K_B = K_{Bo} \exp(-\Delta H_B / RT) \tag{7}$$

and

$$K_C = K_{Co} \exp(-\Delta H_C / RT) \tag{8}$$

where K_{Ao}, K_{Bo} and K_{Co} are the preexponential factors and ΔH_A, ΔH_B and ΔH_C are the heats of adsorption of methanol, isobutene and MTBE respectively.

The values of K_{Ao} (7.36×10^{-18}), K_{Bo} (1.95×10^{-22}), K_{Co} (5.75×10^{-18}), ΔH_A (137,123 J mol^{-1}), ΔH_B (159,388 J mol^{-1}) and ΔH_C (120,744 J mol^{-1}) were found from the least squares fit of the equations 6, 7 and 8 as shown in Figures 4.30, 4.31 and 4.32. Thus,

$$K_A = 7.36x10^{-18} \exp(137{,}123 / RT) \quad (9)$$

$$K_B = 1.95x10^{-22} \exp(159{,}388 / RT) \quad (10)$$

and

$$K_C = 5.75x10^{-18} \exp(120{,}744 / RT) \quad (11)$$

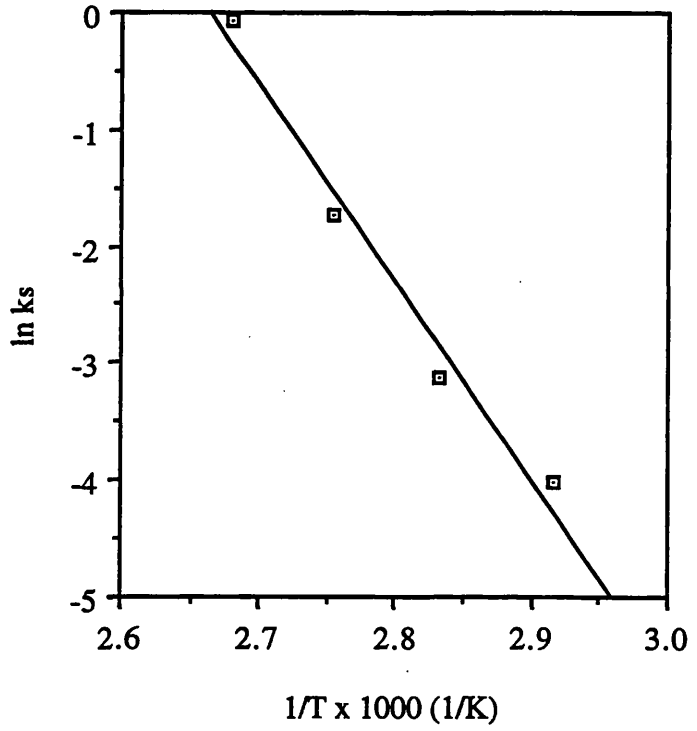

Figure 4.29. Arrhenius plot for K_S.

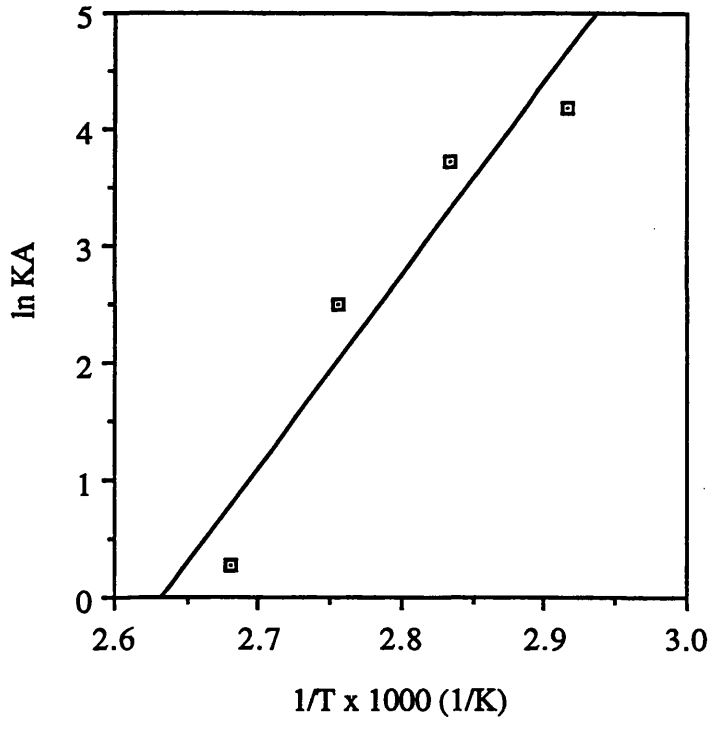

Figure 4.30. van't Hoff plot for K_A.

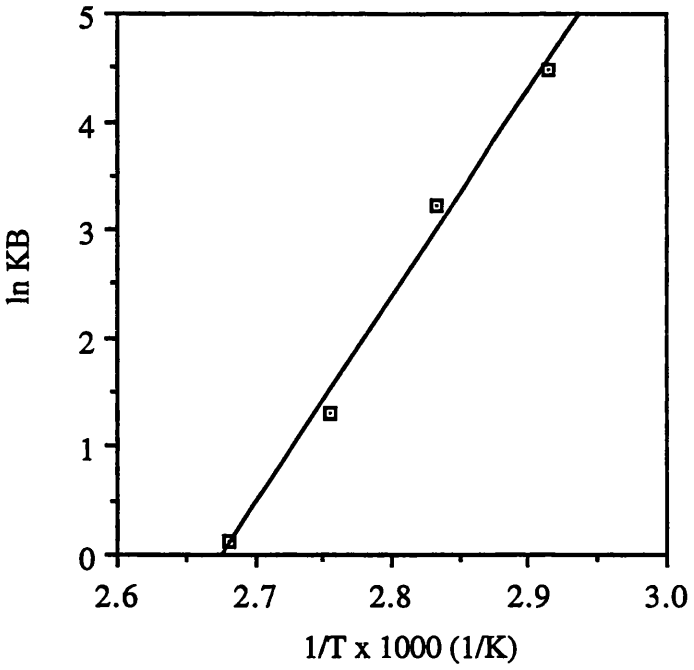

Figure 4.31. van't Hoff plot for K_B.

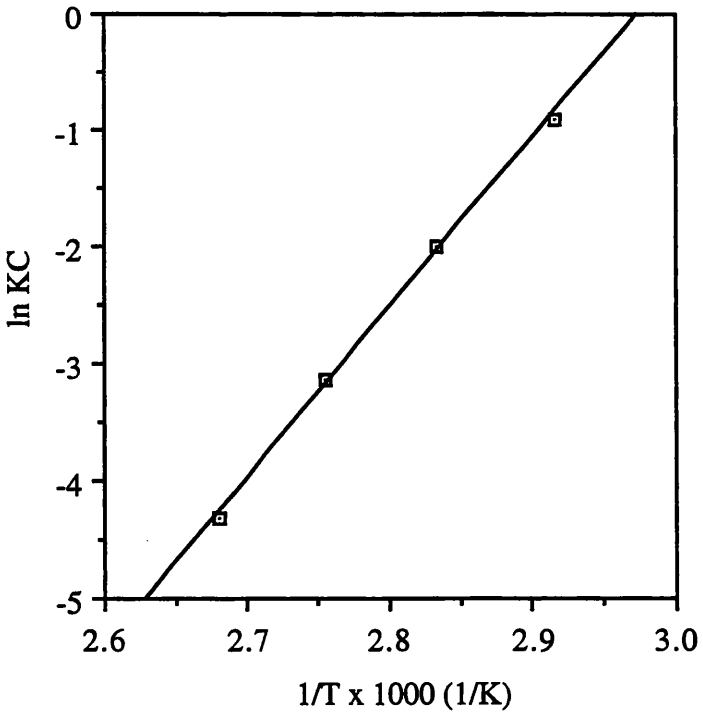

Figure 4.32. van't Hoff plot for K_C.

Figures 4.29 to 4.32 show that when kinetic constants were plotted on a semi-log scale, all data fell on straight lines. This implies that the kinetic constants follow an Arrhenius type of temperature dependency. Therefore, the reaction was controlled by chemical kinetics and not by mass transfer. If the reaction was controlled by mass transfer, then the rate would be given by the following equation.

$$\text{Rate} = k.\Delta C.T^{1.5} \qquad (12)$$

$$\ln [\text{Rate}] = \ln [k.\Delta C] + 1.5 \ln [T]$$

In order to verify this point further, assuming ΔC is constant, rate versus temperature was plotted on a log-log graph (Figure 4.33). Since the slope was 18.7 which is much greater than 1.5, it was concluded that the reaction was free from mass transfer effects.

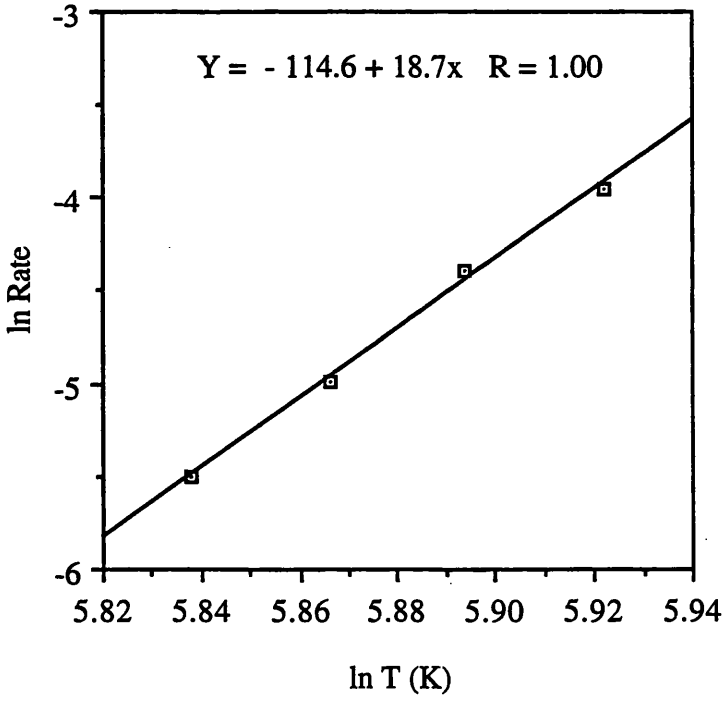

Figure 4.33. Plot of rate of reaction as a function of temperature on a log-log scale.

CHAPTER 5 CONCLUSIONS AND RECOMMENDATIONS

5.1. CONCLUSIONS

The following conclusions were drawn from this study:

1. The synthesis of MFI zeolites was successfully achieved in the laboratory and the rapid crystallization method performed well for zeolites having Si/Al ratio in the range of 10-100. The yields of these zeolites were around 30 grams per batch of synthesis.

2. The calcination of the zeolites to decompose and remove template was successfully achieved by heating the zeolites in an air flow at 873 K temperature maintained for 3 hours. A temperature of 773 K maintained for 5 hours was found insufficient for calcination. This was confirmed by FT-IR spectroscopy.

3. Ion-exchange of the synthesized zeolites was achieved by stirring with a 0.1 molar aqueous solution of hydrochloric acid at ambient temperature for one hour. Alternatively, ion-exchanging was performed using a 1.0 molar aqueous solution of ammonium nitrate at 353 K. Both methods were found equally good.

4. All of the zeolite synthesized were crystalline and of the MFI type as confirmed by the X-ray diffraction data compared with the XRD data of standard MFI zeolite.

5. FT-IR spectroscopy provided a quick and economical method of determining crystallinity of synthesized MFI zeolites. This method was equally supported by X-ray diffraction studies. This method was found applicable both for aluminosilicates and isomorphously substituted zeolites.

6. The synthesized zeolites were found thermally stable up to 1373 K. The water content was found to decrease while the template concentration was observed to increase with increasing Si/Al molar ratio or decreasing aluminum content of the zeolites. This was due to the decrease in hydrophilicity of the zeolites with decreasing aluminum content.

7. Scanning electron microscopy revealed that crystals of the synthesized zeolites were of spherical shape. The crystals of ZCIC-10 zeolite were found to have some amorphous phase. Others of high Si/Al ratio were found free from amorphous material.

8. The elemental composition results showed that the Si/Al molar ratio of the synthesized zeolites agreed quite well with that of ZSM-5 zeolites.

9. The synthesized zeolites possesses good surface properties and pore sizes well suited for MTBE production. The surface area and the micropore area of the synthesized

zeolites were found to increase with increasing Si/Al molar ratio. The median pore diameter values indicate that the zeolites are of the MFI type.

10. The catalytic evaluation of the synthesized zeolites in a packed bed reaction system showed that the activity of the zeolites to produce MTBE was found to increase with increasing temperature in the range 343 to 373 K. The activity of the zeolites showed an increasing trend with decreasing Si/Al molar ratio or increasing aluminum content. All synthesized zeolites were found to have good selectivity for MTBE production.

11. The catalytic evaluation of the isomorphously substituted zeolites at 353 K reaction temperature in a batch reaction system showed that substitution of boron and gallium did not enhance the activity of both the synthesized and commercial MFI zeolites. This was due to the loss of aluminum from the zeolites and lower acidity of boron and gallium compared to aluminum.

12. The hydrothermal treatment of both the synthesized and commercial MFI zeolites with aluminum fluoride in aqueous solution enhanced their activity two to three folds for the reaction of methanol and isobutene to produce MTBE.

13. The investigation of intrinsic kinetics for the heterogeneous reaction of methanol and isobutene to produce MTBE in a batch reaction system using synthesized MFI zeolite catalyst having a Si/Al molar ratio of 10 revealed that the surface reaction rate constant increased with increase in temperature whereas the thermodynamic equilibrium constants and adsorption equilibrium constants decreased with rise in temperature.

14. The reaction of methanol and isobutene to produce MTBE over ZCIC-10 zeolite was found to have an activation energy of 140.8± 0.1 kJ mol^{-1}.

15. The reaction can be represented by Langmuir-Hinshelwood model derived from a mechanism in which methanol adsorbed one active site reacts with isobutene adsorbed on another site and produce MTBE which is then desorbed.

16. The MFI catalyzed reaction of methanol and isobutene to produce MTBE was found first order both in methanol and isobutene and 2.5 orders in MTBE.

5.2. RECOMMENDATIONS

1. Aluminum fluoride treated MFI zeolites have shown enhancement in the activity for the reaction of methanol and isobutene to produce MTBE. These modified MFI zeolites should be studied in depth in order to determine the reaction mechanism. These modified zeolites could prove one of the best alternates to resin catalysts.

2. Aluminum fluoride modification of zeolites other than MFI type such as mordenites, zeolite beta and zeolite Y may also be studied since they have high aluminum contents in their framework.

3. Another method which may be used to enhance the activity of zeolites, for the reaction of methanol and isobutene to produce MTBE, is the hydrothermal treatment of zeolites with other aluminum containing compounds.

CHAPTER 6 REFERENCES

Aboul-Gheit, A.K., F.Z. Yehia and M.Y. El-Awadi (1994). Production of MTBE on solid acid catalysts. *Proceedings of the Second International Conference on Chemistry in Industry*, October 24-26, Manama, Bahrain, Paper no. 34, pp. 1056-1060.

Adams, J. M., J.A. Ballantine, S.H. Graham, R.J. Laub, J.H. Purnell, P.I. Reid, W.Y.M. Shaman and J.M. Thomas (1979). Selective chemical conversions using sheet silicates: Low temperature addition of water to 1-alkenes. *J. Catal.*, v. 58, pp. 238-252.

Adams, J.M., K. Martins, R.W. McCabe and S. Murray (1986). MTBE Production: A comparison of Montmorillonite-derived catalysts with ion-exchange resin. *Clays and Clay Minerals*, v. 34, No. 5, pp. 597-603.

Adams, J.M., S.E. Davies, S.H. Graham and J.M. Thomas (1982). Catalyzed reactions of organic molecules at clay surfaces: Ester breakdown, dimerization and lactonization. *J. Catal.*, v. 78, pp. 197-208.

Al-Jarallah, A. M., M.A.B. Siddiqui and A.K.K. Lee (1988). Kinetics of methyl tertiary butyl ether synthesis catalyzed by ion-exchange resin. *The Canadian J. Chem. Eng.*, v. 66, pp. 802-808.

Ali, A. and S. Bhatia (1990). Methyl tertiary butyl ether formation in a catalytic bed reactor - kinetic and modeling study. *The Chem. Eng. J.*, v. 44, pp. 97-106.

Ancillotti, F., E. Pescarollo, E. Szatmari and L. Lazar (1987). *Hyd. Proc.*, p. 63.

Ancillotti, F., M.M. Mauri and E. Pescarollo (1977). Ion-exchange resin catalyzed addition of alcohols to olefins. *J. Catal.*, v. 46, no. 1, pp. 49-57

Ancillotti, F., M.M. Mauri and E. Pescarollo (1978). Mechanisms in the reaction between olefins and alcohols catalyzed by ion exchange resin. *J. Mol. Catal.*, v. 4, no. 1, pp. 37-48.

Araya, A. and B.M. Lowe (1985). A partial determination of the stability fields of ferrierite and zeolites ZSM-5, ZSM-48 and Nu-10 in the K_2O-Al_2O_3-SiO_2-$NH_2[CH_2]_6NH_2$ system. *J. Chem. Res.*, pp. 192-193.

Argauer, R.J. and G.R. Landolt (1972). *U.S. Patent 3,702,886.*

ASTM D-4365 (1990). Standard test method for determining zeolite area of a catalyst. *Annual Book of ASTM Standards*, v. 05.03, Philadelphia, USA.

Austin, G.T. (1984). Petroleum processing. *Shreve's Chemical Process Industries*, 5th Edition, McGraw-Hill Book Company, pp. 713-747.

Axon, S.A. and J. Klinowski (1989). Isomorphous substitution in zeolite ZSM-5. in Recent Advances in Zeolite Science, J. Klinowski and P.J. Barrie (eds.) Elsevier Science Publishers, B.V. Amsterdam, The Netherlands, *Stud. Surf. Sci. Catal.* v. 52, pp. 113-122.

Bailer, G., H.J. Emeleus, R. Nyholm and A.F. Trotman-Dickenson (1973). *Comprehensive Inorganic Chemistry*, v. 1, pp. 1016-1020, Pergamon Press, New York.

Ballmoos, R. von and J.B. Higgins (1990). Collection of simulated XRD powder patterns from zeolites. *Zeolites*, v. 10, no. 5, pp. 442S-445S.

Barrer, R.M. (1981). *Zeolites*, v. 1, p. 130.

Barrer, R.M. (1982). *Hydrothermal Chemistry of Zeolites*, Academic Press, New York.

Barrer, R.M. and J.F. Cole (1970). *J. Chem. Soc.*, p. 1516.

Barrer, R.M., J.W. Baynham, F.W. Bultitude and W.M. Meier (1959). *J. Chem Soc.*, p. 195.

Becker, K. A. and S. Kowalak (1989). Zeolite catalysts modified with fluorine. in Recent Advances in Zeolite Science, J. Klinowski and P.J. Barrie (eds.) Elsevier Science Publishers, B.V. Amsterdam, The Netherlands,*Stud. Surf. Sci. Catal.* v. 52, pp. 123-132.

Bellusi, G. and V. Fattore (1991). Isomorphic substitution in zeolites: A route for the preparation of novel catalysts. in Zeolite Chemistry and Catalysis, P. A. Jacobs et al. (eds.). Elsevier Science Publishers, B.V. Amsterdam, The Netherlands, *Stud. Surf. Sci. Catal.* v. 69, pp. 79-92.

Bolton, A.P. and M.A. Lanewala (1970). *J. Catal.*, v. 18, p. 154.

Brauer G., (1963). *Handbook of Preparative Inorganic Chemistry*, v. 1, Academic Press, New York.

Briscoe, N., J.L. Casci, J.A. Daniels, D.W. Johnson, M.D. Shanon and A. Stewart (1989). Some aspects of the synthesis, characterization and properties of zeolite Nu-2. in Zeolites: Facts, Figures, Future. P.A. Jacobs and R.A. van Santen (eds.) Elsevier Science Publishers, B.V. Amsterdam, The Netherlands, *Stud. Surf. Sci. Catal.* v. 49, pp. 151-160.

Brockwell, H.L., P.R. Sarathy and R. Trotta (1991). Synthesize ethers. *Hyd. Proc.*, v. 70, no. 9, pp. 133-141.

Broekhoff, J.C.P. and B.G. Linsen (1970). *Physical and Chemical Aspects of Adsorbents and Catalysts*. B.G. Linsen (ed), Academic Press, New York.

Brunauer, S., P.H. Emmett and E. Teller (1938). *J. Am. Chem. Soc.*, v. 60, p. 309.

Bylina, A., J.M. Adams, S.H. Graham and J.M. Thomas (1980). Chemical conversions using sheet silicates. Simple method for producing methyl t-butyl ether. *J. Chem. Soc. Chem. Comm.*, pp. 1003-1004.

Caetano, N.S., J.M. Loureiro and A.E. Rodrigues (1994). Methyl tertiary butyl ether synthesis catalyzed by acid ion-exchange resins: kinetic studies and modeling of multiphase batch reactors. *Chem. Eng. Sci.*, v. 49, no. 24A, pp. 4589-4604.

Chang, K-H., G.T. Kim and W.S. Ahn (1992). Methyl tertiary butyl ether synthesis over titanium-silicalite I catalysts. *Ind. Eng. Chem. Res.*, v. 31, pp. 125-130.

Chase, J.D. (1984). *Catalytic Conversion of Synthetic Gas and Alcohols to Chemicals.* R.G. Herman (ed.), Plenum Press, New York, p. 307.

Chemical Economics Handbook (1994). Gasoline Octane Improvers. *CEH Marketing Report*, SRI International, Menlo Park, California.

Cheng, S., J.T. Wang and C.L. Lin (1991). Layered group (IV) metal phosphates as catalysts for MTBE synthesis. *J. Chinese Chem. Soc.*, v. 38, pp. 529-534.

Chu, C.T.W. and C.D. Chang (1985). *J. Phys. Chem.*, v. 89, p. 1569

Chu, P. (1973). *U.S. Patent 3,709,979.*

Chu, P. and H. Kuhl (1987). Preparation of methyl tertiary butyl ether over zeolite catalysts. *Ind. Eng. Chem. Res.*, v. 26, pp. 365-369.

Clarence, D.C., D.H. Stuart, N.M. Joseph and D.S. Kirk (1985). Insertion of aluminum into high silica content zeolite frameworks. *J. Chem. Soc. Farad. Trans. I*, v. 81, pp. 2215-2224.

Colombo, F., L. Cori, L. Dalloro and P. Delogu (1983). Equilibrium constants for the methyl tertiary butyl ether liquid-phase synthesis by use of UNIFAC. *Ind. Eng. Chem. Fundam.*, v. 22, pp. 219-223.

Coudurier, G. and J.C. Vedrine (1986). Catalytic and acidic properties of boron pentasil zeolite. *Pure Appl. Chem.*, v. 58, no. 10, pp. 1389-1396

Coudurier, G., C. Naccache and J.C. Vedrine (1982). Uses of infrared spectroscopy in identifying ZSM zeolite structure. *J. Chem. Soc. Chem. Commun.*, pp. 1413-1415

Csikos, R., I. Pallay and J. Laky (1980). Practical use of MTBE produced from C4 fraction. *Proceedings of the 10th World Petroleum Congress, Bucharest*, v. 10, no. 5, pp. 107-175.

Csikos, R., I. Pallay, J. Laky, E.D. Radchenko, B.A. Englin and J. A. Roberts (1976). Low-lead fuel with MTBE and C_4 alcohols. *Hyd. Proc.*, v. 55, no. 7, pp. 121-125.

Dartnell, P.L. and K. Cambell (1978). Other aspects of MTBE/methanol use. The Oil and Gas Journal, v. 46, no. 13, pp. 205-212.

DeGarmo, J.L., V.N. Parulekar and V. Pinjala (1992). Consider reactive distillation. *Chem. Eng. Prog.*, v. 88, no. 3, pp. 43-50.

Derouane, E.G., J.B. Nagy, Z. Gabelica, and N. Blom (1982). *Zeolites*, v. 2, p. 299.

Derouane, E.G., L. Baltusis, R.M. Dessau and K. D. Cshmitt (1984). Catalysis by acids and bases. B. Imelik et al. (eds.). Elsevier Science Publishers, B.V. Amsterdam, The Netherlands, *Stud. Surf. Sci. Catal.*, v. 20, p. 135.

Derouane, E.G., S. Detremmerie, Z. Gabelica and N. Blom (1981). Synthesis and characterization of ZSM-5 type zeolites. I. Physico-chemical properties of precursors and intermediates. *Appl. Catal.*, v. 1, p. 201.

Dia, F.Y., M. Suzuki, H. Takahashi, and Y. Saito, (1989). *ACS Symposium Series no. 398*, American Chemical Society, p. 244.

Dixon, P.H.O., V.J. D'Amico, B. Strain, E.M. Jones and L.A. Smith (1989). Catalytic distillation technology and MTBE production, Paper No. AM-89-44. *Presented at the National Petroleum Refiners Association Annual Meeting*, March 19-21, San Francisco, California, USA.

Emmett, P.H. and M. Cines (1947). *J. Phy. Chem.*, v. 51, p. 1248.

Evans, T.W. and K.R. Edlund (1936). Tertiary alkyl ethers, preparation and properties. *Ind. Eng. Chem.*, v. 28, no. 10, pp. 1186-1188.

Fejes, P., I. Marsi, I. Kiricsi, J. Halasz, I. Hannus, A. Rockenbaur, G. Tasi, L. Korecz and G. Schobel (1991). Synthesis, characterization and catalytic activity of V-ZSM-5 zeolites, in Zeolite Chemistry and Catalysis, P. A. Jacobs et al. (eds.). Elsevier Science Publishers, B.V. Amsterdam, The Netherlands, *Stud. Surf. Sci. Catal.* v. 69, pp. 173-180.

Fishel, N. A. (1968). *US Patent 3,413,370.*

Flanigen, E. M. (1973). Molecular sieves. *Advances in Chemistry Series,* no. 121, American Chemical Society, Washington, D.C, USA, p. 119.

Flanigen, E. M., H. Khatami and H. A. Szymanski (1971). Infrared structural studies of zeolites, in Robert F. Gould (ed.) Molecular Sieve Zeolites-1; *Advances in Chemistry Series* no. 101, American Chemical Society, Washington, D.C, USA.

Flanigen, E.M. and D.W. Breck (1960). American Chemical Society 137th meeting, Cleveland, Ohio, USA.

Franz, W., P. Gunther, C.E. Hofstadt (1959). Catalysis on the basis of acid-activated montmorillonites. *Proceedings of the World Petroleum Congress*, New York, v. 3, pp. 123-132.

Gates, B.C. and W. Rodrijuez (1973). General and specific acid catalysis in sulfonic acid resin. *J. Catal.*, v. 31, pp. 27-13.

Gicquel, A. and B. Torck (1983). Synthesis of MTBE catalyzed by ion-exchange resin: influence of methanol concentration and temperature. *J. Catal.*, v. 83, pp. 9-18.

Golubovskaya, E.K., S.V. Dudarev and K.G. Ione (1985). Effect of silica sol (zeolite precursor) composition on the value of its coagulation threshold. *Reac. Kin. Catal. Lett.* v. 28, no. 2, pp. 239-244.

Gosh, A. K. and R. A. Kydd (1985). *Catal. Rev. - Sci. Eng.* v. 27, p. 539.

Grose, R.W. and E.M. Flanigen (1981). *U.S. Patent 4,257,886.*

Gupta, J.C. and J. Prakash (1980). MTBE Technology. *Chem. Eng. World*, v. 15, no. 8, pp. 27-31.

Guttmann A.T. and R.K. Graselli (1983). Esterification of Methacrylic Acid with MTBE-A Process for the Manufacture of Methyl Methacrylate. *Appl. Catal.*, v. 8 , pp. 57-70.

Heath, A. (1977). New additives gives boost to unleaded fuel in Europe. *Chem. Eng.*, v. 84, no. 3, pp. 56c-56f.

Hellmutt, G.K. and K.B. Hermann (1991). Introduction of Cations into Zeolites by solid state reaction in Zeolite Chemistry and Catalysis, P. A. Jacobs et al. (eds.). Elsevier Science Publishers, B.V. Amsterdam, The Netherlands, *Stud. Surf. Sci. Catal.* v. 69, pp. 43-64.

Inui, T., T. Suzuki, M. Inoue, Y. Murakami and Y. Takegami (1984). Structure and Reactivity of Modified Zeolites. P. A. Jacobs et al. (eds.). Elsevier Science Publishers, B.V. Amsterdam, The Netherlands,*Stud. Surf. Sci. Catal.* v. 18, p. 201.

Izquierdo, J.F., F. Cunill, M. Vila, J. Tejero and M. Iborra (1992). Equilibrium constants for methyl tertiary butyl ether liquid-phase synthesis. *J. Chem. Eng. Data*, v. 37, pp. 339-343.

Izquierdo, J.F., F. Cunill, M. Vila, M. Iborra and J. Tejero (1994). Equilibrium constants for methyl tertiary butyl ether and ethyl tertiary butyl ether liquid-phase synthesis using C_4 olefinic cut. *Ind. Eng. Chem. Res.*, v. 33, pp. 2830-2835.

Izumi, Y. (1979). Ethers having tertiary alkyl groups. *Japanese Patent 7,955,507.*

Jacobs, P.A. and R.V. Ballmoos (1982). Framework hydroxyl groups of H-ZSM-5 zeolite. *J. Phys. Chem.*, v. 86, pp. 3050-3052

Jacobs, P.A., H.K. Beyer and J. Valyon (1981). *Zeolites*, v. 1, p. 161.

Jacobs, P.T. and J.A. Martens (1987). Synthesis of ZSM-5 zeolites in the presence of tetrapropylammonium ions. in Synthesis of High-Silica Aluminosilicate Zeolites. P.A. Jacobs and J.A. Martens (eds.). Elsevier Science Publishers, B.V. Amsterdam, The Netherlands,*Stud. Surf. Sci. Catal.*, v. 33, pp. 47-111.

Jacobs, R. and R. Krishna (1993). Multiple solutions in reactive distillation for MTBE synthesis. *Ind. Eng. Chem.*, v. 32, pp. 1706-1709.

Jansen, J.C. and S.T. Wilson (1991). The Preparation of molecular sieves. in Introduction to Zeolite Science and Practice, H. van Bekkum, E.M. Flanigen and J.C. Jansen (eds.) Elsevier Science Publishers, B.V. Amsterdam, The Netherlands, *Stud. Surf. Sci. Catal.* v. 58, pp. 77-136.

Jansen, J.C., F.J. van der Gaag and H. V. Beckum (1984). *Zeolites*, v. 4, p. 369.

Jiru, P. (1982). Influence of controlled structural changes on the catalytic properties of zeolites. in Metal Microstructure in Zeolites. P. A. Jacobs et al. (eds.). Elsevier Science Publishers, B.V. Amsterdam, The Netherlands, *Stud. Surf. Sci. Catal.*, v. 12, , p. 137.

Johnson, M.F.L. (1978). *J. Catal.*, v. 52, p. 425.

Kazi, A.M., J.C. Goodwin, Jr., G. Marcelin and R. Oukaci (1995). Synthesis of MTBE during carbon monoxide hydrogenation: reaction sites required. *Ind. Eng. Chem. Res.*, v. 34, no. 3, pp. 718-721.

Knifton, J.F. (1989). Process and catalysts for the one-step manufacturing of methyl tertiary butyl ether. *European Patent 333,078*, 13pp.

Knifton, J.F. (1992). One-step synthesis of methyl tertiary butyl ether from t-butanol using fluorosulfonic acid-modified clay catalysts. *U.S. Patent 5,157,162*, 8pp.

Knifton, J.F. and J.R. Sanderson (1993). One-step synthesis of methyl tertiary butyl ether from t-butanol using fluorophosphoric acid-modified zeolite catalysts. *U.S. Patent 5,220,078*, 7pp.

Knifton, J.F. and J.R. Sanderson (1994). One-Step Synthesis of Methyl Tertiary Butyl Ether from T-Butanol using Hydrogen Fluoride-Modified Zeolite Catalysts. *U.S. Patent 5,300,697*, 8pp.

Kogelbauer, A., A.A. Nikolopoulos, J.C. Goodwin, Jr. and G. Marcelin (1995). Reactant adsorption and its impact upon MTBE synthesis on Zeolites. *J. Catal.*, v. 152, pp. 122-129.

Kogelbauer, A., M. Ocal, A.A. Nikolopoulos, J.C. Goodwin, Jr. and G. Marcelin (1994). MTBE synthesis on partially alkali-exchanged HY zeolites. *J. Catal.*, v. 148, pp. 157-163.

Kosslick, H., M. Richter, V.A. Tuan, B. Parlitz, K. Szulzewski and R. Fricke (1991). Genesis of Gallosilicates with ZSM-5 structure. Insertion of Ga and zeolitic properties at various steps of crystallization. in Zeolite Chemistry and Catalysis. P. A. Jacobs et al. (eds.). Elsevier Science Publishers, B.V. Amsterdam, The Netherlands, *Stud. Surf. Sci. Catal.* v. 69, pp. 109-117.

Kucherov, A.V. and A.A. Slinkin (1985}. *Zeolites*, v. 5, pp. 320-324.

Kucherov, A.V. and A.A. Slinkin (1986}. *Zeolites*, v. 6, pp. 175-180.

Kucherov, A.V. and A.A. Slinkin (1987a}. *Zeolites*, v. 7, pp. 38-42.

Kucherov, A.V. and A.A. Slinkin (1987b}. *Zeolites*, v. 7, pp. 43-46.

Kucherov, A.V. and A.A. Slinkin (1988}. *Zeolites*, v. 7, pp. 110-116.

Kucherov, A.V. and A.A. Slinkin (1994}. Solid state reaction as a way to transition metal cation introduction into high-silica zeolites. *J. Mol. Catal.*, v. 90, pp. 323-354.

Kulkarni, S.J., H. Hattori and K. Tanabe (1989). Effects of pH during preparation on the physico-chemical acidity and catalytic properties and coking tendencies of H-ZSM-5 type catalysts. *Appl. Catal.*, v. 49, pp. 27-44.

Ladisch, M.R., R.L. Hendrickson, M.A. Brewer and P.J. Westgate (1993). Catalyst induced yield enhancement in a tubular reactor. *Ind. Eng. Chem. Res.*, v. 32, pp. 1888-1894.

Lalik, E., X. Liu and J. Klinowski (1992). Role of gallium in the cataltic activity of zeolite[Si,Ga]-ZSM-5 for methanol conversion. *J. Phys. Chem.*, v. 96, pp. 805-809.

Lok, B.M., F.P. Gortsema, C.A. Messina, H. Rastelli and T.P.Z. Ijod (1982). Zeolite modification - Direct Fluorination. *Preprints, Symposium on Advances in Zeolite Chemistry*, Division of Petroleum Chemistry, Inc., American Chemical Society Meeting, Las Vegas, March 28-April 2.

Mafki (1980). Lead-free or low leaded fuel composition, MTBE production technology. *Technical Brochure of Hungarian Oil and Gas Research Institute*, Hungary.

Mao, R.L.V., A. Ramsaram, S. Xiao, S.T. Le, H.M. Ahmed and G. Denes (1995). Microporous materials prepared by selective removal of silicon from silicalite and ZSM-5 zeolites. *Preprints, Symposium on Synthesis of Zeolites, Layered Compounds and other Microporous Solids.* Division of Petroleum Chemistry Inc., 209th ACS National Meeting, Anaheim, CA, April 2-7, p. 326.

Mao, R.L.V., R. Carli, H. Ahlafi and V. Ragaini (1990). Synthesis of Methyl Tertiary Butyl Ether over Triflic Acid Loaded ZSM-5 and Y Zeolites. *Catal. Letters*, v. 6, pp. 321-330.

Matouq M. and S. Goto (1993). Combined Process for the Production of MTBE from TBA and Methanol. *J. Chem. Eng. Japan,* v. 27, no. 3, pp. 302-306.

Matouq M., T. Tagawa and S. Goto (1993). Liquid-phase Synthesis of MTBE on Heterogeneous Heteropoly Acid Catalysts. *J. Chem. Eng. Japan*, v. 26, no. 3, pp. 254-258.

Matouq M., T. Tagawa and S. Goto (1994). Kinetics of liquid-phase synthesis of MTBE from TBA and methanol catalyzed by ion-exchange resin. *International Journal of Chemical Kinetics*, v. 25, pp. 825-831.

McCabe, R.W., J.M. Adams and K. Martin (1985). Clay and zeolite catalyzed cyclic anhydride formation. *J. Chem. Res.*, v. 11, pp. 356-357.

Milton, R.M. (1968) *Molecular Sieves.* Soc. Chem. Ind., London, p. 199.

Mostowicz, R. and L.B. Sand (1982). *Zeolites*, v. 2, p. 143.

Nastro, A., L. B. Sand (1983). *Zeolites*, v. 3, p 57.

Nastro, A., R. Aiello and C. Colella (1985). Zeolite: synthesis, structure, technology and application. B. Drzaj et al. (eds.). Elsevier Science Publishers, B.V. Amsterdam, The Netherlands, *Stud. Surf. Sci. Catal.*, v. 24, p. 39.

Nayak, V.S. and V.R. Choudhary (1982). Isomerization of m-xylene on H-ZSM-5. Part I: Influence on catalytic activity and selectivity of Si/Al ratio, degree of cation exchange, deammoniation conditions and poisoning of strong acid sites. *Appl. Catal.*, v. 4, pp. 333-352.

New Scientist (1982). Brainwaves reflect the effect of lead on children, v. 94, no. 1301, p. 144.

Nijhuis, S.A., F.P.J.M. Kerkhoj and A.N.S. Mak (1993). Multiple steady states during reactive distillation of MTBE. *Ind. Eng. Chem. Res.*, v. 32, pp. 2767-2774.

Nikolopoulos, A.A., A. Kogelbauer, J. G. Goodwin, Jr. and G. Marcelin (1994b). Effect of dealumination on the catalytic activity of acid zeolites for the gas phase synthesis of MTBE. *Appl. Catal. A: General,* v. 119, pp. 69-81.

Nikolopoulos, A.A., R. Oukaci, J. G. Goodwin, Jr. and G. Marcelin (1992). Gas phase synthesis of MTBE over acid zeolites. *Preprints of the Symposium on Octane and Cetane Enhancement Processes for Reduced Emissions Motor Fuels,* Division of Petroleum Chemistry, Inc. American Chemical Society San Francisco Meeting, April 5-10, San Francisco, California, USA, pp. 787-792.

Nikolopoulos, A.A., R. Oukaci, J. G. Goodwin, Jr. and G. Marcelin (1994a). Selectivity behavior during the equilibrium-limited high temperature formation of MTBE on acid Zeolites. *Catal. Letters,* v. 27, pp. 149-157.

Nishizawa, T., T. Tokumara, Y. Komiyama and Y. Wolonabe (1974). Gasoline compositions with high octane number. *Japanese Patent 7,426,306.*

Nocca, J.L., J. Leonard, J.F. Gaillard and P. Amigues (1989). Process for manufacturing a tertiary alkyl ether by reactive distillation. *U.S. Patent 4,847,431.*

Norris, J.F. and G.W. Rigby (1932). *J. Am. Chem. Soc.*, v. 54, p. 2088.

Ogino, Y., A. Igarashi, and T. Matsuda (1980). Methyl Tertiary Butyl Ether. *Japanese Patent 8,000,323.*

Okazaki, S. and N. Wada (1993). Surface properties and catalytic activities of amorphous niobium phosphate and a comparison with those of H_3PO_4-treated niobium oxide. *Catal. Today,* v. 16, no. 3-4, pp. 349-359.

Panneman, H-J. and A.A.C.M. Beenackers (1995). Synthesis of MTBE catalyzed by acidic ion-exchange resins. influence of the proton activity. *Ind. Eng. Chem. Res.*, v. 34, pp. 4318-4325

Parra, D., J. Tejero, F. Cunill, M. Iborra and J.F. Izquierdo (1994). Kinetic study of methyl tertiary butyl ether liquid phase synthesis using C_4 olefinic cut. *Chem. Eng. Sci.*, v. 49, no. 24A, pp. 4563- 4578.

Pecci, G. and T. Floris (1977). Ether ups antiknock of gasoline. *Hyd. Proc.*, v. 56, no. 12, pp. 98-102.

Pien, S.I. and W.J. Hatcher (1990). Synthesis of methyl tertiary butyl ether on H-ZSM-5 zeolite. *Chem. Eng. Comm.*, v. 93, pp. 257-265.

Price, G.D., J.J. Pluth, J.V. Smith, J.M. Bennett, and R.L. Patton (1982). Crystal structure of tetrapropylammonium fluoride containing precursors to fluoride silicalite. *J. Am. Chem. Soc.*, v. 104, p. 5971.

Quang, D.V., J.F. Gaillard, J. Leonard and J.L. Nocca (1989). Process for manufacturing a tertiary alkyl ether by reactive distillation. *U.S. Patent 4,847,430.*

Rehfinger, A. and U. Hoffmann (1990a). Kinetics of methyl tertiary butyl ether liquid phase synthesis catalyzed by ion-exchange resin-I. Intrinsic rate expression in liquid phase activities. *Chem. Eng. Sci.*, v. 45, no. 6, pp. 1605-1617.

Rehfinger, A. and U. Hoffmann (1990b). Kinetics of methyl tertiary butyl ether liquid phase synthesis catalyzed by ion-exchange resin-II. Macropore diffusion of methanol as rate-controlling step. *Chem. Eng. Sci.*, v. 45, pp. 1619-1626.

Reychler (1907). *Bull. Soc. Chim. Belg.*, v. 21, p. 71.

Reynolds, R.W. (1975). Methyl ether (MTBE) scores well as a high octane gasoline. *The Oil and Gas Journal,* v. 73, no. 24, pp. 50-52.

Rohm and Haas (1992). Amberlyst 15. *Technical Brochure*, Philadelphia, USA.

Rohm and Haas (1996). Polymeric catalyst increases oxygenate output in existing plants with no increase in capital equipment cost. *Hydrocarbon Technology International,* spring 1996, p 27.

Rollmann, L.P. (1984). *Zeolite: Science and Technology*, Martinus Nijhoff Publishers, p. 109.

Sanders, J.V. (1985). *Catalysis: Science and Technology*, Springer, J.R. Anderson and M. Bodart (eds.). New York, v. 7, p. 51.

Santen, van R.A., J. Keijsper, G. Ooms, A.G.T.G. Kortbeek (1986). *New Development in Zeolite Science and Technology*. Murakami et al., (eds.). Elsevier Science Publishers, B.V. Amsterdam, The Netherlands, p. 169.

Satterfield, C. N. (1991). Heterogeneous catalysis in ndustrial practice. Chapter 7, *Acid and Zeolite Catalysis*. McGraw-Hill Inc. New York, p. 229.

Sayed, M.B., A. Auroux and J.C. Vedrine (1989). The effect of boron on ZSM-5 zeolite shape selectivity and activity. *J. Catal.*, v. 116, pp. 1-10.

Sing, K.S.W., D.H. Everret, R.A.W. Haul., L. Moscue,R.A. Pierroti, J. Rowqueral and T. Siemieniewska (1985). *Pure Appl. Chem.*, v. 57, p. 603.

Smith, L.A. (1982). Catalytic distillation process. *U.S. Patent 4,307,254.*

Smith, L.A. (1984). Catalytic distillation structure. *U.S. Patent 4,443,559.*

Smith, L.A. (1990). Method for the preparation of MTBE. *U.S. Patent 4,978,807.*

Snamprogetti (1990). *U.S. Patent 4,039,590.*

Stouthamer, B. and A. Kwantes (1970). Tertiary olefins from cracking. *British Patent 1,176,620.*

Subramaniam, C. and S. Bhatia (1987). Liquid phase synthesis of MTBE catalyzed by ion-exchange resin. *The Canadian J. of Chem. Eng.* v. 65, pp. 613-619.

Sundmacher, K. and U. Hoffmann (1994). Microkinetic analysis of methyl tertiary butyl ether synthesis in chemical potential. *Chem. Eng. Sci.*, v. 49, no. 18, pp. 3077-3089.

Suzuki, K., Y. Kiyozumi, K. Mastsuzaki, and S. Shin (1987). *Appl. Catal.*, v. 35, p. 401.

Suzuki, K., Y. Kiyozumi, S. Shin, K. Fujisawa, H. Watanabe, K. Satio, and K. Noguchi (1986). *Zeolites*, v. 6, p. 290.

Suzuki, K., Y. Kiyozumi, S. Shin, S. Ueda (1985). *Zeolites*, v. 5, p. 11.

Szostak, R. (1989). Molecular Sieves: *Principles of Synthesis and Identification.* Van Nostrand Reinhold Catalysis Series, New York.

Takezono, T. and Y. Fujiwara, (1980). Methods for producing methyl tertiary butyl ether and fuel composition containing the same. *US Patent 4,182,913.*

Tejero, J., F. Cunill and J.F. Izquierdo (1988). *Ind. Eng. Chem. Res.*, v. 27, p. 338.

Tejero, J., F. Cunill and M. Iborra (1987). Molecular mechanism of MTBE synthesis on a sulfonic acid ion exchange resin. *J. Mol. Catal.*, v. 42, pp. 257-268.

Tejero, j., F. Cunill and J.F. Izquierdo (1989). *Ind. Eng. Chem. Res.*, v. 28, p. 1269.

Torck, B., A. Convers, D. Duec, M. Rueil, and P. Mithitenko (1980). Methyl Tertiary Butyl Ether from Methanol and Isobutene. *Ger. Offen.* 3 015346.

Trong on D., S. Kaliaguine and L. Benneviot (1995). Titanium boralites with MFI structure characterized using XRD, XANES, and UV-Visible techniques: Effect of hydrogen peroxide on the preparation. *J. Catal.*, v. 157, p. 235-243.

Vedrine, J.C. (1991). Isomorphous substitution in zeolite frameworks-precedures and characterization in Zeolite Chemistry and Catalysis, P. A. Jacobs et al. (eds.). Elsevier

Science Publishers, B.V. Amsterdam, The Netherlands, *Stud. Surf. Sci. Catal.* v. 69, pp. 25-42.

Vedrine, J.C., G. Coudurier and B.F. Mentzen (1988). Prospective in molecular sieves science. W.H. Flank and T.E. Whyte (eds.). *American Chemical Society Symposium Series* no. 368, American Chemical Society, Washington D.C., p. 66.

Waddams, A.L. (1968). *Chemicals from Petroleum*. Butler and Tanner Ltd., pp. 155-158.

Xu X., Y. Zheng and G. Zheng (1995). Kinetics and effectiveness of catalyst for synthesis of MTBE in catalytic distillation. *Ind. Eng. Chem. Res.*, v. 34, pp. 2232-2236.

Yavaraski, T. and W.J. Hatcher (1989). Adsorption and diffusion in MTBE synthesis over H-ZSM-5. *Presented at the Annual Meeting of AIChE*, November 8, 1989, Session No. 51, San Francisco, California, USA.

Zecchina, A., G. Spoto, S. Bordiga, A. Ferrero, G. Petrini, G. Leofanti and M. Padovan (1991). Framework and extraframework titanium in titanium silicalite, in Zeolite Chemistry and Catalysis, P. A. Jacobs et al. (eds.). Elsevier Science Publishers, B.V. Amsterdam, The Netherlands, *Stud. Surf. Sci. Catal.* v. 69, pp. 251-258.

Zhang, T. and R. Dutta (1995). Integral analysis of MTBE synthesis kinetics. *Ind. Eng. Chem. Res.*, v. 34, pp. 730-740.

Zhdanov, S.P. (1971). Robert F. Gould (ed.) Molecular Sieve Zeolites-1. *Advances in Chemistry Series* no. 101, American Chemical Society, Washington, D.C. p. 20.

APPENDICES

APPENDIX A X-RAY DIFFRACTION PATTERNS

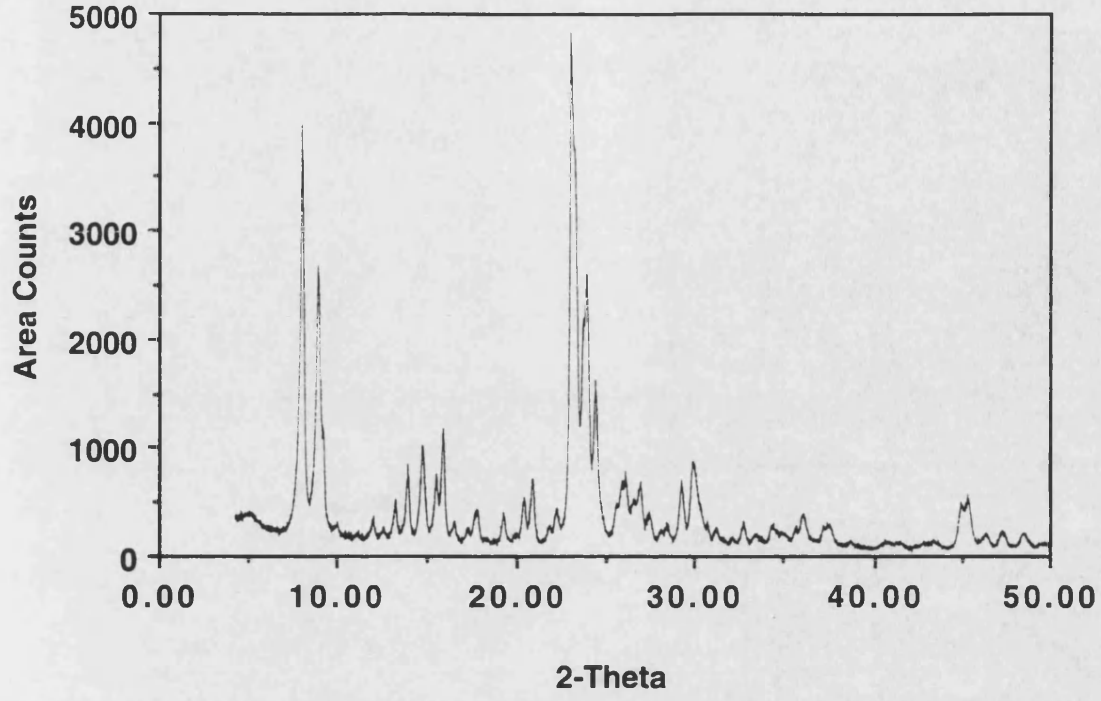

Figure A1. X-ray powder diffraction pattern of ZCIC-15 zeolite.

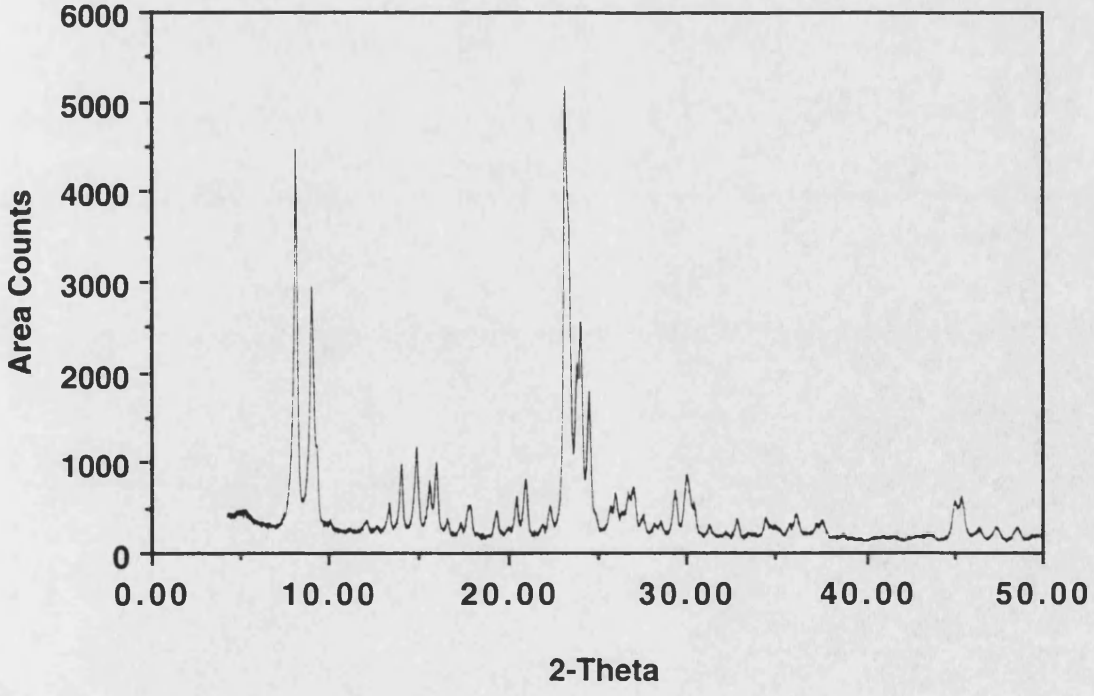

Figure A2. X-ray powder diffraction pattern of ZCIC-20 zeolite.

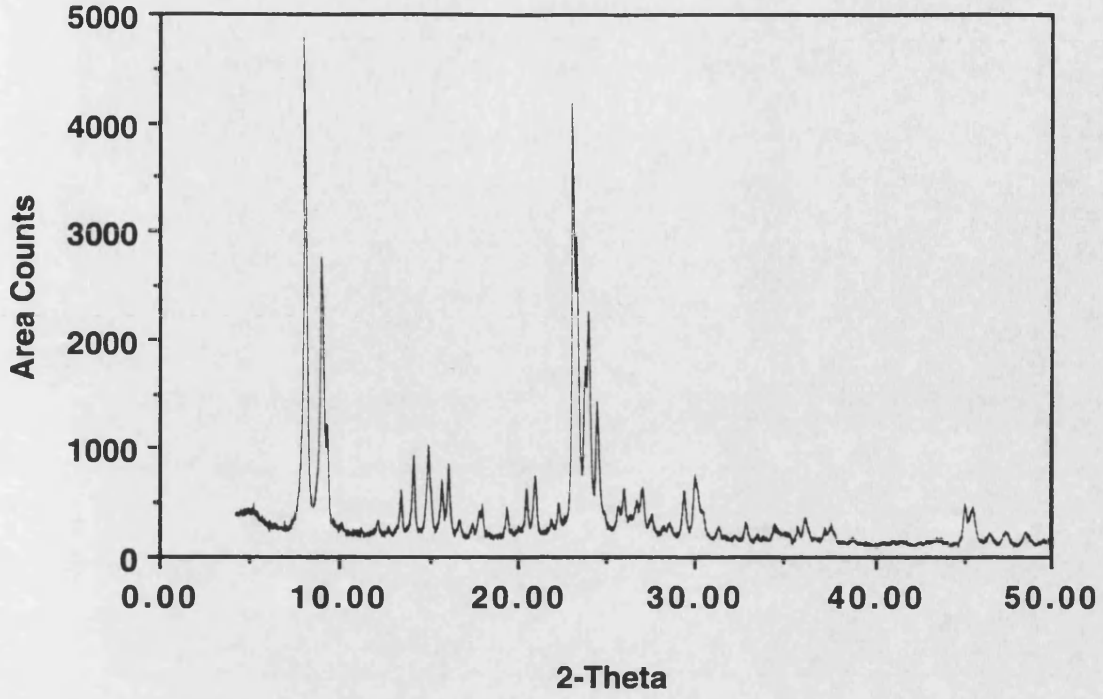

Figure A3. X-ray powder diffraction pattern of ZCIC-25 zeolite.

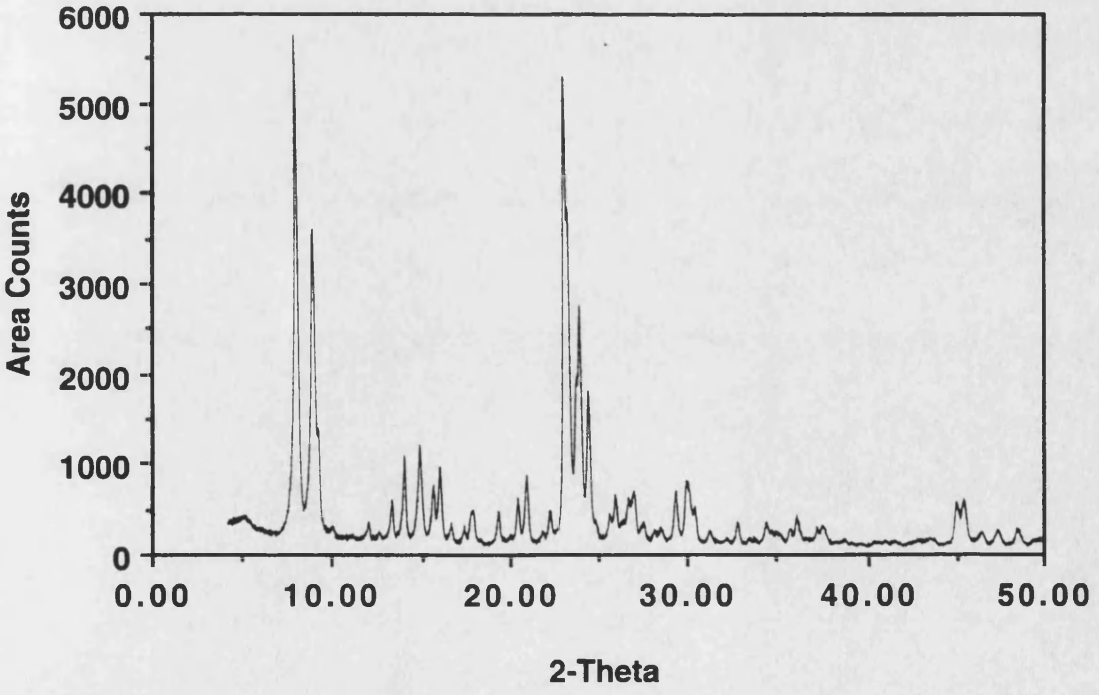

Figure A4. X-ray powder diffraction pattern of ZCIC-50 zeolite.

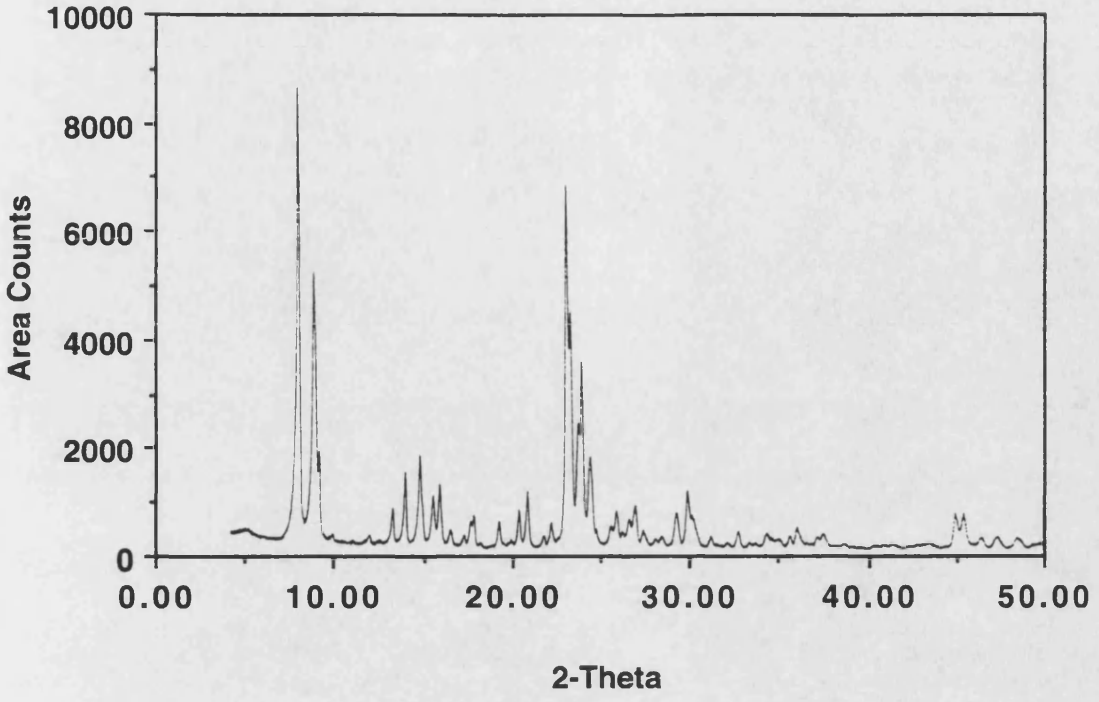

Figure A5. X-ray powder diffraction pattern of ZCIC-75 zeolite.

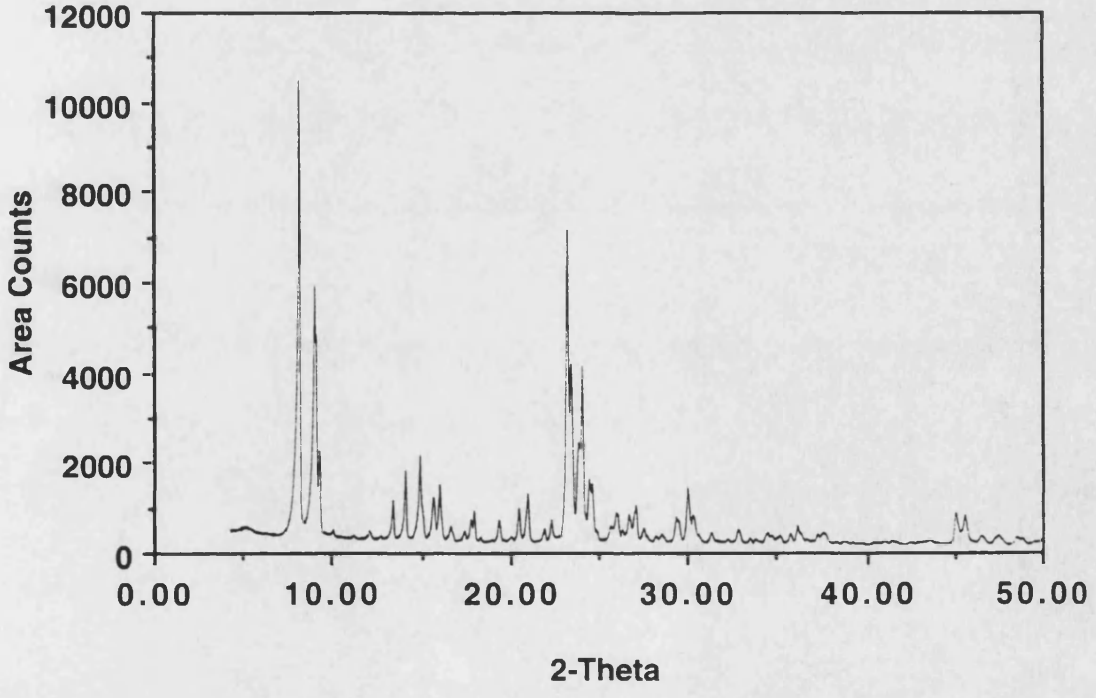

Figure A6. X-ray powder diffraction pattern of ZCIC-100 zeolite.

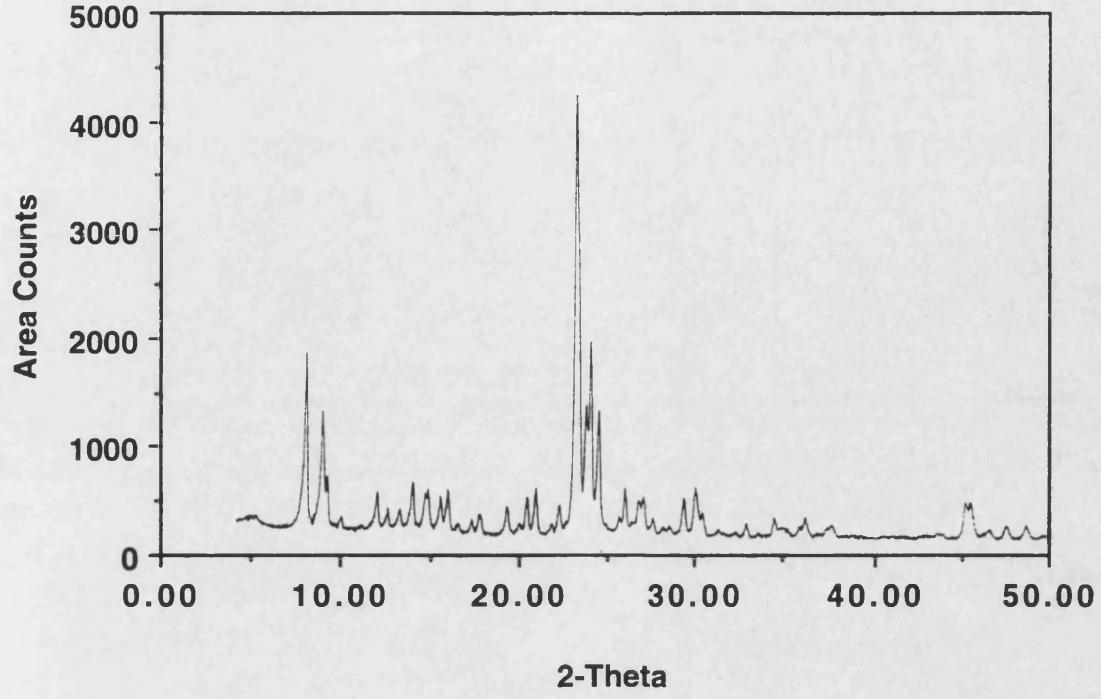

Figure A7. X-ray powder diffraction pattern of B-MFI zeolite.

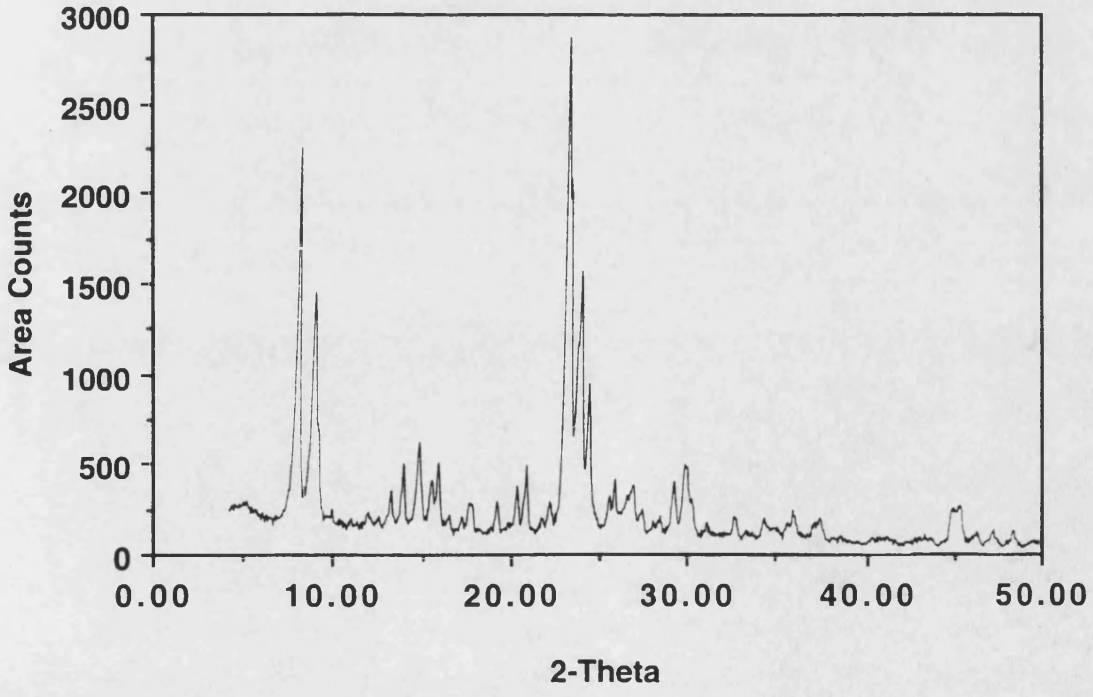

Figure A8. X-ray powder diffraction pattern of Ga-MFI zeolite.

APPENDIX B FT-IR SPECTRA

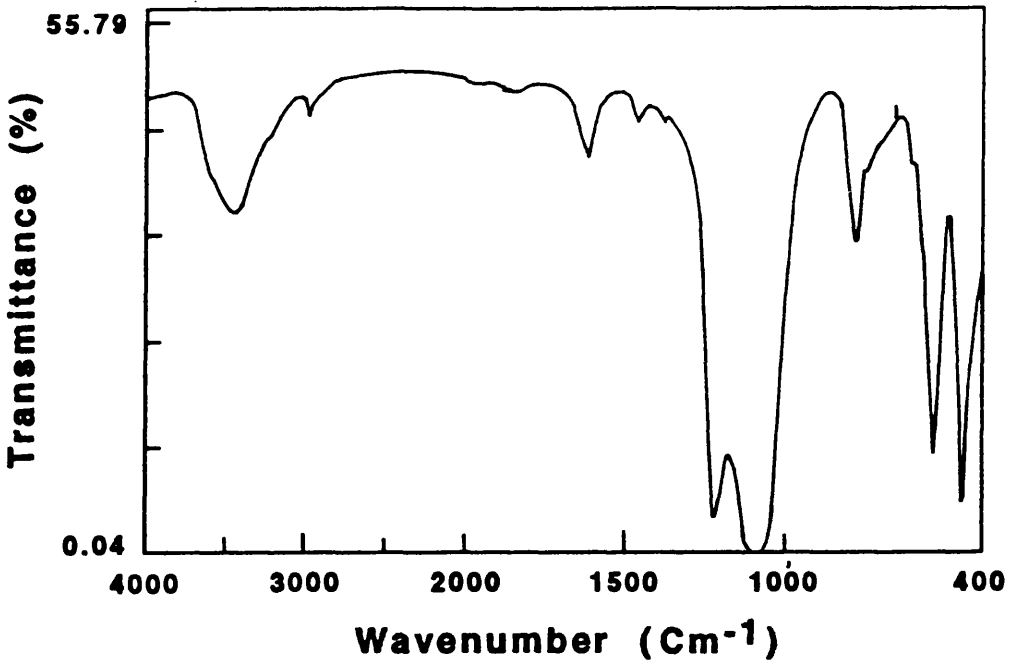

Figure B1. FT-IR spectrum of ZCIC-15 zeolite.

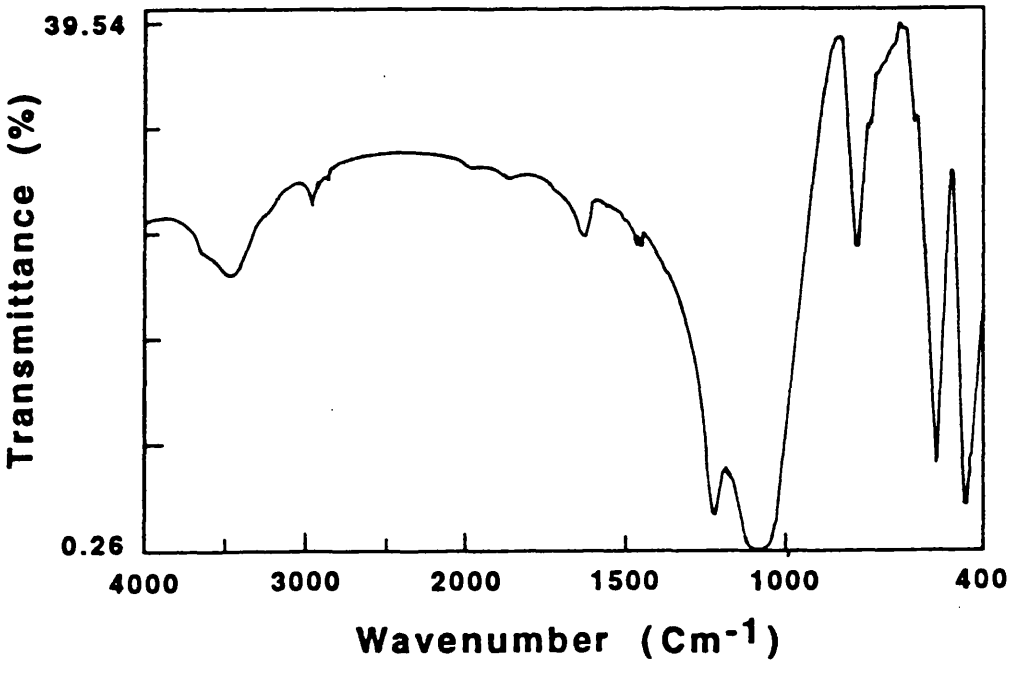

Figure B2. FT-IR spectrum of ZCIC-20 zeolite.

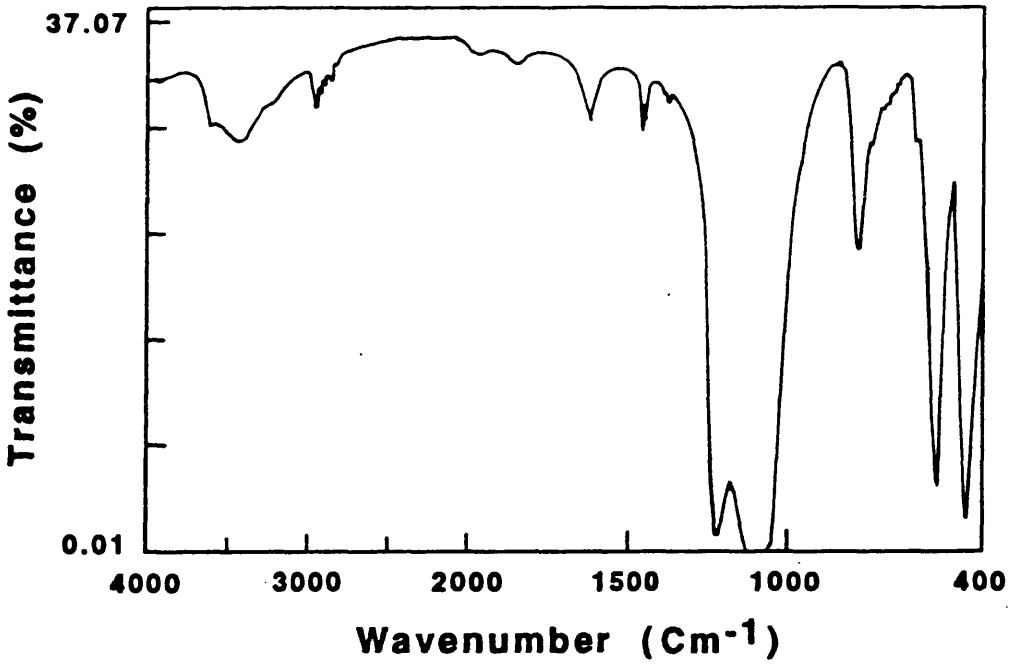

Figure B3. FT-IR spectrum of ZCIC-25 zeolite.

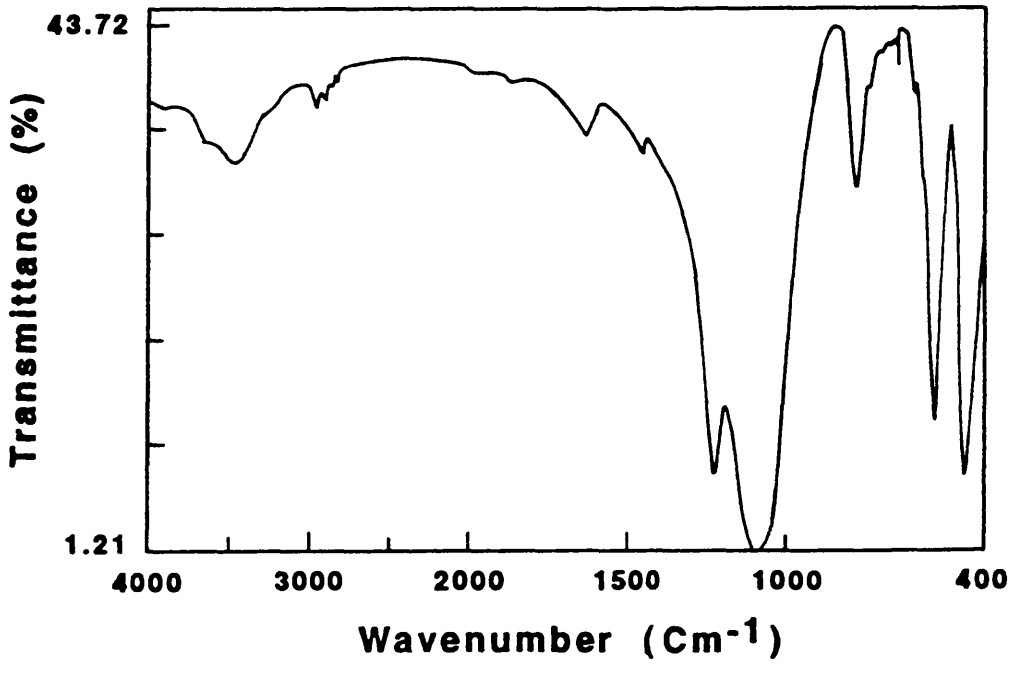

Figure B4. FT-IR spectrum of ZCIC-50 zeolite.

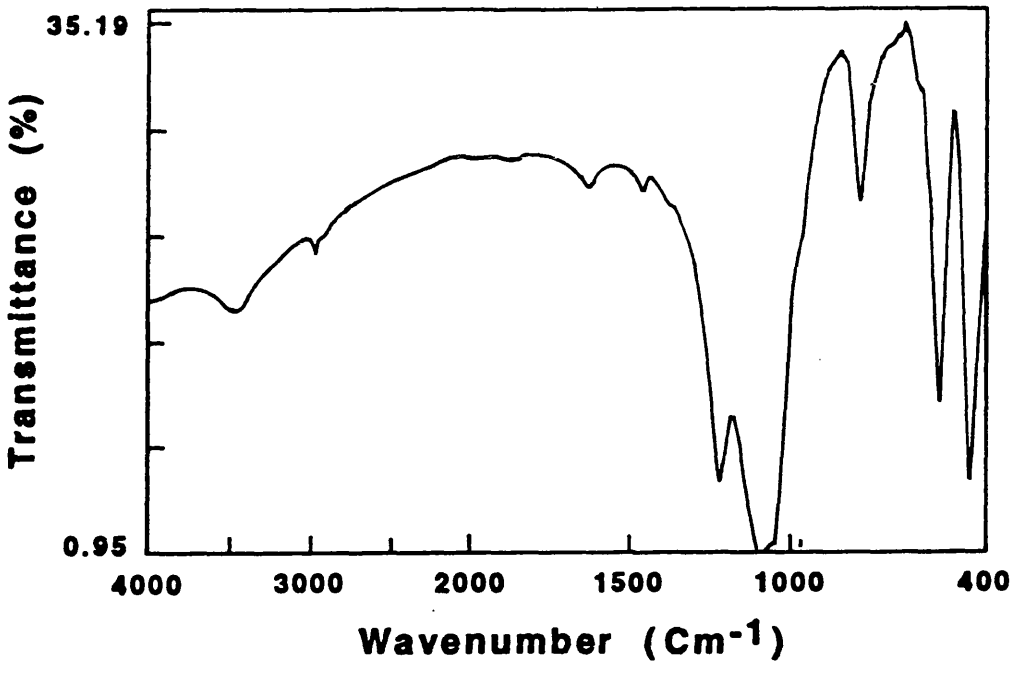

Figure B5. FT-IR spectrum of ZCIC-75 zeolite.

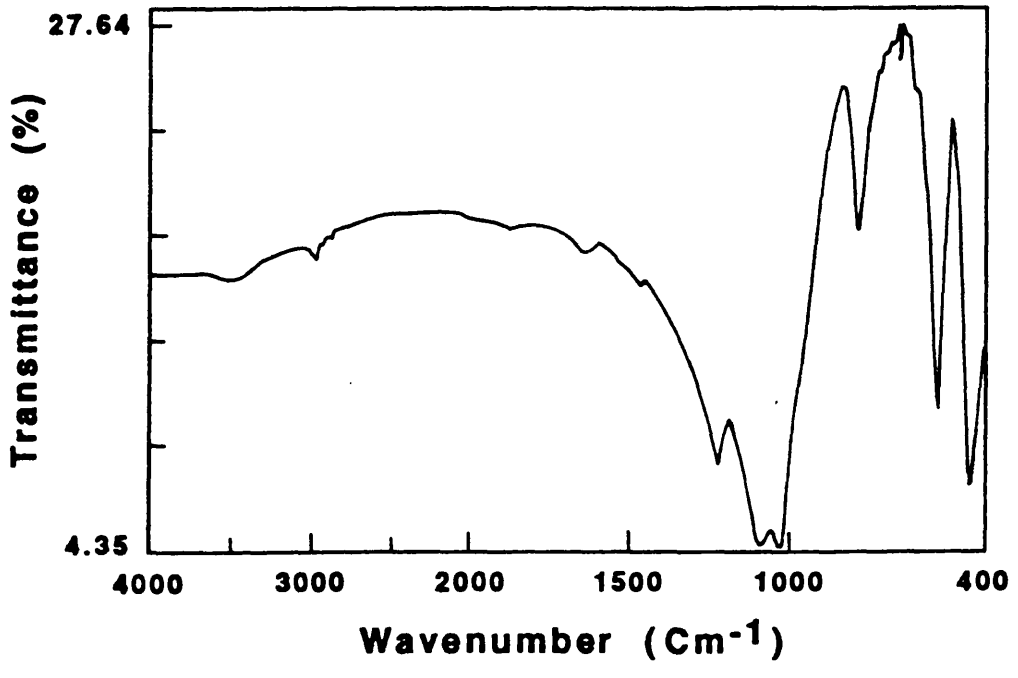

Figure B6. FT-IR spectrum of ZCIC-100 zeolite.

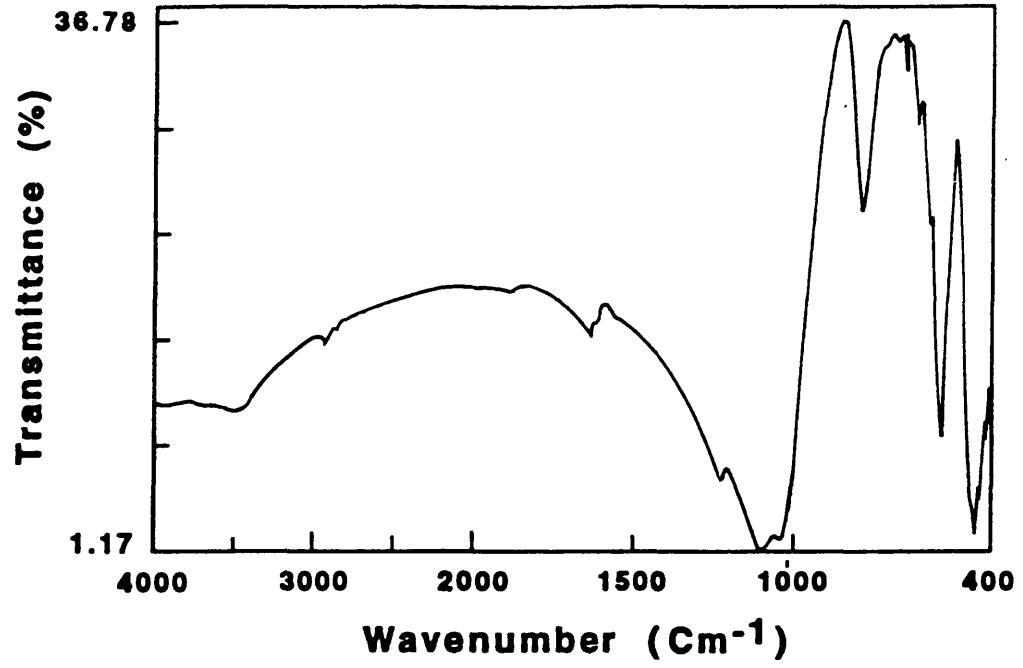

Figure B7. FT-IR spectrum of ZAS-10 zeolite calcined at 500 °C for 5 hours.

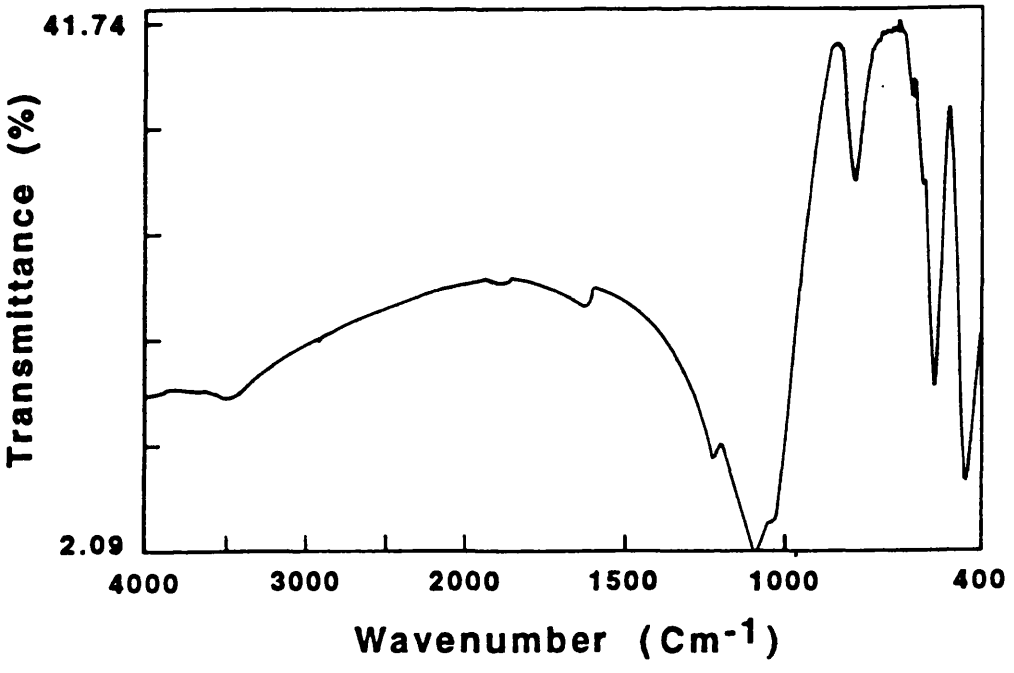

Figure B8. FT-IR spectrum of ZAS-10 zeolite calcined at 600 °C for 3 hours..

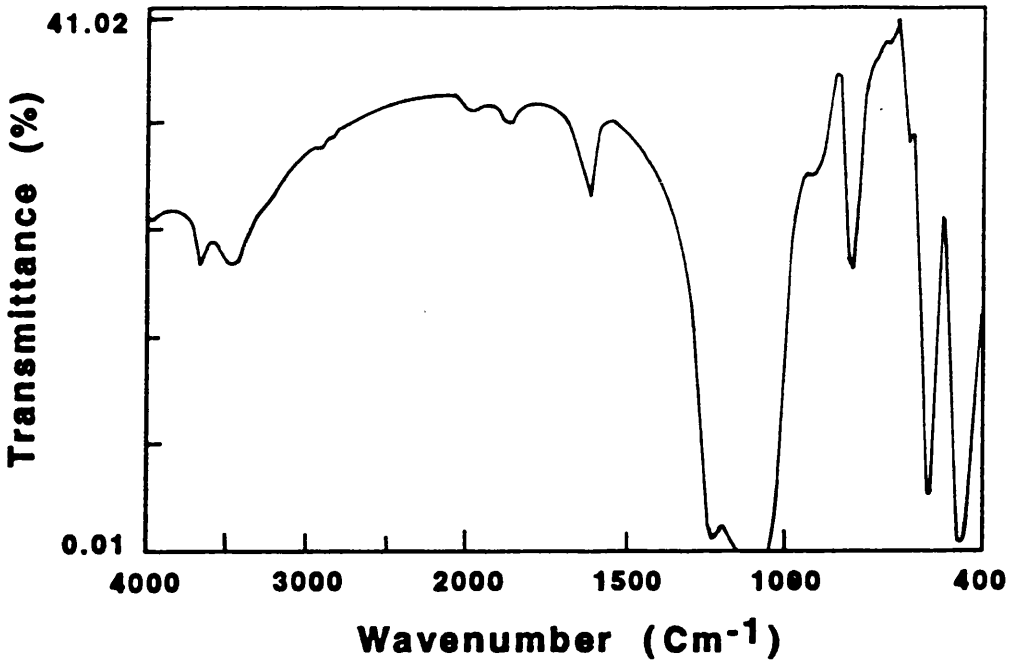

Figure B9. FT-IR spectrum of B-MFI zeolite.

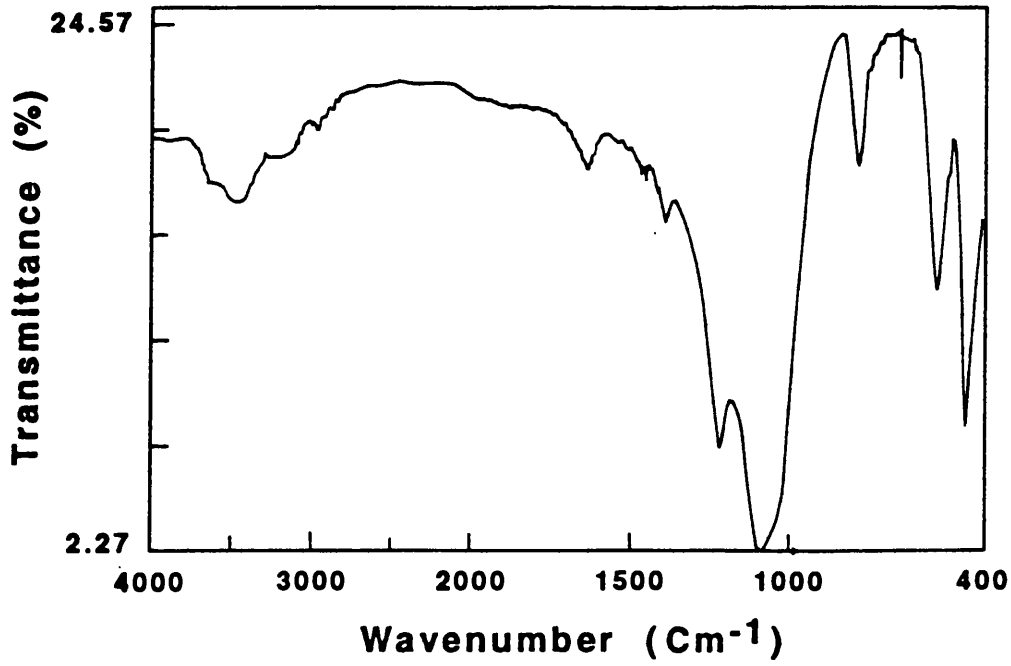

Figure B10. FT-IR spectrum of Ga-MFI zeolite.

APPENDIX C THERMOGRAMS

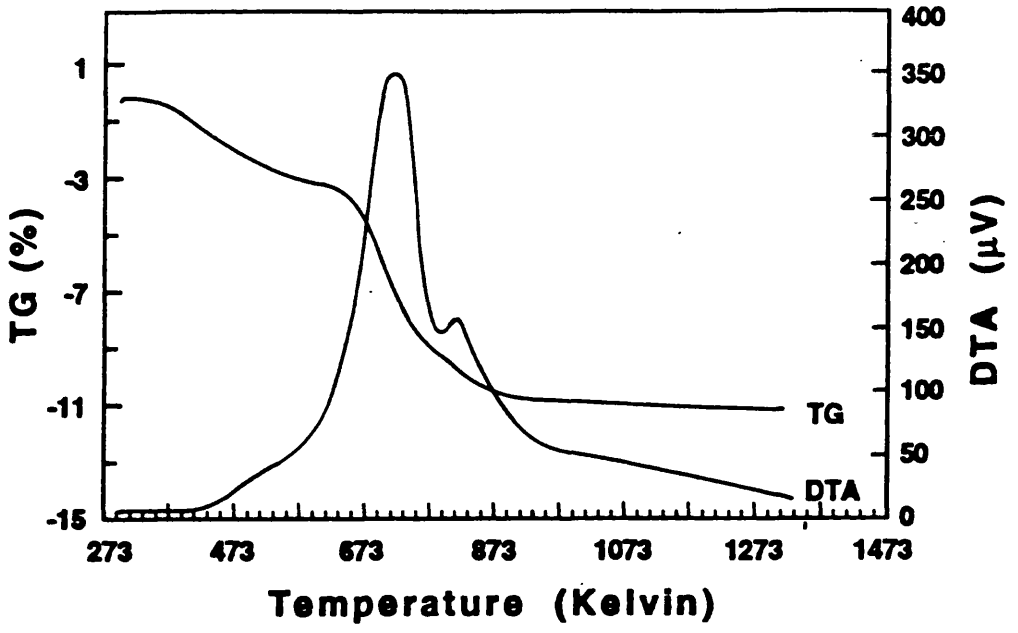

Figure C1. Thermogram of ZCIC-15 zeolite.

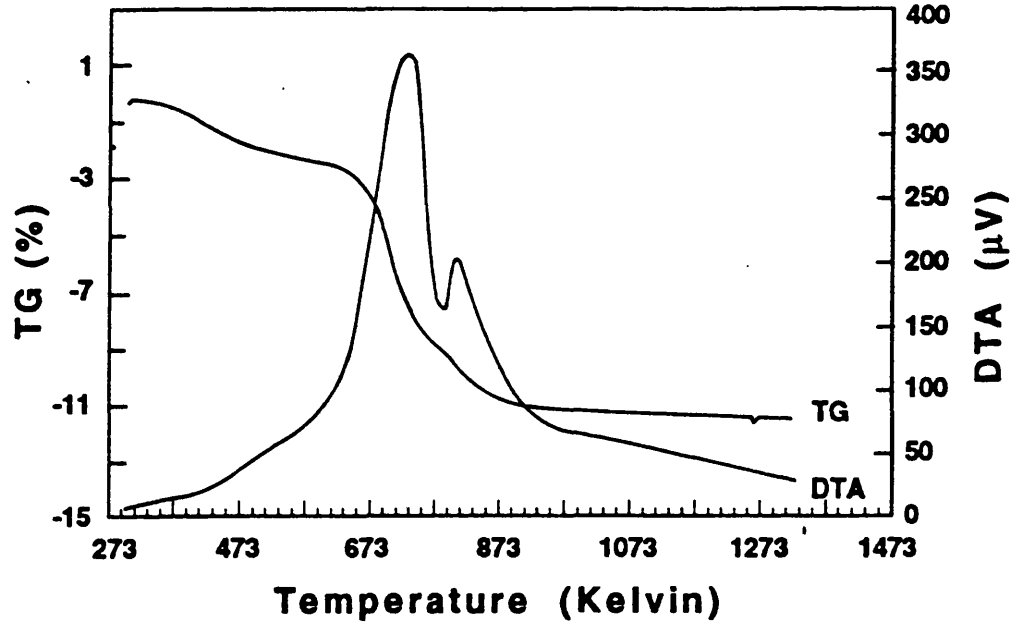

Figure C2. Thermogram of ZCIC-20 zeolite.

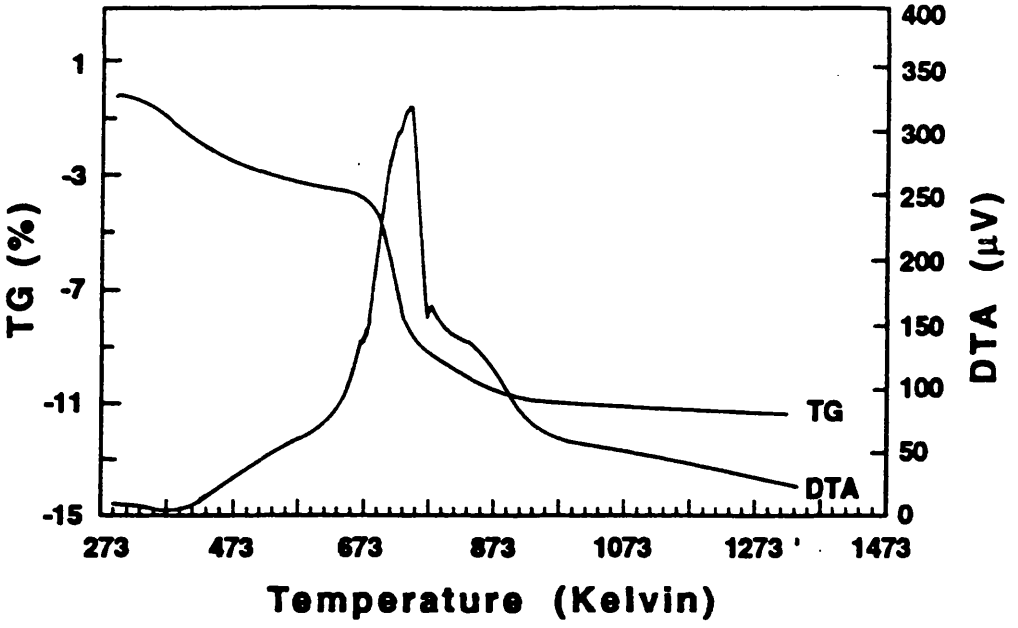

Figure C3. Thermogram of ZCIC-25 zeolite.

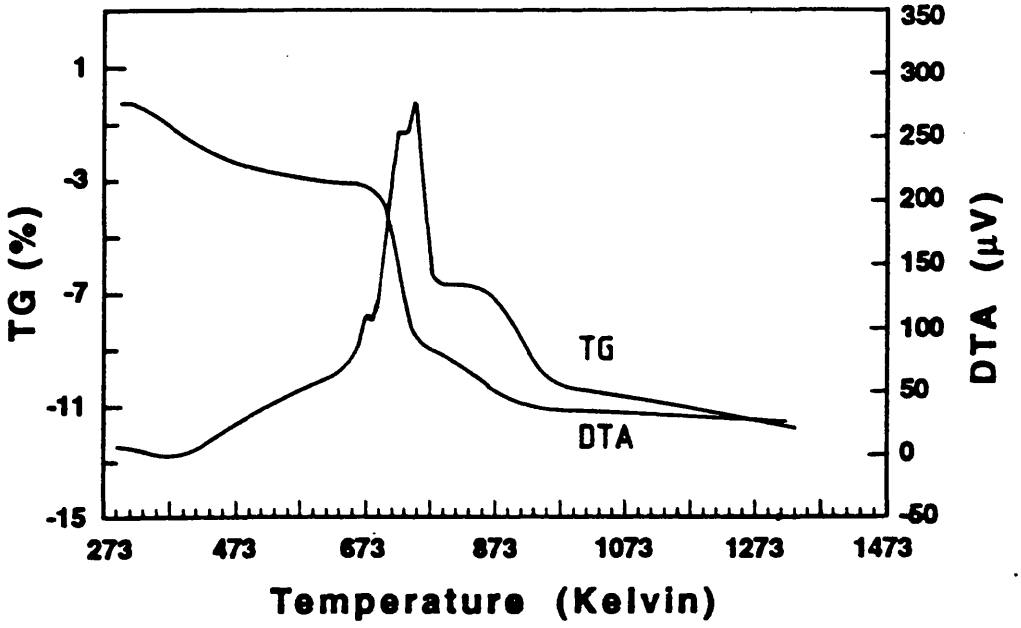

Figure C4. Thermogram of ZCIC-50 zeolite.

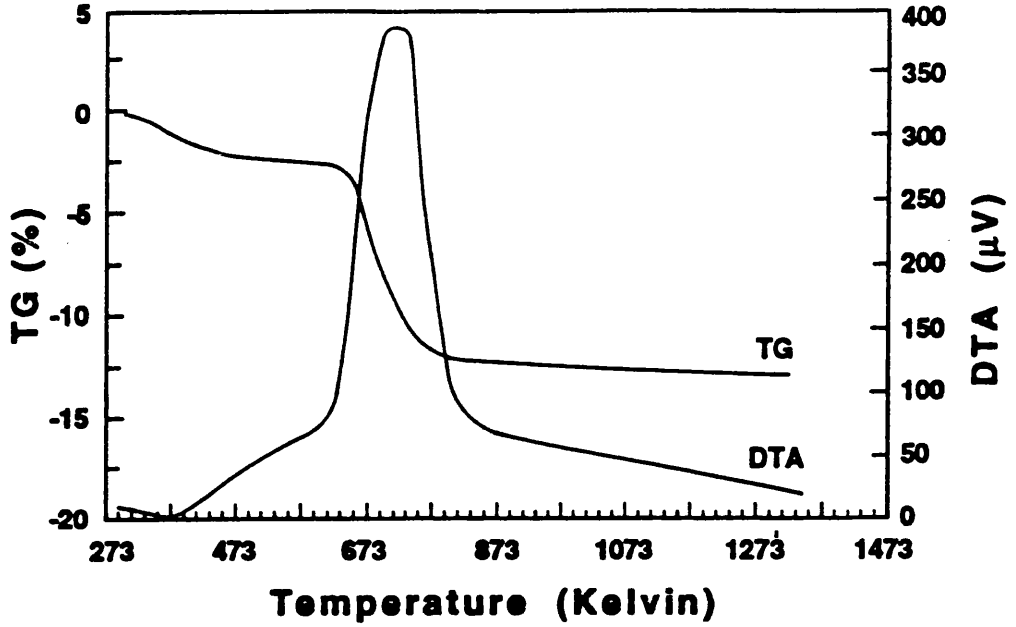

Figure C5. Thermogram of ZCIC-75 zeolite.

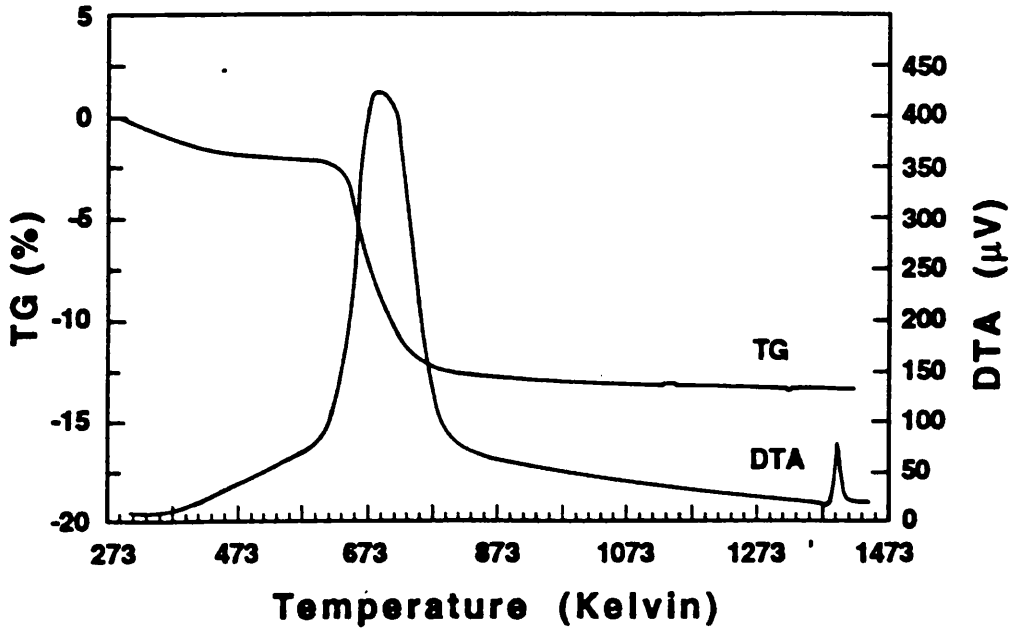

Figure C6. Thermogram of ZCIC-100 zeolite.

APPENDIX D SCANNING ELECTRON MICROGRAPHS

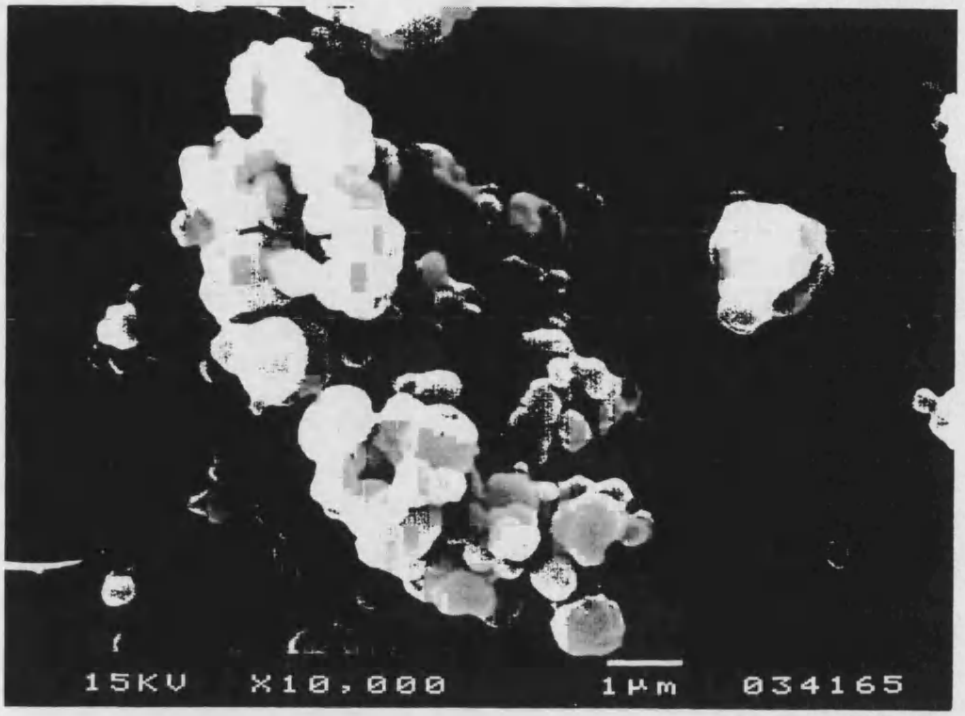

Figure D1. Scanning electron micrograph of ZCIC-15 zeolite.

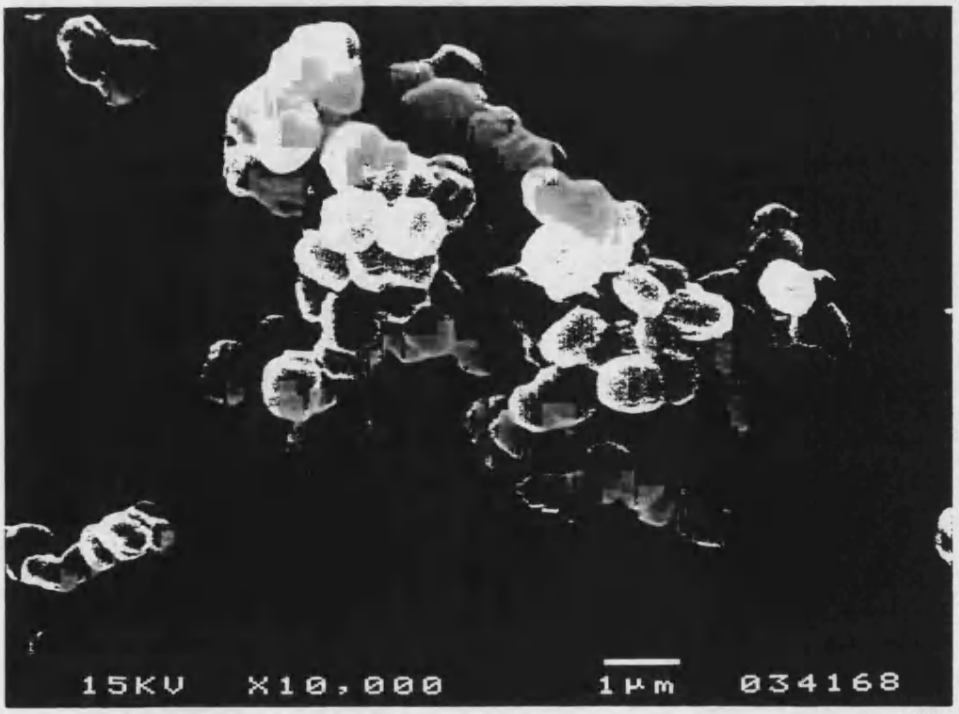

Figure D2. Scanning electron micrograph of ZCIC-20 zeolite.

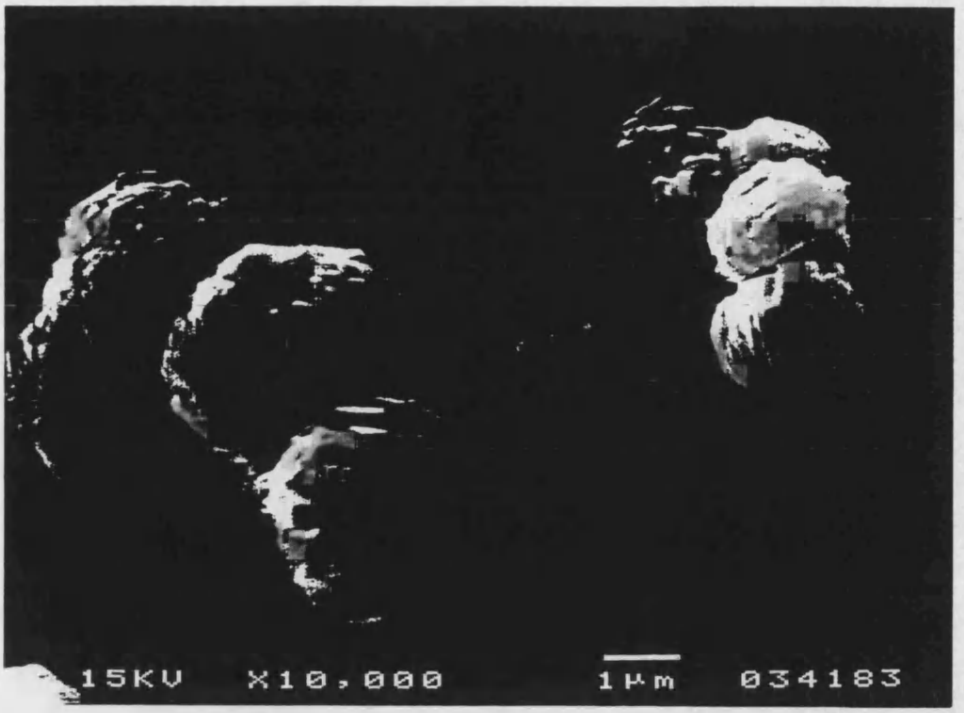

Figure D3. Scanning electron micrograph of ZCIC-25 zeolite.

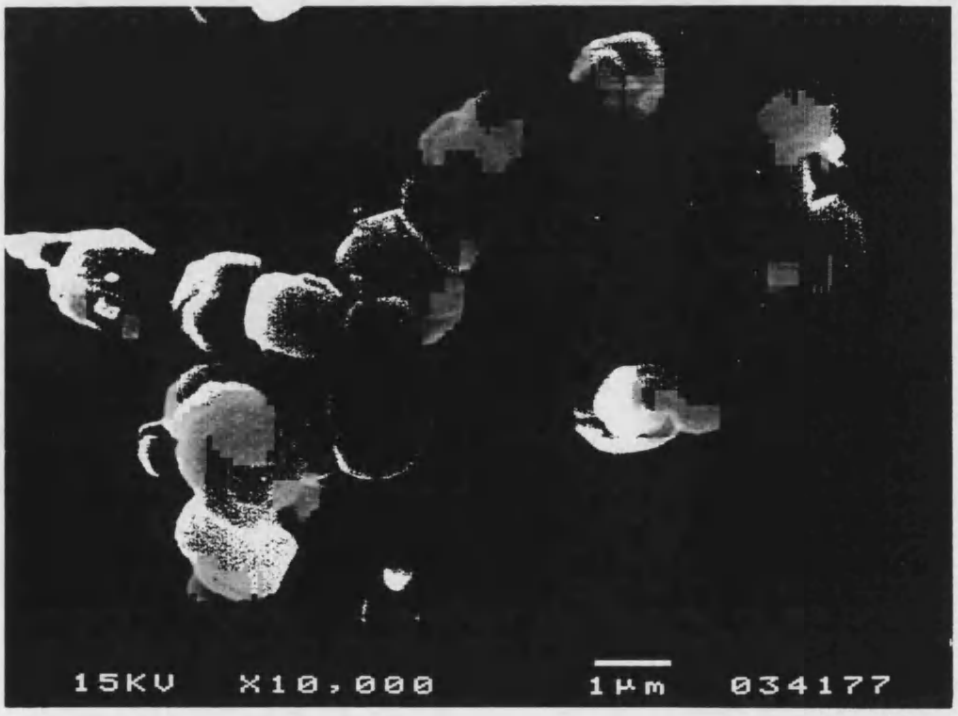

Figure D4. Scanning electron micrograph of ZCIC-50 zeolite.

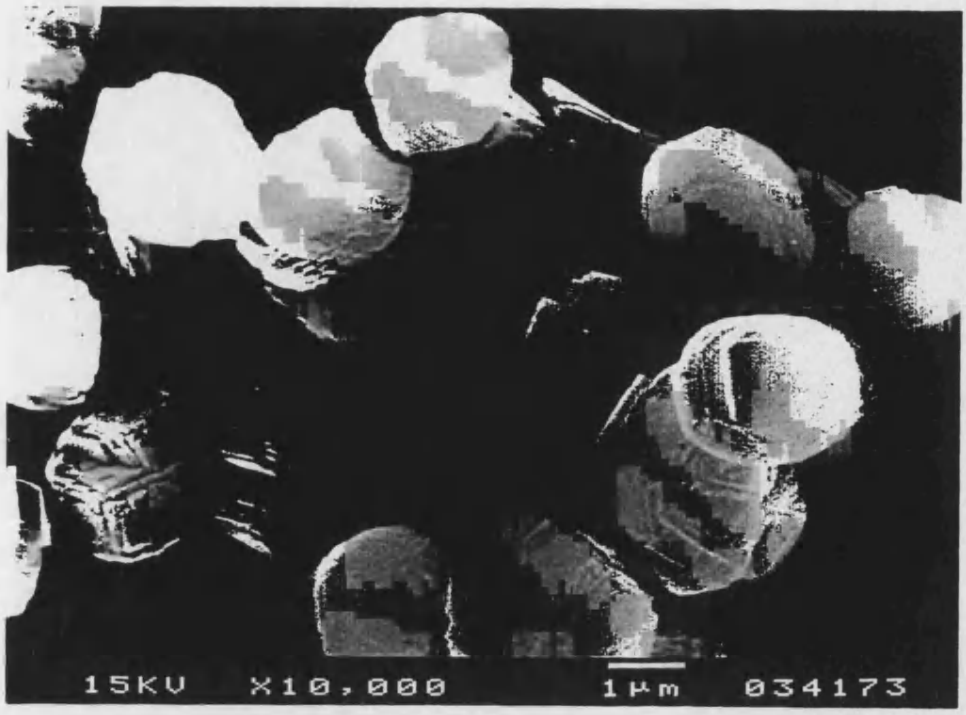

Figure D5. Scanning electron micrograph of ZCIC-75 zeolite.

Figure D6. Scanning electron micrograph of ZCIC-100 zeolite.

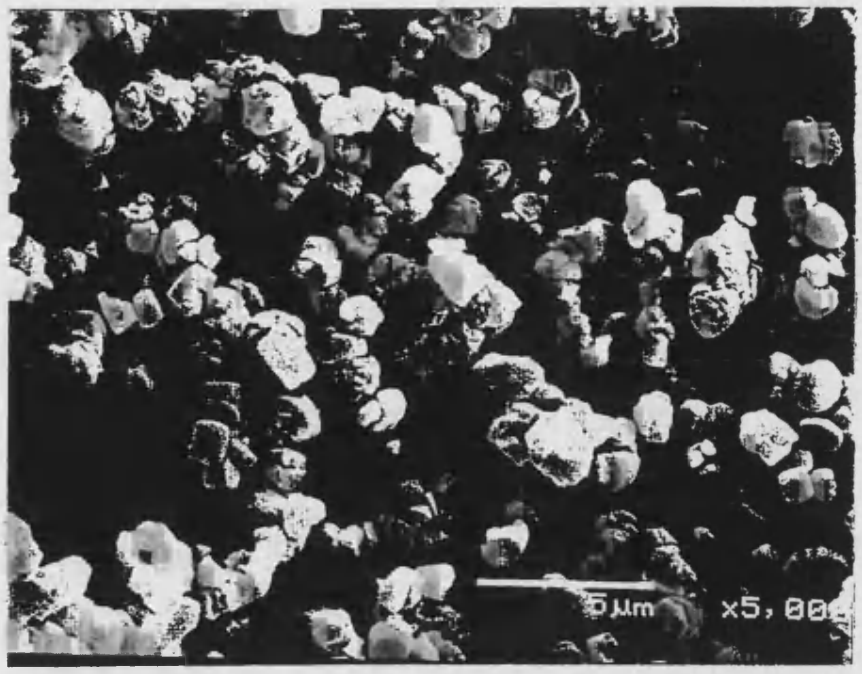

Figure D7. Scanning electron micrograph of B-MFI zeolite.

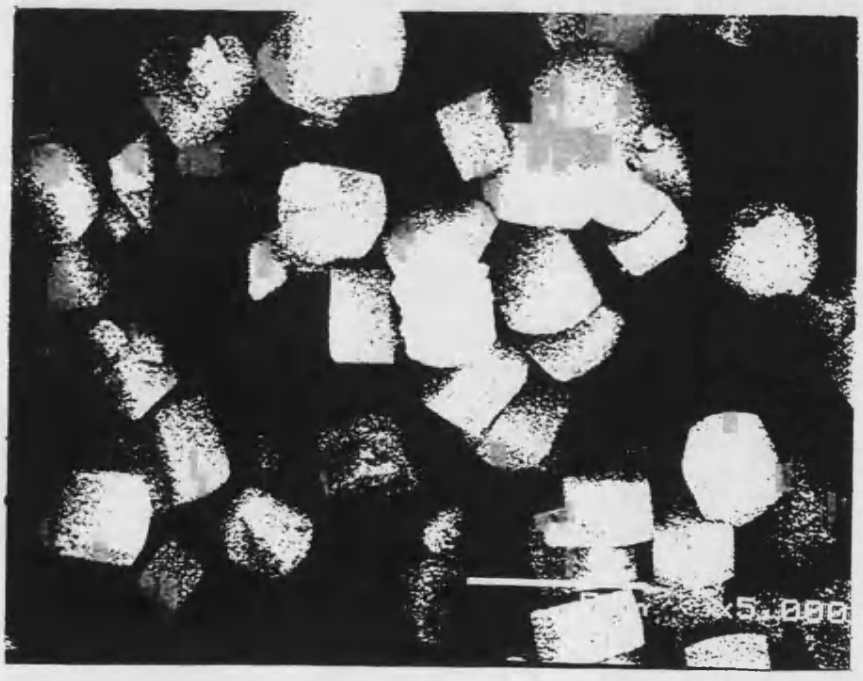

Figure D8. Scanning electron micrograph of Ga-MFI zeolite.

APPENDIX E METHOD OF REACTION PRODUCT ANALYSIS

Analysis of the reaction products was carried out using internal standard method (ASTM method E 260). This technique provides a correction for the relatively high variability of syringe injection and therefore yields a more precise method of analysis. Neither the quantity of solution injected nor change in detector response will alter the area ratio of the components of interest and the internal standard. Prior to analyzing the products, response factors were determined for methanol and MTBE. For this purpose, a number of standard mixtures consist of methanol, MTBE and diisopropyl ether (DIPE) were prepared. An amount, 0.2 microliter, of each standard was injected into the gas chromatograph and the area counts (AC) of all three components were obtained. Then the response factors were determined as follows:

$$\text{Response Factor of MTBE } (RF_{MTBE}) = \frac{\text{moles of MTBE x AC of DIPE}}{\text{moles of DIPE x AC of MTBE}}$$

$$\text{Response Factor of Methanol } (RF_{MeOH}) = \frac{\text{moles of Methanol x AC of DIPE}}{\text{moles of DIPE x AC of Methanol}}$$

After determining the response factor, each reaction product was added with a known amount of DIPE (0.2-0.3 g) as an internal standard, and was analyzed by gas chromatograph to obtain the area counts of methanol, DIPE and MTBE. The following relationships were then used to calculate the amount of MTBE and methanol.

$$\text{Moles of MTBE} = \frac{\text{moles of DIPE x AC of MTBE}}{\text{AC of DIPE}} \times (RF_{MTBE})$$

$$\text{Moles of Methanol} = \frac{\text{moles of DIPE x AC of Methanol}}{\text{AC of DIPE}} \times (RF_{MeOH})$$

The reaction of methanol and isobutene is represented as follows:

Methanol + Isobutene ----------> MTBE

Suppose
initial moles of methanol $= N_A$
initial moles of isobutene $= N_B$
Number of moles of MTBE formed $= X$

Then the above reaction can be represented as

$$(N_A\text{-}X) + (N_B\text{-}X) \longrightarrow X$$

Suppose,

moles of methanol = D

moles of MTBE = E

D and E are related to the moles at the reaction temperature, (N_A - X) and X as follows:

$$(N_A - X) = A \times D \qquad \text{(D-1)}$$

$$\text{and} \quad X = A \times E \qquad \text{(D-2)}$$

where A is a constant which related the moles at room temperature to the moles at reaction temperature. Substitute for X from equation (D-2) into equation (D-1), we get

$$N_A - (A \times E) = A \times D$$

$$N_A = (A \times D) + (A \times E)$$

$$A = N_A / (D+E) \qquad \text{(D-3)}$$

Substitute for A from equation (D-3) into equations (D-1) and (D-2), we get

$$\text{Moles of Methanol} = (N_A - X) = N_A \times D / (D+E) \qquad \text{(D-4)}$$

and

$$\text{Moles of MTBE} = X = N_A \times E / (D+E) \qquad \text{(D-5)}$$

The moles of isobutene were calculated from the stoichiometry of the reaction and the initial concentration of isobutene present in the reaction mixture and are given as (N_B-X).

In heterogeneous catalysis, the concentrations of the components in the reaction are expressed as moles per gram of catalyst. Therefore, the moles of each component was divided by the amount of catalyst charged in the reactor.

APPENDIX F DERIVATION OF THE MODEL EQUATIONS

Rideal-Eley Mechanism

In order to derive an equation for the Rideal-Eley mechanism, consider the case in which reactant A is adsorbed on surface site S and reacts with reactant B in solution. The reaction of methanol (adsorbed A) and isobutene (nonadsorbed B) can be represented by the following elementary steps:

1. **Adsorption** **A + S = A·S**

$$\text{Rate of adsorption of A} = r_{AD} = k_A\left(C_A C_V - \frac{C_{AS}}{K_A}\right) \qquad \text{(F-1)}$$

Where

k_A = Adsorption rate constant of reactant A
C_A = Molar concentration of reactant A
C_V = total molar concentration of active vacant sites per gram of catalyst
$C_{A.S}$ = Molar concentration of reactant A adsorbed on site S
K_A = Adsorption equilibrium constant of reactant A

2. **Surface Reaction** **A·S + B = C·S**

$$\text{Rate of surface reaction} = r_S = k_S\left(C_{AS} C_B - \frac{C_{CS}}{K_S}\right) \qquad \text{(F-2)}$$

k_S = Surface reaction rate constant
C_B = Molar concentration of reactant B
C_V = Total molar concentration of active vacant sites per gram of catalyst
$C_{C.S}$ = Molar concentration of product C adsorbed on site S
K_S = Surface reaction equilibrium constant

3. **Desorption** **C·S = C + S**

$$\text{Rate of desorption} = r_D = k_D\left(C_{CS} - \frac{C_C C_V}{K_C'}\right) \qquad \text{(F-3)}$$

k_D = Desorption rate constant of product C
C_B = Molar concentration of reactant B
C_C = Molar concentration of product C
K_C' = Desorption equilibrium constant of product C

For surface reaction limited mechanism, the rate of consumption of A on the surface is equal to the rate of surface reaction.

$$-r_A = r_S = k_S\left(C_{A.S}C_B - \frac{C_{C.S}}{K_S}\right) \qquad \text{(F-4)}$$

The $C_{C.S}$ and $C_{A.S}$ in the above equation can be replace by measurable quantities. For this purpose, we will use equation (F-1) to obtain $C_{A.S}$. The adsorption of the reactant A is so fast on the surface S that the change in the concentration of A with time is zero ($dC_A/dt = 0$). Thus $r_{AD}/k_A = 0$ since the k_A is very large.
Thus from equation (F-1),

$$\left(C_A C_V - \frac{C_{A.S}}{K_A}\right) = 0$$

Therefore

$$C_{A.S} = K_A C_A C_V \qquad \text{(F-5)}$$

Similarly, the desorption of the product is so fast that the change in the concentration of MTBE with time is zero ($dC_C/dt = 0$). Thus $r_D/k_D = 0$ since the k_D is very large.
Thus from equation (F-3),

$$\left(C_{C.S} - \frac{C_C C_V}{K_C'}\right) = 0$$

Therefore

$$C_{C.S} = C_C C_V / K_C' \qquad \text{(F-6)}$$

From the catalytic site balance, we know that

$$C_t = C_V + C_{A.S} + C_{C.S} \qquad \text{(F-7)}$$

where C_t = total molar concentration of active sites per gram of catalyst (defined as number of active sites per gram of the catalyst /Avogadro's number), and C_V = total molar concentration of active vacant sites per gram of catalyst

Substitute the values of $C_{A.S}$ and $C_{C.S}$ from equation (F-5) and (F-6) into equation (F-7) and rearrange for C_V,

$$C_V = \frac{Ct}{1 + C_A K_A + C_C / K_C'} \qquad \text{(F-8)}$$

Now, substitute the values of $C_{A.S}$, $C_{C.S}$ and C_V into equation (F-4), we get

$$-r_A = r_S = k_S\left(K_A C_A C_B C_V - \frac{C_C C_V}{K_S K_C'}\right)$$

$$-r_A = r_S = k_S C_V \left(K_A C_A C_B - \frac{C_C}{K_S K_C'} \right)$$

$$-r_A = r_S = k_S C_t \frac{(K_A C_A C_B - C_C / K_S K_C')}{1 + K_A C_A + C_C / K_C'}$$

$$-r_A = \frac{k_S C_t K_A C_A C_B - C_C k_S C_t / K_S K_C'}{1 + K_A C_A + C_C / K_C'} \qquad \text{(F-9)}$$

C_t being a constant can be incorporated into k_S.

$$-r_A = k_S K_A \frac{C_A C_B - C_C k_S / K_S K_C'}{1 + K_A C_A + C_C / K_C'} \qquad \text{(F-10)}$$

Let $K_S K_C'/k_S = K_e$ = overall equilibrium constant and $K_C = 1/K_C'$, then the following equation is obtained where a, b and c are the order of reaction with respect to species A, B and C.

$$-r_A = k_S K_A^a \frac{C_A^a C_B^b - C_C^c / K_e}{\left(1 + K_A C_A + K_C C_C\right)^a} \qquad \text{(F-11)}$$

It should be noted that the adsorption equilibrium constant of a given species is exactly the reciprocal of the desorption equilibrium constant of that species (i.e. $K_C = 1/K_C'$).

In case of second possible mechanism where reactant B is adsorbed and reacts with reactant A in solution, the reaction of methanol (adsorbed A) and isobutene (nonadsorbed B) can be represented by the following elementary steps:

1. Adsorption **B + S = B·S**

$$\text{Rate of adsorption of B} = r_{AD} = k_B \left(C_B C_V - \frac{C_{B.S}}{K_B} \right) \qquad \text{(F-12)}$$

Where

k_B = Adsorption rate constant of reactant B

C_B = Molar concentration of reactant B

C_v = Total molar concentration of active vacant sites per gram of catalyst

$C_{B.S}$ = Molar concentration of reactant B adsorbed on site S

K_B = Adsorption equilibrium constant of reactant B

2. Surface reaction **B·S + A = C·S**

$$\text{Rate of surface reaction} = r_S = k_S \left(C_{B.S} C_A - \frac{C_{C.S}}{K_S} \right) \qquad \text{(F-13)}$$

K_S = Surface reaction rate constant

C_A = Molar concentration of reactant A

$C_{C.S}$ = Molar concentration of product C adsorbed on site S

K_S = Surface reaction equilibrium constant

3. Desorption **C·S = C + S**

$$\text{Rate of desorption} = r_D = k_D\left(C_{C.S} - \frac{C_C C_V}{K_C'}\right) \qquad \text{(F-14)}$$

k_D = Desorption rate constant of product C

C_C = Molar concentration of product C

$C_{C.S}$ = Molar concentration of product C adsorbed on site S

K_C' = Desorption equilibrium constant of product C

and the equation for the case where B is adsorbed and reacts with A in solution will be as follows:

$$-r_A = k_S K_B^b \frac{C_A^a C_B^b - C_C^c / K_e}{\left(1 + K_B C_B + K_C C_C\right)^b} \qquad \text{(F-15)}$$

Langmuir-Hinshelwood Mechanism

In the case of the Langmuir-Hinshelwood mechanism, reaction takes place between molecules A and B adsorbed on two adjacent active sites and the kinetic equation will be in the form as given below:

$$-r_A = k_S K_A^a K_B^b \frac{C_A^a C_B^b - C_C^c / K_e}{\left(1 + K_A C_A + K_B C_B + K_C C_C\right)^{a+b}} \qquad \text{(F-16)}$$

APPENDIX G

PROPERTIES OF MTBE, METHANOL AND ISOBUTENE

Table G1. Physical, chemical and thermal properties of MTBE.

Molecular weight	88.15
Elemental analysis, wt%	
Carbon / Hydrogen / Oxygen	68.1 / 13.7 / 18.2
C/H weight ratio	5.0
Density @ 15 °C, g cm^{-3}	0.75
Boiling point @ 760 mmHg, °C (K)	55.3 (328)
Freezing point, °C (K)	-108.6 (164.5)
Vapor density, calculated, (air = 1)	3.1
Solubility @ 20 °C (25 °C), wt%	
MTBE in water	4.0 (5.0)
Water in MTBE	1.3 (1.5)
Viscosity, cSt	
@ 37.8 °C (311 K),	0.31
@ 20 °C (293 K), cp	0.35
@ -20 °C (253 K), cp	0.60
Refractive index @ 20 °C (293 K)	1.37
Dielectric constant	4.5
Surface tension, din cm^{-2}	19.4
Latent heat of vaporization (25 °C), kCal kg^{-1} (kJ kg^{-1})	81.7 (342)
Specific heat @ 25 °C, Cal g^{-1} _C^{-1}	0.5
Lower heating value, kCal kg^{-1} (kJ kg^{-1})	8,400 (35146)
Flammability limits in Air, vol%	
Lower limit / Upper limit	1.7 / 8.4
Auto ignition temperature, °C (K)	435 (708)
Flash point, closed cup, °C (K)	-25.6 (247)
Blending octane number	
RON * / MON *	116 / 98
(RON + MON)/2*	107

*Octane numbers were obtained for a blend of 10 vol% of MTBE in unleaded base gasoline having 94.3 RON and 84.3 MON. Laboratory engine research and motor octane rating procedures are not suitable for use with neat oxygenates such as MTBE.

Table G2. Physical, chemical and thermal properties of methanol.

Molecular weight	32.0
Elemental analysis, wt%	
Carbon / Hydrogen / Oxygen	37.5 / 12.6 / 49.9
C/H weight ratio	3.0
Specific gravity @ 15 °C (288 K)	0.79
Reid vapor pressure (RVP)	
37.8 °C, kPa (psi)	31.7 (4.6)
25 °C, kPa (psi)	15.8 (2.3)
Blending RVP, kPa (psi)	414 (60.0)
Boiling point, °C (K)	65.0 (338)
Freezing point, °C (K)	-93 (180)
Specific heat, kJ kg^{-1} $°C^{-1}$ (Btu lb^{-1} $°F^{-1}$)	2.5 (0.60)
Solubility @ 21 °C (294 K), wt%	
Methanol in water	100
Water in methanol	100
Viscosity @ 40 °C, cSt (cP)	0.46 (0.58)
Dielectric constant	32.6
Latent heat of vaporization, kCal kg^{-1} (kJ kg^{-1})	260 (1088)
Lower heating value, kCal kg^{-1} (kJ kg^{-1})	4650 (19456)
Flammability limits in Air, vol%	
Lower limit / Upper limit	7.0 / 36.0
Autoignition temperature, °C (K)	470 (743)
Flash point, closed cup, °C (K)	11 (284)
Refractive Index	1.33
Blending octane number	
RON* / MON*	123 / 91
(RON+MON)/2*	107

*Octane number (RON and MON) obtained for a blend of 10 volume percent methanol in a base gasoline having RON clear 94.3 and MON clear 84.3. Laboratory RON and MON rating procedures are not suitable to measure the octane number of pure oxygenates.

Table G3. Physical, chemical and thermal properties of isobutene.

Molecular weight	56.104
Boiling point @ 760 mm Hg, °C (K)	-6.9 (266.2 K)
Melting point @ 760 mm Hg, °C (K)	-140.4 (132.6 K)
Saturated vapor pressure, mm Hg	
@ 25 °C (298 K)	3.0
@ 100 °C (373 K)	18.4
Density of liquid isobutene, g cm^{-3}	
@ 10 °C (283 K)	0.61
@ 25 °C (298 K)	0.59
Latent heat of vaporization, kJ kg^{-1}	
@ 20 °C (293 K)	371
@ 100 °C (373 K)	247

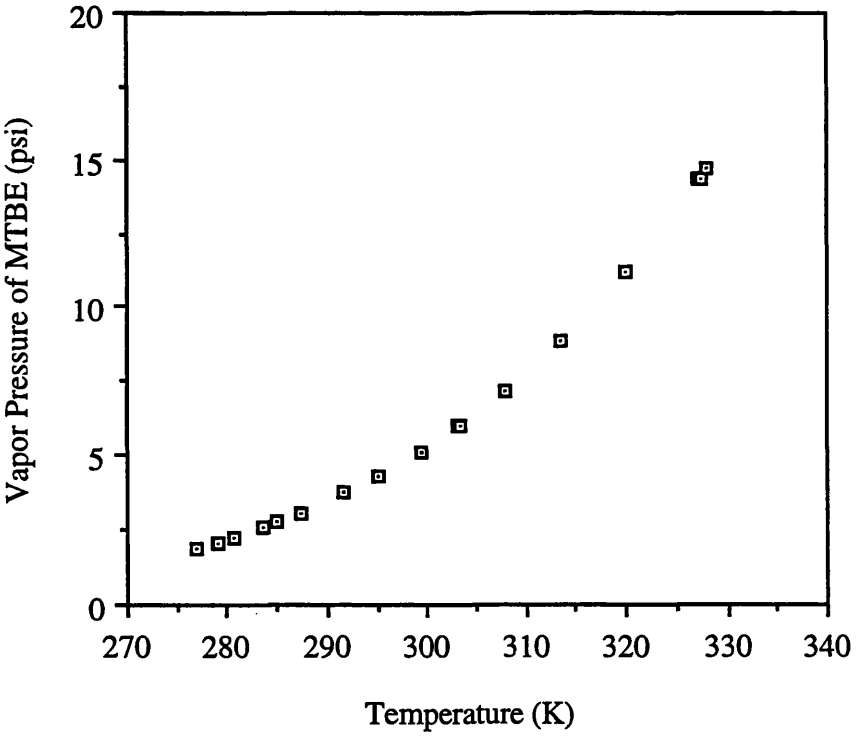

Figure G1. Vapor pressure of MTBE as a function of temperature.

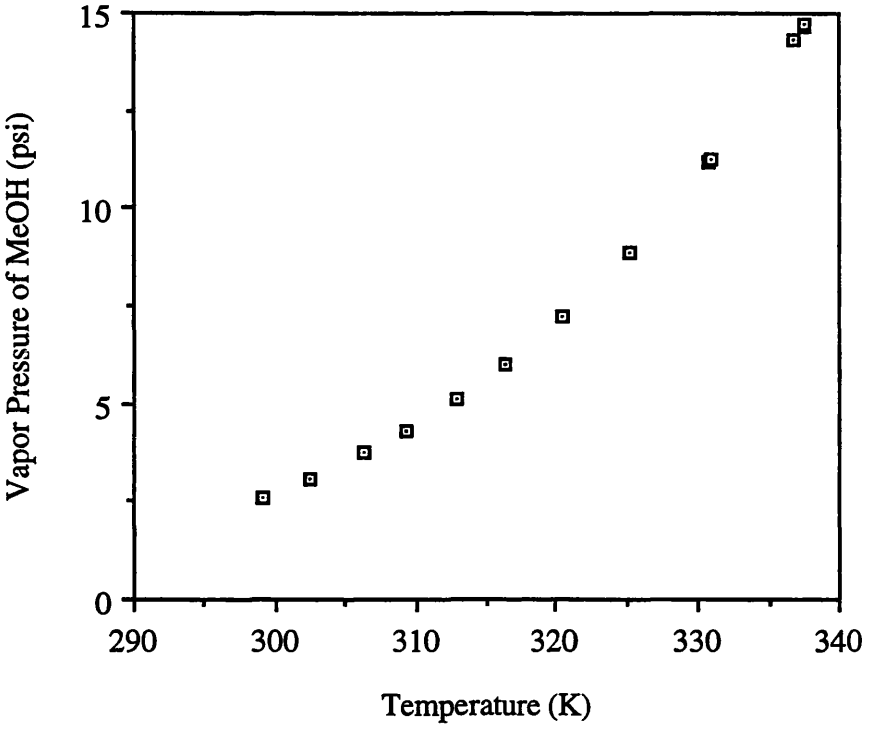

Figure G2. Vapor pressure of methanol as a function of temperature.

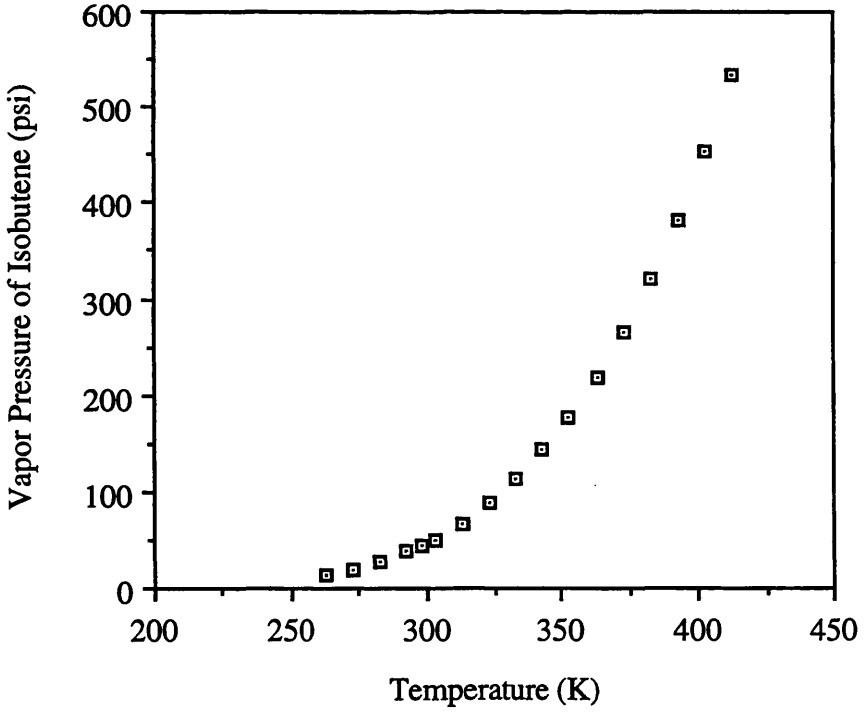

Figure G3. Vapor pressure of isobutene as a function of temperature.

APPENDIX H KINETIC REACTION STUDY DATA

H1. Effect of stirring speed on the rate of reaction

Reaction Temperature: 353 K
Stirrer Speed: 600 rpm
Catalyst: 15.0 grams ZCIC-10
Methanol: 136 grams (4.25 moles)
Isobutene: 119 grams (2.13 moles)
Methanol-to-Isobutene molar ratio: 2.0

Time hour	Methanol mol g^{-1}	Isobutene mol g^{-1}	MTBE mol g^{-1}	Percent Isobutene Conversion
0.00	2.83E-01	1.42E-01	0.00	0.0
0.08	2.83E-01	1.41E-01	0.2E-03	0.1
0.25	2.82E-01	1.40E-01	1.4E-03	1.0
0.50	2.80E-01	1.38E-01	3.3E-03	2.4
1.00	2.79E-01	1.37E-01	4.6E-03	3.3
1.50	2.77E-01	1.35E-01	6.3E-03	4.4
2.00	2.74E-01	1.32E-01	9.3E-03	6.6
2.50	2.73E-01	1.31E-01	10.8E-03	7.6
3.00	2.70E-01	1.28E-01	13.2E-03	9.3
3.50	2.68E-01	1.26E-01	15.3E-03	10.8
4.00	2.66E-01	1.24E-01	17.2E-03	12.2
4.50	2.63E-01	1.21E-01	20.3E-03	14.3
5.00	2.62E-01	1.20E-01	21.5E-03	15.2
5.50	2.59E-01	1.18E-01	24.1E-03	17.0
6.00	2.58E-01	1.17E-01	24.5E-03	17.3

Reaction Temperature: 353 K
Stirrer Speed: 800 rpm
Catalyst: 15.0 grams ZCIC-10
Methanol: 136 grams (4.25 moles)
Isobutene: 119 grams (2.13 moles)
Methanol-to-Isobutene molar ratio: 2.0

Time hour	Methanol mol g^{-1}	Isobutene mol g^{-1}	MTBE mol g^{-1}	Percent Isobutene Conversion
0.00	2.83E-01	1.42E-01	0.00	0.0
0.08	2.83E-01	1.41E-01	2.00E-04	0.2
0.25	2.81E-01	1.40E-01	2.00E-03	1.5
0.50	2.79E-01	1.37E-01	4.80E-03	3.4
1.00	2.77E-01	1.35E-01	6.60E-03	4.7
1.50	2.74E-01	1.33E-01	9.00E-03	6.3
2.00	2.70E-01	1.28E-01	1.33E-02	9.4
2.50	2.68E-01	1.26E-01	1.54E-02	10.9
3.00	2.65E-01	1.23E-01	1.88E-02	13.3
3.50	2.61E-01	1.20E-01	2.19E-02	15.5
4.00	2.59E-01	1.17E-01	2.46E-02	17.4
4.50	2.54E-01	1.13E-01	2.89E-02	20.4
5.00	2.53E-01	1.11E-01	3.07E-02	21.7
5.50	2.49E-01	1.07E-01	3.44E-02	24.3
6.00	2.48E-01	1.07E-01	3.50E-02	24.7

Reaction Temperature: 353 K
Stirrer Speed: 1000 rpm
Catalyst: 15.0 grams ZCIC-10
Methanol: 136 grams (4.25 moles)
Isobutene: 119 grams (2.13 moles)
Methanol-to-Isobutene molar ratio: 2.0

Time hour	Methanol mol g^{-1}	Isobutene mol g^{-1}	MTBE mol g^{-1}	Percent Isobutene Conversion
0.00	2.83E-01	1.42E-01	0.00	0.0
0.08	2.83E-01	1.41E-01	1.00E-03	0.7
0.25	2.81E-01	1.40E-01	2.10E-03	1.5
0.50	2.78E-01	1.37E-01	5.00E-03	3.5
1.00	2.76E-01	1.35E-01	6.90E-03	4.9
1.50	2.74E-01	1.32E-01	9.40E-03	6.7
2.00	2.69E-01	1.28E-01	1.40E-02	9.9
2.50	2.67E-01	1.25E-01	1.62E-02	11.4
3.00	2.64E-01	1.22E-01	1.98E-02	14.0
3.50	2.60E-01	1.19E-01	2.30E-02	16.2
4.00	2.58E-01	1.16E-01	2.58E-02	18.2
4.50	2.53E-01	1.11E-01	3.04E-02	21.5
5.00	2.51E-01	1.09E-01	3.22E-02	22.7
5.50	2.47E-01	1.05E-01	3.62E-02	25.5
6.00	2.47E-01	1.05E-01	3.68E-02	26.0

H2. Effect of amount of catalyst on the rate of reaction

Reaction Temperature: 353 K
Stirrer Speed: 1000 rpm
Catalyst: 2.5 grams
Methanol: 136 grams (4.25 moles)
Isobutene: 119 grams (2.13 moles)
Methanol-to-Isobutene molar ratio: 2.0

Time hour	Methanol mol g^{-1}	Isobutene mol g^{-1}	MTBE mol g^{-1}	Percent Isobutene Conversion
0.00	2.83E-01	1.42E-01	0.00	0.0
0.08	2.83E-01	1.42E-01	6.00E-05	0.0
0.25	2.83E-01	1.41E-01	4.20E-04	0.3
0.50	2.82E-01	1.41E-01	1.00E-03	0.7
1.00	2.82E-01	1.40E-01	1.38E-03	1.0
1.50	2.81E-01	1.40E-01	1.88E-03	1.3
2.00	2.81E-01	1.39E-01	2.80E-03	2.0
2.50	2.80E-01	1.38E-01	3.24E-03	2.3
3.00	2.79E-01	1.38E-01	3.96E-03	2.8
3.50	2.79E-01	1.37E-01	4.60E-03	3.2
4.00	2.78E-01	1.36E-01	5.16E-03	3.6
4.50	2.77E-01	1.36E-01	6.08E-03	4.3
5.00	2.77E-01	1.35E-01	6.44E-03	4.5
5.50	2.76E-01	1.34E-01	7.24E-03	5.1
6.00	2.76E-01	1.34E-01	7.36E-03	5.2

Reaction Temperature: 353 K
Stirrer Speed: 1000 rpm
Catalyst: 7.5 grams
Methanol: 136 grams (4.25 moles)
Isobutene: 119 grams (2.13 moles)
Methanol-to-Isobutene molar ratio: 2.0

Time hour	Methanol mol g^{-1}	Isobutene mol g^{-1}	MTBE mol g^{-1}	Percent Isobutene Conversion
0.00	2.83E-01	1.42E-01	0.00	0.0
0.08	2.83E-01	1.42E-01	1.50E-04	0.1
0.25	2.82E-01	1.41E-01	1.05E-03	0.7
0.50	2.81E-01	1.39E-01	2.50E-03	1.8
1.00	2.80E-01	1.38E-01	3.45E-03	2.4
1.50	2.79E-01	1.37E-01	4.70E-03	3.3
2.00	2.76E-01	1.35E-01	7.00E-03	4.9
2.50	2.75E-01	1.34E-01	8.10E-03	5.7
3.00	2.73E-01	1.32E-01	9.90E-03	7.0
3.50	2.72E-01	1.30E-01	1.15E-02	8.1
4.00	2.70E-01	1.29E-01	1.29E-02	9.1
4.50	2.68E-01	1.26E-01	1.52E-02	10.7
5.00	2.67E-01	1.26E-01	1.61E-02	11.4
5.50	2.65E-01	1.24E-01	1.81E-02	12.8
6.00	2.65E-01	1.23E-01	1.84E-02	13.0

Reaction Temperature: 353 K
Stirrer Speed: 1000 rpm
Catalyst: 12.0 grams
Methanol: 136 grams (4.25 moles)
Isobutene: 119 grams (2.13 moles)
Methanol-to-Isobutene molar ratio: 2.0

Time hour	Methanol mol g^{-1}	Isobutene mol g^{-1}	MTBE mol g^{-1}	Percent Isobutene Conversion
0.00	2.83E-01	1.42E-01	0.00	0.0
0.08	2.83E-01	1.41E-01	2.90E-04	0.2
0.25	2.81E-01	1.40E-01	2.02E-03	1.4
0.50	2.79E-01	1.37E-01	4.80E-03	3.4
1.00	2.77E-01	1.35E-01	6.62E-03	4.7
1.50	2.74E-01	1.33E-01	9.02E-03	6.4
2.00	2.70E-01	1.28E-01	1.34E-02	9.5
2.50	2.68E-01	1.26E-01	1.56E-02	11.0
3.00	2.64E-01	1.23E-01	1.90E-02	13.4
3.50	2.61E-01	1.20E-01	2.21E-02	15.6
4.00	2.59E-01	1.17E-01	2.48E-02	17.5
4.50	2.54E-01	1.12E-01	2.92E-02	20.6
5.00	2.52E-01	1.11E-01	3.09E-02	21.8
5.50	2.49E-01	1.07E-01	3.48E-02	24.5
6.00	2.48E-01	1.06E-01	3.53E-02	24.9

Reaction Temperature: 353 K
Stirrer Speed: 1000 rpm
Catalyst: 15.0 grams
Methanol: 136 grams (4.25 moles)
Isobutene: 119 grams (2.13 moles)
Methanol-to-Isobutene molar ratio: 2.0

Time hour	Methanol mol g^{-1}	Isobutene mol g^{-1}	MTBE mol g^{-1}	Percent Isobutene Conversion
0.00	2.83E-01	1.42E-01	0.00	0.0
0.08	2.83E-01	1.41E-01	1.00E-03	0.7
0.25	2.81E-01	1.40E-01	2.10E-03	1.5
0.50	2.78E-01	1.37E-01	5.00E-03	3.5
1.00	2.76E-01	1.35E-01	6.90E-03	4.9
1.50	2.74E-01	1.32E-01	9.40E-03	6.7
2.00	2.69E-01	1.28E-01	1.40E-02	9.9
2.50	2.67E-01	1.25E-01	1.62E-02	11.4
3.00	2.64E-01	1.22E-01	1.98E-02	14.0
3.50	2.60E-01	1.19E-01	2.30E-02	16.2
4.00	2.58E-01	1.16E-01	2.58E-02	18.2
4.50	2.53E-01	1.11E-01	3.04E-02	21.5
5.00	2.51E-01	1.09E-01	3.22E-02	22.7
5.50	2.47E-01	1.05E-01	3.62E-02	25.5
6.00	2.47E-01	1.05E-01	3.68E-02	26.0

H3. Effect of MTBE in the reaction mixture on the rate of reaction

Reaction Temperature: 343 K
Stirrer Speed: 1000 rpm
Catalyst: 15.0 grams ZCIC-10
Methanol: 136 grams (4.25 moles)
Isobutene: 119 grams (2.13 moles)
MTBE: 2.53 grams (2.9×10^{-2} moles)
Methanol-to-Isobutene molar ratio: 2.0

Time hour	Methanol mol g^{-1}	Isobutene mol g^{-1}	MTBE mol g^{-1}	Percent Isobutene Conversion
0.00	2.83E-01	1.42E-01	0.00	0.0
0.08	2.83E-01	1.41E-01	2.00E-04	0.1
0.25	2.83E-01	1.41E-01	4.00E-04	0.3
0.50	2.83E-01	1.41E-01	8.00E-04	0.6
1.00	2.82E-01	1.40E-01	1.80E-03	1.3
1.50	2.80E-01	1.38E-01	3.20E-03	2.3
2.00	2.78E-01	1.36E-01	5.20E-03	3.7
2.50	2.75E-01	1.34E-01	7.90E-03	5.6
3.00	2.73E-01	1.31E-01	1.03E-02	7.2
3.50	2.69E-01	1.28E-01	1.40E-02	9.9
4.00	2.67E-01	1.25E-01	1.64E-02	11.6
4.50	2.64E-01	1.23E-01	1.90E-02	13.4
5.00	2.63E-01	1.21E-01	2.06E-02	14.6
5.50	2.62E-01	1.20E-01	2.16E-02	15.3
6.00	2.61E-01	1.19E-01	2.25E-02	15.9

Reaction Temperature: 353 K
Stirrer Speed: 1000 rpm
Catalyst: 15.0 grams ZCIC-10
Methanol: 136 grams (4.25 moles)
Isobutene: 119 grams (2.13 moles)
MTBE: 2.53 grams (2.9×10^{-2} moles)
Methanol-to-Isobutene molar ratio: 2.0

Time hour	Methanol mol g^{-1}	Isobutene mol g^{-1}	MTBE mol g^{-1}	Percent Isobutene Conversion
0.00	2.83E-01	1.42E-01	0.00	0.0
0.08	2.83E-01	1.41E-01	2.00E-04	0.1
0.25	2.82E-01	1.40E-01	1.20E-03	0.8
0.50	2.81E-01	1.39E-01	2.70E-03	1.9
1.00	2.79E-01	1.38E-01	3.90E-03	2.7
1.50	2.78E-01	1.36E-01	5.40E-03	3.8
2.00	2.75E-01	1.33E-01	8.30E-03	5.9
2.50	2.72E-01	1.30E-01	1.15E-02	8.1
3.00	2.67E-01	1.25E-01	1.64E-02	11.6
3.50	2.63E-01	1.21E-01	2.04E-02	14.4
4.00	2.60E-01	1.19E-01	2.29E-02	16.2
4.50	2.55E-01	1.14E-01	2.80E-02	19.8
5.00	2.53E-01	1.12E-01	2.99E-02	21.1
5.50	2.50E-01	1.08E-01	3.36E-02	23.8
6.00	2.49E-01	1.07E-01	3.45E-02	24.3

Reaction Temperature: 363 K
Stirrer Speed: 1000 rpm
Catalyst: 15.0 grams ZCIC-10
Methanol: 136 grams (4.25 moles)
Isobutene: 119 grams (2.13 moles)
MTBE: 2.53 grams (2.9×10^{-2} moles)
Methanol-to-Isobutene molar ratio: 2.0

Time hour	Methanol mol g^{-1}	Isobutene mol g^{-1}	MTBE mol g^{-1}	Percent Isobutene Conversion
0.00	2.83E-01	1.42E-01	0.00	0.0
0.08	2.83E-01	1.41E-01	8.00E-04	0.6
0.25	2.81E-01	1.39E-01	2.20E-03	1.5
0.50	2.77E-01	1.36E-01	5.90E-03	4.2
1.00	2.75E-01	1.33E-01	8.30E-03	5.9
1.50	2.71E-01	1.29E-01	1.26E-02	8.9
2.00	2.69E-01	1.27E-01	1.45E-02	10.2
2.50	2.62E-01	1.21E-01	2.11E-02	14.9
3.00	2.53E-01	1.11E-01	3.02E-02	21.3
3.50	2.47E-01	1.05E-01	3.63E-02	25.6
4.00	2.37E-01	9.56E-02	4.60E-02	32.5
4.50	2.35E-01	9.34E-02	4.82E-02	34.1
5.00	2.31E-01	8.88E-02	5.28E-02	37.3
5.50	2.28E-01	8.60E-02	5.56E-02	39.3
6.00	2.24E-01	8.27E-02	5.89E-02	41.6

Reaction Temperature: 373 K
Stirrer Speed: 1000 rpm
Catalyst: 15.0 grams ZCIC-10
Methanol: 136 grams (4.25 moles)
Isobutene: 119 grams (2.13 moles)
MTBE: 2.53 grams (2.9×10^{-2} moles)
Methanol-to-Isobutene molar ratio: 2.0

Time hour	Methanol mol g^{-1}	Isobutene mol g^{-1}	MTBE mol g^{-1}	Percent Isobutene Conversion
0.00	2.83E-01	1.42E-01	0.00	0.0
0.08	2.82E-01	1.40E-01	1.40E-03	1.0
0.25	2.80E-01	1.38E-01	3.30E-03	2.3
0.50	2.72E-01	1.31E-01	1.10E-02	7.8
1.00	2.67E-01	1.25E-01	1.62E-02	11.4
1.50	2.59E-01	1.17E-01	2.47E-02	17.4
2.00	2.58E-01	1.16E-01	2.52E-02	17.8
2.50	2.53E-01	1.11E-01	3.07E-02	21.7
3.00	2.39E-01	9.74E-02	4.42E-02	31.2
3.50	2.32E-01	9.04E-02	5.12E-02	36.1
4.00	2.25E-01	8.36E-02	5.80E-02	40.9
4.50	2.15E-01	7.37E-02	6.79E-02	47.9
5.00	2.08E-01	6.59E-02	7.57E-02	53.5
5.50	2.01E-01	5.93E-02	8.23E-02	58.1
6.00	1.96E-01	5.40E-02	8.76E-02	61.9

H4. Effect of reaction temperature on the rate of reaction

Reaction Temperature: 343 K
Stirrer Speed: 1000 rpm
Catalyst: 15.0 grams ZCIC-10
Methanol: 136 grams (4.25 moles)
Isobutene: 119 grams (2.13 moles)
Methanol-to-Isobutene molar ratio: 2.0

Time hour	Methanol mol g^{-1}	Isobutene mol g^{-1}	MTBE mol g^{-1}	% Isobutene Conversion	dMTBE/dt
0.00	2.83E-01	1.42E-01	0.00	0.0	4.10E-03
0.08	2.83E-01	1.41E-01	8.00E-04	0.6	4.10E-03
0.25	2.82E-01	1.40E-01	1.40E-03	1.0	4.09E-03
0.50	2.80E-01	1.39E-01	3.00E-03	2.1	4.08E-03
1.00	2.79E-01	1.37E-01	4.40E-03	3.1	4.07E-03
1.50	2.77E-01	1.35E-01	6.80E-03	4.8	4.05E-03
2.00	2.74E-01	1.32E-01	9.80E-03	6.9	4.03E-03
2.50	2.73E-01	1.31E-01	1.08E-02	7.6	4.01E-03
3.00	2.71E-01	1.29E-01	1.25E-02	8.8	4.00E-03
3.50	2.69E-01	1.27E-01	1.45E-02	10.2	3.98E-03
4.00	2.68E-01	1.26E-01	1.53E-02	10.8	3.96E-03
4.50	2.66E-01	1.24E-01	1.76E-02	12.4	3.94E-03
5.00	2.61E-01	1.19E-01	2.22E-02	15.7	3.92E-03
5.50	2.60E-01	1.18E-01	2.32E-02	16.4	3.90E-03
6.00	2.59E-01	1.18E-01	2.41E-02	17.0	3.88E-03
10.00	2.44E-01	1.02E-01	3.96E-02	28.0	3.71E-03
11.00	2.40E-01	9.83E-02	4.33E-02	30.6	3.66E-03
16.00	2.22E-01	8.06E-02	6.10E-02	43.1	3.41E-03
18.00	2.16E-01	7.39E-02	6.77E-02	47.8	3.30E-03
21.00	2.06E-01	6.43E-02	7.73E-02	54.6	3.12E-03
26.00	1.91E-01	4.95E-02	9.21E-02	65.1	2.80E-03
31.00	1.78E-01	3.63E-02	1.05E-01	74.3	2.44E-03
36.00	1.67E-01	2.51E-02	1.17E-01	82.3	2.05E-03
41.00	1.58E-01	1.59E-02	1.26E-01	88.8	1.62E-03
45.00	1.52E-01	1.01E-02	1.32E-01	92.8	1.26E-03
51.00	1.46E-01	4.30E-03	1.37E-01	97.0	6.73E-04
53.00	1.45E-01	3.20E-03	1.38E-01	97.8	4.67E-04
56.00	1.44E-01	2.20E-03	1.39E-01	98.4	1.46E-04

Reaction Temperature: 353 K
Stirrer Speed: 1000 rpm
Catalyst: 15.0 grams ZCIC-10
Methanol: 136 grams (4.25 moles)
Isobutene: 119 grams (2.13 moles)
Methanol-to-Isobutene molar ratio: 2

Time hour	Methanol mol g^{-1}	Isobutene mol g^{-1}	MTBE mol g^{-1}	% Isobutene Conversion	dMTBE/dt
0.00	2.83E-01	1.42E-01	0.00	0.0	6.80E-03
0.08	2.82E-01	1.41E-01	1.00E-03	0.7	6.79E-03
0.50	2.78E-01	1.37E-01	5.00E-03	3.5	6.72E-03
1.00	2.76E-01	1.35E-01	6.90E-03	4.9	6.64E-03
2.00	2.69E-01	1.28E-01	1.40E-02	9.9	6.48E-03
3.00	2.64E-01	1.22E-01	1.98E-02	14.0	6.33E-03
4.00	2.58E-01	1.16E-01	2.58E-02	18.2	6.17E-03
5.00	2.51E-01	1.09E-01	3.22E-02	22.7	6.01E-03
6.00	2.47E-01	1.05E-01	3.68E-02	26.0	5.84E-03
8.00	2.34E-01	9.19E-02	4.97E-02	35.1	5.52E-03
10.00	2.23E-01	8.12E-02	6.04E-02	42.7	5.19E-03
12.00	2.13E-01	7.11E-02	7.05E-02	49.8	4.86E-03
14.00	2.04E-01	6.18E-02	7.98E-02	56.4	4.52E-03
15.00	1.95E-01	5.30E-02	8.86E-02	62.5	4.18E-03
16.00	1.87E-01	4.50E-02	9.66E-02	68.2	3.84E-03
18.00	1.79E-01	3.77E-02	1.04E-01	73.4	3.49E-03
20.00	1.73E-01	3.11E-02	1.11E-01	78.1	3.14E-03
21.00	1.67E-01	2.51E-02	1.17E-01	82.2	2.79E-03
23.00	1.62E-01	1.99E-02	1.22E-01	85.9	2.43E-03
26.00	1.57E-01	1.54E-02	1.26E-01	89.1	2.07E-03
28.00	1.53E-01	1.16E-02	1.30E-01	91.8	1.71E-03
30.00	1.50E-01	8.60E-03	1.33E-01	93.9	1.34E-03
33.00	1.48E-01	6.30E-03	1.35E-01	95.6	9.67E-04
34.00	1.46E-01	4.70E-03	1.37E-01	96.7	5.92E-04
36.00	1.46E-01	4.50E-03	1.37E-01	96.8	4.98E-04
37.50	1.46E-01	3.90E-03	1.38E-01	97.2	2.14E-04
38.50	1.46E-01	3.80E-03	1.38E-01	97.3	1.19E-04

Reaction Temperature: 363 K
Stirrer Speed: 1000 rpm
Catalyst: 15.0 grams ZCIC-10
Methanol: 136 grams (4.25 moles)
Isobutene: 119 grams (2.13 moles)
Methanol-to-Isobutene molar ratio: 2.0

Time hour	Methanol mol g^{-1}	MTBE mol g^{-1}	Isobutene mol g^{-1}	% Isobutene Conversion	dMTBE/dt
0.00	2.83E-01	1.42E-01	0.00	0.0	1.24E-02
0.08	2.82E-01	1.40E-01	1.40E-03	1.0	1.23E-02
0.25	2.79E-01	1.38E-01	4.00E-03	2.8	1.22E-02
0.50	2.73E-01	1.31E-01	1.05E-02	7.4	1.21E-02
1.00	2.69E-01	1.27E-01	1.47E-02	10.4	1.17E-02
2.00	2.59E-01	1.17E-01	2.42E-02	17.1	1.10E-02
3.00	2.48E-01	1.06E-01	3.54E-02	25.0	1.04E-02
4.00	2.38E-01	9.66E-02	4.50E-02	31.8	9.76E-03
5.00	2.26E-01	8.43E-02	5.73E-02	40.5	9.13E-03
6.00	2.20E-01	7.82E-02	6.34E-02	44.8	8.52E-03
7.50	2.11E-01	6.94E-02	7.22E-02	51.0	7.92E-03
8.10	2.03E-01	6.17E-02	7.99E-02	56.4	7.34E-03
9.50	1.96E-01	5.47E-02	8.69E-02	61.4	6.77E-03
10.10	1.90E-01	4.82E-02	9.34E-02	66.0	6.22E-03
11.50	1.84E-01	4.23E-02	9.93E-02	70.2	5.68E-03
12.20	1.79E-01	3.68E-02	1.05E-01	74.0	5.16E-03
13.30	1.74E-01	3.19E-02	1.10E-01	77.4	4.64E-03
14.50	1.69E-01	2.75E-02	1.14E-01	80.6	4.15E-03
15.00	1.65E-01	2.36E-02	1.18E-01	83.3	3.67E-03
16.20	1.62E-01	2.02E-02	1.21E-01	85.7	3.20E-03
17.90	1.59E-01	1.72E-02	1.24E-01	87.8	2.75E-03
18.70	1.56E-01	1.47E-02	1.27E-01	89.6	2.31E-03
19.00	1.54E-01	1.26E-02	1.29E-01	91.1	1.88E-03
20.00	1.53E-01	1.09E-02	1.31E-01	92.3	1.47E-03
21.30	1.51E-01	9.70E-03	1.32E-01	93.2	1.08E-03
22.20	1.51E-01	8.80E-03	1.33E-01	93.8	6.96E-04
22.70	1.50E-01	8.30E-03	1.33E-01	94.2	3.29E-04
23.40	1.49E-01	8.20E-03	1.33E-01	94.2	1.86E-04
23.60	1.49E-01	8.10E-03	1.34E-01	94.3	1.16E-04

Reaction Temperature: 373 K
Stirrer Speed: 1000 rpm
Catalyst: 15.0 grams ZCIC-10
Methanol: 136 grams (4.25 moles)
Isobutene: 119 grams (2.13 moles)
Methanol-to-Isobutene molar ratio: 2.0

Time hour	Methanol mol g^{-1}	Isobutene mol g^{-1}	MTBE mol g^{-1}	% Isobutene Conversion	dMTBE/dt
0.00	2.83E-01	1.42E-01	0.00	0.0	1.92E-02
0.08	2.81E-01	1.39E-01	2.60E-03	1.8	1.91E-02
0.25	2.78E-01	1.36E-01	5.80E-03	4.1	1.88E-02
0.50	2.67E-01	1.26E-01	1.61E-02	11.4	1.85E-02
1.00	2.61E-01	1.19E-01	2.25E-02	15.9	1.77E-02
2.00	2.49E-01	1.07E-01	3.45E-02	24.4	1.63E-02
3.00	2.32E-01	9.05E-02	5.11E-02	36.1	1.49E-02
4.00	2.09E-01	6.73E-02	7.43E-02	52.5	1.34E-02
5.00	2.01E-01	5.91E-02	8.25E-02	58.3	1.20E-02
6.00	1.93E-01	5.16E-02	9.00E-02	63.6	1.06E-02
6.10	1.87E-01	4.51E-02	9.65E-02	68.1	9.84E-03
7.00	1.82E-01	4.04E-02	1.01E-01	71.5	9.13E-03
7.60	1.78E-01	3.60E-02	1.06E-01	74.6	8.42E-03
8.00	1.74E-01	3.19E-02	1.10E-01	77.4	7.71E-03
8.90	1.70E-01	2.83E-02	1.13E-01	80.0	7.00E-03
9.10	1.66E-01	2.43E-02	1.17E-01	82.8	6.15E-03
9.30	1.64E-01	2.20E-02	1.20E-01	84.5	5.58E-03
9.90	1.62E-01	1.99E-02	1.22E-01	86.0	5.02E-03
10.00	1.60E-01	1.80E-02	1.24E-01	87.3	4.45E-03
10.70	1.58E-01	1.63E-02	1.25E-01	88.5	3.89E-03
11.00	1.56E-01	1.42E-02	1.27E-01	89.9	3.04E-03
11.50	1.55E-01	1.37E-02	1.28E-01	90.4	2.76E-03
12.00	1.54E-01	1.24E-02	1.29E-01	91.2	2.06E-03
12.50	1.53E-01	1.15E-02	1.30E-01	91.9	1.22E-03
13.00	1.53E-01	1.11E-02	1.31E-01	92.2	6.56E-04
13.30	1.53E-01	1.10E-02	1.31E-01	92.2	3.76E-04
13.40	1.53E-01	1.09E-02	1.31E-01	92.3	9.66E-05

APPENDIX I PARAMETER ESTIMATION RESULTS

I1. Rideal-Eley mechanism in which methanol (reactant A) is adsorbed and reacts with isobutene (reactant B) in solution to produce MTBE and surface reaction is the rate controlling step of the reaction (k_S is the surface reaction rate constant).

$$-r_A = k_S K_A \frac{C_A^a C_B^b - C_C^c / K_e}{\left(1 + K_A C_A + K_C C_C\right)}$$

T, K	K_e	A	B	C	k_S	K_A	K_B	K_C	$\sqrt{\Sigma r^2}$
343	6.71	1.0	1.0	0.5	4.60E-01	3.44E-01	-	3.54E+02	2.20E-02
353	3.51	1.0	1.0	0.5	1.82E-08	3.52E-07	-	3.64E+01	3.67E-02
363	1.91	1.0	1.0	0.5	1.42E-08	2.87E-07	-	2.03E+01	4.99E-02
373	1.07	1.0	1.0	0.5	7.18E-09	3.91E-09	-	2.54E-07	7.82E-02
343	6.71	1.0	1.0	1.0	4.28E-01	3.45E-01	-	2.76E+01	1.75E-02
353	3.51	1.0	1.0	1.0	6.04E-01	4.58E-01	-	1.64E+02	3.26E-02
363	1.91	1.0	1.0	1.0	8.74E-01	4.89E-01	-	4.44E+02	8.73E-02
373	1.07	1.0	1.0	1.0	1.77E-08	5.50E-08	-	2.73E+01	7.82E-02
343	6.71	1.0	1.0	1.5	4.12E-01	3.28E-01	-	4.51E-01	1.29E-02
353	3.51	1.0	1.0	1.5	5.37E-01	4.58E-01	-	1.44E+01	2.59E-02
363	1.91	1.0	1.0	1.5	7.71E-01	6.19E-01	-	6.47E+01	3.98E-02
373	1.07	1.0	1.0	1.5	1.07E+00	6.40E-01	-	3.16E+02	7.27E-02
343	6.71	1.0	1.0	2.0	3.49E-02	7.59E+03	-	2.23E-05	8.84E-03
353	3.51	1.0	1.0	2.0	8.81E-02	6.36E+00	-	1.17E-08	1.78E-02
363	1.91	1.0	1.0	2.0	7.01E-01	6.37E-01	-	7.23E+00	2.99E-02
373	1.07	1.0	1.0	2.0	9.22E-01	7.96E-01	-	4.26E+01	6.48E-02
343	6.71	1.0	1.0	2.5	3.54E-02	2.64E+04	-	4.23E-04	7.20E-03
353	3.51	1.0	1.0	2.5	5.83E-02	1.24E+04	-	2.33E-05	1.04E-02
363	1.91	1.0	1.0	2.5	1.00E-01	2.07E+04	-	1.11E-04	1.72E-02
373	1.07	1.0	1.0	2.5	3.32E-01	3.24E+00	-	2.22E-08	4.65E-02
343	6.71	1.0	1.0	3.0	3.55E-02	1.38E+04	-	1.87E-01	6.68E-03
353	3.51	1.0	1.0	3.0	5.87E-02	1.77E+04	-	1.80E-04	9.48E-03
363	1.91	1.0	1.0	3.0	1.02E-01	2.90E+04	-	2.58E-04	1.08E-02
373	1.07	1.0	1.0	3.0	1.74E-01	3.21E+04	-	3.68E-04	2.50E-02

I2. Rideal-Eley mechanism in which isobutene (reactant B) is adsorbed and reacts with methanol (reactant A) in solution to produce MTBE and surface reaction is the rate controlling step of the reaction (k_S is the surface reaction rate constant).

$$-r_A = k_S K_B \frac{C_A^a C_B^b - C_C^c / K_e}{\left(1 + K_B C_B + K_C C_C\right)}$$

T, K	K_e	A	B	C	k_S	K_A	K_B	K_C	$\sqrt{\Sigma r^2}$
343	6.71	1.0	1.0	0.5	4.04E-01	-	3.73E-01	3.29E+02	2.20E-02
353	3.51	1.0	1.0	0.5	2.02E-08	-	2.76E-07	1.32E+01	3.67E-02
363	1.91	1.0	1.0	0.5	1.27E-08	-	1.92E-07	7.28E+00	5.00E-02
373	1.07	1.0	1.0	0.5	2.91E-09	-	8.67E-03	5.75E+03	7.82E-02
343	6.71	1.0	1.0	1.0	3.93E-01	-	3.62E-01	2.74E+01	3.35E-02
353	3.51	1.0	1.0	1.0	5.16E-01	-	4.59E-01	1.15E+02	3.26E-02
363	1.91	1.0	1.0	1.0	7.24E-01	-	5.61E-01	4.34E+02	4.62E-02
373	1.07	1.0	1.0	1.0	1.72E-08	-	4.84E-08	1.18E+01	7.82E-02
343	6.71	1.0	1.0	1.5	3.78E-01	-	3.43E-01	4.64E-01	1.29E-02
353	3.51	1.0	1.0	1.5	4.99E-01	-	4.66E-01	1.39E+01	2.59E-02
363	1.91	1.0	1.0	1.5	6.96E-01	-	6.18E-01	5.51E+01	3.98E-02
373	1.07	1.0	1.0	1.5	9.40E-01	-	6.80E-01	3.01E+02	3.25E-02
343	6.71	1.0	1.0	2.0	2.23E-02	-	2.03E+01	7.75E-01	8.43E-03
353	3.51	1.0	1.0	2.0	8.41E-02	-	1.36E+01	1.44E-02	1.78E-02
363	1.91	1.0	1.0	2.0	6.56E-01	-	6.28E-01	6.52E+00	2.99E-02
373	1.07	1.0	1.0	2.0	8.60E-01	-	7.76E-01	3.93E+01	6.48E-02
343	6.71	1.0	1.0	2.5	1.68E-02	-	9.41E+01	2.44E-01	4.29E-03
353	3.51	1.0	1.0	2.5	3.14E-02	-	3.42E+01	9.20E-02	9.56E-03
363	1.91	1.0	1.0	2.5	6.78E-02	-	1.62E+01	1.42E-01	1.67E-02
373	1.07	1.0	1.0	2.5	2.64E-01	-	3.00E+00	7.14E-09	4.61E-02
343	6.71	1.0	1.0	3.0	1.55E-02	-	2.57E+02	2.02E-10	1.07E-03
353	3.51	1.0	1.0	3.0	2.54E-02	-	1.31E+02	4.34E-11	2.28E-03
363	1.91	1.0	1.0	3.0	4.80E-02	-	6.28E+01	2.19E-10	2.34E-03
373	1.07	1.0	1.0	3.0	6.77E-02	-	1.22E+05	7.13E+03	1.17E-02

I3. Langmuir-Hinshelwood mechanism in which both methanol (reactant A) and isobutene (reactant B) are adsorbed on separate sites and react to produce MTBE and surface reaction is the rate controlling step of the reaction (k_S is the surface reaction rate constant)

$$-r_A = k_S K_A K_B \frac{C_A^a C_B^b - C_C^c / K_e}{(1 + K_A C_A + K_B C_B + K_C C_C)^{a+b}}$$

T, K	K_e	A	B	C	k_S	K_A	K_B	K_C	$\sqrt{\Sigma r^2}$
343	6.71	1.0	1.0	0.5	8.00E-01	4.59E-01	6.03E-01	7.41E+01	2.12E-02
353	3.51	1.0	1.0	0.5	1.25E-09	7.22E-04	4.64E-04	5.98E+03	3.67E-02
363	1.91	1.0	1.0	0.5	8.90E-10	1.47E-03	1.05E-03	1.30E+04	4.99E-02
373	1.07	1.0	1.0	0.5	8.18E-10	2.61E-03	1.89E-03	2.34E+04	7.82E-02
343	6.71	1.0	1.0	1.0	6.77E-01	5.09E-01	6.03E-01	1.42E+01	1.72E-02
353	3.51	1.0	1.0	1.0	9.39E-01	5.59E-01	6.98E-01	3.95E+01	3.15E-02
363	1.91	1.0	1.0	1.0	1.39E+00	5.76E-01	8.10E-01	8.65E+01	4.44E-02
373	1.07	1.0	1.0	1.0	2.80E-09	9.90E-04	6.14E-04	7.70E+03	7.82E-02
343	6.71	1.0	1.0	1.5	6.36E-01	4.96E-01	5.90E-01	1.26E+00	1.29E-02
353	3.51	1.0	1.0	1.5	7.90E-01	6.39E-01	7.21E-01	8.59E+00	2.56E-02
363	1.91	1.0	1.0	1.5	1.12E+00	7.40E-01	8.66E-01	2.40E+01	3.85E-02
373	1.07	1.0	1.0	1.5	1.68E+00	6.86E-01	9.50E-01	7.46E+01	7.02E-02
343	6.71	1.0	1.0	2.0	1.50E-01	5.58E+00	9.64E-01	3.41E-08	8.70E-03
353	3.51	1.0	1.0	2.0	3.33E-01	1.13E+00	1.16E+00	8.73E-02	1.77E-02
363	1.91	1.0	1.0	2.0	9.26E-01	8.51E-01	8.88E-01	4.86E+00	2.97E-02
373	1.07	1.0	1.0	2.0	1.27E+00	9.34E-01	1.02E+00	1.98E+01	6.37E-02
343	6.71	1.0	1.0	2.5	1.78E-02	6.59E+01	8.80E+01	4.05E-01	3.70E-03
353	3.51	1.0	1.0	2.5	4.35E-02	4.15E+01	2.49E+01	1.35E-01	8.90E-03
363	1.91	1.0	1.0	2.5	1.76E-01	1.22E+01	3.70E+00	4.35E-02	1.63E-03
373	1.07	1.0	1.0	2.5	9.36E-01	1.30E+00	1.12E+00	1.34E-02	4.60E-03
343	6.71	1.0	1.0	3.0	1.74E-02	6.49E+01	9.05E+01	7.79E-02	1.75E-03
353	3.51	1.0	1.0	3.0	3.15E-02	5.26E+01	5.21E+01	1.33E-10	3.47E-03
363	1.91	1.0	1.0	3.0	4.84E-02	3.48E+02	5.31E+02	1.65E+02	4.01E-03
373	1.07	1.0	1.0	3.0	7.42E-02	5.16E+03	7.50E+03	1.46E+03	1.25E-02

I4. Langmuir-Hinshelwood mechanism in which adsorption of methanol (reactant A) is the rate controlling step of the reaction (K_a is the adsorption rate constant)

$$-r_A = K_a \frac{C_A^a - C_c^c / K_e C_B^b}{\left(1 + K_B^b C_B^b + K_A^a C_C^c / K_e C_B^b + K_C^c C_C^c\right)}$$

T, K	K_e	A	B	C	K_a	K_A	K_B	K_C	$\sqrt{\Sigma r^2}$
343	6.71	1.0	1.0	0.5	3.83E-00	4.83E+03	1.29E+03	2.51E-07	2.19E-02
353	3.51	1.0	1.0	0.5	1.18E-00	1.32E+03	7.68E+02	1.72E-07	3.53E-02
363	1.91	1.0	1.0	0.5	8.73E-01	8.29E+02	4.51E+02	5.18E-08	4.75E-02
373	1.07	1.0	1.0	0.5	1.03E-02	1.57E+02	8.54E-11	7.00E-07	7.58E-02
343	6.71	1.0	1.0	1.0	1.35E-01	1.13E+01	6.16E+01	7.69E+01	3.78E-03
353	3.51	1.0	1.0	1.0	1.41E-01	1.12E+01	7.60E+01	9.83E+01	9.40E-03
363	1.91	1.0	1.0	1.0	1.37E-01	1.17E+01	7.53E+01	7.27E+01	2.80E-03
373	1.07	1.0	1.0	1.0	1.36E-01	8.39E+00	8.99E+01	4.62E+01	7.62E-02
343	6.71	1.0	1.0	1.5	2.08E-02	3.30E+01	4.40E+00	1.85E-04	2.37E-03
353	3.51	1.0	1.0	1.5	4.31E-02	5.75E+01	2.15E+01	1.66E-08	4.45E-03
363	1.91	1.0	1.0	1.5	3.22E-02	2.89E+01	1.39E+01	6.99E-05	6.92E-03
373	1.07	1.0	1.0	1.5	3.13E-00	1.76E+03	2.44E+03	9.06E-04	1.53E-02
343	6.71	1.0	1.0	2.0	1.29E-02	7.08E+01	9.81E-11	3.72E-08	2.52E-03
353	3.51	1.0	1.0	2.0	1.10E-02	4.57E+01	1.15E-09	1.21E-07	4.53E-03
363	1.91	1.0	1.0	2.0	1.17E-02	3.58E+01	6.68E-01	5.40E-06	7.25E-03
373	1.07	1.0	1.0	2.0	1.76E-02	3.37E+01	6.66E+00	2.23E-03	1.61E-02
343	6.71	1.0	1.0	2.5	1.24E-02	2.19E+02	2.59E-08	5.39E-08	2.56E-03
353	3.51	1.0	1.0	2.5	1.04E-02	1.40E+02	3.29E-08	8.42E-02	4.60E-03
363	1.91	1.0	1.0	2.5	1.05E-02	1.03E+02	3.30E-08	9.16E-10	7.17E-03
373	1.07	1.0	1.0	2.5	9.28E-03	5.35E+01	1.65E-12	8.48E-03	1.54E-02
343	6.71	1.0	1.0	3.0	1.20E-02	6.49E+02	4.62E-08	2.59E-06	2.78E-03
353	3.51	1.0	1.0	3.0	9.94E-03	4.12E+02	5.52E-08	3.07E-06	4.96E-03
363	1.91	1.0	1.0	3.0	1.01E-02	2.91E+02	3.30E-07	6.43E+00	7.47E-03
373	1.07	1.0	1.0	3.0	8.85E-03	1.56E+02	1.65E-08	3.91E-07	1.47E-02

I5. Langmuir-Hinshelwood mechanism in which desorption of MTBE (reactant C) is the rate controlling step of the reaction (K_d is the desorption rate constant)

$$-r_A = K_d K_C^c \frac{C_A^a C_B^b - C_c^c / K_e}{\left(1 + K_A^a C_A^a + K_B^b C_B^b + K_C^c K_e C_A^a C_B^b\right)}$$

T, K	K_e	A	B	C	K_d	K_A	K_B	K_C	$\sqrt{\Sigma r^2}$
343	6.71	1.0	1.0	0.5	2.21E-01	2.71E-05	5.98E-05	5.30E+04	2.28E-02
353	3.51	1.0	1.0	0.5	4.08E-08	2.32E+01	5.84E-01	3.62E-06	3.67E-02
363	1.91	1.0	1.0	0.5	1.77E-08	2.08E+02	2.80E-03	3.00E-06	5.00E-02
373	1.07	1.0	1.0	0.5	3.28E-08	7.22E+02	2.37E-03	9.69E-06	7.82E-02
343	6.71	1.0	1.0	1.0	1.02E+00	2.48E-04	2.65E+03	8.70E+01	1.57E-02
353	3.51	1.0	1.0	1.0	1.34E+00	1.91E-05	3.88E-05	1.59E+04	3.09E-02
363	1.91	1.0	1.0	1.0	1.98E+00	4.09E-06	9.02E-06	6.24E+03	4.81E-02
373	1.07	1.0	1.0	1.0	6.02E-08	8.34E-08	5.40E-08	9.47E+01	2.24E-02
343	6.71	1.0	1.0	1.5	7.06E+00	8.54E-06	1.01E+03	1.85E+00	1.08E-02
353	3.51	1.0	1.0	1.5	6.72E+00	3.38E-06	4.43E+02	1.80E+00	2.23E-02
363	1.91	1.0	1.0	1.5	6.06E+00	4.09E-04	3.08E+05	5.91E+02	3.50E-02
373	1.07	1.0	1.0	1.5	8.45E+00	1.54E-04	3.28E-04	2.07E+04	7.24E-02
343	6.71	1.0	1.0	2.0	2.35E+00	1.35E+01	2.53E+01	2.43E-01	2.09E-02
353	3.51	1.0	1.0	2.0	6.02E+00	6.79E+01	1.38E+02	1.22E+00	1.86E-02
363	1.91	1.0	1.0	2.0	1.52E+01	2.04E+01	7.16E+02	1.23E+00	3.73E-02
373	1.07	1.0	1.0	2.0	2.31E+01	9.85E-04	2.24E+05	4.25E+01	5.96E-02
343	6.71	1.0	1.0	2.5	1.94E+02	2.00E-06	4.44E+03	6.56E-01	3.18E-03
353	3.51	1.0	1.0	2.5	1.74E+02	3.26E-06	2.50E+03	6.63E-01	7.39E-03
363	1.91	1.0	1.0	2.5	2.18E+02	1.67E-05	6.25E+03	1.11E+00	1.40E-02
373	1.07	1.0	1.0	2.5	2.80E+02	1.50E-04	1.39E+04	1.73E+00	3.95E-02
343	6.71	1.0	1.0	3.0	2.36E+03	1.76E+01	1.07E+03	1.92E-01	1.08E-03
353	3.51	1.0	1.0	3.0	6.19E+00	7.63E+01	1.23E+02	1.08E-02	3.67E-03
363	1.91	1.0	1.0	3.0	5.55E+04	1.69E+02	1.41E+03	1.11E-01	2.36E-02
373	1.07	1.0	1.0	3.0	4.12E+03	3.19E+03	1.29E+05	1.30E+00	1.15E-02